Extractive Metallurgy 1

Extractive Metallurgy 1

Basic Thermodynamics and Kinetics

Alain Vignes

ISTE

WILEY

First published 2011 in Great Britain and the United States by ISTE Ltd and John Wiley & Sons, Inc.

Apart from any fair dealing for the purposes of research or private study, or criticism or review, as permitted under the Copyright, Designs and Patents Act 1988, this publication may only be reproduced, stored or transmitted, in any form or by any means, with the prior permission in writing of the publishers, or in the case of reprographic reproduction in accordance with the terms and licenses issued by the CLA. Enquiries concerning reproduction outside these terms should be sent to the publishers at the undermentioned address:

ISTE Ltd
27-37 St George's Road
London SW19 4EU
UK

www.iste.co.uk

John Wiley & Sons, Inc.
111 River Street
Hoboken, NJ 07030
USA

www.wiley.com

© ISTE Ltd 2011

The rights of Alain Vignes to be identified as the author of this work have been asserted by him in accordance with the Copyright, Designs and Patents Act 1988.

Library of Congress Cataloging-in-Publication Data

Vignes, Alain.
Extractive Metallurgy 1/ Alain Vignes.
p. cm.
Includes bibliographical references and index.
ISBN 978-1-84821-160-5
1. Metallurgy--Handbooks, manuals, etc. 2. Extraction (Chemistry)--Handbooks, manuals, etc. I. Title.
TN671.V54 2011
669--dc22

2010031981

British Library Cataloguing-in-Publication Data
A CIP record for this book is available from the British Library
ISBN 978-1-84821-160-5

Printed and bound in Great Britain by CPI Antony Rowe, Chippenham and Eastbourne.

Table of Contents

Preface xi

Chapter 1. Metallurgical Thermochemistry 1

1.1. Introduction 1
1.2. Quantities characterizing the state of a system and its evolution 3
1.2.1. The types of operations 3
1.2.2. Stoichiometric description of a chemical system 4
1.2.3. Evolution of a system's state: degree of advancement of a reaction 6
1.2.4. Characteristic quantities of a phase's composition 11
1.3. Thermodynamic fundamentals of reactions 16
1.3.1. Reaction enthalpy 16
1.3.2. Gibbs free energy of a system, affinity of a reaction and chemical potential of a component 18
1.3.3. Expressions of the chemical potential and activities of a component 21
1.3.4. Affinity of a reaction: law of mass action (thermodynamic modeling of a process) 28
1.3.5. Applications 32
1.4. Phase diagrams 36
1.4.1. Binary phase diagrams 36
1.4.2. Ternary phase diagrams 36
1.5. Bibliography 39

Chapter 2. Oxides, Sulfides, Chlorides and Carbides 41

2.1. Introduction 41
2.2. Metal-oxygen/metal-sulfur systems activities in the intermediate phases 42

2.2.1. Phase diagrams 42
2.2.2. Component activities in the intermediate phases 46
2.3. Standard Gibbs free energy: temperature diagrams for oxides – Ellingham-Richardson diagrams 51
2.3.1. Stoichiometric oxides 51
2.3.2. Unstoichiometric compounds 54
2.3.3. Thermodynamic data for the reduction of oxides by a reducing gas 58
2.4. Thermodynamic data for sulfides and chlorides 58
2.4.1. Ellingham-Richardson diagram for sulfides 58
2.4.2. Stability diagrams for the (M-O-S) systems 60
2.4.3. Ellingham-Richardson diagram for chlorides 62
2.4.4. Stability diagrams of $M-O_2-Cl_2$ systems 62
2.5. Metal-carbon phase diagrams and the Ellingham-Richardson diagram for carbides 63
2.6. Carbon and carbon oxide reactions 67
2.6.1. Oxidation reactions 67
2.6.2. Boudouard's reaction 68
2.6.3. The different types of coal 70
2.7. Bibliography 71

Chapter 3. Metal Solutions, Slags and Mattes 73

3.1. Introduction 73
3.2. Metal solutions 74
3.2.1. Phase diagrams and activities of liquid alloys components 74
3.2.2. Activities and solubilities of metalloids in metal solutions 83
3.2.3. Solubility and precipitation of oxide and sulfide compounds in metals 92
3.3. Mattes 93
3.3.1. Structure and physical properties of sulfide melts (mattes) 93
3.3.2. Thermodynamic data for the binary Fe-S, Ni-S, Cu-S and Pb-S systems 95
3.3.3. Thermodynamic data of ternary mattes 97
3.3.4. Thermodynamic data for M-O-S systems 99
3.4. Slags 106
3.4.1. Structure and physical properties 106
3.4.2. Phase diagrams and activities 110
3.4.3. Phase diagrams and activities of oxide mixtures forming the basis of metallurgical slags $CaO-SiO_2-Al_2O_3-MgO$ 111
3.4.4. Phase diagrams and activities of mixtures of $CaO-SiO_2-Al_2O_3-MgO$ oxides and reducible (iron, manganese and chrome) oxides 115
3.5. Bibliography 127

Chapter 4. Aqueous Electrolytic Solutions and Salt Melts 131

4.1. Introduction 131
4.2. Thermodynamics of aqueous electrolyte solutions 131
4.2.1. Chemical potentials and activities of the components of electrolyte aqueous solutions 132
4.2.2. Aqueous solutions of acids and bases 138
4.2.3. Aqueous solutions of metallic salts: complexation and speciation 148
4.2.4. Solubility of oxides and hydroxides 156
4.2.5. Solubility of salts 165
4.2.6. Solubility of gases in an aqueous solution 171
4.3. Thermodynamics of salt melts (fluxes) 173
4.3.1. Compositions and physical properties of fluxes 174
4.3.2. Thermodynamic properties 174
4.3.3. Solubility of oxides in halides 177
4.4. Bibliography 179

Chapter 5. Reaction Kinetics 183

5.1. Introduction 183
5.2. Rate of a chemical reaction 184
5.2.1. Definitions 184
5.2.2. Expressions of the rate of a chemical reaction 186
5.3. Homogeneous precipitation 189
5.3.1. Thermodynamics of primary nucleation 190
5.3.2. Nucleation and primary particle formation processes 191
5.3.3. Secondary nucleation 193
5.4. Kinetics and mechanism of heterogeneous reactions 194
5.4.1. Mechanism of heterogeneous chemical reactions 194
5.4.2. Rates of heterogeneous reactions in fluid-solid systems 195
5.4.3. Experimental rates of gasification reactions 197
5.4.4. Experimental rates of oxide and sulfide dissolution by acid-base reactions 202
5.4.5. Rates of heterogeneous chemical reactions in fluid-fluid systems 206
5.4.6. Experimental rates of transfer processes 207
5.4.7. Experimental rates of gas-liquid reactions 209
5.5. Reaction rates for in situ conversion of a solid particle 211
5.5.1. Reduction of an oxide in solid state by carbon monoxide or hydrogen 211
5.5.2. Roasting of a zinc sulfide particle 214
5.6. Heterogeneous precipitation 215
5.6.1. Deposition mechanism 216

5.6.2. Silicon deposition by heterogeneous thermal decomposition of silane . . . 216
5.7. Bibliography . . . 217

Chapter 6. Transport Kinetics . . . 219

6.1. Introduction . . . 219
6.1.1. Identification of the rate-limiting step . . . 222
6.2. Equations of change and relationships between diffusion fluxes and driving forces . . . 223
6.2.1. Equations of change (in terms of the fluxes) . . . 223
6.2.2. Relationships between diffusion fluxes, driving forces and transport properties . . . 225
6.3. Interphase mass or heat transport (mass and heat transfer) . . . 227
6.3.1. Definitions of heat and mass transfer coefficients . . . 227
6.3.2. Kinetics of diffusion-controlled processes . . . 229
6.4. Mass and heat transfer coefficients . . . 236
6.4.1. Mass and heat transfer (across a phase boundary) between two semi-infinite and stagnant phases . . . 237
6.4.2. Heat and mass transfer between a flat wall and a fluid flowing along the flat surface in forced convection: boundary layer theory . . . 239
6.4.3. Heat and mass transfer between particles, drops or bubbles and a continuous fluid phase . . . 243
6.5. Overall kinetics of extraction processes under mixed control . . . 247
6.5.1. Extraction process-type gasification . . . 247
6.5.2. Transfer process-type solvent extraction . . . 249
6.5.3. Note on the rule of addition of resistances acting in series . . . 250
6.6. Bibliography . . . 251

Chapter 7. Particulate Kinetics . . . 253

7.1. Introduction . . . 253
7.2. Gasification/leaching of a particle . . . 254
7.2.1. Non-porous particles . . . 254
7.2.2. Porous particles (pellets) . . . 259
7.3. Heterogeneous precipitation: growth rate of the particles . . . 263
7.4. *In situ* conversion of a solid particle . . . 264
7.4.1. Non-porous particle: the shrinking unreacted core model . . . 265
7.4.2. In situ conversion of a porous particle: the grain pellet model . . . 269
7.5. Conversion of a particle undergoing strong exo- or endothermic chemical reactions . . . 270
7.5.1. Exothermic chemical reactions . . . 270
7.5.2. Endothermic chemical reactions . . . 275

7.6. Transfer processes between two fluid phases, one phase being dispersed (as drops or bubbles) in the second phase 276
7.6.1. Heat transfer 276
7.6.2. Mass transfer 277
7.6.3. Hydrogen removal from liquid steel bath by injection of inert gas bubbles 278
7.7. Bibliography 280

Chapter 8. Electrochemical Reactions 283

8.1. Overview of electrochemical processes 283
8.2. Equilibrium electric potential of an elementary electrochemical reaction 285
8.2.1. Nernst equation 285
8.2.2. Electrode potentials in aqueous solutions 288
8.2.3. Equilibrium potential metal/ion $E_{M/M^{z+}}$ in molten salts 292
8.3. Electrochemical equilibria of metals and metalloids (Pourbaix diagrams) 292
8.3.1. Diagram of electrochemical equilibria of water 293
8.3.2. Pourbaix diagram for metal-water systems 294
8.3.3. Pourbaix diagram for the Fe, Cu and Zn-Cl-H_2O systems 300
8.3.4. Pourbaix diagrams for the M-NH_3-H_2O systems 302
8.3.5. Pourbaix diagrams for the M-HCN-H_2O systems 304
8.3.6. Pourbaix diagrams for the M-S-H_2O systems 305
8.4. Electrochemical kinetics 306
8.4.1. Rate of an elementary electrochemical reaction: Tafel's Law 307
8.4.2. Diffusion-controlled rate of an elementary electrochemical reaction 312
8.4.3. Rate of a redox chemical reaction 313
8.5. Redox electrochemical reactions 314
8.5.1. Cementation or displacement reaction 315
8.5.2. Leaching (dissolution) of metals 319
8.6. Bibliography 322

List of Symbols 325

Index 337

Summaries of Other Volumes 345

Preface

Extractive metallurgy is the art of extracting metals from their ores and refining them.

This book deals with the processes, operations, technologies and processing routes of extractive metallurgy, i.e. the (production) extraction of metals from ores, concentrates (enriched ores), scraps and other sources and their refining to liquid metals before casting or to solid metals.

In many books dealing with metallurgy, the introduction starts by recalling the steps of the progress of metallurgy. These steps, according to and since Lucrèce, are identical to those of human progress: the copper age, the bronze age, the iron age, the silicon age[1]. According to Mohen[2], the considerable role attributed to the three principal metals in the development of human societies must not be overstressed or overvalued. It is nonetheless true that "metallurgy is the most advanced prehistoric manifestation of the mastery of natural resources" (Mohen). Extracting copper from its ore dates back to the middle of the fifth millennium before our age and extracting iron from its ore dates from the beginning of the second millennium before our age.

The winning (production) of metals and alloys today is still one of the basic industries of the transformation of matter. Metals and alloys still are essential resources for metallic, mechanic, electromagnetic, electric and even electronic industries (silicon is treated as a metal).

---

1 S.L. SASS, *The Substance of Civilization: Materials and Human History from the Stone Age to the Age of Silicon*, Arcade Publishing, 1999.

2 J.P. MOHEN, *Métallurgie préhistorique*, Masson, Paris, 1990.

This industry is characterized by:

– Production (of primary metal) ranging from 1,345 million tons (Mt) of steel a year to 138,000 tons of titanium, in 2007[3].

Steel	Aluminum	Copper	Zinc	Lead	Nickel	Magnesium	Titanium
1,345	38	15.6	10.6	7.0	1.66	0.79	0.138

Table 1. *World Metal Production in 2007*

– Very high growth rates in the years 1950 to 1973, and again since 2000. The production of steel was 200 million tons in 1950. The production of aluminum increased from 2 million tons in 1950 to 10 million tons in 1973, reaching 38 million tons in 2007. If in developed countries the growth in terms of tonnage has strongly slowed in recent decades, this is due to a smaller consumption of these products owing to the increase in mechanical and physical properties of the materials and parts forged from these materials, thus requiring less material for the same usage. However the annual production of steel in China increased from 182 million tons in 2002 to 489 million tons in 2007[4].

– Production costs varying by a factor of 20 to 25 between steel and titanium. The three principal costs in metal production are investment, ore and energy consumption. The energy consumption is about 20 GJ/ton of steel, 80 GJ/ton of aluminum and 160 GJ/ton of titanium. Hence the permanent research into improvements of the processes or operations and/or the development of new processes.

– Very high recycling rates. Recycled steel represents 46% of iron sources in worldwide steel production. The “electric furnace processing route” produces 35% of steel. It uses 75% less energy than the integrated route. The recycling rate of aluminum represents 25% of total production and the energy consumption from recycled aluminum represents 5% (energy reflow) of energy consumption from the ore. The production of primary zinc is 7.4 million tons and from recycled zinc is 2.1 million tons. In the case of lead, the production from recycled lead is greater than 50%.

– Very high quality products with degrees of purity (i.e. contents of harmful impurities) for the finished products, comparable to the purity of materials for electronics and with very narrow concentration ranges of the alloying elements, to obtain physical or mechanical properties with very small dispersions. For metal castings reaching 300 tons, steel grades with carbon content of less than 25 ppm,

3 US Geological Survey, *Minerals Commodity Summaries and Minerals Yearbook*, 2007.

4 Source: IISI (International Iron and Steel Institute).

and sulfur and phosphorus content of less than 20 ppm or even 10 ppm can be guaranteed. The impurities in liquid aluminum after electrolysis and refining are <3 ppm for Li, <1 ppm for Ni and <1/10 ppm for H. The contents of each impurity in copper for electric wire must be <1 ppm. Achieving these chemical performances coupled to research into the lowest energy consumption requires perfect mastery of the process and thus a profound knowledge of its technology.

– The energy consumption and reduction of pollution (rejected CO_2, SO_2 and dust) from the production of metals have become major objectives, leading to the development of new processes or product lines.

– Non-ferrous metal ores often have very low contents of many rare or noble metals, whose extraction and recuperation often constitutes essential steps for the global production economy. Such extraction requires very complex processing routes for recovering rare or precious metals.

Often the metal can or could be produced via several processing routes. The industrial processing routes for a given metal are to a large extent dependent on economic considerations, i.e. the cost of raw materials, cost of energy, cost of equipment and market conditions.

The raw materials for the production of metals and alloys are the ores on one hand and recovered and recycled products on the other:

– the ores. The ores of Sn, Fe, Mn, Cr, Al, Ni are oxides. The ores of many non-ferrous metals, e.g. Cu, Ni, Pb, Zn, Cd, Mo, are sulfides;

– the recycled metals (Fe, Al, Cu, Zn, Pb);

– the steel plant dust containing metals or oxides (Zn, Cd, Pb);

– the residues from leaching operations, e.g. the red muds, a residue containing titanium, vanadium, gallium produced by bauxite leaching during the Bayer process, the gold cyanide sludge;

– the drosses, slags and scoria treated to recover rare metals or to eliminate harmful components.

The operations of mineralogy are known as ore-dressing. In the general case, the ore must be concentrated to free it from minerals of no value, called the gangue, whose main components are oxides (SiO_2, Al_2O_3, CaO, MgO). This is done using physical operations: grinding (comminution) or fragmentation of the ore to small sizes to allow easy separation, then separation by sedimentation and enrichment by flotation, magnetic sorting etc., leading to a raw material enriched in components.

The operations of extractive metallurgy treat ores, concentrates and recycled metals. These are mixtures of oxides or sulfides. The processing routes of the ore's

treatment, raw or enriched, together with the technologies used in these routes depend first of all on the ore's nature and its metal content.

Thus iron ore is practically pure iron oxide (hematite or magnetite), with a content of iron of the order of 65% and several percent of silica (SiO_2). The basic treatment will be the direct reduction of the iron oxide.

Alternatively, the ores can be treated to give an essentially pure chemical compound of the metal and this compound may be converted to give the metal. For example, aluminum's ore (bauxite), is composed of alumina (Al_2O_3, 30–60%), iron oxide (Fe_2O_3, 1–30%) and silica (1–10%). The first phase of the ore's treatment will be the separation of these oxides to obtain the pure alumina, which will be reduced in a second phase by electrolysis in molten salts.

The copper sulfide ores, whose copper content is very low, exceptionally reaching 5%, undergo processes of mineralogy (flotation) to obtain concentrates containing Cu (20–25%), Fe (30%) and S (30%). The separation of copper sulfide from iron sulfide via a selective roasting constitutes the first step of the treatment. The second step is a copper converting.

Zirconium ore, zircon (silicate of zirconium and hafnium, i.e. $ZrSiO_4$ and $HfSiO_4$), is converted into gas chlorides whose separation is possible before the reduction of zirconium chloride to very pure zirconium.

Extraction and refining operations may be carried out by pyrometallurgical, hydrometallurgical, halide and electrometallurgical processes:

– *pyrometallurgy* involves processes carried out at high temperatures divided into:

- *primary pyrometallurgy*, which converts the ore or concentrate to impure metal generally in liquid form. The main operations are oxide reduction, sulfide roasting, smelting and converting;

- *secondary pyrometallurgy* is the treatment of the liquid metal, obtained either directly in the first step or by remelting metallic recycled products. It consists of several refining operations, mainly the removal of harmful elements left in the liquid metal (deoxidation, dehydrogenation, etc.) and addition of the alloying elements;

– *hydrometallurgy* consists of operations of primary metallurgy performed in aqueous solutions, at relatively low temperatures and often under high pressure, such as leaching, precipitation and solvent extraction;

– *hydroelectrometallurgy* consists of salt electrolysis in an aqueous solution, yielding the metal in a solid state. Electrorefining constitutes a refining process of the metal obtained in a first electrolysis;

– *pyroelectrometallurgy* consists of processes employing electrolysis (reduction), either of mattes or oxides (e.g. Al_2O_3) or chlorides (e.g. $MgCl_2$) into molten salts, yielding the metal in a liquid state;

– *chlorometallurgy* consists of the following processes:

- *chlorination* of a highly reactive metal oxide, such as titanium or zirconium,

- *separation* of the chlorides via physical processes: distillation and extractive distillation,

- *reduction* of chlorides by metallothermic reduction.

The upholding into operation of an existing processing unit, the improvement of an industrial operation, the implementation of a new technology (not formerly used in the unit) and the development of a new process all fall within technical considerations, as well as economic considerations. In this series, economical considerations will not be discussed, for obvious reasons, but sound economic decisions rest on in-depth technical analyses of the processes and operations. Such in-depth analyses are based on process engineering principles. These methods use mathematical models allowing us to simultaneously take into account the elementary processes and their couplings[5]. These mathematical models are sets of fundamentally-based differential equations derived from thermodynamics, kinetics, heat flow, fluid flow, mass transfer and electromagnetic phenomena. Modeling will thus be at the heart of all the analyses here. The solutions to these differential equations, via analytical or numerical methods, allow us to achieve sound quantitative previsions. Analytical solutions of these equations of partial derivatives have been established in numerous instances, but only for specific cases. They are nonetheless interesting as they reveal the influence of certain factors or parameters on the processes. This leads to very useful dimensionless numbers. These analytical solutions and the dimensionless equations are presented and used in these volumes. For the numerical methods of the solution of equation systems, the reader is referred to specialized publications.

The subject of extractive metallurgy is also addressed in two other publications written by myself and published by ISTE. This volume deals with the fundamentals

---

5 J. SZEKELY, "The mathematical modeling revolution in extractive metallurgy", *Metallurgical Transactions B*, Vol. 19B, p. 525-540, 1988, and H.Y. SOHN, "The coming-of-age of process engineering in extractive metallurgy", *Metallurgical Transactions B*, Vol. 22B, p. 737-754, 1991.

of thermodynamics and kinetics of the extraction processes. The second volume, *Metallurgical Reaction Processes*, deals with the extraction and refining unit processes. The third volume, *Processing Operations and Routes*, deals with the operations and technologies used in industrial production and industrial processing routes, i.e. the combination of steps or operations used to convert the available ore to metal, illustrated by flowsheets.

This book is intended not only for students of metallurgical and mechanical engineering who want to acquire the bases of this technology, decreasingly taught in universities and engineering schools, but also for engineers confronted with a new production problem, either directly (management of a industrial operation or development of a new process) or indirectly (in the definition of a materials' specification).

It is conceived to be accessible to any student or engineer with general chemistry and physics training. It only necessitates elementary knowledge in chemistry, thermodynamics and chemical kinetics. One of the objectives of this book is to allow the easy consultation of books and technical publications dealing with this field.

This book is the result of my chemical engineering training, courses taught in the Écoles des Mines of Nancy and Paris (France), visits to industrial plants, research performed in collaboration with industry, studies and common work as a consultant and as an industrialist in direct contact with numerous producers of metallic parts. I would like to thank, more particularly, engineers from the research centers of Arcelor-Mittal (IRSID), Alcan (ex-Péchiney), Cezus and Eramet for their advice and authorized opinions.

I would most particularly like to thank Professors Jean Philibert and André Pineau. Finally this book is dedicated to Professors Pierre Le Goff and Pierre-Marie Fourt.

Alain VIGNES

February 2011

Chapter 1

Metallurgical Thermochemistry

1.1. Introduction

The industrial *processing route* for the production of a metal, from its ore or concentrate to a refined metal, consists of a combination or sequence of *operations* (illustrated conveniently by means of a flowsheet, see [VIG 11c], Chapter 10), performed in *reactors*. In a *unit operation* a single *extraction process* is performed, such as the roasting of a sulfide ore or the reduction of an oxide or a transfer process (removal of a component from a phase) such as a solvent extraction. *In some operations, such as in blast furnaces, several processes occur in sequence* from iron ore to hot metal *in the same reactor.*

These operations are carried out in different conditions: discontinuous (batch, closed), continuous (open) and semi-continuous (semi-batch), see Figure 1.2.1.

Metallurgical processes, occurring in the operations of extraction and refining of metals and alloys, involve homogeneous chemical reactions or heterogeneous chemical reactions (between reactants present in two phases, the reaction occurring at the interface between the two phases).

In the first part of this chapter the physical quantities allowing the quantitative description of the state (and its evolution) of a reaction mixture undergoing a chemical reaction are defined. The second part deals with the fundamentals of thermodynamics for these reactions.

The thermodynamic analysis of reactions constitutes the first unavoidable step of the study of these extraction processes.

Extractive Metallurgy 1: Basic Thermodynamics and Kinetics Alain Vignes
© 2011 ISTE Ltd. Published 2011 by ISTE Ltd.

Thermodynamics provides three important pieces of information:

– it allows the calculation of the energy balance, i.e. the energy (thermal or electric) that needs to be provided or extracted for the reaction to occur at a certain temperature and pressure;

– it allows the calculation of the maximum possible degree of advancement (i.e. the extent) of a reaction and the maximum possible fractional conversion of the reactants, in different operating conditions, which constitute what can be called the *thermodynamic modeling* of a process.

– it allows the determination of operating conditions (T, P, initial composition of the reaction mixture), optimizing the maximum possible fractional conversion of the reactants.

The thermodynamic quantities and data necessary for the prediction of operating conditions of processes are of two types:

– *thermodynamic functions*: enthalpy, Gibbs free energy (free enthalpy), affinity of a reaction, activity of a phase's component, law of mass action, equilibrium constant of a reaction;

– *phase diagrams*: graphs that show which phases (and their extension) are present in a binary, ternary system. The coordinates of these diagrams are various parameters: for instance: temperature (ordinate) and composition (abscissa), see section 1.4. These equilibrium diagrams are quantitatively related to the thermodynamic functions of the systems they describe.

A thermodynamic analysis is often sufficient to predict the maximum possible extent of reactions carried out at high temperatures, especially in the case of reactions between fluid phases, for which the process rates are not limited by slow diffusion phenomena in solid phases or by chemical reactions. It can then be considered that the reaction is indeed occurring: until the total consumption of a reactant or until it nearly reaches equilibrium state for a closed system; or is occurring through a succession of equilibrium states, in the case of a semi-batch system during the continuous injection of a reactant.

The extent of this presentation comes from the fact that in the literature (books and publications) dealing with this field, many definitions and expressions can be found for the same quantities, especially for the activities of components. All these different definitions are presented in this chapter in order to help the reader interpret and understand future readings.

1.2. Quantities characterizing the state of a system and its evolution

The progress of a chemical reaction can be expressed by a single quantity: the degree of advancement (or extent) ξ, see equation [1.2.5]. The fractional conversion of the reactants, see equation [1.2.7], depends on the degrees of advancement of the reactions occurring during the process. The corresponding equations depend on the type of operations, see Figure 1.2.1.

1.2.1. *The types of operations*

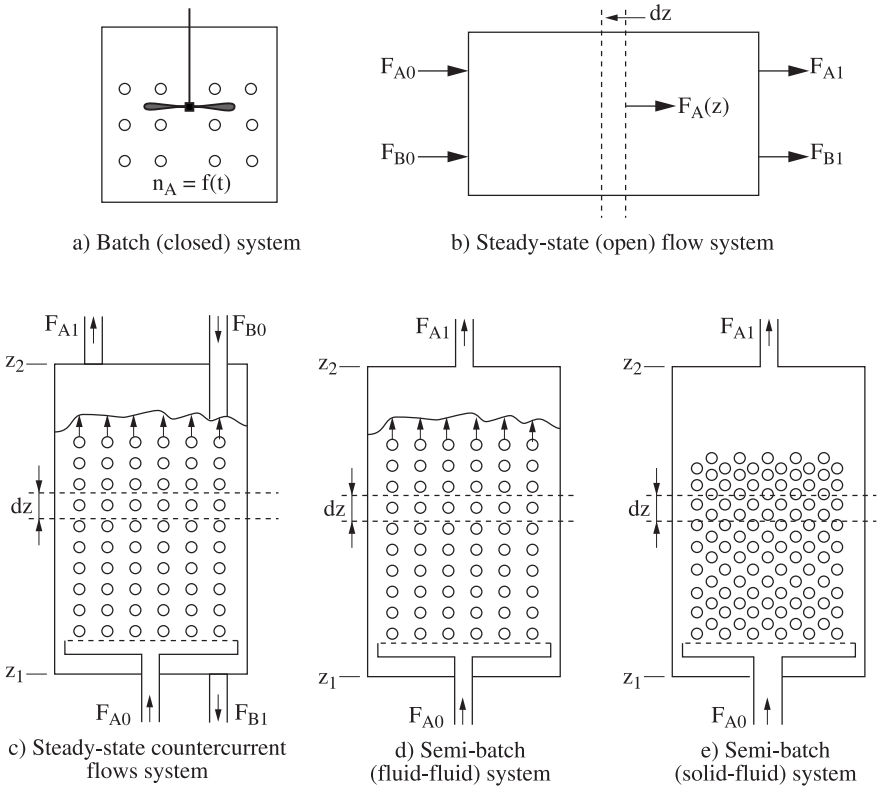

Figure 1.2.1. *Types of operations and contacting patterns for fluid-fluid (c and d) and fluid-solid (e) systems*

The different operations can be performed under three modes: a discontinuous mode, a continuous mode and a semi-continuous mode:

– In a *discontinuous operation*, the reactants are charged into the reactor, mixed and left to react for a certain time. The reaction mixture is then discharged. These reactors are qualified as *batch (closed)*, as there is no flow of matter in or out of the reactor, see Figure 1.2.1a.

– In a *continuous operation*, the reactor is an *open system* that has one or more openings through which the reactants are introduced and one or more exits from where the products of the process are extracted. Thus, there is one (in the case of a homogeneous reaction) or several flows of matter (in the case of a heterogeneous reaction) getting in and out of the reactor. The steady state is the normal operating regime of this operation: steady state plug flow for a homogeneous system (reaction), see Figure 1.2.1b; or steady-state countercurrent or co-current flows for a two-phase system with various contacting patterns, see Figure 1.2.1c.

– in a *semi-continuous operation*, in a *semi-open (semi-batch) system reactor*, one of the reactants or one phase is introduced at the start of the operation (discontinuous charging, for example a charge of solid particles or a liquid phase). The other reactant is continuously introduced during the operation (continuous feed), for instance a gas phase injected as bubbles into a liquid bath, see Figure 1.2.1d, or a gas phase blown through a bed of solid particles, see Figure 1.2.1e. The reactions proceed as long as the reactants are added.

1.2.2. *Stoichiometric description of a chemical system*

We consider the following reaction (homogeneous or heterogeneous) occurring in the indicated direction:

$$\nu_A A(\alpha) + \nu_B B(\beta) \rightarrow \nu_R R(\alpha) + \nu_S S(\beta) \qquad [1.2.1]$$

A, B, R and S are the components (elements, molecules or compounds), and α and β are the phases in which the components are present.

Although the number of molecules can vary in a system during the reaction, the number of elements ("*chemical elements*") does not vary. Thus, the stoichiometric coefficients ν of the reaction are not arbitrary. They satisfy the conservation equations of the elements, see equations [1.2.12b].

Besides this, during the reaction there is conservation of matter. The mass conservation law leads to the *stoichiometric equation* between the stoichiometric coefficients:

$$\nu_A M_A + \nu_B M_B = \nu_R M_R + \nu_S M_S \qquad [1.2.2]$$

For a system in which several chemical reactions may occur, it is important to have a criterion that gives the number r of independent (distinct) reactions necessary to determine the chemical composition of the system when the equilibrium state has been reached. This number is equal to the difference between the number n of non-inert (reacting) components, and the number e of the chemical elements [PRI 54]:

$$r = n - e \qquad [1.2.3]$$

1.2.2.1. *The Gibbs phase rule*

The phase rule that gives the number of *intensive variables w* (T, P and mole fractions) determining the physicochemical state of a multiphase system at equilibrium can be either written as:

$$w = (n - r) + 2 - \phi \qquad [1.2.4a]$$

where ϕ is the number of phases at the same pressure p and at the same temperature T, [PRI 54] or as:

$$w = C_{(independent)} + 2 - \phi \qquad [1.2.4b]$$

where the number of independent components is equal, at most, to the number of chemical elements [ROS 83].

For instance, a system composed of three phases and three components: $CO_3Ca(s)$, $CaO(s)$ and $CO_2(g)$, undergoing the following reaction:

$$CO_3Ca(s) = CaO(s) + CO_2(g)$$

is mono-variant w = 1 and at equilibrium, its physicochemical state is entirely determined by the set temperature. At a temperature T, the pressure of CO_2 at equilibrium with the two solid phases is determined. If the reaction is carried out in the presence of an inert gas under a pressure P, the reaction and CO_2 gas release against the pressure P, will only occur at one temperature fixed by P.

DUHEM THEOREM.– Regardless of the number of phases, components and chemical reactions occurring in the system, the equilibrium states of a closed system, whose initial masses (or number of moles) of each component in each phase is given, are completely determined by two independent variables.

1.2.3. *Evolution of a system's state: degree of advancement of a reaction*

The fractional conversion rates of the reactants can be expressed as a function of a single quantity: the *degree of completion or degree of advancement (extent)* of the reaction ξ.

1.2.3.1. *For a closed system*

The reaction mixture (mono- or multiphase) within a closed container contains n_j molecules of each component j:

– at the initial state: $n_{A0}\ n_{B0}\ n_{R0}\ n_{S0}\ \{\sum n_{j0} + n_{inert}\}$;

– at a time t: $n_A(t)\ n_B(t)\ n_R(t)\ n_S(t)\ \{\sum n_j(t) + n_{inert}\}$.

In the course of reaction [1.2.1], the variations of the number of moles of each component are proportional to the corresponding stoichiometric coefficients of the reaction (*law of definite proportions*):

$$dn_A / -\nu_A = dn_B / -\nu_B = dn_R / \nu_R = dn_S / \nu_S = d\xi \qquad [1.2.5]$$

where $\xi(t)$ is the reaction's degree of advancement, at time t. It is an *extensive variable* that can take any positive value.

Convention: the stoichiometric coefficients v are all positive (an inverse convention is often used).

For a degree of advancement ξ of the reaction, $\nu_R \,.\, \xi$ moles of R and $\nu_S \,.\, \xi$ moles of S are produced, $\nu_A \,.\, \xi$ moles of A and $\nu_B \,.\, \xi$ moles of B have been consumed. The molar balance of each component is written:

$$n_A(t) - n_{A0} = -\nu_A \,.\, \xi(t) \qquad [1.2.6a]$$

$$n_B(t) - n_{B0} = -\nu_B \,.\, \xi(t) \qquad [1.2.6b]$$

$$n_R(t) - n_{R0} = +\nu_R \,.\, \xi(t) \qquad [1.2.6c]$$

$$n_S(t) - n_{S0} = +\nu_S \,.\, \xi(t) \qquad [1.2.6d]$$

The state at time t of a mono- or a multiphase reaction mixture, in which a chemical reaction is occurring, is determined by the initial number of moles of each component n_{ij}, by the degree of advancement of the reaction $\xi(t)$ and by two physical variables (T and P).

The *fractional conversion of a reactant*[1] is the ratio of the number of moles of reactant having reacted to the number of moles initially present:

$$\chi_A(t) = (n_{A0} - n_A(t)) / n_{A0} \quad [1.2.7]$$

with the following relationship between the fractional conversion of reactants A and B:

$$n_{A0} \cdot \chi_A / \nu_A = n_{B0} \cdot \chi_B / \nu_B \quad [1.2.8]$$

The fractional conversion of a reactant is an intensive variable, independent of the initial number of moles, ranging from 0 (initial state) to 1 (final state).

These fractional conversions can be expressed as a function of the degree of advancement ξ of the reaction by:

$$\chi_A(t) = \nu_A.\xi(t) / n_{A0} \quad [1.2.9a]$$

$$\chi_B(t) = \nu_B.\xi(t) / n_{B0} \quad [1.2.9b]$$

1.2.3.2. *Closed system within which several chemical reactions occur*

The molar balance of each component can be expressed as a function of the degrees of advancement of the reactions occurring, by:

$$n_j(t) = n_{j0} + \sum(\pm\nu_{jr}) \cdot \xi_r \quad [1.2.10]$$

where the sign before the stoichiometric coefficient is negative if the component is a reactant for a reaction r, and positive if the component (possibly the same one) is a product in a reaction r'. The fractional conversions, at time τ, for the reactants in one or more reactions are given by:

$$\chi_A(t) = \{\sum\nu_A \cdot \xi(\tau)\} / n_{A0} \quad [1.2.11]$$

EXAMPLE.– For a system that initially involves two reactants: an oxide and carbon, undergoing simultaneous reactions:

$$1/y\ M_xO_y(s) + CO(g) \rightarrow x/y\ M(s) + CO_2(g) \quad (R)$$

$$C(s) + CO_2(g) \rightarrow 2\ CO(g) \quad (B)$$

1 The fractional conversion makes sense only for reactants.

where ξ_R is the degree of advancement of the oxide reduction by carbon monoxide and ξ_B is the degree of advancement of the Boudouard reaction (B). The state of the system may be described by these degrees of advancement. For example, the numbers of molecules (or masses) of each component present at a specific time are given by the following balances:

$$n_{MxOy} = n°_{MxOy} - \xi_R/y$$

$$n_M = (x/y)\,\xi_R$$

$$n_C = n°_C - \xi_B \qquad [1.2.12a]$$

$$n_{CO} = -\xi_R + 2\,\xi_B;$$

$$n_{CO2} = \xi_R - \xi_B$$

$$p_{CO} = \{-\xi_R + 2\,\xi_B\}\ P / \xi_B$$

$$p_{CO2} = \{\xi_R - \xi_B\}\ .\ P / \xi_B$$

The state of the system may also be described by the conservation equations of elements M, C and O:

– for the metal M: $n°_{MxOy} = n_{MxOy} + x n_M$;

– for the carbon: $n°_C = n_C + n_{CO} + n_{CO2}$; and [1.2.12b]

– for the oxygen: $n°_{MxOy} = n_{MxOy} + y n_{CO} + 2\,y n_{CO2}$.

It is easy to verify that these two sets of equations are equivalent.

1.2.3.3. *Open system*

In the *law of definite proportions*, see equation [1.2.5], in terms of F, the molar flow rates of each constituent in and out of the reactor can be expressed by:

$$\frac{(F_{A0} - F_{A1})}{-\nu_A} = \frac{(F_{B0} - F_{B1})}{-\nu_B} =$$

$$\frac{(F_{Re0} - F_{R1})}{\nu_R} = \frac{(F_{S0} - F_{S1})}{\nu_S} \qquad [1.2.13]$$

For an open system and a single phase in convective flow within a tubular reactor, the fractional conversion of reactants A and B presents in this phase, between the entry and exit of the reactor (see Figure 1.2.1.b) can be expressed by:

$$\chi_{A1} = \frac{\left(F_{A0} - F_{A1}\right)}{F_{A0}} \qquad [1.2.14a]$$

$$\chi_{B1} = \frac{\left(F_{B0} - F_{B1}\right)}{F_{B0}} \qquad [1.2.14b]$$

The degree of advancement of the reaction in moles per time unit reached at the exit of the reactor, can be written as:

$$\xi_1 = \frac{\left(F_{A0} - F_{A1}\right)}{\nu_A} = \frac{\left(F_{B0} - F_{B1}\right)}{-\nu_B} \qquad [1.2.15]$$

Under a steady-state flow regime, these two quantities do not vary over time, but vary from point-to-point along the flow path:

$$\chi_A(z) = \frac{\left(F_{A0} - F_A(z)\right)}{F_{A0}} \qquad [1.2.16]$$

and:

$$\xi(z) = \frac{\left(F_{A0} - F_A(z)\right)}{\nu_A} = \frac{\left(F_{B0} - F_B(z)\right)}{\nu_B} \qquad [1.2.17]$$

with:

$$\frac{\left(F_{A0} \cdot \chi_A(z)\right)}{\nu_A} = \frac{\left(F_{B0} \cdot \chi_B(z)\right)}{\nu_B} \qquad [1.2.18]$$

For a length dz, we have:

$$\left(\frac{F_{A0}}{\nu_A}\right) \cdot \left(\frac{d\chi_A}{dz}\right) = \left(\frac{F_{B0}}{\nu_B}\right) \cdot \left(\frac{d\chi_B}{dz}\right) \qquad [1.2.19]$$

For a two-phase system α and β, *with concurrent flows of both phases*, with reactant A present in phase α and reactant B in phase β, the previous relationships are all valid.

For a two-phase system *with countercurrent flows of both phases*, see Figure 1.2.1c, with reactant A present in phase α and reactant B in phase β, we have:

$$\left(\frac{F_{A0}}{\nu_A}\right).\left(\frac{d\chi_A}{dz}\right) = -\left(\frac{F_{B0}}{\nu_B}\right).\left(\frac{d\chi_B}{dz}\right) \qquad [1.2.20]$$

when $z = z_1$, $\chi_A(z_1) = 0$ and when $z = z_2$: $\chi_B(z_2) = 0$ and:

$$\chi_B(z) - \chi_B(z_1) = -\left(\frac{\nu_B}{\nu_A}\right)\left(\frac{F_{A0}}{F_{B0}}\right).\chi_A(z) \qquad [1.2.21]$$

1.2.3.4. *Semi-batch system*

1.2.3.4.1. First case

A gas A(α) is blown through a stationary liquid bath β, or through a fluidized bed of particles B, see Figures 1.2.1d and 1.2.1e and section 18.4.

When the flow rate of gas A is such that phase β can be considered homogeneous, the composition of this phase evolves over time. The fractional conversion of reactant B(β) for a blowing time τ is:

$$\chi_B(\tau) = \{n_{B0} - n_B(\tau)\} / n_{B0} \qquad [1.2.22]$$

For a steady flow of phase α, the inlet molar flow rate of reactant A (F_{Ae}) is constant during the operation, but the outlet molar flow rate $F_{As}(t)$ varies over time. The number of moles of B(β) that still have to be consumed decreases with time. The fractional conversion of reactant A at each instant is given by:

$$\chi_A(t) = \{F_{A0} - F_{A1}(t)\} / F_{A0} \qquad [1.2.23]$$

It decreases over time. A global fractional conversion, during time τ, can thus be defined by:

$$\chi_A(\tau) = \frac{F_{A0}.\tau - \int F_{A1}(t)\,dt}{F_{A0}.\tau} \qquad [1.2.24]$$

Equation [1.2.8] is therefore written:

$$\frac{\{F_{A0}.\tau.\chi_A(\tau)\}}{\nu_A} = \frac{\{n_{B0}.\chi_B(\tau)\}}{\nu_B} \qquad [1.2.25]$$

where $F_{A0} . \tau$ is the number of moles of reactant A injected into the reactor over a time τ. Equation [1.2.25] is equivalent to equations [1.2.8] and [1.2.18]. During this time τ, a number of moles of reactant A equal to $\{F_{A0} . \tau . \chi_A(\tau)\}$ have reacted.

1.2.3.4.2. Second case

A gas A(α) is blown through a fixed bed of solid particles B, see Figure 1.2.1e and Figure 3.3.2 in [VIG 11c].

When the height of the bed is such that the fractional conversion of the stationary reactant B varies along the length z of the fixed bed, the fractional conversion of reactant A – $\chi_A(z, t)$ – and of reactant B – $\chi_B(z, t)$ – depend on z and t. Along a length dz of the particle bed, we thus have:

$$\left(\frac{F_{A0}}{\nu_A}\right).\left(\frac{d\chi_A}{dz}\right) = \left(\frac{n_{B0}}{\nu_B}\right).\left(\frac{d\chi_B}{dt}\right) \qquad [1.2.26]$$

when $z = z_1$, $\chi_A(z_1) = 0$ and when $t = 0$, $\chi_B = 0$.

During time τ, if $F_{A0}. \tau$ moles of A pass through the fixed bed of B particles, the fractional conversion of both reactants are connected by equation [1.2.25].

1.2.4. *Characteristic quantities of a phase's composition*

Many quantities characterizing the composition of a phase are used. Every one of them is used for a special purpose, hence the necessity of introducing and defining them with precision.

We consider in a phase, in convective or non-convective flow, an elementary volume that is small enough that its composition may be considered uniform (this elementary volume being in motion or not).

Let $m_j(t)$ be the mass and $n_j(t)$ the number of moles of component j, of molar (atomic) mass M_j, at a given time in the elementary volume V. This mass $m_j(t)$ varies over time, following the advancement of the reaction(s). It can also vary by inlet or outlet of matter from the considered volume:

$$n_j = m_j / M_j \qquad [1.2.27]$$

The *(mass) density* ρ of the phase is defined as:

$$\rho = \sum m_j / V \qquad [1.2.28]$$

The *molar* (*mole) fraction* of component j is defined as:

$$x_j = n_j / \sum n_j = n_j / n \quad \text{with} \quad \sum x_j = 1 \qquad [1.2.29]$$

where n is the total number of moles present in the elementary volume (this number is not usually constant).

The *mass fraction* of component j is defined as:

$$w_j = m_j / \sum m_j \quad \text{with} \quad \sum w_j = 1 \qquad [1.2.30]$$

Metallurgists often use the *mass percentage*, represented by %j, for components present in low concentrations:

$$\%j = 100 w_j \qquad [1.2.31]$$

The relation between the molar fraction and the mass percentage is:

$$x_j = \{\%j / M_j\} / \sum\{(\%j) / M_j)\} \qquad [1.2.32]$$

and in a *binary* solution, very dilute in component j:

$$x_j \approx (\%j) \, . \, \{M_s / 100 \, M_j\} \qquad [1.2.33]$$

where M_s is the molar mass of the "solvent".

The *molar concentration*, or *molality* C_j, of component j, which is often represented by [A] for component A, is the number of moles n_j per unit volume:

$$C_j = n_j / V, \quad C_A = [A] = n_A / V \quad \text{and} \quad C = \sum C_j \qquad [1.2.34]$$

For a dilute solution, for the elements present in low concentrations:

$$x_j = C_j \times v_{MS} \qquad [1.2.35]$$

where v_{MS} is the specific molar volume of the solvent. For instance, in the case of water, $v_{Ms} = 18$ cm^3/mol.

The *mass concentration* of component j is the mass of component j per unit volume:

$$\rho_j = m_j / V \qquad [1.2.36]$$

The *molality* is the number of moles of component j dissolved in 1,000 g of solvent, often designated by $<m_j>$. For a dilute solution:

$$<m_j> = x_j \times 1{,}000 / M_{(solvent)} \qquad [1.2.37]$$

For a gaseous phase, the *partial pressure* of component j is defined as:

$$p_j = P \,.\, x_j \qquad [1.2.38]$$

and for a perfect gas (mix) in the elementary volume V:

$$p_j = n_j \,.\, R \,.\, T / V = C_j \,.\, RT \qquad [1.2.39]$$

and:

$$P = (\sum n_j) \,.\, RT / V \qquad [1.2.40]$$

In the case of a phase, in convective flow through a straight section Ω, we can also express all the quantities that are specific to the phase's composition at a given point and time by the flow rate of this phase and the fluxes (flow rates by unit surface) of each component. We can define the following instantaneous values through a section Ω:

– the *volumetric flow rate* Q(z,t) is the volume of the phase passing through the section Ω during a unit of time;

– the linear velocity of the flow u is given by:

$$u(z,t) = Q(z,t) / \Omega; \qquad [1.2.41]$$

– the *mass flow rate* through section Ω is given by:

$$G(z,t) = Q.\, \rho = \sum F_j(z,t).\, M_j \qquad [1.2.42]$$

where $F_j(z,t)$ is the *molar flow rate* of component j. This is equal to the number of moles of component j passing through the section Ω at time t during a time unit. $F_j \,.\, M_j$ is the mass flow rate of component j at z and t.

The expression of a component's molar fraction at each section of a reactor remains the same. In equation [1.2.29], the number of moles n_j have to be replaced by the molar flow rate F_j (moles/sec) of each component, leading to:

$$x_j(z,t) = F_j(z,t) / \sum F_j \quad [1.2.43]$$

and:

$$C_j(z,t) = F_j / Q \quad [1.2.44]$$

At the section Ω, the expression of the partial pressure is as follows:

$$p_j = PF_j / \sum F_j = F_j\, RT / Q \quad [1.2.45]$$

The total pressure at the section Ω is given by:

$$P = (\sum F_j)\, RT / Q \quad [1.2.46]$$

1.2.4.1. *Expressions of these quantities as a function of the reactions' degree of advancement*

1.2.4.1.1. For a closed system

For a closed mono- or multiphase system of mass m (constant), all the definitions of the characteristic quantities of the composition of each phase are applicable at each instant. Quantities vary over time, owing to the chemical reactions and mass transfer between phases that occur in the system.

In the presence of a gas phase, the reactor can operate under a constant pressure and the volume of the gas phase V will vary with the extent of the reaction or, under constant volume V, the pressure of the gas phase will vary in the same way. The volume or the total pressure of the gas phase will vary during the progress of the reactions owing to the variation of the number of moles $\sum n_j$.

Assuming that the perfect gas law can be applied, at a given time where the pressure is P and the temperature is T (see equation [1.2.40]), we have:

$$PV(g) / RT = \{\sum n_{ji}(g) + n_{inert}(g) + \Delta\nu(g)\, .\, \xi(t)\} \quad [1.2.47]$$

where $n_{ji}(g)$ and $n_{inert}(g)$ are the number of moles of the components (reactants, products and inert materials) initially present in the gas phase and where $\Delta\nu(g)$ corresponds to:

$$\Delta\nu(g) = (\nu_R + \nu_S - \nu_A - \nu_B)(g)$$

In the initial state:

$$P_iV_i = RT_i\{\sum n_{ji}(g) + n_{inert}(g)\} \quad [1.2.48]$$

Thus, the variation of PV/T (see equation [1.2.47]) is then given by:

$$PV/T = \{P_i V_i / T_i\} \,.\, (1 + \lambda(g) \,.\, \xi(t)) \qquad [1.2.49]$$

where:

$$\lambda(g) = \Delta\nu(g) / \{\sum n_{ji}(g) + n_{inert}(g)\} \qquad [1.2.50]$$

For an operation where the volume of the gas phase is constant, this equation gives the variation of the pressure as a function of the degree of advancement of the reaction. The concentration of a gas component varies as follows:

$$C_A = C_{Ai} - (\nu_A / \Delta\nu)\,(P - Pi) / RT \qquad [1.2.51]$$

For an operation under constant pressure, the gas phase volume varies as follows:

$$V(g) / T = \{V_i(g) / T_i\}\,(1 + \lambda(g) \,.\, \xi) \qquad [1.2.52]$$

The volume of the gas phase varies with the advancement of the reaction (ξ), as the reaction consumes or produces gas molecules $\lambda(g) > 0$ or < 0 and:

$$C_A = \frac{n_A}{V_g} = \left(\frac{T}{T_i}\right)\frac{(n_{Ai} - \nu_A.\xi)}{(1 + \lambda(g).\xi)} \qquad [1.2.53]$$

The concentration of reactant A can be expressed as a function of the corresponding fractional conversion, by:

$$C_A = \frac{C_{Ai}(1 - \chi_A)}{(1 + \varepsilon_A.\chi_A)} \qquad [1.2.54]$$

$$\varepsilon_A = (\Delta\nu / \nu_A)\, n_{Ai} / \{\sum n_{ji} + n_{inert}\} = \lambda(g) \,.\, (n_{Ai} / \nu_A) \qquad [1.2.55]$$

1.2.4.1.2. Open system with a gas phase in a steady-state convective flow

For an open system a tubular reactor of a Z-length cross-section Ω and a convective gas phase plug flow, the pressure P_e and volumetric gas flow rate Q_e are set at the entry of the reactor. This is in order to overcome the pressure drop along the reactor and to allow the fluid to flow out against a fixed set pressure (atmospheric pressure or counter-pressure). The volumetric flow rate Q varies along the reactor with the advancement of the reaction, according to an equation that is similar to that of a closed reactor, see equation [1.2.49]:

$$Q(z)P(z) / T = \{Q_e P_e / T_e\} . (1 + \lambda(g) . \xi(z)) \quad [1.2.56]$$

where the pressure drop $\Delta P(z) = P(z) - P_e$ along the reactor also depends on the gas flow rate (or on the linear velocity of the gas phase), see Chapter 3 of [VIG 11c], section 3.2.2.1.

The expressions of the concentration of the reactant within the gas phase, as a function of degree of advancement of the reaction or fractional conversion of the reactant, are similar to those within a closed system, see equations [1.2.53] and [1.2.54].

1.3. Thermodynamic fundamentals of reactions

Readers may want to refer to the following references for additional information [GAS 81, KUB 79, PRI 54].

1.3.1. *Reaction enthalpy*

A chemical reaction or a physical process, such as dissolution, evaporation and fusion, is either exothermic or endothermic. If the chemical reaction is exothermic, it produces heat that has to be released into the external environment; if not, the temperature of the reaction mixture will increase. If the chemical reaction is endothermic it absorbs heat. The external environment therefore has to provide some heat to the reaction system; if not, the temperature of the reaction mixture will decrease.

The temperature of the system has to be maintained at a desired value in order to control:

– the reaction kinetics; and

– the maximum possible degree of advancement that will be reached at equilibrium.

The knowledge of the sign of the reaction enthalpy allows the determination, *a priori*, of the direction of variation of the maximum extent of the reaction with temperature, see Figure 1.3.4.

Let us consider reaction [1.2.1]:

$$\nu_A A(\alpha) + \nu_B B(\beta) \rightarrow \nu_R R(\alpha) + \nu_S S(\beta) \quad [1.3.1]$$

carried out at constant temperature and pressure (1 atm) in a system where, in the initial state, both reactants A and B are in stoichiometric quantities and in their *standard state* (pure body in its stable physical state, at temperature T and a pressure of 1 atm), without any products R and S. The heat that has to be provided or extracted by/from the external environment for the reaction to be complete (total consumption of reactants A and B; degree of advancement $\xi = 1$). Even if, in fact, at the given temperature the reaction tends towards an equilibrium state is *the standard enthalpy of the reaction* at this temperature at a pressure of 1 atm. It is represented by $\Delta H°_r$:

– for an exothermic reaction $\Delta H°_r < 0$; [1.3.2]

– for an endothermic reaction $\Delta H°_r > 0$.

For an advancement $\Delta\xi$ of the reaction, the variation in enthalpy of the system is:

$$\Delta H°_r \,.\, \Delta\xi \qquad [1.3.3]$$

For an adiabatic process the system is isolated from the external environment. The reaction produces or absorbs heat and thus heats or cools the reaction system.

The standard enthalpy of reaction r at a temperature T can be calculated from the *standard enthalpies of formation* of the reaction components: $\Delta H_f°$ (T, p = 1 atm) by:

$$\Delta H_r°(T) = \{\nu_R \Delta H°_{r(R)}(T) + \nu_S \Delta H°_{r(S)}(T)\} - \qquad [1.3.4]$$

$$\{\nu_A \Delta H°_{r(A)}(T) + \nu_B \Delta H°_{r(B)}(T)\}$$

The standard enthalpy of formation of a component at a temperature T can be calculated from the standard enthalpy of formation at 298.1K, from the molar enthalpy of a possible physical state change between 298K and T and from the specific heat of the component:

$$\Delta H_{r(j)}°(T) = \Delta H°_{r(j)}(298K) + C_{p(j)}(T - 298K) \qquad [1.3.5]$$

The thermodynamic tables give the values of: standard enthalpies of formation of components $\Delta H°_f$ (298.1K; 1 atm); molar enthalpies of physical state change (latent heat of fusion or evaporation); and variations of specific heats of components with temperature [STU 71].

1.3.2. *Gibbs free energy of a system, affinity of a reaction and chemical potential of a component*

The *Gibbs free energy* (free enthalpy) G of a system in which a reaction is occurring at a constant temperature and pressure is given by:

$$G^{sys}(t) = \sum n_j(t) \,.\, \mu_j(t) \qquad [1.3.6]$$

where $n_j(t)$ is the number of moles of component j present at time t within an element of volume. $\mu_j(t)$ is its *chemical potential*, which depends on the temperature, pressure and composition of the phase in which the component is dissolved at time t:

$$\mu_j = (\delta G^{sys} / \delta n_j)_{ni \,=\, constant} \qquad [1.3.7]$$

The chemical potential of component j is the variation in Gibbs free energy of the phase in which it is present, when 1 mole of component j is added to this phase.

During a process carried out at constant time T and pressure P, the variation of the Gibbs free energy of the system between the initial and final state, is:

$$\Delta G^{sys} = G_{E.F} - G_{E.I} \qquad [1.3.8]$$

For the advancement $\Delta\xi$ of a reaction, the variation in Gibbs free energy ΔG of the system is given by:

$$\Delta G_r = \{(\nu_R.\mu_R + \nu_S.\mu_S) - (\nu_A.\mu_A + \nu_B.\mu_B)\} \,.\, \Delta\xi \qquad [1.3.9]$$

The standard Gibbs free energy of formation of a compound (of stoichiometric composition) at temperature T from its *chemical elements* in their standard state at this temperature and under 1 atm pressure:

$$xX + yY \rightarrow X_xY_y \qquad [1.3.10]$$

is given by:

$$\Delta G^\circ_{f(XxYy)}(T,\, p = 1 \text{ atm}) = \mu^o_{X_xY_y} - (x\mu^\circ_X + y\mu^\circ_Y) \qquad [1.3.11a]$$

where μ° are the *standard chemical potentials* (the potential of a pure species in its physical state at the given temperature under a pressure of 1 atm) of the chemical elements and the pure components in their stable physical state. By definition, *the values of the standard chemical potentials of chemical elements are equal to zero under the following conditions:*

p = 1 atm, T = 298.1K

$$\mu^\circ_{Fe}, \mu^\circ_{S}, \mu^\circ_{Si} = 0 \quad \text{and} \quad \mu^\circ_{O2}, \mu^\circ_{H2,} \mu^\circ_{N2,} \mu^\circ_{Cl2} = 0 \qquad [1.3.11b]$$

But at a different temperature their values are not equal to zero, as the values of the entropy and specific heat of the chemical elements are not equal to zero:

$$\Delta G^\circ_f(T) = \{\Delta H^\circ_f(T) - T \,.\, \Delta S^\circ_f(T)\} \qquad [1.3.12]$$

For a chemical reaction carried out at a temperature T between reactants in stoichiometric quantities and in their standard state, the variation of standard Gibbs free energy of the complete reaction ($\xi = 1$) – even if in fact the reaction tends towards a an equilibrium state ($\xi^* < 1$) – between the initial state and the final state can be expressed as a function of the standard chemical potentials of the components μ_j°, as:

$$\Delta G_r(\xi = 1) = \Delta G^\circ_r(T) = (\nu_R.\mu^\circ_R + \nu_S.\mu^\circ_S) - (\nu_A.\mu^\circ_A + \nu_B.\mu^\circ_B) \qquad [1.3.13a]$$

The standard Gibbs free energy of the reaction $\Delta G^\circ_r(T)$ can thus be expressed as a function of the standard free energies of formation of the components as:

$$\Delta G^\circ_r(T) = (\nu_R.\Delta G^\circ_{f(R)} + \nu_S.\Delta G^\circ_{f(S)}) - (\nu_A.\Delta G^\circ_{f(A)} + \nu_B.\Delta G^\circ_{f(B)}) \qquad [1.3.13b]$$

According to the law of conservation of chemical elements, this relation is true at any temperature. The standard Gibbs free energies of formation $\Delta G^\circ_{f(A)}$ are determined by calorimetric measurements and data are found in thermodynamic tables [STU 71], see Chapter 2.

The *affinity* of reaction [1.3.1], occurring in the forward direction (as indicated), is defined as [PRI 50][2]:

$$A_r = -dG_r / d\xi = (\nu_A.\mu_A + \nu_B.\mu_B - \nu_R.\mu_R - \nu_S.\mu_S) = \sum(\nu_j.\mu_j) \qquad [1.3.14]$$

The affinity is the *instantaneous driving force* of the reaction. It is an intensive quantity: a linear combination of chemical potentials (expressed in $J.mol^{-1}$), while the variation of the system's Gibbs free energy ΔG^{sys} is an extensive quantity, depending on the number of moles and expressed in Joules.

In English textbooks, the affinity is called the *reaction's Gibbs free energy* and is represented by:

---

2 $A = -\sum \nu_j \mu_j$ where the stoichiometric coefficients of reactants are negative and those of the products are positive.

$$A_r = - \text{“}\Delta G_r\text{”} \qquad [1.3.15]$$

written here as “ΔG_r” to show that it is not a variation in free energy.

Similarly, the *standard affinity of the reaction A°(T, p =1 atm)* is defined as the standard free energy of reaction [1.3.13] but with opposite signs, even though it is a variation and not an instantaneous quantity:

$$A°_r(T,P = 1 \text{ atm}) = - \Delta G°_r(T) \qquad [1.3.16]$$

1.3.2.1. *The De Donder equation and the equilibrium state of a chemical reaction*

For a spontaneous chemical reaction to occur, the free energy of the system must decrease. The variation in free energy between the initial and final state, see equation [1.3.8], must be negative:

$$\Delta G^{sys} = G_{E.F} - G_{E.I} < 0 \qquad [1.3.17]$$

A reaction starts and proceeds as long as its affinity remains positive $A_r > 0$, or as long as:

$$A_r \,.\, d\xi > 0 \qquad [1.3.18]$$

This inequality is due to De Donder [PRI 54].

During the combustion of coal, for example, the chemical energy $A.\, d\xi$ is completely degraded into heat released to the external environment.

As an example, in a closed system we consider a mixture whose reactants are initially present in stoichiometric quantities where there are no products R and S. Two cases are possible for the variation in Gibbs free energy of the reaction mixture as a function of the degree of advancement ξ, see Figure 1.3.1. It can decrease in a monotonous way or present a minimum:

– If the Gibbs free enthalpy of the reaction mixture decreases in a monotonous way, the affinity of the reaction remains positive (curve I in Figure 1.3.1) when ξ goes from 0 to 1:

$$A_r(\xi) = - (dG_r / d\xi) > 0 \qquad [1.3.19]$$

Complete consumption of the reactants occurs if they are initially in stoichiometric proportions. If one reactant is in excess, complete consumption of the second reactant will occur.

– If the variation in Gibbs free energy of the mixture goes through a minimum for a degree of advancement ξ^* (curve II in Figure 1.3.1), the reaction mixture evolves towards an equilibrium state. Between the initial state ($\xi = 0$) and the equilibrium state ($\xi = \xi^*$), $A_r(\xi)$ remains positive. The composition of the reaction mixture at equilibrium corresponds to the minimum of the curve, thus:

$$A_r(\xi^*) = -\left(dG_r / d\xi\right)_{equilibrium} = 0 \qquad [1.3.20]$$

The affinity is equal to zero at equilibrium. This equation will be used to determine the state of the reaction mixture (its composition ξ^*) at equilibrium, thus the maximum fractional conversion at this temperature, see section 1.3.4.

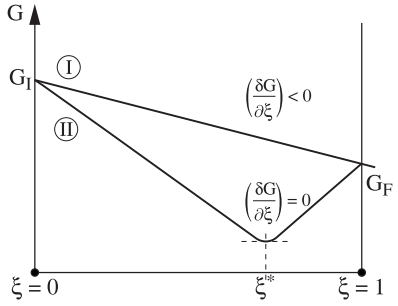

Figure 1.3.1. *Variation of Gibbs free energy G of a stoichiometric mixture ($n_{Ai} = n_A$, $n_{Bi} = n_B$, $n_{Ri} = n_{Si} = 0$) as a function of the degree of advancement of the reaction ξ.*
Curve I = complete reaction.
Curve II = reaction reaching an equilibrium ξ^*

1.3.3. *Expressions of the chemical potential and activities of a component*

The chemical potential μ_j of a component j in a solution can be expressed in many different ways, which can explain the different definitions of the activity coefficient of a component.

1.3.3.1. *Chemical potential, activities and reference states*

The basic expression of the chemical potential μ_j of component j in phase α is given by:

$$\mu_j(\alpha) = \zeta_j(T,P) + RT \ln a_j \qquad [1.3.21]$$

where a_j is the *Raoultian activity* of component j and $\zeta_j(T,P)$ is the potential of pure component j in the same physical state as phase α in which it is dissolved. This defines the activity of the component according to Raoult's law, see Figure 1.3.2.

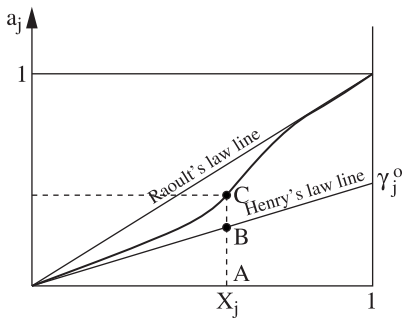

Figure 1.3.2. *Diagrammatic illustration of the relation between Raoultian activity $a_j = \gamma_j.x_j$ and Henrian activity $f_j.x_j$, with f_j = AC/AB in a binary system with complete mutual solubility, with negative deviations from ideal Raoultian behavior*

For instance, for liquid mixtures at temperatures below the melting point of the pure component, the reference state for that component is the metastable supercooled liquid.

It is often convenient to choose the stable form (i.e. standard state) as a reference state for the component at temperature T and P = 1 atm. The chemical potential of component j is then *referred to* its standard chemical potential μ°_j, which defines a new activity a°_j:

$$\mu_j(\alpha) = \mu^\circ_j(T,P = 1 \text{ atm}) + RT \ln a^\circ_j \qquad [1.3.22]$$

a°_j, which we call the *standard activity* referring to *the standard state of component j*, i.e. its physical state at temperature T and P = 1 atm (the a° notation is used to show that the reference state corresponds to the standard one).

It may be verified that:

$$\zeta_j(T,P) = \mu^\circ_j(T) + \Delta g_j^{(SC)} \qquad [1.3.23]$$

where $\Delta g_j^{(SC)}$ is the molar free energy of the physical state (phase) change (SC) of component j at the given temperature, from its standard state to the physical state of the solution in which it is dissolved.

The relation between both activities is:

$$a^\circ_j / a_j = \exp(\Delta g_j^{(SC)} / RT) \qquad [1.3.24]$$

Depending on the standard state (ss) of a solute M (gas, liquid or solid) at the temperature of the reaction and the physical state of phase α in which it is dissolved:

$$\Delta g_j^{(SC)}\{l(ss) \rightarrow g(\alpha)\} = \Delta g^{(\text{evaporation or sublimation})} = -RT \ln p^\circ_j \qquad [1.3.25a]$$

$$\Delta g_j^{(SC)}\{g(ss) \rightarrow l(\alpha)\} = \Delta g^{(\text{condensation})} = RT \ln p^\circ_j \qquad [1.3.25b]$$

where p°_j is the vapor pressure of the pure species j. The thermodynamic tables give the variations of vapor pressure of the elements and pure species with temperature.

$$\Delta g^{(SC)}\{s(ss) \rightarrow l(\alpha)\} = \Delta g^{(\text{fusion})} \qquad [1.3.25c]$$

where $\Delta g_j^{(\text{fusion})}$ is the free molar energy of the fusion of component j at the given temperature. This may be evaluated from the enthalpy of fusion by:

$$\Delta g_j^{(\text{fusion})} = (1 - T / T_f) \,.\, \Delta H_j^{(\text{fusion})} \quad (\text{with } \Delta H_j^{(\text{fusion})} > 0) \qquad [1.3.26]$$

If $T < T_f$, then $\Delta g_j^{(\text{fusion})}(T) > 0$.

Within a binary solution (with complete mutual solubility: $x_j = 0$ to 1) where the standard physical states of both components are the same, at the solution temperature, see Figure 1.3.2, we have:

$$a_j = a^\circ_j$$

In a gas phase considered as a perfect gas:

$$p_j = P \,.\, x_j(g) \qquad [1.3.27]$$

where p_j is the partial pressure of component j in a gas mixture and P is the total pressure, the pressures are expressed in atmospheres. The Raoultian activity, see equation [1.3.21], of a component $a_j(g)$ is equal to the molar fraction of the component within the phase:

$$a_j(g) = x_j(g) \qquad [1.3.28]$$

– if the standard state of component j at temperature T is gaseous, the standard activity, see equation [1.3.22], is equal to the partial pressure of the component:

$$a^\circ_j(g) = p_j \qquad [1.3.29]$$

– if the standard state of component j at temperature T is liquid, see equations [1.3.24] and [1.3.25a]:

$$a^\circ_j(g) = p_j / p^\circ_j \qquad [1.3.30]$$

In a condensed phase, for a non-ideal solution the deviation from the ideal for each component is expressed by a coefficient γ_j, called the *Raoultian activity coefficient* γ_j. This is defined by (see Figure 1.3.2):

$$a_j = \gamma_j \, . \, x_j \qquad [1.3.31]$$

where:

$$\gamma_j \rightarrow 1 \text{ when } x_j \rightarrow 1 \qquad [1.3.32]$$

– if the standard physical state of component j at the given temperature T is gaseous, the activities of component j in the liquid phase may be estimated from the partial pressure of component j in the gas phase in equilibrium with the liquid phase, see equation [1.3.29]:

$$a^\circ_j(l) = a^\circ_j(g) = p_j \qquad [1.3.33a]$$

$$a_j(l) = p_j / p^\circ_j \qquad [1.3.33b]$$

– if the standard physical state of component j at temperature T is liquid, the activities of component j in the liquid phase may be estimated from the partial pressure of component j within the gas phase in equilibrium with the liquid phase, see equation [1.3.30]:

$$a_j(l) = a^\circ_j(l) = p_j / p^\circ_j \qquad [1.3.34]$$

1.3.3.2. *Activity of a component according to Henry's law*

The Raoultian activity a_j of a component j, see equations [1.3.21] and [1.3.31], in a condensed phase is expressed as the product:

$$a_j = f_j \, . \, \gamma_{j(0)} \, . \, x_j \qquad [1.3.35]$$

which defines another activity coefficient f_j, where $\gamma_{j(0)}$ is the value of the Raoultian activity coefficient at infinite dilution of component j (see Figure 1.3.2):

$$\gamma_j \rightarrow \gamma_{j(0)} \text{ when } x_j \rightarrow 0 \qquad [1.3.36]$$

where RT ln $\gamma_{j(0)}$ is the free energy of solution of one mole of component j in the solution at infinite dilution, the component being in the same physical state as the solution.

The coefficient f_j is called the *Henrian activity coefficient*. For a dilute solution, this coefficient gives the deviation from Henry's law (see Figure 1.3.2):

$$f_j = AC / AB \rightarrow 1 \text{ when } x_j \rightarrow 0 \qquad [1.3.37a]$$

A *new Henrian activity* $\tilde{a}_j$ is thus defined:

$$\tilde{a}_j = f_j \,.\, x_j \qquad [1.3.37b]$$

The chemical potential, referring to the standard potential, can thus be written as (see equation [1.3.22]):

$$\mu_{j(l)} = \mu^\circ_j + \Delta g^\circ_{j(0)}{}^{(sol)} + RT \ln f_j \,.\, x_j = \eta^\circ_j + RT \ln f_j \,.\, x_j \qquad [1.3.38]$$

where $\Delta g^\circ_{j(0)}{}^{(sol)}$ is the free energy of solution of one mole of component j in its standard physical state at temperature T in a solution at infinite dilution:

$$\Delta g^\circ_{j(0)}{}^{(sol)} = RT \ln \gamma_{j(0)} + \Delta g_j^{(SC)} \qquad [1.3.39]$$

The "standard" activity a_j°, see equations [1.3.22], [1.3.24] and [1.3.39], can be written as:

$$a^\circ_j = \exp(\Delta g_j^{(S.C)} / RT) \,.\, f_j \,.\, \gamma_{j(0)} \,.\, x_j = \exp(\Delta g^\circ_{j(0)}{}^{(sol)} / RT) \,.\, f_j \,.\, x_j \qquad [1.3.40]$$

1.3.3.3. *Dilute metal solutions*

For dilute metal solutions, the mass percentage %j of component j is quite often used instead of the molar fraction for its content in the solution. By substituting the chemical potential expression (see formula [1.3.38]) and mole fraction by the mass percentage (see equation [1.2.32]), we have:

$$\mu_j = \mu^\circ_j + \Delta g^\circ_{j(0)}{}^{(diss)} + RT \ln(M_{(solvent)} / 100\, M_j) + RT \ln(f_j \,.\, \%j)$$

$$= \eta^\circ_{j(\%J)} + RT \ln(f_j . \%j) \qquad [1.3.41a]$$

$$a_j^\circ = \exp(\Delta g_j^{(SC))} / RT)\, (M_{(solvent)} / 100\, M_j) \,.\, (f_j \,.\, \gamma_{j(0)} \,.\, \%j)$$

$$= \exp(\Delta g^\circ_{j(1\%)}{}^{(sol)} / RT) \,.\, (f_j \,.\, \%j) \qquad [1.3.41b]$$

where $\Delta g_{j(1\%)}{}^{(sol)}$ is the free energy of solution of one mole of component j in a hypothetical solution containing 1% in weight of component j that would follow Henry's law up to a content of 1% ($f_j = 1$ for %j = 1).

$$\Delta g^\circ_{j(1\%)}{}^{(sol)} = \Delta g^\circ_{j(0)}{}^{(sol)} + RT \ln(M_{(solvent)} / 100\, M_j) \qquad [1.3.42]$$

The $\Delta g^{\circ}_{j(1\ \%)}{}^{(sol)}$ values can be found in tables for some elements in solution and a few liquid metals (mainly iron), see Table 3.2.2 (Chapter 3). A new activity is thereby defined:

$$\tilde{\mathbf{a}}_{\mathbf{j}\ (1\ \%)} = f_j\ .\ \%j \qquad [1.3.42b]$$

For dilute metal solutions of several components, the activity coefficient f_j of a solute is expressed as the product of the activity coefficients:

$$f_j = f^{i}_j\ f^{k}_j\ \ldots..\ f^{n}_j \qquad [1.3.43]$$

with:

$$\log f^{k}_j = e^{k}_j\ .\ \%k \qquad [1.3.44]$$

thus:

$$\log f_j = \sum e^{k}_j\ .\ \%k \qquad [1.3.45]$$

where e^{k}_j are the interaction coefficients (see Chapter 3, Table 3.2.3). For more concentrated solutions, second-order coefficients are needed in order to represent the thermodynamic properties of these solutions. But we will not have to use them.

1.3.3.4. *Electrolytic aqueous solutions*

In electrolytic aqueous solutions, the molar concentration C_j, see equation [1.2.34], or the molality $<m_j>$, see equation [1.2.37], of an electrolyte molecule or ion is used instead of the molar fraction for its content in the solution. The expression of the chemical potential can thus be written, see equation [1.3.38], as:

$$\mu_j = \mu^{\circ}_j + \Delta g^{\circ}_{j(0)}{}^{(sol)} + RT \ln V_{Ms} + RT \ln f_j\ .\ C_j = \eta^{\circ}_{j(C)} + RT \ln f_j\ .\ C_j \qquad [1.3.46a]$$

$$\tilde{\mathbf{a}}_{\mathbf{j}\ C} = f_j\ .\ C_j \qquad [1.3.46b]$$

where $\Delta g^{\circ}_{j(0)}{}^{(sol)} + RT \ln V_{Ms}$ is the free energy of solution of one mole of an electrolyte in a hypothetical solution at a concentration of 1 mole/liter, which would follow Henry's law up to a concentration of 1 mole/liter ($f_j = 1$ for $C_j = 1$). This hypothetical solution is called the *Henrian solution at 1 mole/liter*.

In the same way, the expression of the chemical potential as a function of the molality is:

$$\mu_j = \mu^{\circ}_j + \Delta g^{\circ}_{j(0)}{}^{(sol)} + RT \ln M_{(solvent)} / 1\ 000 + RT \ln f_j\ .\ <m_j> \qquad [1.3.47]$$

1.3.3.5. *Metal-metalloid solutions*

The dissolution of metalloids (O, S, P, H, N) in metal solutions (Fe, Cu, Al, Pb, Ti, etc.) in the liquid state is represented by the reaction:

$$1/2\ X_2(g) \rightarrow \underline{X}_{(M)} \text{ (dissolved in the metal M)} \qquad [1.3.48a]$$

At the temperature of liquid metals, the standard physical state of these metalloids is gaseous and they are dissolved in the metals as an element.

The affinity of dissolution [1.3.48] of half a mole of oxygen in a metal M is expressed by:

$$A^{(diss)} = -\Delta G^{(diss)} = 1/2\ \mu_{(X2)} - \mu_{\underline{X}(M)} \qquad [1.3.48b]$$

The expression of the chemical potential $\mu_{\underline{X}(M)}$, by taking the standard physical state of the element i.e. a gas, as the reference chemical potential, is given by:

$$\mu_{X(M)} = 1/2\ \mu^\circ_{(X2)} + RT \ln a^\circ_X \qquad [1.3.49a]$$

or, see equations 1.3.39 and 1.3.42, by:

$$\mu_{\underline{X}(M)} = 1/2\ \mu^\circ_{(X2)} + 1/2\ \Delta g^\circ_{X2(0)}{}^{(sol)} + RT \ln(f_X \,.\, x_X) \qquad [1.3.49b]$$

$$\mu_{\underline{X}(M)} = 1/2\ \mu^\circ_{(X2)} + 1/2\ \Delta g^\circ_{X2(1\%)}{}^{(sol)} + RT \ln f_X \,.\, \%X \qquad [1.3.49c]$$

The values of the free energies of a solution of half a mole of a gas component under a pressure of 1 atm in some liquid metals can be found in the literature. They can either correspond to solution at infinite dilution – $1/2\ \Delta g_{X2(0)}{}^{(sol)}$ – or to a solution in a 1wt % solution of component j – $1/2\ \Delta g_{(X2)(1\ \%)}{}^{(sol)}$ (see Chapter 3, Table 3.2.2).

The affinity of dissolution [1.3.48] is given by:

$$A = -1/2\ \Delta g^\circ_{X2(0)}{}^{(sol)} + RT \ln\{(p_{X2})^{1/2} / f_X \,.\, x_X\} \qquad [1.3.50a]$$

$$A = -1/2\ \Delta g^\circ_{(X2)(1\%)}{}^{(sol)} + RT \ln\{(p_{X2})^{1/2} / f_X \,.\, \%\underline{X}\} \qquad [1.3.50b]$$

At equilibrium between the metal solution and gas phase, the activities can be written as:

$$a^\circ_{X(M)} = (p_{X2})^{1/2} \qquad [1.3.51a]$$

$$\tilde{\mathbf{a}}_{\mathbf{X(M)}} = f_X \,.\, x_X = K_p\ (p_{X2})^{1/2} \qquad [1.3.51b]$$

where:

$$RT \ln K_p = -1/2\ \Delta g^\circ_{X2(0)}{}^{(sol)}$$

$$\tilde{\mathbf{a}}_{\mathbf{X}\,(1\%)} = f_X\ .\ \%X = K'\ (p_{X2})^{1/2} \qquad [1.3.51c]$$

where:

$$RT \ln K_{1\ \%} = -1/2\ \Delta g^\circ_{(X2)(1\%)}{}^{(sol)}$$

The solubility of an element X within the liquid metal at a given temperature depends on the partial pressure of component X_2 in the gas phase in contact and at equilibrium with the metallic phase. The isobars p_{X2} are drawn in the phase diagrams (M-O and M-S), see Figures 2.2.1 to 2.2.9.

1.3.3.6. *Gibbs-Duhem equation*

The Gibbs-Duhem equation between the activities of components in a solution makes it possible to calculate the activity of one component A in a solution if the activities of the other components are known:

$$\sum x_j\ .\ d \ln a_j = 0 \qquad [1.3.52]$$

In a binary solution, this equation enables calculation of the activity of component B in a solution from the activity of component A.

In the case of metal-metalloid solutions, knowledge of the partial oxygen or sulfur pressure in the gas phase, at equilibrium with M-O or M-S solutions, enables calculation of the activity of the metallic element, see formula [1.3.33].

In a ternary solution, it is possible to calculate the activities of both components from the activity of the third component [DAR 50, SCH 55].

1.3.4. *Affinity of a reaction: law of mass action (thermodynamic modeling of a process)*

The basic thermodynamic quantity featuring the evolution of a chemical reaction is its affinity, see equation [1.3.14]. The affinity or "driving force" of the reaction is the sum of two terms:

$$A_r = -\Delta G_r(T) = -\Delta G_r^\circ(T) + RT \ln \frac{\left(a_A^\circ\right)^{\nu_A} \cdot \left(a_B^\circ\right)^{\nu_B}}{\left(a_R^\circ\right)^{\nu_R} \cdot \left(a_S^\circ\right)^{\nu_S}} \qquad [1.3.53]$$

The first term is the standard Gibbs free energy of the reaction (with an opposite sign). This is the algebraic sum of the standard free energies of formation of the components of the reaction, see equation [1.3.13b]. Basic data on the standard free energy of the formation of oxides, sulfides, chlorides and carbides (the main components of the metallurgical processes), are given in Chapter 2. The second term is a function of the "standard activities" of the components, see equation [1.3.22], in the phase within which they are present. Fundamentals of thermodynamics and basic data on activities of components of metallic solutions, mattes and slags are given in Chapter 3 and for electrolytic solutions and fluxes (molten salts) in Chapter 4.

In a closed system, a reaction carried out at constant T and P evolves as long as its affinity is positive. If the reaction evolves towards a state of equilibrium (reversible reaction) when this state is reached, affinity A is then equal to zero and:

$$\Delta G^\circ_r(T) = -RT \ln \frac{\left(a^\circ_R\right)^{\nu_R} \cdot \left(a^\circ_S\right)^{\nu_S}}{\left(a^\circ_A\right)^{\nu_A} \cdot \left(a^\circ_B\right)^{\nu_B}} = -RT \ln K^\circ(T) \qquad [1.3.54]$$

where K°(T) is the standard *equilibrium (or mass action) constant*, *K°(T,P = 1 atm)*. The law of mass action is:

$$K^\circ(T) = \frac{\left(a^\circ_R\right)^{\nu_R} \cdot \left(a^\circ_S\right)^{\nu_S}}{\left(a^\circ_A\right)^{\nu_A} \cdot \left(a^\circ_B\right)^{\nu_B}} \qquad [1.3.55]$$

The equilibrium or mass action constant is written with the quantities related to the products at the numerator and those related to the reactants at the denominator.

A high value of K° shows that the operating conditions are favorable to production of the desired products and a low value shows that the reaction will not proceed very far. The reaction is said to be irreversible.

NOTE.– There will be as many definitions of the equilibrium constant as definitions of activities. When the activities are expressed as a function of the mass percentage (%j) of the components, $K_{[1\%]}$ will then stand for the equilibrium constant and similarly, for each definition of the activity, the same will be observed.

The variation of the standard equilibrium constant K°(T) with the temperature is a function of the standard enthalpy of the reaction, see equation [1.3.3]:

$$d \ln K^\circ / dT = \Delta H^\circ_r / RT^2 \qquad [1.3.56]$$

The variation of the equilibrium constant with temperature depends upon the endo- or exothermic character of the reaction, see Figure 1.3.3:

– for an exothermic reaction $\Delta H_r < 0$: K decreases as the temperature increases;

– for an endothermic reaction $\Delta H_r > 0$: K increases as temperature increases.

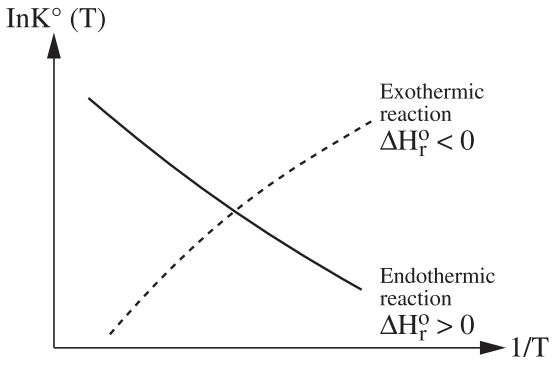

Figure 1.3.3. *Variation with temperature of the equilibrium constant for an exothermic and an endothermic reaction (see equation [1.3.56])*

When the reaction's affinity remains positive during its advancement (for an irreversible reaction), if the reactants are in stoichiometric proportions the reaction evolves until $\xi = 1$ (curve I, Figure 1.3.1), with complete consumption of the reactants. When reactant A is in excess there will be complete consumption of the second reactant and the reaction mixture will be composed of residual reactant A and the products of the reaction will be in stoichiometric proportions. The composition of the reaction mixture will thus be known.

For a reversible reaction, when a reaction evolves towards and reaches an equilibrium state (curve II, Figure 1.3.1), the activities being a function of the corresponding contents of the components in the phase in which they are present, the law of mass action in principle allows the calculation of the degree of advancement that will be reached at equilibrium and therefore the maximal fractional conversion of reactants. By characterizing the initial composition by factor α, see equation [1.3.58]:

$$\xi_{equilibrium} = f\{\alpha, K(T)\} \qquad [1.3.57]$$

– If the reaction is endothermic, the maximum degree of advancement increases with increasing temperature.

– If the reaction is exothermic, the degree of advancement decreases as the temperature increases (see Figure 1.3.4).

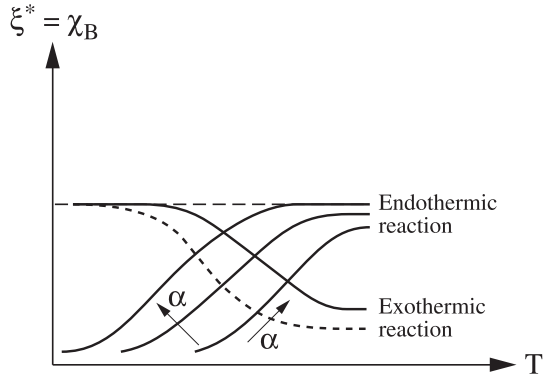

Figure 1.3.4. *Variation of the degree of advancement ξ^* (which would be reached at equilibrium) as a function of temperature, and of ratio α (see equation [1.3.58]) for an endothermic and an exothermic reaction*

For a reversible reaction, a high fractional conversion of one of the reactants (see Figure 1.3.4), can be obtained by acting:

– on the temperature (first term of the affinity: RT ln K°(T)); or

– on the initial composition of the reaction mixture. If reactant A is in excess with regards to reactant B, the fractional conversion of reactant B will be closer to the unit, as α becomes greater:

$$\text{if} \quad n_{Ai} = \alpha \nu_A \quad \text{with } \alpha > 1 \text{ and } n_{Bi} = \nu_B,$$

$$\text{then} \quad \chi_{A(max)} = 1 / \alpha; \chi_{B(max)} \rightarrow 1 \text{ and } \xi_{(max)} \rightarrow 1 \qquad [1.3.58]$$

The greater α, the more the curves will be displaced in the direction that increases the temperature domain where the conversion of B is complete (see Figure 1.3.4); or

– by extracting one of the products of the reaction, the reactants can thus be entirely consumed.

The importance of knowing the reaction's enthalpy, or at least its sign, is to be noted in predicting the direction of variation with the temperature of the degree of advancement of a reaction.

For an open system in a steady flow, the degree to which a reversible reaction will advance between the entry and exit of the reactor varies in the same way.

For closed, open or semi-open systems, the use of the law of action mass as a prediction tool is possible and instructive for a number of reaction mixtures, for which the components' activities can be expressed simply by their content in their respective phases.

By minimization of the system's free energy, numerical methods allow calculation of the composition of the reaction mixture at equilibrium. They are presented in thermodynamic books.

Thermodynamic modeling using the laws of mass action allows completely valid numerical previsions to be used for a certain number of chemical reactions in extractive metallurgy. Let us consider, for example, reaction [1.2.1] being carried out in gas phase in a closed system. At equilibrium we will thus have:

$$K_p(T) = \frac{\left(p_R\right)^{\nu_R} \cdot \left(p_S\right)^{\nu_S}}{\left(p_A\right)^{\nu_A} \cdot \left(p_B\right)^{\nu_B}} \qquad [1.3.59]$$

By using equations [1.2.39] and [1.2.53], the degree of advancement of a reaction at equilibrium can be calculated as a function of the initial composition.

For reactions between components present in liquid phases (metallic phase, matte, slag and gas phase), examples of such modeling are given in Chapters 5, sections 5.4 and 5.5, and in Chapter 6, section 6.4.6 of [VIG 11b].

1.3.5. *Applications*

1.3.5.1. *Calculation of the theoretical quantity of oxygen necessary to convert one mole of metal into an oxide*

In a closed system, with the metallic sample being in contact with a limited quantity of oxygen, the partial pressure of oxygen will decrease during the conversion. The oxidation will stop when the equilibrium pressure of the oxygen with the metal and oxide is reached. The degree of advancement of a reaction, which is equal to the fractional conversion of the metal into an oxide, may be evaluated by the following material balance for the reaction:

	2 M(s) + O_2(g) → 2 FeO(s)			n_t(g)
Initial number of moles	2	a	0	a + b
Number of moles at time t	2 – 2 ξ	a – ξ	2 ξ	a + b – ξ

where b is the number of inert moles and ξ is the degree of advancement of the reaction, thus:

$$p_{O2} = P(a - \xi) / (a + b - \xi)$$

and the affinity of the reaction is:

$$A = RT \ln K_p°(T) + RT \ln p_{O2}$$

In a closed system, of constant volume, under initial pressure P_i:

$$p_{O2} = P_i(a - \xi) / (a + b)$$

The maximum degree of advancement of the reaction, if equilibrium is reached, is then equal to:

$$\xi^* = [a(K_p°(T) \cdot P_i - 1) - b] \ / K_p°(T)P_i$$

To obtain the complete conversion of 2 moles of metal, they have to be put in contact with:

$$a = [K_p°(T) \cdot P_i + b] / [K_p°(T) \cdot P_i - 1]$$

moles of oxygen.

– If K°(T) is very large, i.e. if the standard affinity oxide formation is very large, there will be complete consumption of the oxygen. If a ≤ 1, the fractional conversion of 2 moles of metal into oxide is:

$$\chi_{M(max)} = \xi_{eq} = a$$

– If K°(T) is close to 1, to convert 2 moles of metal into oxide the amount of oxygen necessary is >> 1.

In a closed system, *under a constant pressure P*, the reaction will continue as long as:

$$p_{O2} = P(a - \xi) / (a + b - \xi) > p^*_{O2}$$

The maximum degree of advancement of the reaction is equal to:

$$\xi^* = [a(K_p^\circ(T) \,.\, P_i - 1) - b] / [K_p^\circ(T)\, P_i - 1]$$

so to convert 2 moles of metal into oxide, the amount of oxygen necessary is equal to:

$$\xi^* = 1 \rightarrow a = [K_p^\circ(T) \,.\, P_i - 1 + b\,] / [K_p^\circ(T) \,.\, P_i - 1]$$

moles of oxygen.

In a semi-open system (section 1.2.3), by blowing oxygen over the metal sample (a bed of particles, see Figure 1.2.1.e), if the pressure of the oxygen at entry is constant and greater than the equilibrium pressure, the process will continue until complete conversion of the metal into an oxide. The total amount of oxygen consumed is equal to the amount in a closed system operating under constant pressure (equation [1.2.26]).

Chapter 4, section 4.2.2.3 of [VIG 11b] presents two examples of thermodynamic modeling of solid gas heterogeneous reactions.

1.3.5.2. *Determination of the equilibrium composition of a system of several components between several phases where several distinct chemical reactions occur*

For a system subjected to a constant temperature and pressure, the state of the system is completely determined by the number of moles of each component initially present in every phase (Duhem theorem), see section 1.2.2.1. The number of moles of each component in each phase at equilibrium is calculated using expression [1.2.10] as a function of the degree of advancement at equilibrium of each distinct reaction, see equation [1.2.3]. The degrees of advancement are calculated by the laws of mass action of the distinct reactions.

EXAMPLE.– Carbothermic reduction of silica into SiC.

For an initial charge of 1 mole of SiO_2 and $n°_C$ moles of carbon we want to calculate the composition of the reaction mixture at equilibrium.

In the initial state we have $n°_{SiO2}$ and $n°_C$. In the final state we have n_{SiO2}, n_{SiC}, $n_{SiO}(g)$, n_{CO} and n_C, i.e. five unknowns.

The evolution of the system is described by two reactions, see section 1.2.2:

$$SiO_2(s) + C(s) \rightarrow SiO(g) + CO(g)$$

$$SiO(g) + 2\ C(s) \rightarrow SiC(s) + CO(g)$$

As the SiO(g) produced by the first reaction is consumed by the second reaction, the first reaction evolves until complete consumption of SiO_2, thus $n_{SiO2} = 0$. The system therefore has four unknowns that can be determined using the three conservation equations of the elements, see equation [1.2.12b]:

– balance Si: $n°_{SiO2} = 1 = n_{SiC} + n_{SiO}$;

– balance C: $n°_C = n_{Si} + n_{CO} + n_C$;

– balance O: $2\ n°_{SiO2} = 2 = n_{SiO} + n_{CO}$;

and the law of mass action for the second reaction:

$$K = p_{CO} / p_{SiO} = n_{CO} / n_{SiO}$$

The composition of the system in the final state is given by:

$$n_{SiO} = 2 / (1 + K), \qquad n_{SiC} = (K - 1) / (1 + K),$$

$$n_{CO} = 2\ K / (1 + K), \qquad n_C = n°_C - (3\ K - 1) / (1 + K).$$

NOTE.– using the degrees of advancement as intermediate variables is quite useful in the case of systems that involve solid and gas components, see Chapter 4, section 4.2.2 of [VIG 11b].

1.4. Phase diagrams

Phase diagrams are graphical representations of the effect of physico-chemical parameters on chemical or electrochemical equilibriums, or of phase transformations on a map whose coordinates are the parameters. The equilibriums between two components of a chemical reaction or two phases of a given system are represented by lines. If the conditions of equilibrium of all chemical reactions or phase transformations likely to occur in a given system are taken into account, then the families of lines are obtained that represent all the equilibrium conditions. The regions inside the lines are then predominance regions for the components (for chemical reactions) and stability regions for the solid species. As we will see in chapter 2, we can extract a great deal of thermodynamic information from phase diagrams. Numerous phase diagrams are used:

– *phase diagrams* or *constitution diagrams* representing the effect of temperature (ordinate) and composition (abscissa) on phase transformations in binary and ternary systems, see Chapter 2, section 2.2.1.

– *stability (predominance) diagrams* for ternary systems of a metal and two metalloids (oxygen and sulfur for example). Their parameters (and coordinates) that control the equilibrium state of the various phases of the system are the partial pressures of the volatile components, see Chapter 2, section 2.4.2 of [VIG 11b].

– p*otential -pH diagrams*, known as *Pourbaix diagrams*, for aqueous systems are diagrams of the electrochemical equilibria of metals and metalloids showing the predominant regions for the complexes formed with water and stability regions for the phases, see Chapter 8, section 8.3.2.

1.4.1. *Binary phase diagrams*

The main types of *binary phase diagrams* are relatively familiar. They are presented in Chapter 2, section 2.2 and Chapter 3, section 3.4.

1.4.2. *Ternary phase diagrams*

The phase diagram of a ternary system requires 3D: two for the composition and one for the temperature. The composition is given by the position of a point inside an equilateral triangle whose corners represent the three pure components of the system. The temperature axis is perpendicular to the composition plane. The vertical faces of the prism represent the three binary systems.

This 3D diagram enables visualization of the surfaces separating the liquid phase(s) from the underlying solid phases [CHA 81, PRE 04, RHI 56], see Figure 1.4.1.

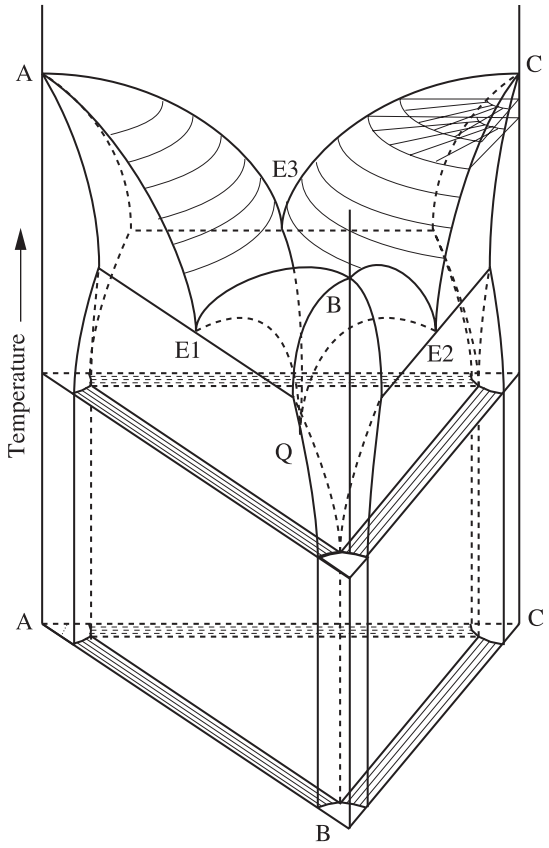

Figure 1.4.1. *Equilibrium phase diagram for a ternary system. Pictorial view of a ternary system ABC composed of three binary eutectics E_1, E_2 and E_3 and a ternary eutectic Q [HUM 66]*

Such a diagram shows the existence of three solid ternary solutions that correspond to three solidus surfaces and three liquidus surfaces. The liquidus surfaces meet two-by-two along the curves E_1Q, E_2Q and E_3Q (the *valleys*) concurrent at a point Q, which represents a liquid at equilibrium, at one temperature, with the three solid phases. After complete solidification, the solid is composed of three phases.

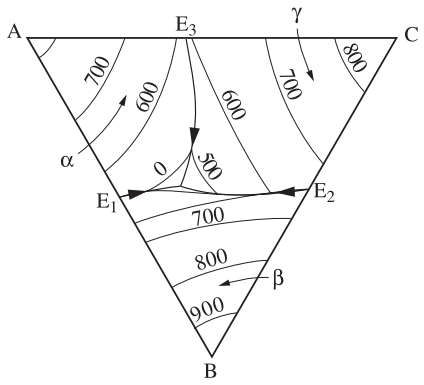

Figure 1.4.2. *Equilibrium diagram showing the valleys or boundary lines that separate the primary phase fields in plane view. Isothermal lines indicate the temperature contours of the liquidus surfaces*

Usually in a projection, see Figure 1.4.2, appear the (curves of the) *valleys* between two liquidus surfaces (in solid line). The *isotherms* of the liquidus surfaces, the tie-lines the binary or ternary components and solid phases formed during cooling, see Figure 3.4.2. We can thus visualize the composition domains where one phase is liquid above a given temperature. These are very important data for the choice of slag composition that has to present, at a given temperature, the most extended liquid domain possible.

In an isothermal section we may see the one-phase regions α, β and γ, the 2-phase regions with the "tie-lines", and the three-phase triangles (see Figure 1.4.3).

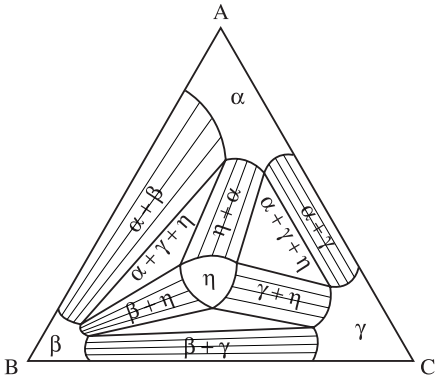

Figure 1.4.3. *Isothermal section above the eutectic point of a ternary system, similar to the system in Figure 1.4.1*

An example of a complex ternary diagram corresponding to the SiO_2-CaO-Al_2O_3 system, is presented in Chapter 3 in Figure 3.4.2. Many more examples of ternary system phase diagrams of slags and mattes can be found in Chapter 3.

1.5. Bibliography

[CHA 81] P. CHAMPION, L. GUILLET, P. POUPEAU, *Diagrammes de Phases des Matériaux Cristallins*, 2nd edition, Masson, Paris, 1981.

[DAR 50] L.S. DARKEN, *J. Am. Chem. Soc.*, Vol. 72, 2909, 1950.

[GAS 81] D.R. GASKELL, *Introduction to Metallurgical Thermodynamics*, 2nd edition, McGraw-Hill, New York, 1981.

[HUM 66] W. HUME-ROTHERY, *The Structure of Alloys of Iron*, Pergamon Press, 1966.

[KUB 79] O. KUBASCHEWSKI, E. EVANS, C.B. ALCOCK, *Metallurgical Thermochemistry*, 5th edition, Pergamon Press, Oxford, 1979.

[PRE 04] B. PREDEL, M. HOCH, *Phase Diagrams and Heterogeneous Equilibria: A Practical Introduction*, Springer Verlag, 2004.

[PRI 54] I. PRIGOGINE, R. DEFAY, *Chemical Thermodynamics* (translated by D.H. Everett), Longmans-Green, London, 1954.

[RHI 56] F.N. RHINES, *Phase Diagrams in Metallurgy,* McGraw-Hill, New York, 1956.

[ROS 83] T. ROSENQUIST, *Principles of Extractive Metallurgy*, McGraw-Hill, New York, 1983.

[SCH 55] R. SCHUHMANN, *ActaMet*, Vol. 3, pp. 219-226, 1955.

[STU 71] D.R. STULL, H. PROPHET, *JANAF Thermochemical Tables. Second Edition*, National Standard Reference Data System, 1971.

[VIG 11b] A. VIGNES, *Extractive Metallurgy 2: Metallurgical Reaction Processes*, ISTE Ltd, London and John Wiley and Sons, New York, 2011.

[VIG 11c] A. VIGNES, *Extractive Metallurgy 3: Processing Operations and Routes*, ISTE Ltd, London, and John Wiley and Sons, New York, 2011.

Chapter 2

Oxides, Sulfides, Chlorides and Carbides

2.1. Introduction

Almost all metals are extracted from oxides and sulfides. These compounds are extracted from ores by dressing operations: crushing, grinding, sizing, sorting and flotation.

The reduction of oxides is the basic extraction process of extractive metallurgy. It leads to the formation of a metallic phase.

The extraction of sulfides into oxides constitutes a step in the production of the corresponding metals.

Chlorides are obtained by attacking titanium, zirconium, aluminum and magnesium ores with chlorine and a reducing agent (carbochlorination), enabling their separation and purification by distillation.

Conversely, the formation of oxide or/and sulfide inclusions in liquid metals, by precipitation, is one of the basic processes of metal refining.

The basic thermodynamic quantities relative to these compounds are:

– the phase diagrams of the binary (M-O, M-S, M-Cl, M-C) and ternary (M-O-S, M-O-Cl) systems, showing the regions of stability of the various phases (intermediate phases and stoichiometric compounds) of these systems as a function of temperature, composition, partial pressures of the metalloids, and so on;

Extractive Metallurgy 1: Basic Thermodynamics and Kinetics Alain Vignes
© 2011 ISTE Ltd. Published 2011 by ISTE Ltd.

– the standard enthalpies and Gibbs free energies of formation of these compounds; and

– the activities of components in the intermediate phases of the systems.

Theoretically, the phase diagrams can be established from the variations with composition of the free energy G of all possible phases and thus of the chemical potentials of the components in each phase [PHI 02, RIC 48, RIC 74]. Therefore, there is a very close relationship between phase diagrams and free energy curves and component activities in these phases. As a result, a great deal of thermodynamic information can be extracted from these phase diagrams [RIC 74].

In this chapter, the phase diagrams, thermochemical data for the intermediate phases and stoichiometric compounds (in the solid state) of these systems (Ellingham-Richardson diagrams and stability or predominance diagrams) are presented.

The features of these diagrams and corresponding thermodynamic data for liquid metallic solutions, liquid oxide solutions (slags) and liquid sulfide solutions (mattes) are presented in Chapter 3.

2.2. Metal-oxygen/metal-sulfur systems activities in the intermediate phases

2.2.1. *Phase diagrams*

The phase diagrams of some important systems (M-O and M-S) are shown in Figures 2.2.1 to 2.2.9.

In the solid state, three different types of systems can be distinguished:

– the systems where metalloid solubility in the metal is so low that the metal may be considered pure and where the oxides and sulfides may be considered to be stoichiometric compounds: Fe_2O_3, NiO, CuO and Cu_2O, SiO_2, Al_2O_3, Cu_2S, PbS;

– the systems where metalloid solubility in the metal is so low that the metal may be considered pure and where some oxides or sulfides are intermediate phases (FeO, FeS) with a more or less wide composition range (see Figures 2.2.1 and 2.2.6); and

– the systems where the oxygen solubility in the metal is high (Ti-O and Zr-O systems) and where oxides or sulfides are intermediate phases (see Figure 2.2.5).

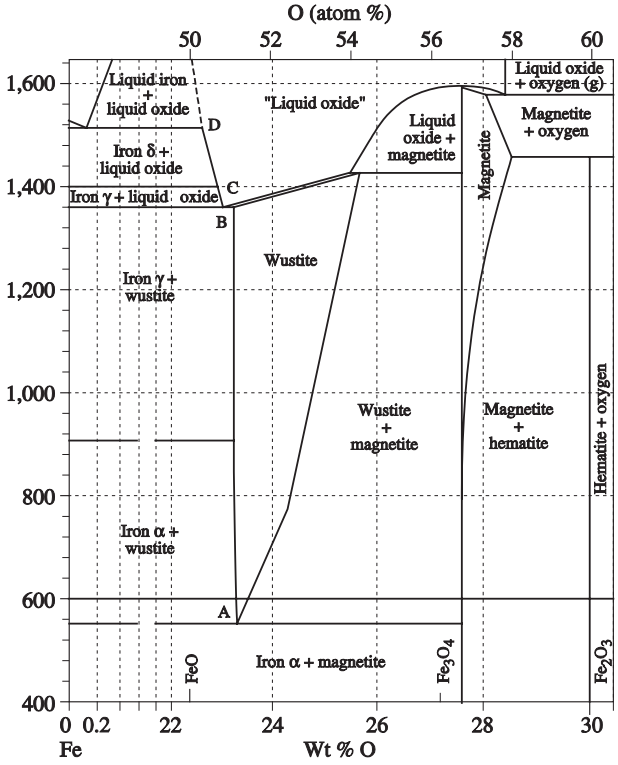

Figure 2.2.1. *Phase diagram for the iron-oxygen system [HAN 58]*

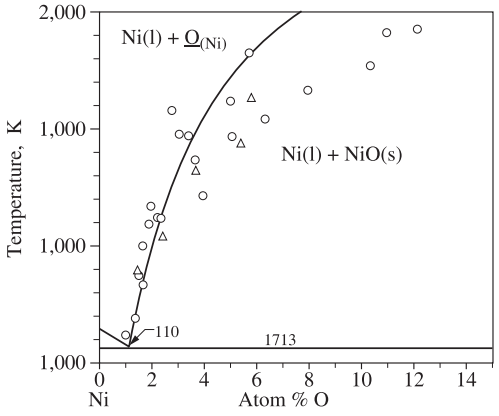

Figure 2.2.2. *Phase diagram for the nickel–oxygen system [KEL 87]*

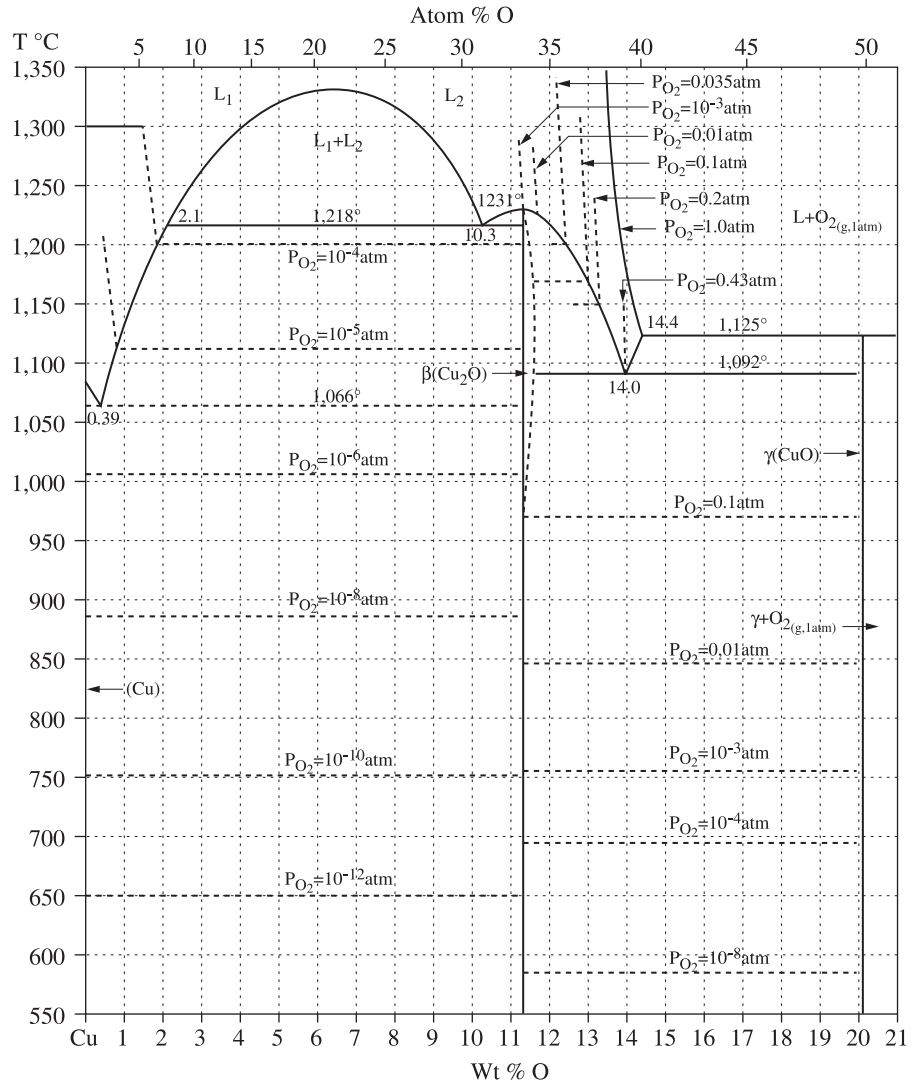

Figure 2.2.3. *Phase diagram for the copper-oxygen system [HAN 58]*

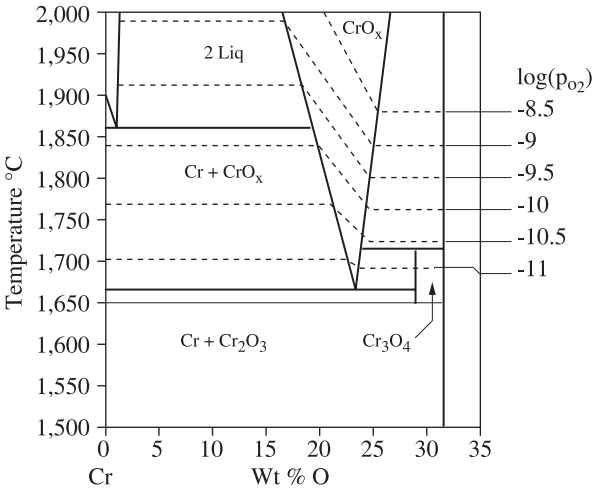

Figure 2.2.4. *Phase diagram for the chromium–oxygen system [HOL 04]*

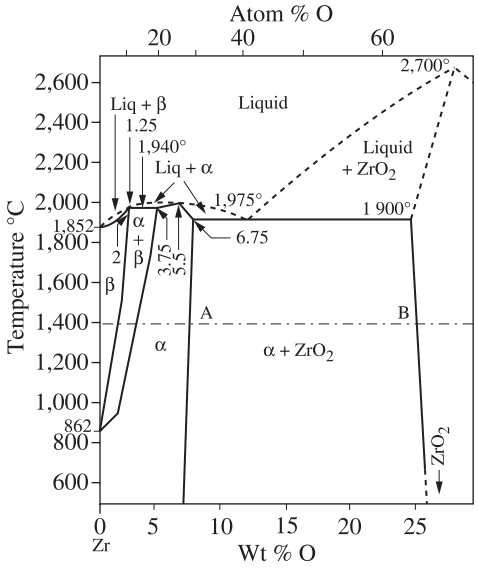

Figure 2.2.5. *Phase diagram for the zirconium–oxygen system [HAN 58]*

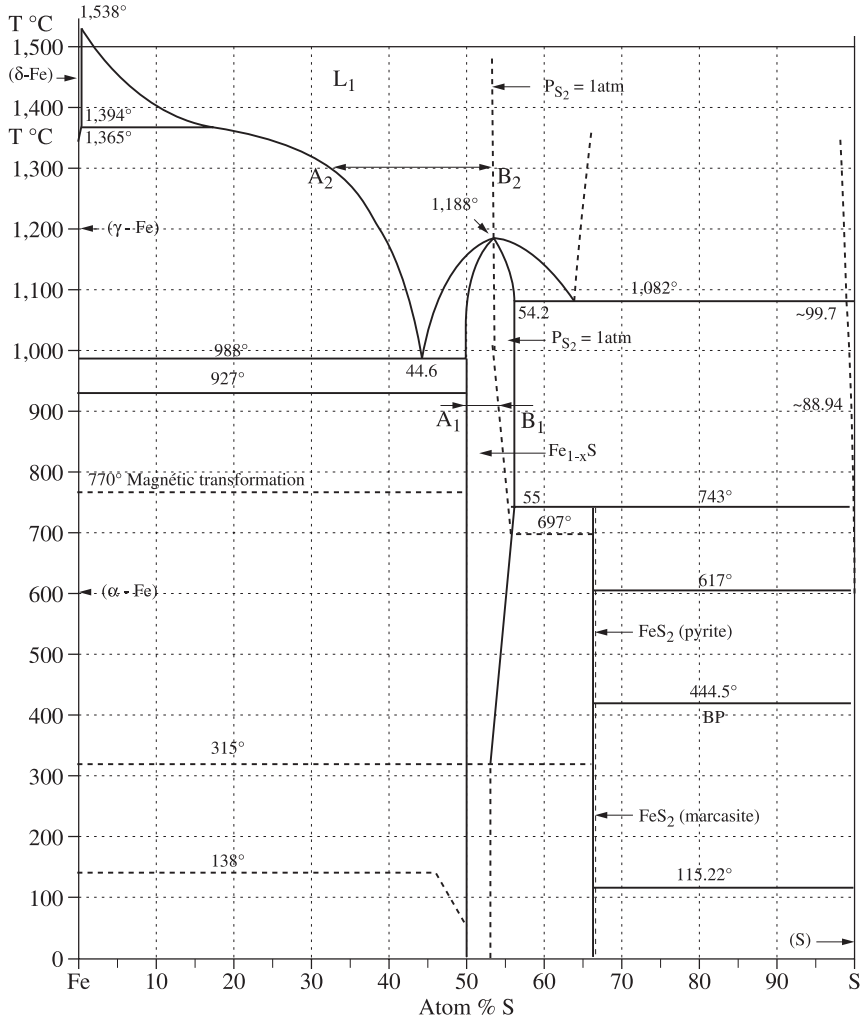

Figure 2.2.6. *Phase diagram for the iron-sulfur system [MAS 86]*

2.2.2. *Component activities in the intermediate phases*

In these phase diagrams, the oxygen (or sulfur) isobars are drawn. As these diagrams are equilibrium diagrams, the phases are in equilibrium between themselves, two-by-two, and in equilibrium with the gas phase in contact with them. The content in element X (O or S) in the different phases depends on the partial pressure (p_{O2} or p_{S2}) in the gas phase and vice versa (see Chapter 1, section 1.3.3.5).

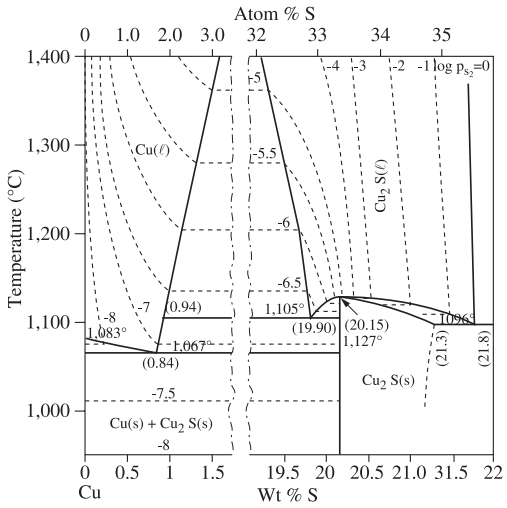

Figure 2.2.7. *Phase diagram for the copper-sulfur system [ELL 76]*

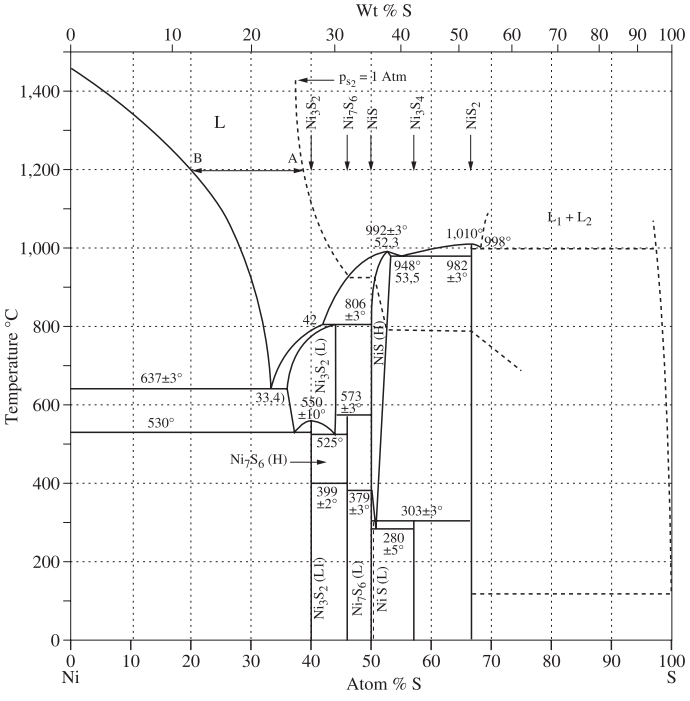

Figure 2.2.8. *Phase diagram for the nickel-sulfur system [HAN 58]*

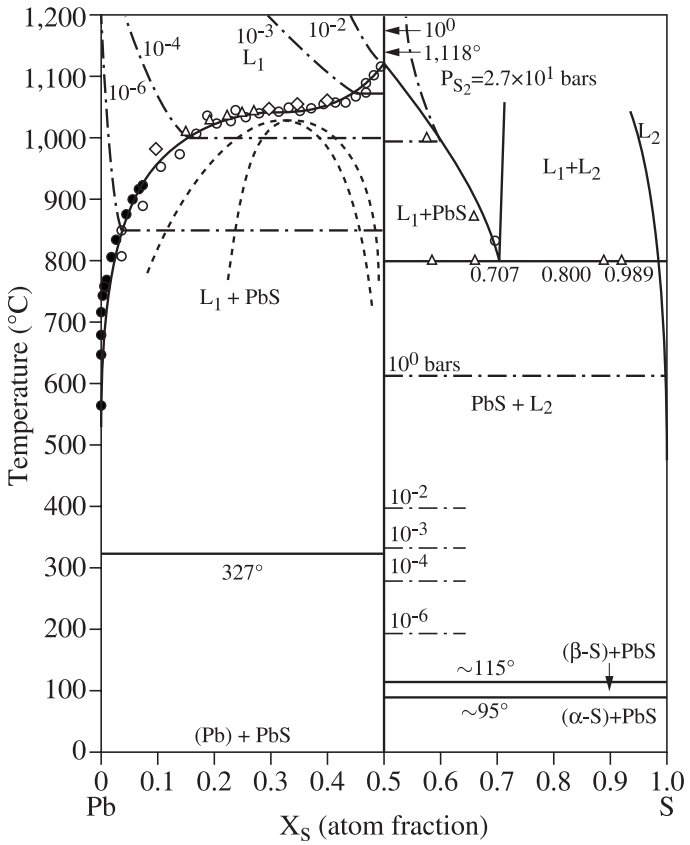

Figure 2.2.9. *Phase diagram for the lead-sulfur system [SHA 87]*

We may represent these equilibriums as resulting from a dissolution reaction of oxygen (or sulfur) in the metallic or intermediate phases, see reaction [1.3.48a] in Chapter 1. Like the metallic phase, see Chapter 1, section 1.3.3.5, the intermediate phases (solid or liquid) can be described by the activities of the elements: metal M and oxygen O (or sulfur S), even if the physical states of these components in these phases are not elements but ions. Thus the chemical potential of oxygen (or sulfur) in the intermediate phases is given by expression [1.3.49] and the standard activity $a°_X$ of the metalloid in each phase by expression [1.3.51a]:

$$a°_X = (p_{X2})^{1/2} \qquad [2.2.1]$$

The corresponding activity of the metallic element in each phase is calculated by the Gibbs-Duhem equation, see equation [1.3.52].

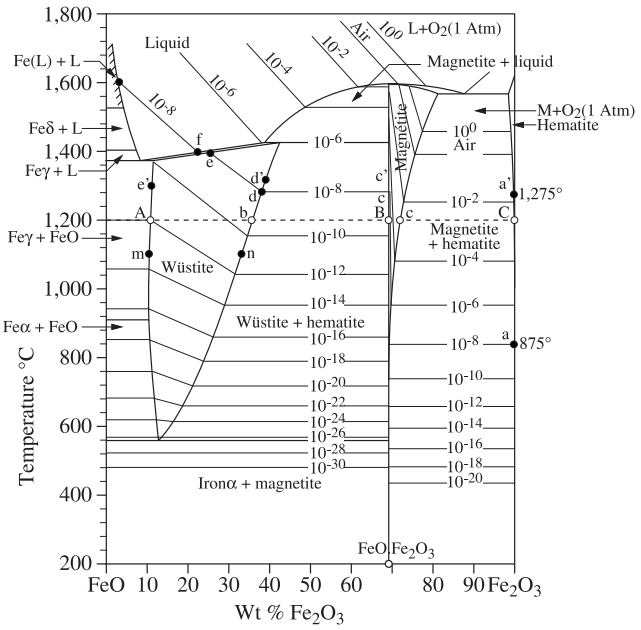

Figure 2.2.10. *Phase diagram for the FeO-Fe_2O_3 system. Thin continuous lines are the oxygen isobars (p_{O2} in atm) [MUA 65]*

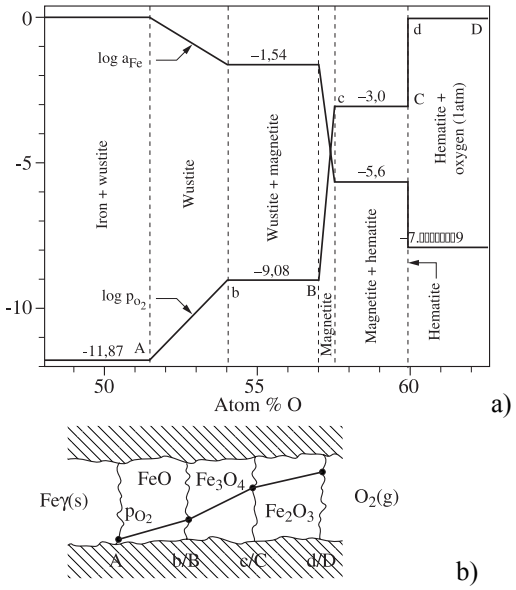

Figure 2.2.11. *Iron-oxygen system: a) variation of p_{O2}, ^{a}Fe with composition [ROS 83]; and b) variation of p_{O2} in the oxide layers growing on the metal during oxidation*

In Figure 2.2.10, the oxygen isobars are drawn in a FeO-Fe_2O_3 diagram. It will be noticed that the wüstite composition range does not include the stoichiometric FeO composition. The limit of the intermediate "FeO" phase on the iron-rich side of the diagram corresponds to a molar oxygen content >50% ($Fe_{0,95}O$) above the stoichiometric FeO composition. This comes from the fact that the "FeO" oxide can only exist for the ratios O/Fe > 1. Indeed, the Fe-O diagram (see Figure 2.2.1) presents a two-phase domain – solid or liquid Fe + solid or liquid oxide – present in the ternary diagrams (see Chapter 3, Figures 3.4.9, 3.4.10 and 3.4.12).

In Figure 2.2.11a, at point A the pressure p^*_{O2} is the equilibrium pressure (or oxygen potential) between the metallic phase (Fe saturated in oxygen) and wüstite phase (saturated in oxygen). At points b/B, p^*_{O2} is the equilibrium pressure between the wüstite phase (saturated in oxygen) and magnetite. The variation in pressure between both limits of magnetite is very high. It is the same for hematite, which is considered as a stoichiometric compound. The variation in p^*_{O2} can also be drawn across a section of the physical M-O system, see Figure 2.2.11b.

For a metal in contact with oxygen at a pressure of 1 atm, at high temperature and at the surface of the metal, different oxide layers of different thicknesses will form, depending on their growth kinetics. The oxygen pressures (or activities) at the Fe/FeO, FeO/Fe_3O_4, Fe_3O_4/Fe_2O_3 and Fe_2O_3/gas phase interfaces correspond to points A, B, C and D in Figure 2.2.11a. When the oxide can be considered a stoichiometric compound, such as the oxide Fe_2O_3, the corresponding layer has a quasi-uniform composition, but the oxygen partial pressure varies significantly through the layer.

It is the same for the Fe-S, Ni-S, Co-S and Cu-S systems, see Figures 2.2.6 to 2.2.9. The sulfides of iron "$Fe_{(1-x)}S$", cobalt "$Co_{(1-y)}S$" and copper "Cu_2S" all present a relatively extended stability (existence) domain. For instance, the existence domain of the "iron sulfide" ranges from the stoichiometric composition "FeS" in equilibrium with iron (point A_1) to $Fe_{(1-x)}S$ (point B1), see Figure 2.2.6. The sulfur partial pressure at equilibrium with the sulfide varies from very low values for the stoichiometric compound FeS, to the atmospheric pressure (point B_1). The iron sulfide saturated in sulfur above 743°C can only exist for pressures p_{S2} > 1 atm.

Sulfides rich in sulfur, e.g. FeS_2, NiS_2, Co_3S_4, are not stable. They undergo decomposition at relatively low temperatures by liberating sulfur and yielding a stable sulfide. At 700°C, the partial pressure of sulfur at equilibrium with pyrite and pyrrhotite is equal to 1 atm:

$$FeS_2 \rightarrow Fe_{0,9}S + 0.5\ S_2(g)$$

2.3. Standard Gibbs free energy: temperature diagrams for oxides – Ellingham-Richardson diagrams

The Ellingham-Richardson diagrams for oxides (see Figure 2.3.1) and sulfides (see Figure 2.4.1) [ELL 44, RIC 48, RIC 74] are graphical representations of the variation with temperature of:

– the standard Gibbs free energies (free enthalpies) of formation $\Delta G°_{f\ \text{“MexSy”}}$ (T, p = 1 atm) of “stoichiometric” oxides (or sulfides) or for the stoichiometric composition of a non-stoichiometric oxide, see Chapter 1, equation [1.3.11]. These quantities can be determined by calorimetric measurements. The values of the standard free energies of formation of the oxides for the stoichiometric composition can be found in the following tables [KUB 79];

– the RT ln p^*_{X2} values, where p^*_{X2} is the partial oxygen (or sulfur) pressure at the metal/oxide (or metal/sulfide) interface, or at the interface between two intermediate phases.

2.3.1. *Stoichiometric oxides*

When the solubility of oxygen in the metal is very low and the corresponding oxide may be considered a stoichiometric compound, the formation of the oxide may be considered the result of the chemical reaction between the metal and oxygen in the gas phase, yielding the stoichiometric oxide:

$$2(x/y)M(s \text{ or } l) + O_2(g) \rightarrow (2/y)M_xO_y(s \text{ or } l) \qquad [2.3.1a]$$

The Gibbs free energy or affinity of the reaction of oxide formation from its metal (see Chapter 1, equation [1.3.11a]) is given by:

$$A_{r(MxOy)} = \{-(2/y)\,\Delta G°_{f(MxOy)}\} + RT \ln p_{O2} \qquad [2.3.1b]$$

$\Delta G°_{f(MxOy)}$ is the standard Gibbs free energy (T, p = 1 atm) of formation of one mole of oxide, the reactants and products being in their standard state at the reaction temperature. The oxygen pressure at equilibrium with the metal and oxide is given by:

$$RT \ln p^*_{O2} = \{(2/y)\,\Delta G°_{f(MxOy)}\} \qquad [2.3.2]$$

The formation of an oxide is an exothermic reaction $\Delta H_f°(T) < 0$ (see Chapter 1, equation [1.3.2]) occurring with a decrease of the number of gas moles, thus $\Delta S°(T) < 0$ (see equation [1.3.12]):

$$\Delta G°_f(T) = \{\Delta H°_f(T) - T\,.\,\Delta S°_f(T)\} \qquad [2.3.3]$$

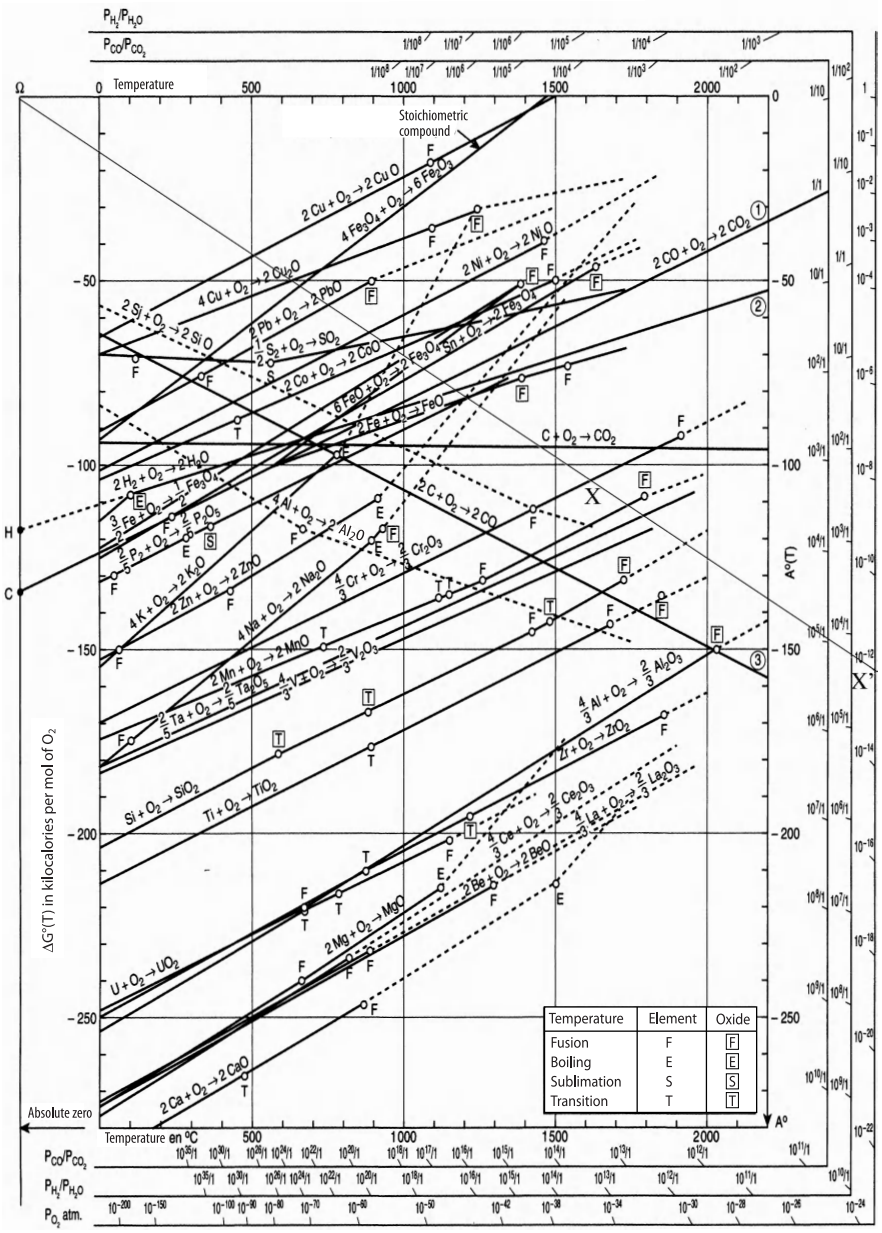

Figure 2.3.1. *Ellingham-Richardson diagram: Gibbs free energy–temperature diagram for oxides [OLE 63, RIC 74]*

The *standard free energies of formation* as a function of temperature, in the case of oxides, are shown in Figure 2.3.1[1].

The variation with temperature of the standard free energy (T, p = 1 atm) of formation of one mole of Cu_2O:

$$2\ Cu(s) + 1/2\ O_2(g) \rightarrow Cu_2O\ (s)$$

(both Cu_2O and CuO are stoichiometric in the solid state, see Figure 2.2.3) is given, in the tables, by the following equation:

$$\Delta G°_{f(Cu2O)} = -40{,}500 - 3.92\ T \log T + 29.5\ T \text{ (cal/mole) when } T < 1{,}356K$$

It is often adequate to represent $\Delta G_f°$ as a linear function of temperature by the equation:

$$\Delta G_f° = -39{,}850 + 15\ T \text{ (cal/mole)}$$

The curves of the standard free energy of formation of oxides are therefore composed of straight line segments; each segment corresponding to a physical state of the metal or oxide. In each state, the standard enthalpies of formation and entropies of the oxides vary very slightly with temperature. The change of slope for each segment is due to a variation in the system's entropy. From now on, we shall call them *Ellingham (straight) lines*.

Ellingham lines for the formation of solid or liquid oxides have a positive slope because of the decrease in the number of gas moles occurring during the reaction. The standard affinity for oxide formation decreases as the temperature increases: the metal is decreasingly oxidizable.

When the oxide is formed from metal vapor (e.g. zinc above 906°C under atmospheric pressure), the upward slope of the Ellingham straight line is correspondingly greater, as the reduction in entropy is greater than when the metal is a solid or liquid. The affinity of the reaction of zinc oxide formation depends on the partial zinc pressure. The Ellingham (dotted) line for the zinc in the gaseous state corresponds to a partial pressure of zinc equal to 1 atm:

$$Zn(g) + O_2(g) \rightarrow 2\ ZnO\ (s \text{ or } l) \qquad [2.3.4a]$$

$$A = -2\ \Delta G°_f + RT \ln p_{Zn} \cdot p_{O2} \qquad [2.3.4b]$$

1 A detailed analysis of the curves drawn in the Ellingham-Richardson diagram can be found in [RIC 74].

The standard free energy of formation corresponds to $p_{Zn} = p_{O2} = 1$ atm.

Oxidation of some metals and carbon yields gaseous sub-oxides:

$$2\ Si(s) + O_2(g) \rightarrow 2\ SiO(g) \qquad [2.3.5]$$

$$4\ Al(s \text{ or } l) + O_2(g) \rightarrow 2\ Al_2O(g) \qquad [2.3.6]$$

$$2\ C(s) + O_2(g) \rightarrow 2\ CO(g) \qquad [2.3.7]$$

whose affinity of formation is given by the following equation, for instance:

$$A_f = -2\ \Delta G^\circ_f + RT \ln\{p_{O2} / (p_{SiO})^2\} \qquad [2.3.8]$$

For these sub-oxides, the Ellingham lines have a negative slope due to the increase of the number of gas molecules during the reaction.

The standard affinities $A^\circ_f = -\Delta G^\circ_f$ of metal oxide formation are positive for any temperature. The higher the standard affinity of oxide formation (i.e. the closer the corresponding line is to the lower part of the graph), the more stable the oxide and more difficult it will be to reduce it.

In the Ellingham diagram for the oxides, see Figure 2.3.1, three different scales can be observed on the right-hand side. The scale on the extreme right-hand side is designed so that oxygen pressure (in atm) in equilibrium with any particular metal-metal oxide system can be read directly from the diagram for any desired temperature. A straight line passing by point Ω (at the top left-hand corner) and by the point of the considered Ellingham straight line at the desired temperature cuts the oxygen pressure scale at a point corresponding to the partial oxygen pressure at temperature T in equilibrium with both phases. For the Cr/Cr_2O_3 equilibrium at 1,600°C, $p^*_{O2} = 10^{-12}$ atm, which is line ΩXX' in Figure 2.3.1.

2.3.2. *Unstoichiometric compounds*

For some unstoichiometric compounds, the Ellingham lines correspond to $RT \ln p^*_{X2}$ values where p^*_{X2} is the partial oxygen (or sulfur) pressure corresponding to the equilibrium between the metal and oxide (or sulfide) or between two intermediate phases. The Ellingham lines, for the different equilibriums of the Fe-O system, are drawn in Figure 2.3.2. Each segment gives the variation of $RT \ln p^*_{O2}$ with temperature for the different equilibriums between two adjacent phases: Fe/Fe_3O_4 at 570 °C, Fe/"FeO", "FeO"/Fe_3O_4 and Fe_3O_4/Fe_2O_3. We can obtain the corresponding oxygen pressure from the oxygen scale. In the case of the Fe/"FeO" equilibrium at 1,200 °C (at point A), the p^*_{O2} value read on the

oxygen scale is 10^{-12} atm. We have indicated the position of the corresponding point A of the Ellingham curve in the FeO-Fe_2O_3 phase diagram, see Figures 2.2.10 and 2.2.11. The pressure p_{O2} read on these diagrams is equal to 10^{-12} atm.

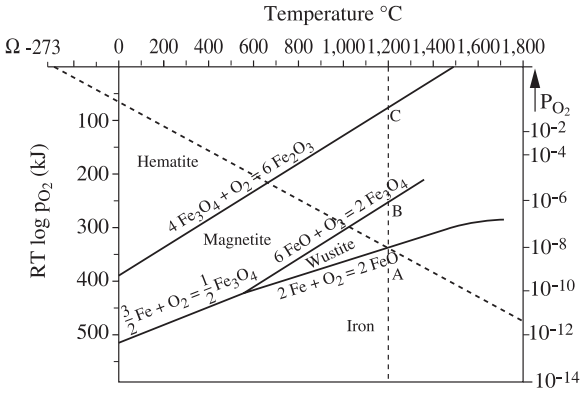

Figure 2.3.2. *Ellingham diagram for the indicated equilibriums of the iron-oxygen system*

For the wüstite/magnetite FeO/Fe_3O_4 equilibrium at 1,200°C, $p^*_{O2} = 10^{-9}$ atm, which is the same value as those indicated (point B) in Figures 2.2.10 and 2.2.11. For the magnetite/hematite equilibrium (point C), at 1,200 °C, $p^*_{O2} = 10^{-3}$ atm.

The equilibrium between a metal saturated in oxygen and an oxide (or sulfide) saturated in metal, may be represented by the reaction:

$$O^*_{(\text{in the metal saturated in oxygen})} = (O)^*_{(\text{in the oxide saturated in metal})} \qquad [2.3.9a]$$

(the notation O is conventional and does not stand for the oxygen state in both phases), where (see Chapter 1, equation [1.3.51]):

$$a^\circ_{O(M)} = a^\circ_{(O(MxOy))} = (p^*_{O2})^{1/2} \qquad [2.3.9b]$$

Thus, for instance, in the case of the "FeO" oxide the variation of RT ln p^*_{O2} as a function of temperature is given by the following equation (see Figure 2.3.2):

$$2\,Fe(s) + O_2(g) \rightarrow 2\,\text{"FeO"}(s)_{(\text{saturated in iron})}$$

$$RT \ln p^*_{O2} = -124{,}100 + 30\,T \text{ (cal/mole } O_2) \qquad [2.3.10a]$$

$$\text{for } 848 < T < 1{,}642\text{K}$$

$$2\,Fe(l) + O_2(g) \rightarrow \rightarrow 2\,\text{"FeO"}(l)_{(\text{saturated in iron})}$$

$$RT \ln p^*_{O2} = -111{,}100 + 21.8\ T \text{ (cal/mole } O_2) \qquad [2.3.10b]$$

$$\text{for } 1{,}808 < T < 2{,}000K$$

For the stoichiometric (hypothetical) "FeO" compound:

$$\Delta G^\circ_{\text{"FeO"}} = -54{,}000 + 9.88\ T \text{ (cal/FeO mole)}$$

In the case of (Ti-O, Zr-O) systems, where the solubility of oxygen in the metal is high (see Figure 2.2.5), the Ellingham straight line for ZrO_2 oxide, for instance, corresponds to the free energy of formation of the oxide for its stoichiometric composition and not to the oxygen pressure for the Zr/ZrO_2 equilibrium.

For these unstoichiometric compounds or the intermediate phases a pseudo-activity $\hat{a}_{\text{"MaXb"}}$ of a compound M_aA_b can be defined as:

$$\hat{a}_{MaAb} = K^\circ_{MaXa} \cdot (a^\circ_M)^a \cdot (a^\circ_A)^b \qquad [2.3.11]$$

By taking the stoichiometric composition as the reference state:

$$\hat{a}_{MaAb} = 1$$

$$RT \ln K^\circ = -\Delta G^\circ_{f\text{"MaAb"}} = -RT \ln (p^*_{O2})^{1/2}$$

where $\Delta G^\circ_{f\ \text{"MaAb"}}$ is the standard free energy of formation of the stoichiometric compound and p^*_{O2} is the equilibrium oxygen partial pressure for the stoichiometric composition, see equation [2.3.2]. For the intermediate phase, Cu_2S of the Cu-S system, $\hat{a}_{Cu2S}$ remains very close to one on either side of the stoichiometric composition (see Figure 2.3.3).

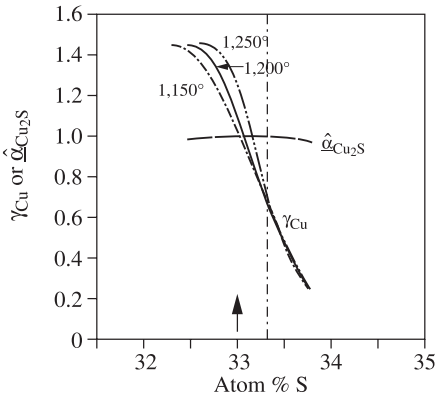

Figure 2.3.3. *Pseudo-activity $\hat{a}_{(Cu2S)}$ in the liquid intermediate phase Cu_2S [BAL 76]*

Other pseudo-activities may be defined from other reference states. This is the case for the "FeO" oxide. As the stoichiometric composition of the FeO oxide is out of the oxide existence domain (in the solid state), a pseudo-activity of the FeO component may be defined with, as the reference state, the composition of the oxide in equilibrium with the metallic phase saturated in oxygen, which corresponds to the pressure $p^*_{O2(Fe/FeO)}$ (see expression 2.3.10):

$$\hat{a}_{(FeO)(Fe/FeO)} = 1$$

$$\hat{a}_{FeO} = \hat{K}^\circ \cdot a^\circ_{Fe} \cdot a^\circ_{O} \qquad [2.3.12]$$

where:

$$RT\ln \hat{K}^\circ = -RT \ln(p^*_{O2(Fe/FeO)})^{1/2} \qquad [2.3.13]$$

and:

$$\hat{a}_{(FeO)} = a^\circ_{Fe} \cdot (p_{O2} / p^*_{O2(Fe/FeO)})^{1/2}$$

and $\hat{a}_{(FeO)}$ can be calculated by [DAR 45]:

$$\hat{a}_{(FeO)} = -\int \left(\frac{x_O}{x_{Fe}} - 1 \right) d \log \left(p_{O_2} \right)^{1/2}$$

The curves of variation of $\hat{a}_{(FeO)}$, a°_{Fe}, and $(p_{O2}/p^*_{O2(Fe/FeO)})^{1/2}$ for the "FeO" oxide are drawn in Figure 2.3.4.

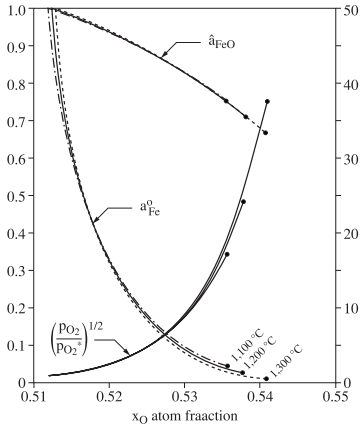

Figure 2.3.4. *Activities $\hat{a}_{(FeO)}$, a°_{Fe}, and $(p_{O2}/p^*_{O2(Fe/FeO)})^{1/2}$ in the wüstite phase fields at different temperatures [DAR 46]*

2.3.3. *Thermodynamic data for the reduction of oxides by a reducing gas*

In the Ellingham-Richardson diagram (see Figure 2.3.1), on the right-hand side, two other scales permit the direct reading of the ratios p_{H2}/p_{H2O} and p_{CO}/p_{CO2} for the reduction of an oxide by H_2 or by CO at equilibrium:

$$(1/y)M_xO_y + \{H_2(g) \text{ or } CO(g)\} \rightarrow (x/y)M(g,l,s) + \{H_2O \text{ or } CO_2\} \qquad [2.3.14]$$

The ratio of partial pressures $(p_{H2}/p_{H2O})^*$ at equilibrium with the metal and oxide at all temperatures can be graphically obtained by drawing a line passing by point H and the point of the Ellingham line considered at the chosen temperature.

Likewise for the third scale, by drawing a line passing by point C and the point of the Ellingham line considered, at the desired temperature, we can obtain the ratio of the partial pressures $(p_{CO}/p_{CO2})^*$ at equilibrium with the metal and oxide.

These data will be used for the thermodynamic analysis of oxide reduction reactions in Chapter 4 of [VIG 11b].

2.4. Thermodynamic data for sulfides and chlorides

2.4.1. *Ellingham-Richardson diagram for sulfides*

The Ellingham straight lines drawn in Figure 2.4.1 correspond to the standard free molar energy of formation of stoichiometric sulfides[2]:

$$2\ (x/y)M(s \text{ or } l) + S_2(g) \rightarrow (2/y)M_xS_y(s \text{ or } l) \qquad [2.4.1a]$$

$$A_{r(MxSy)} = \{-(2/y)\ \Delta G°_{f(MxSy)}\} + RT \ln p_{S2} \qquad [2.4.1b]$$

and the pressure p^*_{S2} at equilibrium with the stoichiometric compound is given by:

$$RT \ln p^*_{S2} = (2/y)\ .\ \Delta G°_{f(MxSy)} \qquad [2.4.1c]$$

In the case of iron sulfides, FeS (see Figure 2.2.6), the stoichiometric composition nearly corresponds to the limit of the metal-sulfide:

$$2\Delta G°_{f(FeS)} = -71{,}820 + 25.12\ T \text{ (cal/mol) between 139 and 906°C}$$

2 A detailed analysis of the diagram can be found in [RIC 74]

The Ellingham diagram presents two scales that permit to read directly the partial pressure of sulfur p^*_{S2} or the ratio $(p_{H2S}/p_{H2})^*$, which would be in equilibrium with the metal-metal sulfide reaction [2.4.1] or reaction [2.4.2]:

$$Mn + H_2S \rightarrow MnS + H_2 \qquad [2.4.2]$$

The location of the Ellingham straight lines for the Mg or Ca sulfides explains the desulfurizing power of these metals in desulfurization operations of liquid steel (see Chapter 7, section 7.2.4.1 of [VIG 11b]).

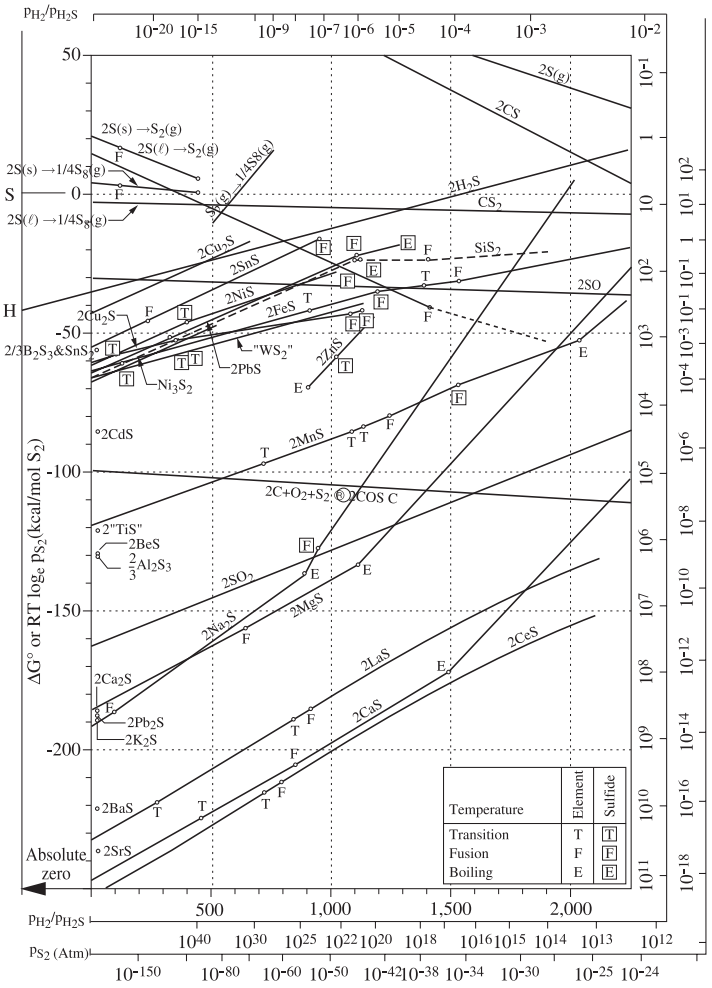

Figure 2.4.1. *Ellingham-Richardson Diagram: Gibbs free energy – temperature diagram for sulfides [RIC 74]*

2.4.2. *Stability diagrams for the (M-O-S) systems*

Roasting is the oxidation of metal sulfides to give either metal oxide and sulfur dioxide, see reaction [6.2.1], or metal and sulfur dioxide, see reaction [6.2.12] (Chapter 6 of [VIG 11b]):

$$MS(s) + 3/2\ O_2(g) \rightarrow MO(s) + SO_2(g) \qquad [2.4.3]$$

$$MS(s) + O_2(g) \rightarrow M(s) + SO_2(g) \qquad [2.4.4]$$

Furthermore, in the gas phase the following reaction (and equilibria) occurs:

$$1/2\ S_2(g) + O_2(g) \rightarrow SO_2(g) \qquad [2.4.5]$$

The number of distinct reactions to be taken into account is equal to three: six components minus three chemical elements (S, O and M), see Chapter 1, equation [1.2.3]. If the temperature is fixed, the composition of the gas mixture is defined by the partial pressure of any two of the gaseous components [p_{S2} and p_{O2}] or [p_{O2} and p_{SO2}]. For a fixed gas composition, the number of condensed phases in equilibrium with the gas phase is equal to one (Gibbs phase rule, see equation [1.2.4a]). So, for a fixed-gas composition the composition and therefore nature of the condensed phase in equilibrium with the gas is fixed. Thus the phase relations in the ternary system at constant temperature may be described in a two-dimensional diagram where the two coordinates are the partial pressures of two of the gaseous components. For a system of two condensed phases (equations [2.4.3] or [2.4.4]) and one gas phase, the variance of the system is equal to one and an equilibrium between two condensed phases is represented by a line on such a diagram.

Stability (or predominance or existence) diagrams show, at a given temperature, the areas of oxide, sulfide or metal stability as a function of the partial pressures [p_{S2} and p_{O2}] or [p_{O2} and p_{SO2}] in the gas phase. In this chapter, we present the stability diagram based on the partial pressures [p_{S2} and p_{O2}]. The stability diagram based on the partial pressures [p_{O2} and p_{SO2}] is presented in Chapter 6, section 6.2.1.1 of [VIG 11b].

In Figure 2.4.2, the vertical lines p_{S2} = cste correspond to the metal-sulfide equilibrium pressures, see equation [2.4.1a]. The horizontal lines p_{O2} = cste correspond to the metal-oxide or oxide-oxide equilibrium pressures, see equation [2.3.1a].

The lines with positive slopes represent the equilibrium for the reaction:

$$\text{“sulfide”} + y\ O_2(g) \rightarrow \text{“oxide”} + y'\ S_2(g) \qquad [2.4.6]$$

which is the sum of equations [2.3.1a] and [2.4.1a], whose slope is equal to the ratio of the stoichiometric coefficients (y/y').

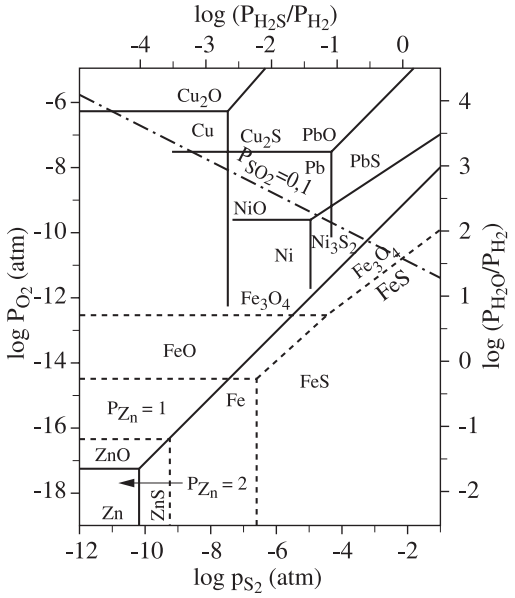

Figure 2.4.2. *Stability diagrams for the sulfides and oxides of the M-O-S systems for various elements at 1,027°C [YAZ 79]*

On either side of these straight lines, reaction [2.4.6] will evolve towards the formation of the compound indicated in the zone considered.

The straight line, with a negative slope, represents the relationship between the pressures p_{O2} and p_{S2}, for $p_{SO2} = 0.1$ atm at equilibrium for the reaction [2.4.5]:

$$K°(T) = p_{SO2} / (p_{S2})^{1/2} \cdot p_{O2} \qquad K°(T) = 1.174 \times 10^{9} \text{ at } 1{,}200\ °C$$

At 1,027°C and a partial pressure p_{SO2} of the order 0.1–0.2 atm and pressure $p_{S2} < 10^{-8}$ atm, the stable phase (at equilibrium) with the copper sulfide is the copper Cu°. Likewise for the lead sulfide, when $p_{S2} < 10^{-4}$ atm. In the case of iron sulfide, the stable phase in equilibrium with the sulfide is Fe_3O_4 when $p_{S2} < 10^{-2}$ atm. Similarly, in the case of nickel under a pressure $p_{SO2} = 0.1$ atm at equilibrium, the stable phase in equilibrium with the sulfide, as is the oxide. At 1,453°C, when $p_{SO2} = 0.1$ atm, the stable phase with the sulfide is nickel Ni° (see Chapter 3, Figure 3.3.7).

2.4.3. *Ellingham-Richardson diagram for chlorides*

In titanium, zirconium and hafnium metallurgy, chlorides are intermediate components between the oxides and corresponding metals, allowing the separation and purification of metals by distillation. Silicon chlorides are the intermediate components in silicon metallurgy. In Figure 2.4.3, the Ellingham lines for the chlorides of some metals are drawn. As we will see in Figure 3.2.2, Chapter 3 of [VIG 11b], the formation of an oxichloride (for instance MoO_2Cl_2) may occur.

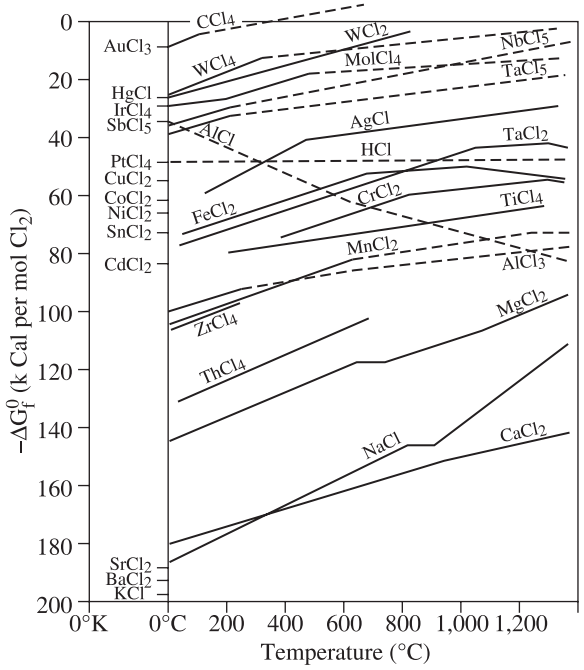

Figure 2.4.3. *Ellingham diagram for chlorides [ROS 83]*

2.4.4. *Stability diagrams of M-O_2-Cl_2 systems*

The stability diagrams of Zn-O_2-Cl_2, Fe-O_2-Cl_2- and Cr-O_2-Cl_2 systems are shown in Figures 2.4.4a, b and c. (see also Figures 3.2.2a and b, Chapter 3 of [VIG 11b]). The lines with a positive slope correspond to the equations:

$$ZnO + Cl_2(g) \rightarrow \rightarrow ZnCl_2(g) + 1/2\ O_2(g)$$

$$\Delta G°(800°C) = -32{,}270 \text{ (kJ/mole)} \quad [2.4.7]$$

$$1/3\ Fe_2O_3 + Cl_2(g) \rightarrow 2/3\ FeCl_3(g) + 1/2\ O_2(g)$$

$$\Delta G°(800°C) = +25{,}844 \text{ (kJ/mole)} \quad [2.4.8]$$

Under a gas stream equimolecular in chlorine and oxygen, zinc chloride is stable, and both iron oxide and chrome oxide are stable. The chlorination of these oxides can be achieved by a highly reducing gas (very low p_{O2}) or in presence of either C or CO (see Chapter 3, section 3.2.2.2 of [VIG 11b]).

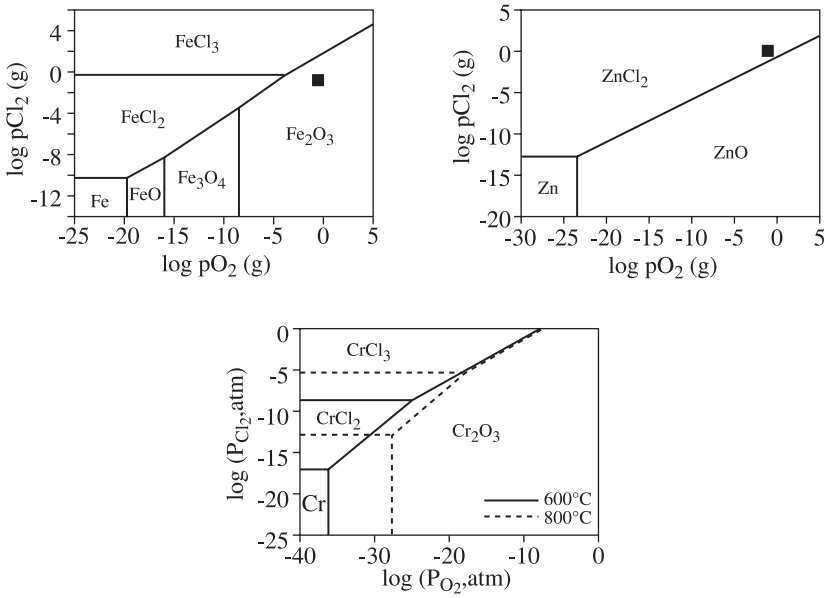

Figure 2.4.4. *Stability diagrams for the systems: a) Fe-O_2-Cl_2; b) Zn-O_2-Cl_2 at 800°C [TEE 99]; and c) Cr-O_2-Cl_2 [KAN 98]*

2.5. Metal-carbon phase diagrams and the Ellingham-Richardson diagram for carbides

The phase diagrams of both Fe-C and Cr-C systems are presented in Figures 2.5.1 and 2.5.2. The high solubility of carbon in γ iron and the very low solubility of carbon in chromium can be observed. Carbides are stoichiometric compounds, whose Ellingham straight lines are drawn in Figure 2.5.3. As the number of gas molecules does not vary during the formation of the carbides, their standard free energy of formation is nearly constant, except when a state change occurs.

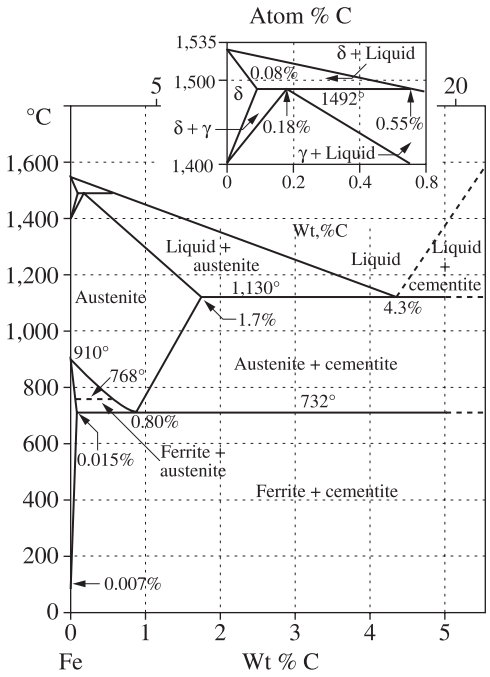

Figure 2.5.1. *Fe-C system phase diagram [HAN 58]*

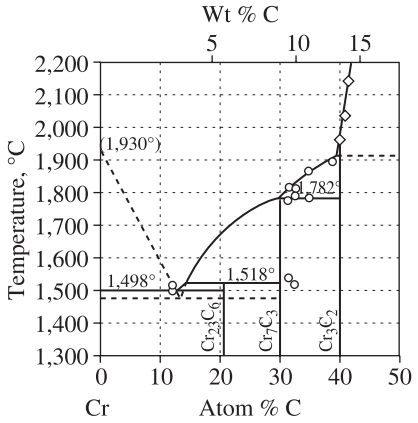

Figure 2.5.2. *Cr-C system phase diagram [HAN 58]*

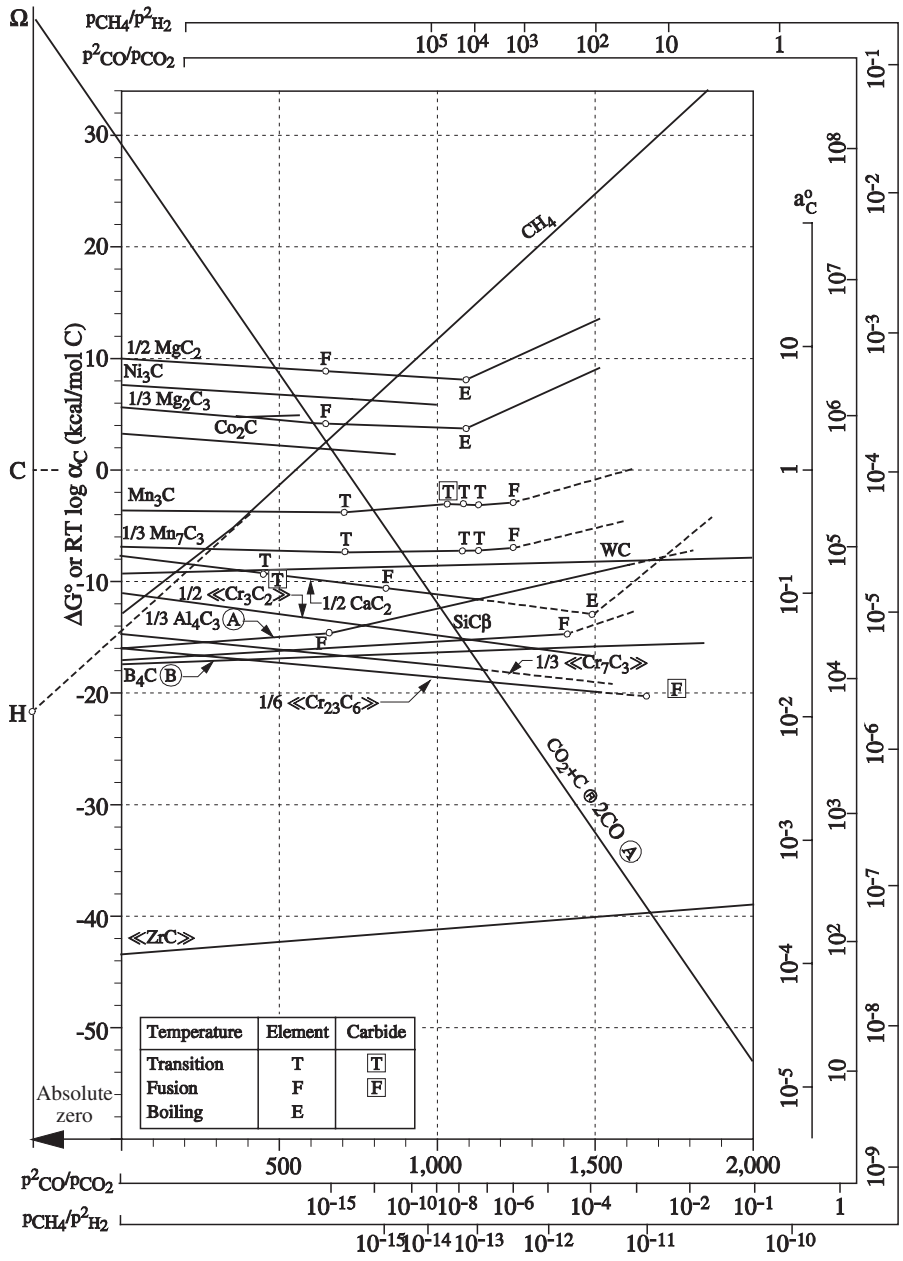

Figure 2.5.3. *Ellingham diagram for carbides: Gibbs free energy of formation of carbides [ANC 73]*

The standard free energy of formation of nickel and cobalt carbides is positive. The standard free energy of formation of cementite becomes negative when T > 800°C and then remains very low. Cementite is actually a metastable phase that decomposes into iron and carbon. The standard free energy of formation of Cr, Mn, Si and Al carbides is negative but relatively low. The standard free energy of titanium and zirconium carbide formations is very high (in absolute value).

In the same way as with oxides, see reaction [2.3.9a], we can thermodynamically describe the metal-carbide equilibria by the following reaction:

$$C_{(\text{in the metal saturated in carbon})} = C_{(\text{in the carbide saturated in metal})} \quad [2.5.1a]$$

$$a°_{C(M)} = a°_{C(MxCy)} \quad [2.5.1b]$$

The first scale in this diagram, see Figure 2.5.3, allows the graphical determination of the standard activity of carbon at equilibrium between the metal saturated in C and the carbide saturated in metal at a given temperature, by plotting a line from point C and the point of the Ellingham straight line of the carbide considered at temperature T.

In this diagram, the lines corresponding to the standard free energy of methane formation ($C(s) + 2\ H_2 \rightarrow CH_4$) and carbon oxide by the Boudouard reaction ($CO_2 + C \rightarrow 2\ CO$) are drawn, see section 2.6.2. These two curves allow the standard energies of carbide formation by carburization of the metal either by CH_4, or CO to be determined (see Chapter 4 of [VIG 11b], Figure 4.1.1 and sections 4.2.2.2 and 4.3.5). The formation of a carbide and/or the carburization of a metal occur by reaction with carburizing gases (CH_4 and CO) which, by decomposition at the surface of the metallic phase, supplies the necessary carbon. For example, in the case of chromium carbide:

$$3/2\ Cr(s \text{ or } l) + CH_4(g) \rightarrow 1/2\ Cr_3C_2(s) + 2\ H_2(g) \quad [2.5.2a]$$

$$A_2 = -(1/2\ \Delta G°_{f(Cr3C2)} - \Delta G°_{f(CH4)}) + RT \ln\{p_{CH4} / (p_{H2})^2\} \quad [2.5.2b]$$

The standard affinity $A_2°$ of this reaction is greater than the standard affinity of the formation of carbide by direct reaction with carbon. In addition, the affinity remains positive even for very low $P_{CH4}/(P_{H2})^2$ ratios.

On the right-hand side of the Ellingham diagram, two other scales allow the graphical determination of the ratios of partial pressures $P_{CH4}/(P_{H2})^2$ and $(P_{CO})^2/P_{CO2}$ at equilibrium for both carburization reactions of metal by CH_4 or CO.

In the case of chrome carbide formation by CO:

$$3/2\ Cr + 2\ CO \rightarrow 1/2\ Cr_3C_2 + CO_2 \qquad [2.5.3a]$$

$$A = -(1/2\ \Delta G°_{f(Cr3C2)} + \Delta G°_{f(CO2)} - 2\ \Delta G°_{f(CO)} + RT\ \ln\{(p_{CO})^2 / p_{CO2}\} \qquad [2.5.3b]$$

The standard affinity is positive but very low for temperatures below 1,050°C. It is lower than the standard affinity of the carburization by direct reaction. The formation of chromium carbide by carburization of metal by CO does not occur at high temperature. This is because CO is very stable – the higher the temperature, the more stable is CO.

Chapter 4 of [VIG 11b] deals with the carburization of metals by CO, in section 4.2.2.2 and Figure 4.2.3b.

2.6. Carbon and carbon oxide reactions

2.6.1. *Oxidation reactions*

In the Ellingham-Richardson diagram, see Figure 2.3.1, Ellingham's straight lines relative to the combustion reactions of hydrogen, carbon and carbon monoxide CO are drawn.

At low temperature, the combustion of carbon produces CO_2. At high temperature it produces CO:

$$C(s) + O_2(g) \rightarrow CO_2 \qquad [2.6.1]$$

$$A°_1 = -\Delta G°(T) = 94{,}200 + 0.2\ T\ (cal/mole\ O_2)$$

The reaction is highly exothermic $\Delta H° = -94{,}200$ (cal/mole O_2) and the variation of standard affinity with temperature is very low. The Ellingham straight line is nearly horizontal. This is because there is no variation in the number of gas molecules.

The reaction:

$$2\ C(s) + O_2(g) = \rightarrow 2\ CO \qquad [2.6.2]$$

$$A°_2 = -\Delta G°\ (T) = 53{,}400 + 41.9\ T\ (cal/mole\ O_2)$$

is exothermic and the standard affinity of formation of the carbon monoxide CO increases as temperature increases. The corresponding Ellingham straight line has a negative slope, see Figure 2.3.1. The reaction occurs with an increase in the number

of gas molecules. Carbon monoxide becomes more stable as the temperature gets higher.

The reaction:

$$2\ CO(g) + O_2(g) \rightarrow 2\ CO_2(g) \qquad [2.6.3]$$

$$A°_3 = -\Delta G°_3(T) = 135{,}000 - 41.50\ T\ (cal/mole\ O_2)$$

is exothermic and the standard affinity of the reaction decreases as the temperature increases. The Ellingham straight line has a positive slope. In the Figure 2.3.1, the reaction occurs with a decrease in the number of gas molecules.

$$A_3 = A°\{-\Delta G°(T)\} + RT\ \ln\{(p_{CO})^2\ .\ p_{O2} / (p_{CO2})2\} \qquad [2.6.4]$$

The Ellingham line drawn in the diagram, see Figure 2.3.1, corresponds to a value of the ratio $p_{CO}/p_{CO2} = 1$. It cuts the vertical axis (0K) at C and the first scale on the left-hand side (p_{O2}) at the point corresponding to the ratio $p_{CO}/p_{CO2} = 1$. The value of the oxygen pressure, p^*_{O2} at temperature T, in equilibrium with a gas phase, where $p_{CO}/p_{CO2} = 1$

$$\Delta G°_3(T) = RT\ \ln\ p^*_{O2} \qquad [2.6.5]$$

can be obtained by drawing a line on Figure 2.3.1 from point Ω and the point of the Ellingham line at the desired temperature. The intersection of this line with the scale on the right-hand side gives the pressure p^*_{O2}.

NOTE.– the standard affinities (free enthalpies) of these reactions correspond to the compositions of the gas, with $p_{O2} = p_{CO2} = p_{CO} = 1$ atm.

The mechanism and combustion rate of carbon are presented in Chapter 5, section 5.4.3 and Figure 5.4.1.

2.6.2. *Boudouard's reaction*

The Ellingham line of Boudouard's reaction (or carbon gasification and gas regeneration reaction) is drawn in Figure 2.5.3:

$$CO_2(g) + C(s) \rightarrow 2CO(g) \qquad [2.6.6]$$

$$A°_B(T) = -\Delta G°(T) = RT\ \ln\ K_B(T) =$$

$$-40{,}900(-38{,}700) + 41.7\ (40.5)T\ (cal/mole)$$

The standard affinity of this reaction only becomes positive above 666°C. The reaction is endothermic and occurs with an increase of the number of gas molecules, and the Ellingham straight line has a negative slope. The maximum degree of conversion of CO_2 into CO and therefore the reducing gas regeneration power increases with temperature.

Thermodynamically, Boudouard's reaction gets close to completion above <900°C. In fact, it is very slow below 950–1,100°C. This temperature depends on the nature of the carbon (its reactivity) and the presence of catalyzing species.

The inverse dissociation reaction of CO is an exothermic reaction, whose standard affinity is only positive at low temperatures (T < 666°C). The reaction is very slow below 1,000–1,100°C. It requires a highly reducing environment, therefore very high p_{CO}/p_{CO2} ratios. At high temperatures, the CO can be considered metastable.

The affinity of Boudouard's reaction is given by:

$$A = A°(-\Delta G°_B(T)) + RT \ln\{p_{CO2} / (p_{CO})^2\} \quad [2.6.7]$$

Thus, at equilibrium:

$$\log\{p_{CO2} / (p_{CO})^2\} = 8{,}677(8{,}891) / T - 8.874(9.06) \quad [2.6.8]$$

As $p_{CO} + p_{CO2} = P$, the ratio of the partial pressures $(p_{CO2}/p_{CO})^*$ at equilibrium depends on the total pressure:

$$\left(\frac{p_{CO_2}}{p_{CO}}\right)^* = \frac{\left(2P + K_B - \sqrt{\left(K_B^2 + 4K_B.P\right)}\right)}{\left(\sqrt{\left(K_B^2 + 4K_B.P - K_B\right)}\right)} \quad [2.6.9]$$

The curves corresponding to the equilibrium of Boudouard's reaction, plotted in the Rosenquist diagram (see Figure 4.2.3a, Chapter 4 of [VIG 11b]) and in Chaudron diagram (see Figure 4.2.4b, Chapter 4 of [VIG 11b]), respectively, represent the variations of the $(p_{CO2}/p_{CO})^*$ and $p_{CO}/(p_{CO} + p_{CO2})^*$ ratios as a function of temperature and they are drawn for P = 1 atm. The mechanism and kinetics of Boudouard's reaction are presented in Chapter 5, section 5.4.3.

2.6.3. *The different types of coal*

Coals are divided into five main categories, whose denomination and features are presented in Table 2.6.1.

	Lignite	Sub-bituminous	Bituminous (high volatiles)	Bituminous (low volatiles)	Anthracite
Calorific power inferior on dry product, Kcal/kg	3,500-4,500	4,500-6,500	6,500-7,800	6,500-7,800	7,800-8,500
Humidity	25-50%	14-25%	5-10%	5-10%	1-6%
Volatile materials	50%	25-50%	30-40%	15-25%	< 10%
Ash content	30-50%	20-30%	10-20%	10-20%	0-10%

Table 2.6.1. *Coals and their characteristics*

Metallurgical coke is obtained by coking – heating coal in the absence of air so that the volatile components are driven off – bituminous, low volatile (23–27%) coals. The baking is carried out in an oven at temperatures as high as 1,000°C so that the fixed carbon and ash are fused together. The coke particles must be strong enough to resist the weight of overburden in the blast furnace. The injection of (bituminous) coal into blast furnaces by replacing a fraction of coke was industrially developed in the 1990s because of the cost difference between both combustibles, reaching injected quantities of 180 kg/t Fe for 300 kg/t Fe of coke.

The composition of the some cokes is presented in Table 2.6.2.

Fixed carbon %	Ash %	P %	S %	Volatile materials %	Humidity %
89	9.5	0.02	0.30	1.50	5
88	10.5	0.025	0.30		
86	12	0.03	0.50		

Table 2.6.2. *Composition of cokes*

2.7. Bibliography

[ANC 73] M.F. ANCEY-MORET, Y. DENIELY, *Mem. Sic. Rev. Met*., Vol. 70, No. 4, pp. 301-317, 1973.

[BAL 76] C.W. BALE, J.M. TOGURI, *Canadian Metallurgical Quarterly*, Vol. 15, No. 4, 305-318, 1976.

[BAR 77] I. BARIN, O. KNACKE, O. KUBASCHEWSKI, *Thermodynamics of Inorganic Substances*, 2nd ed., Springer Verlag, Berlin, 1977.

[DAR 46] L.S. DARKEN, R.W. GURRY, *JACS*, Vol. 67, pp. 1398, 1945 and Vol. 68, pp. 798-816, 1946.

[ELL 44] H.J.T. ELLINGHAM, *J. Soc. Chem. Ind.*, Vol. 63, pp. 125-133, 1944.

[ELL 76] J.F. ELLIOTT, *Metallurgical Transactions B*, Vol. 7B, 17-33, March 1976.

[HAN 54] T. HANSEN-ELLIOTT, J. ROSENQUIST, *Iron and Steel Institute*, Vol. 176, 37-57, 1954.

[HAN 58] M. HANSEN, *Constitution of Binary Alloys*, 2nd ed., Metallurgy and Metallurgical Engineering Series, McGraw Hill, 1958, R.P. ELLIOTT, First supplement, 1965, F.A. SHUNK, Second supplement, 1969.

[HOL 04] L. HOLAPPA, X. XIAO, *Journal South African Institute of Mining and Metallurgy*, pp. 429-437, August 2004.

[KAN 98] N. KANARI, B.R. REDDY, I. GABALLAH, *Metallurgical and Materials Transactions B*, Vol. 29B, pp. 729-737, August 1998.

[KEL 87] H.H. KELLOG, *Canadian Metallurgical Quarterly*, Vol. 26, No. 4, pp. 285-298, 1987.

[KUB 79] O. KUBASCHEWSKI, E. EVANS, C.B. ALCOCK, *Metallurgical Thermochemistry*, 5th ed., Pergamon Press, Oxford, 1979.

[MAS 86] T.B. MASSALLSKI, *Binary Alloy Phase Diagrams*, Vol. 1 and 2, ASM, 1986.

[MUA 65] A. MUAN, E.F. OSBORNE, *Phase Equilibria among Oxides in Steelmaking*, Addison-Wesley Publishing Co, Reading, MA, 1965.

[OLE 63] M. OLETTE, M.F. ANCEY-MORET, *Revue de Métallurgie*, pp. 561-581, June 1963.

[PHI 02] J. PHILIBERT *et al*., *Métallurgie*, *du Minerai au Matériau*, Chapters 2-3, 2nd ed., Dunod, Paris, 2002.

[RIC 48] F.D. RICHARDSON, J.H.E. JEFFES, *J. Iron, Steel, Inst*., Vol. 160, pp. 261-270, November 1948.

[RIC 74] F.D. RICHARDSON, *Physical Chemistry of Melts in Metallurgy*, Vol. 1, Academic Press, Oxford, 1974.

[ROS 83] T. ROSENQUIST, *Principles of Extractive Metallurgy*, McGraw-Hill, New York, 1983.

[SHA 87] R.C. SHARMA, J.C. LIN, Y.A. CHANG, *Metallurgical Transactions B*, Vol. 18B, pp. 237-243, March 1987.

[STU 71] D.R. STULL, H. PROPHET, *JANAF Thermochemical Tables*, National Standard Reference Data System, 1971.

[TEE 99] J.K.S. TEE, D.J. FRAY, *JOM*, pp. 24-27, August 1999.

[VIG 11b] A. VIGNES, *Extractive Metallurgy 2: Metallurgical Reaction Processes*, ISTE Ltd, London and John Wiley and Sons, New York, 2011.

[VIG 11c] A. VIGNES, *Extractive Metallurgy 3: Processing Operations and Routes*, ISTE Ltd, London and John Wiley and Sons, New York, 2011.

[YAZ 79] A. YAZAWA, *Metallurgical Transactions B*, Vol. 10B, pp. 307-321, September 1979.

Chapter 3

Metal Solutions, Slags and Mattes

3.1. Introduction

Smelting, converting, and refining processes involve homogeneous and heterogeneous reactions. The optimization of these processes (optimization of the initial and operating conditions) is based on the possibility of estimating the affinity of the reactions occurring and the possible equilibrium state has been reached.

The basic thermodynamic function controlling the evolution of a chemical reaction is its affinity or its "driving force" (see Chapter 1, section 1.3.2 and equations [1.3.14] and [1.3.53]). Chapter 2 deals with the thermochemical data leading to the calculation of the first term of affinity: the *standard affinity* (or standard Gibbs free energy, see Equation [1.3.16] in Chapter 1 of this book), which depends on the Gibbs free energy of formation of the reaction components. In this chapter, the thermodynamic data necessary to calculate the second term of affinity are presented. They correspond to the activities of components of the reaction occurring in metal solutions, slags and mattes as a function of temperature and composition, at each instant in each phase.

Knowledge of the components activities is extremely important for the prediction of direction and degree of reaction advancement, especially as metallic solutions, slags and mattes often show very large deviations from ideal cases. Let us consider the following extraction reaction:

$$\underline{M}_{(\text{dissolved in liquid iron})} + O_2(g) \rightarrow (MO)_{(\text{dissolved in a slag})} \qquad [3.1.1]$$

whose affinity, A, is given by:

Extractive Metallurgy 1: Basic Thermodynamics and Kinetics Alain Vignes
© 2011 ISTE Ltd. Published 2011 by ISTE Ltd.

$$A = (-\Delta G^\circ_r) + RT \ln p_{O2} + RT \ln a^\circ_{M(Fe)}/a^\circ_{(MO)} \quad [3.1.2]$$

If the activity $a^\circ_{\underline{M(Fe)}}$ is low and the activity $a^\circ_{(MO)}$ is high, extracting the M element from the metallic phase will be difficult and vice versa. Another illustration of the importance of knowing the activities of components is when we want to determine the direction of a reaction, as presented in [VIG 11b], Chapter 4, section 4.1.2 and Figure 4.1.2.

There is no question in this chapter of dealing, in a relatively exhaustive manner, with measurement and/or estimation from models of thermodynamic quantities, especially the activities of the components. The aim is to present the data found in tables, books and papers, bringing out the features in order to help orient the reader during the study of these pieces of information.

3.2. Metal solutions

3.2.1. *Phase diagrams and activities of liquid alloy components*

3.2.1.1. *Typical systems: silver-copper, lead-zinc and copper-zinc systems*

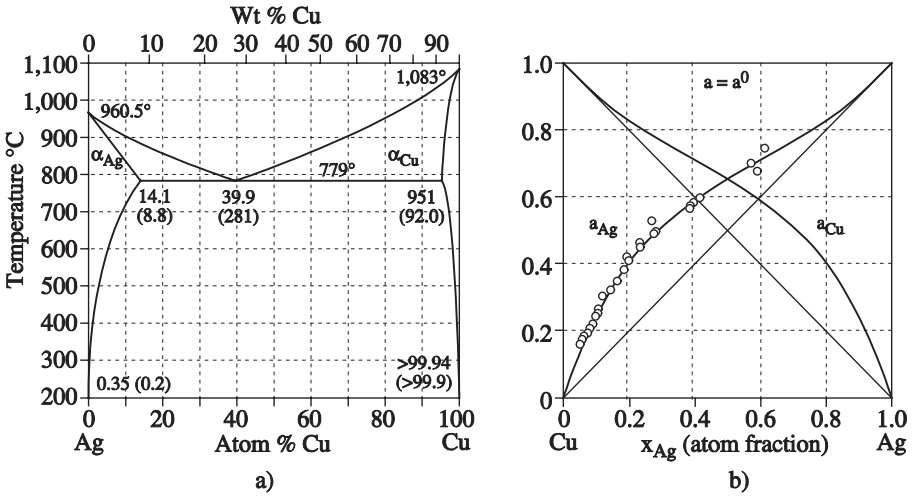

Figure 3.2.1. *Ag-Cu system: a) phase diagram; and b) Cu and Ag activities at 1,400K [HOW 89]*

The silver-copper system (see Figure 3.2.1a) is representative of binary eutectic systems, with stable terminal phases of limited extension. The Raoultian or standard activities (see equations [1.3.21], [1.3.22] and [1.3.24] in Chapter 1) of both components in the liquid solution at 1,127°C (see Figure 3.2.1b) present a positive deviation from ideality. They show a tendency for these two components to segregate as the temperature is lowered, the Ag-Ag and Cu-Cu attractions being stronger than the Ag-Cu attraction, as shown in the phase diagram.

The Pb-Zn phase diagram, see Figure 3.2.2a, presents a miscibility gap between 419 and 800°C, separating two liquid phases. The activities of both elements in these two stable terminal phases, see Figure 3.2.2b, at 600°C exhibit very strong positive deviations from Raoult's law, resulting from a weak Pb-Zn attraction.

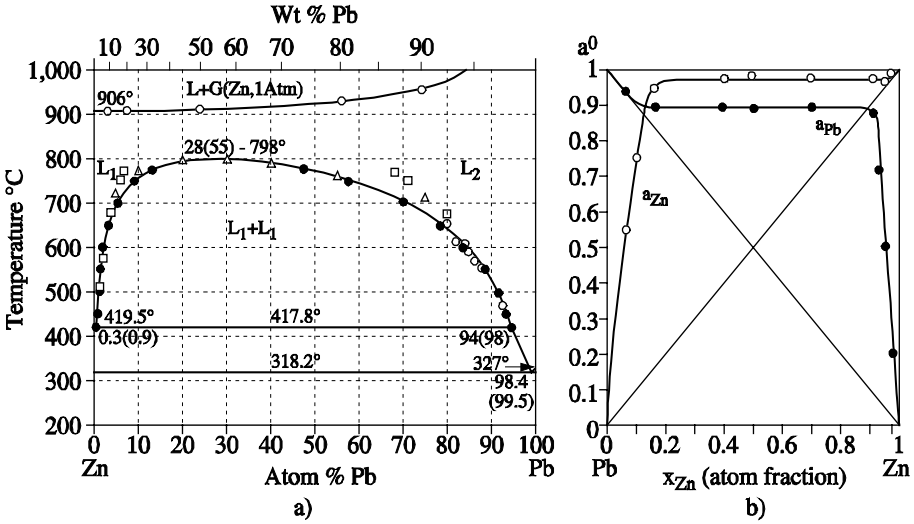

Figure 3.2.2. *Zn-Pb system: a) phase diagram; and b) Zn and Pb activities at 600°C [LUM 52, MAC 65]*

The Cu-Zn system contains several intermediate solid phases resulting from a strong Cu-Zn attraction, see Figure 3.2.3a. The activities of copper and zinc in the liquid phase at 1,060°C under a pressure of p_{Zn} = 4 atm, see Figure 3.2.3b, exhibit negative deviations from ideality.

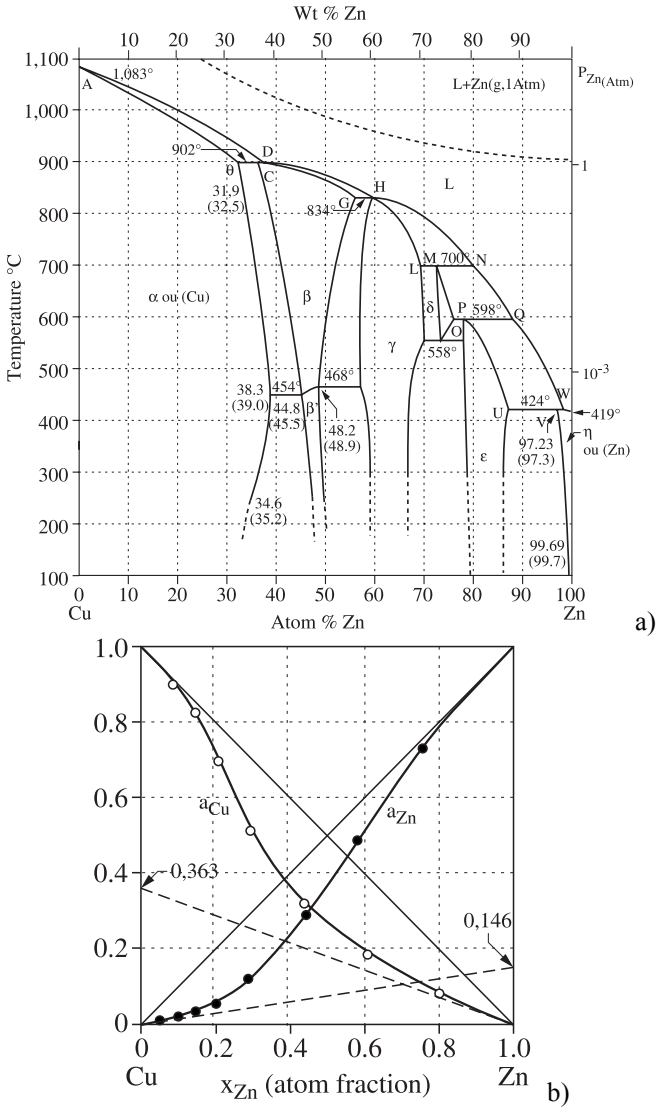

Figure 3.2.3. *Cu- Zn system: a) phase diagram; and b) activities at 1,060°C and p = 4 atm [DAR 53]*

3.2.1.2. *Activities of metals in liquid copper*

Copper as copper blister, at the end of the processing route, contains several metallic impurities. The extraction of these impurities via thermo-chemical routes

can be obtained, either by oxidation or by volatilization of these elements (see [VIG 11b], Chapter 7, section 7.4). For these two refining processes, knowing the Raoultian activity coefficient $\gamma_{j(0)}$ at infinite dilution (see equation [1.3.36]), of the impurity in copper indicates whether or not it can be easily extracted. The higher the $\gamma_{j(0)}$, the greater the affinity of the oxidation reaction, see equation [3.1.2]. Regarding volatilization of the impurities, the greater the product (vapor pressure of the impurity by this coefficient), the easier the volatilization (see equation [1.3.34]), at high dilution:

$$p_M = p^\circ_M \cdot \gamma_{M(0)(Cu)} \cdot x_M$$

In Table 3.2.1 some values of this activity coefficient in copper and of the vapor pressure of some metallic elements are presented. The extraction of elements, such as Pt, Pd and Au, should be difficult because of the low activity coefficient values. On the other hand, the extraction of iron, lead and nickel by oxidation should be easy, because of the high activity coefficient values of these elements.

Element	*Raoultian activity coefficient at infinite dilution $g_{j(0)}$, at 1,200°C*	*p°_M (atm) at 1,200°C*
Au	0.34	$4.9 \cdot 10^{-7}$
Ag	4.8	$2.2 \cdot 10^{-4}$
Pt	0.03	$6.4 \cdot 10^{-13}$
Pd	0.06	$8.5 \cdot 10^{-7}$
Cu	1	$4.5 \cdot 10^{-6}$
Pb	5.7	$1.9 \cdot 10^{-2}$
Ni	2.8	$2.8 \cdot 10^{-8}$
Cd	0.73	
Sb	0.013	$7.9 \cdot 10^{-2}$
As	0.0005	
Sn	0.11	$6.5 \cdot 10^{-6}$
In	0.32	$8.1 \cdot 10^{-4}$
Fe	15	$7.8 \cdot 10^{-8}$
Zn(l) under p = 10 atm	0.11	10
Si	0.1	10^{-6}
Al	0.008	$1.3 \cdot 10^{-5}$

Table 3.2.1. *Raoultian activity coefficients at infinite dilution $\gamma_{\alpha(0)}$ (see equation [1.3.36] of this book) in liquid copper and vapor pressures at 1,200°C of the metals [YAZ 69]*

3.2.1.3. *Phase diagrams and activities of Si, Mn, and Cu in liquid iron*

In Figure 3.2.4 the activity curves (see equation [1.3.22]), of several metallic elements (Si, Mn and Cu in liquid iron), at 1,600°C are drawn (These elements present a total miscibility with iron at this temperature and the standard activity is equal to the Raoultian activity, see equation [1.3.24].). Some values of the Raoultian activity coefficient, at infinite dilution $\gamma_{j(0)}$, of the Henrian activity coefficients f_j^k and of the molar free energies of solution of some elements in iron are presented in Table 3.2.2. Interaction coefficients e_i^j (see equation [1.3.44]), between elements in solution in liquid iron at 1,600°C are presented in Table 3.2.3.

Element and reference physical state	*Raoultian activity coefficient at infinite dilution $\gamma_{\varphi 0}$ at 1,600°C (see equation [1.3.36] in this book)*	*Henrian activity coefficient f_j (see equation [1.3.37])*	*Molar free energy of solution at infinite dilution (cal/mol) (see equation [1.3.39])*	*Molar free energy of solution in a 1% solution (cal/mol) (see equation [1.3.42])*
Al (liquid)	0.029			-15,100 – 6.67 T
Cr (liquid) Cr (solid)	1 ; 1.12		4,600 – 2.17 T	-9.01 T 4,600 – 11.18 T (4,000 – 10.9 T)
Cu (liquid)	7-10		11,370 – 2.16 T	11,370 – 11.62 T
Mn (liquid)	1.48			1,450 – 9.12 T
Si (liquid)	0.018, 0.0052, 0.00724, $\log \gamma_{Si(0)} = 1.21 – 6{,}100/T$			-31,400 – 3.60 T -28,000 – 2.20 T
Ni (liquid)	0.62			-1,800 – 0.25 T
C (graphite)	10^{-3}		+5,400-4.0 T	+5,400 – 10.10 T
1/2 O_2 (1 atm)		$\log f_O = -0.10$ (%O) $\log f_O = -0.15$ (% Si)		-28,000 – 0.69 T (-27,930 – 0.62 T)
1/2 P_2 (1 atm)		$\log f_P = -0.062$ (%P)		-29,200 – 4.60 T
1/2 S_2 (1 atm)		$\log f_S = -0.03$ (%S)		-32,280 + 5.60 T (-31,250 + 5.27 T)
1/2 H_2 (1 atm)				+8,720 + 7.28 T (7,631 + 7.67 T)
1/2 N_2 (1 atm)				+ 860 + 5.71 T

Table 3.2.2. *Raoultian activity coefficients at infinite dilution, Henrian activity coefficients at 1,600°C and molar free energy of solution of metals and metalloids in liquid iron [RIS 74b]*

Element j	e^i_C	e^j_H	e^f_N	e^j_O	e^i_S
Al	0.43	0.013	0.28	–3.9	0.035
C	0.14	0.06	0.13	–0.13	0.11
Cr	–0.024	–0.002	–0.047	–0.04	–0.011
Mn	–0.012	–0.001	–0.02	–0.021	–0.026
N	0.13	0	0	0.057	0.007
O	–0.34	–0.19	–0.05	–0.2	–0.27
P	0.051	0.011	0.045	0.07	0.29
S	0.046	0.008	0.007	–0.133	0.028
Si	0.08	0.027	0.047	–0.131	0.063

Table 3.2.3. *Interaction coefficients e_i^j in dilute solutions of ternary iron base alloys for C,H,N,O and S elements at 1,600°C [TUR 96]; see also [BOD 63, ELL 63]*

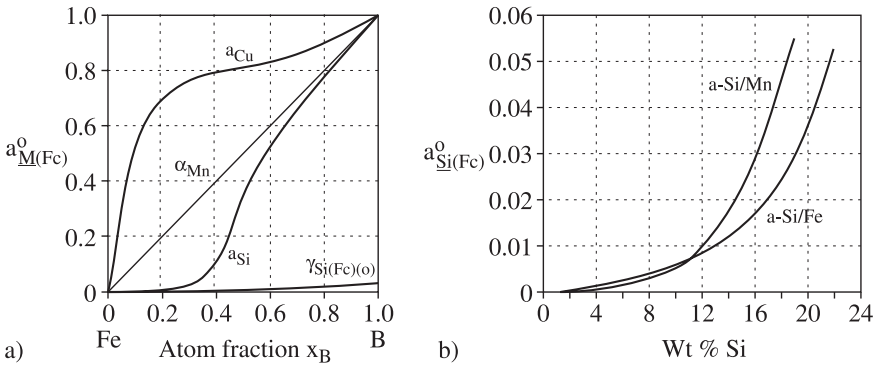

Figure 3.2.4. *a) Raoultian activities of copper, manganese and silicon in solution in molten iron at 1,600°C [WAR 62]; and b) activities of silicon in carbon-saturated Fe-Si-C and Mn-Si-C systems at 1,600°C [OLS 97]*

The Fe-Mn and Fe-Ni solutions at 1,600 °C are very close to ideality.

In the Fe-Cu system (see Figures 3.2.5a and b), the standard activities at 1,600°C present a strong positive deviation from ideality, which results from strong Cu-Cu and Fe-Fe interactions and a weak Cu-Fe interaction. Copper should be easily extracted from iron. As a matter of fact, that is not what happens, as the standard affinity of formation (the free energy of formation) of copper oxide is very low at this temperature (see Figure 2.3.1 of this book).

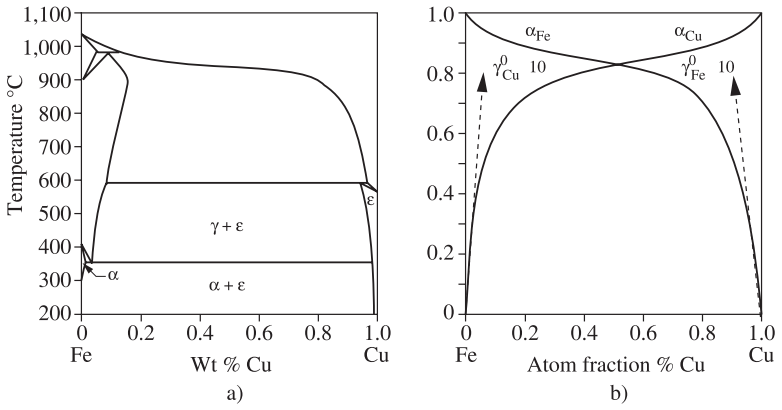

Figure 3.2.5. *Fe-Cu system: a) phase diagram; b) activities at 1,600°C [ROS 83]*

In the Fe-Si system, the silicon activity shows a strong negative deviation from ideality, which is due to a very strong Fe-Si interaction. Silicon does indeed form a compound with iron (FeSi) with a congruent fusion at around 1,410°C. The very low values of the activity coefficient, $\gamma_{Si(0)}$ at 1,600°C are very dispersed, see Table 3.2.2. Because of this strong negative deviation from ideality, silicon should be difficult to extract from liquid iron. This is not the case, however, as the standard affinity of silica formation is very high, see Figure 2.3.1 in this book.

The variations of silicon activity within the Fe-Si-C and Mn-Si-C alloys saturated in carbon, as a function of the content in silicon at 1,600°C, are drawn in Figure 3.2.4b.

3.2.1.4. *Activity and solubility of carbon in liquid iron*

The solution of carbon (graphite) in liquid iron can be represented by the following reaction:

$$C(s) \rightarrow \underline{C}_{(\text{dissolved in liquid iron})} \qquad [3.2.1a]$$

whose affinity:

$$A_C^{(diss)} = \mu°_C - (\mu°_C + RT \ln a°_{C(Fe)}) = RT \ln a°_{\underline{C}(Fe)}$$

can be represented by the following equations [RIS 56] (see equations [1.3.40] and [1.3.41b] of this book):

$$A_C^{(sol)} = -5{,}400 + 4.0\ T - 4.57\ T \log f_C\ .\ x_C \text{ (cal/mole)} \qquad [3.2.1b]$$

$$A_C^{(sol)} = -5{,}400 + 10.40\ T - 4.57\ T \log f_C\ .\ \%C\ (cal/mole) \qquad [3.2.1c]$$

Due to the strong Fe-C bond leading to the formation of cementite in the solid state, the carbon activity in liquid iron has to present a very strong negative deviation from ideality. The variation of the "standard" activity $a°_{\underline{C}(Fe)}$ at 1,600°C as a function of the carbon content is shown in Figure 3.2.6a. The slope at the origin (see equation [1.3.40] of this book) is equal to:

$$a°_{\underline{C}(Fe)} / x_C = \gamma_{C(Fe)(0)}\ .\ \exp(\Delta g_C^{(fusion)} / RT) = 0.575 \text{ for } x_C = 0 \qquad [3.2.2]$$

The standard activity of C, $a°_{\underline{C}(Fe)}$, in iron saturated in C, at equilibrium with graphite, is equal to one (reference state). The variation in Henrian activity of C in iron ($\tilde{a}_{\underline{C}(Fe)} = f_C\ .\ x_C$) (see equation [1.3.37b]), is shown in Figure 3.2.6b. The activity $\tilde{a}_{\underline{C}(Fe)}$ at saturation ($f_C\ .\ x_C$) is equal to 1.75. In the Ellingham diagram (see Figure 2.5.3), the carbon activity scale corresponds to the standard activity $a°_{\underline{C}(Fe)}$.

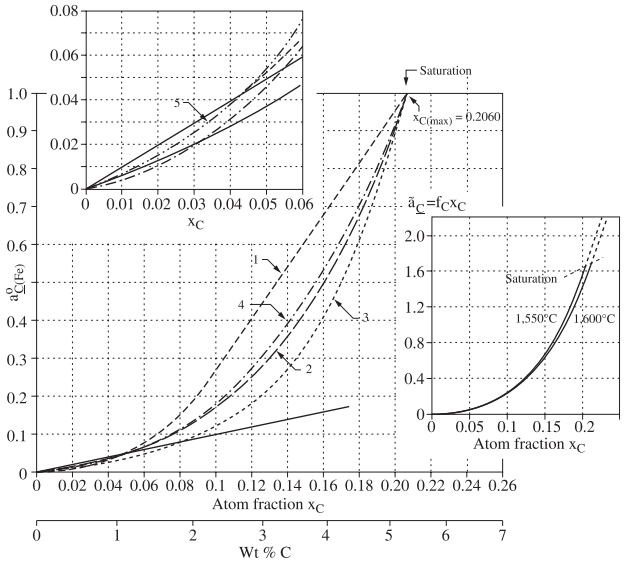

Figure 3.2.6. *Activity of carbon within the iron-carbon system at 1,550°C: a) standard activity $a°_C$ (reference state graphite) [OET 94]; and b) Henrian activity ($\tilde{a}_C = f_C.x_C$) [ELL 63]*

The molar free energy of carbon (graphite) solution in liquid iron and at infinite dilution, is given by [RIS 56] (see equation [1.2.39] of this book):

$$\Delta g_{\underline{C}(Fe)(0)}^{(sol)} = \{RT \ln \gamma_{C(Fe)(0)} + \Delta g_C^{(fusion)}\} = 5{,}400 - 4.0\ T\ (cal/mole) \qquad [3.2.3]$$

where:

$$\Delta g_C^{(fusion)} = 38{,}500 - 7.74\ T$$

thus:

$$RT \ln \gamma_{C(Fe)(0)} = -33{,}100 + 3.74\ T \text{ (cal/mole)}$$

and

$$\gamma_{C(Fe)(0)} = 10^{-3} \text{ at } 1{,}600°C$$

The variation of the carbon Henrian activity coefficient f_C (see equation [1.3.37]) as a function of the carbon content in liquid iron is plotted in Figure 3.7a:

$$\log f_{C(Fe)} = \{4{,}350 / T\}\ [1 + 4.10^{-4}\ (T - 1{,}770)]\ \{1 - (x_{Fe})^2\} \qquad [3.2.4a]$$

$$\log f_{C(Fe)} = 0.2\ (\%C) \text{ when } \%C < 1 \text{ at } T = 1{,}600°C \qquad [3.2.4b]$$

and the activity coefficient variations f^k_C (see equation [1.3.43]) as a function of the alloy content in steel are plotted in Figure 3.2.7b.

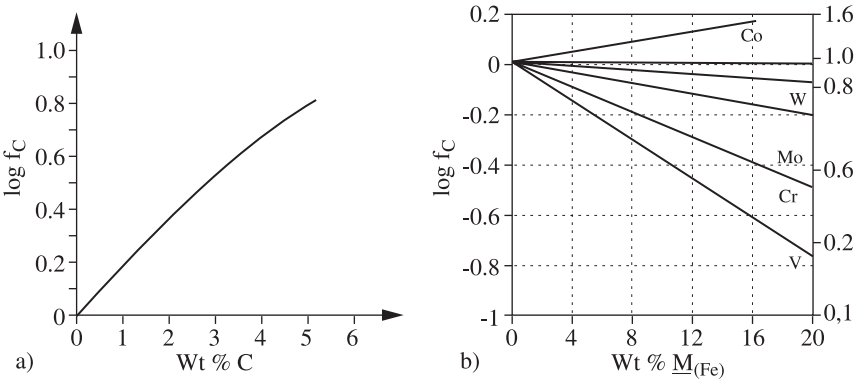

Figure 3.2.7. *a) Henrian activity coefficient $f_{C(Fe)}$ of carbon in liquid iron at 1,550°C, b) Henrian activity coefficient of carbon $f_{C(Fe)}$ in ternary alloys, relative to the values in pure iron at 1,600°C as a function of the alloy concentration (see equation [1.3.44]) [BRA 65]*

The solubility of carbon in iron is given by:

$$\log x_{\underline{C}(Fe)}(sat) = -560 / T - 0.375 \qquad [3.2.5a]$$

At 1,550°C: $x_{\underline{C}(Fe)}(sat) = 0.2060$ and $\%\underline{C}_{(Fe)}(sat) = 5.1\ \%$ (see Figure 3.2.6a)

The solubility of carbon in a Fe-Si alloy significantly decreases with silicon content, see Figure 3.2.8, due to the strong Si-C bond resulting in the formation of SiC carbide:

$$\%\underline{C}_{(Fe\text{-}Si)}(sat) = 0.65 + 0.00254\ T - 0.34\ \%\underline{Si}_{(Fe)} \qquad [3.2.5b]$$

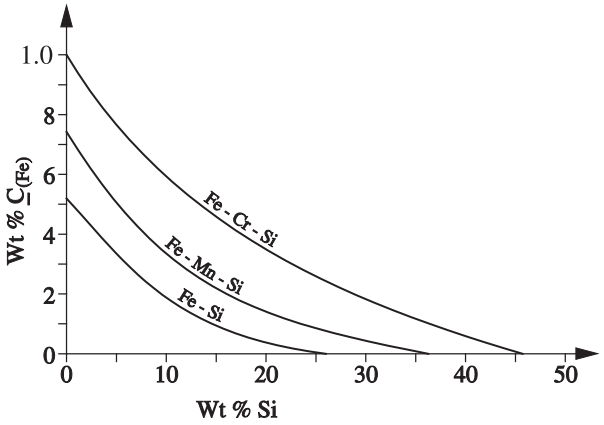

Figure 3.2.8. *Carbon solubilities at 1,600°C in ferroalloys (approximation): Fe-Si, Fe-Mn-Si and Fe-Cr-Si [ROS 83]*

3.2.1.5. *Carbon activity in liquid manganese*

$$\Delta g_{C(Mn)(1\ \%)}^{(sol)} = 10{,}000 - 14.25\ T\ (cal/mole)\ (Kim) \qquad [3.2.6a]$$

$$\ln \gamma_{C(Mn)(0)} = -4.1 + 5{,}040 / T\ (cal/mole)\ \text{between 1,673 and 1,773K}$$

and in ferromanganese:

$$\log f_{C(Fe)} = 0.03\ (\%C) + 0.0136\ (\%C)^2 + 0.0867\ (\%Fe) \qquad [3.2.6b]$$

3.2.2. *Activities and solubilities of metalloids in metal solutions*

3.2.2.1. *Sulfur and oxygen in liquid copper*

Copper-oxygen (see Figure 2.2.3) and copper-sulfur (see Figure 2.2.7) systems present a miscibility gap between 1,065 and 1,325°C. The variations in content of O and S in the liquid copper-rich phase (L_1) at 1,200°C are drawn as a function of the partial pressures p_{O2} and p_{S2} in the stability diagram (see Chapter 2, section 2.4.2, Figure 2.4.2 and Figure 3.2.9).

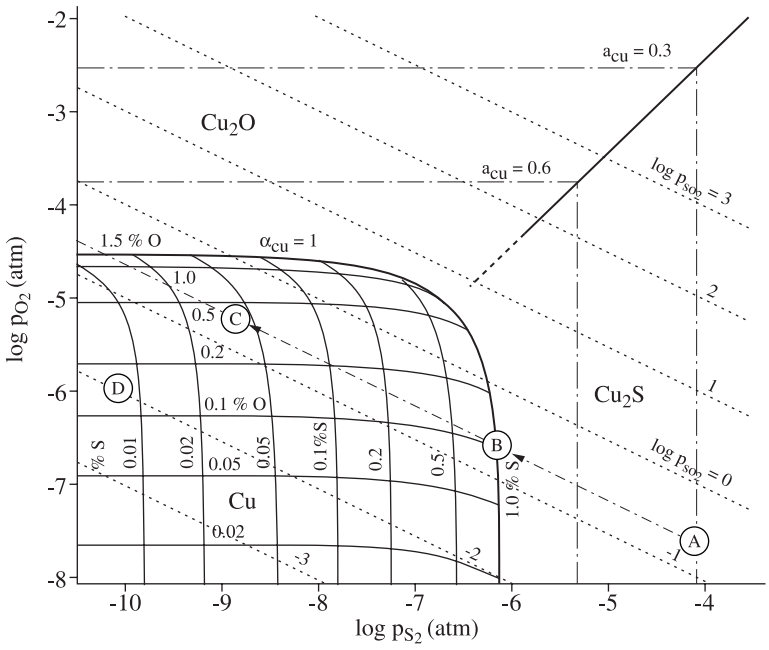

Figure 3.2.9. *Stability diagram for the Cu-O-S system at 1,200°C [YAZ 69]*

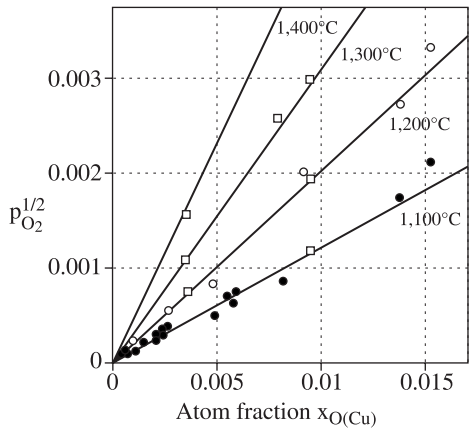

Figure 3.2.10. *Standard activities of oxygen as a function of the oxygen atom fraction in liquid copper* $a°_{\underline{O}(Cu)} = p^{1/2}{}_{O2}\,(atm^{1/2})$ *(see equation [1.3.51a] and Table 3.2.4 of this book) [FRU 69]*

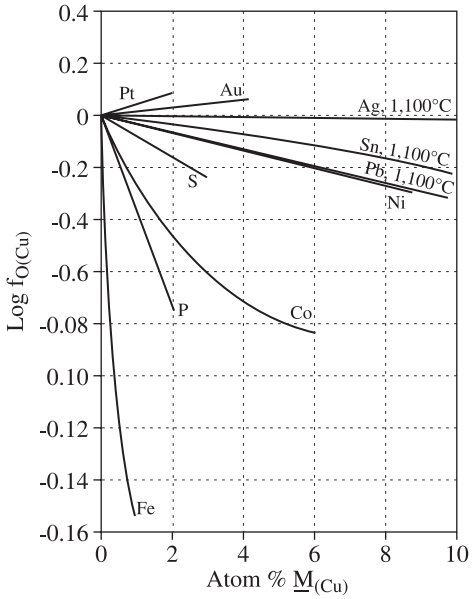

Figure 3.2.11. *The influence of alloying elements on the activity coefficient of oxygen in liquid copper at 1,200°C (or 1,100°C where indicated) log $f_O^k = e_O^k.\%k$ (see equation [1.3.44]) [RIC 74]*

The data concerning oxygen and sulfur activities in liquid copper are gathered in Tables 3.2.4a and b, and in Figures 3.2.10 to 3.2.12 (see Chapter 1, section 1.3.3.5. of this book).

$$1/2\ O_2(g) \rightarrow O_{(\text{dissolved in copper})} \qquad [3.2.7a]$$

$$\log p_{O2}^{1/2} / f_O\ .\ \%O_{(Cu)} = -3{,}950 / T + 0.584$$

$$\Delta g_{O(Cu)(1\ \%)}^{(sol)} = -18{,}051 + 2.66\ T\ (\text{cal/mole})$$

$$1/2\ S_2(g) \rightarrow S_{(\text{dissolved in copper})} \qquad [3.2.8a]$$

$$\log p_{S2}^{1/2} / f_S\ .\ \%S_{(Cu)} = -5{,}440 / T + 0.815$$

$$\Delta g_{S(Cu)(1\ \%)}^{(sol)} = -24{,}860 + 3.72\ T\ (\text{cal/mole})$$

$$\log f_O^0 = -311.3\ .\ (\%O) / T;\ \log f_O^S = -242.6\ .\ (\%S) / T$$

$$\log f_S^S = -281.6\ .\ (\%S) / T;\ \log f_S^O = -485.2\ .\ (\%O) / T$$

Table 3.2.4a. *Cu-O-S system thermodynamic data (equations [3.2.7a] and [3.2.8a]) [YAZ 69]*

$$1/2\ O_2(g) \rightarrow O_{(Cu)} \qquad [3.2.7b]$$

$$\Delta g_{O(Cu)(1\ \%)}^{(sol)} = -85{,}930 + 7.21\ T\ (J/mole)$$

$$1/2\ S_2(g) \rightarrow S_{(Cu)} \qquad [3.2.8b]$$

$$\Delta g_{S(Cu)(1\ \%)}^{(sol)} = -102{,}230 + 7.53\ T\ (J/mole)$$

$$1/2\ H_2(g) \rightarrow H_{(dissolved\ in\ copper)}$$

$$\Delta g_{H(1\ \%)}^{(sol)} = 10{,}400 - 10.8\ T\ (cal/mole)$$

Table 3.2.4b. *Cu-O-S system thermodynamic data (equations [3.2.7b] and [3.2.8b]) [JAC 71]*

Figure 3.2.10 shows the curves of variation of the standard activity of oxygen in Cu-O solution. $a°_{\underline{O}(Cu)} = (p_{O2})^{1/2}$ as a function of the mole fraction $x_{\underline{O}}$ (see equation [1.3.51a]). The slope at the origin corresponds to the molar free energy of a solution of half a mole of oxygen in liquid copper at infinite dilution, see equation [1.3.50]. As these curves are straight lines, the Henrian activity coefficient $f_{O(Cu)} = 1$ (see equation [1.3.37]), up to a content of 1.5 atom%. The values of the Raoultian activity coefficient at infinite dilution $(p_{O2})^{1/2} / x_O = a°_{\underline{O}(Cu)} / x_O = \gamma_{O(Cu)(0)}$, 0.122 at 1,100°C and 0.204 at 1,200°C, are in agreement with the data presented in Table 3.2.4. Figure 3.2.11 shows the effect of alloying elements on the Henrian activity coefficient f_O^k (see equation ([1.3.44]) of oxygen in liquid copper at 1,200°C.

In Figure 3.2.12, the curves of $(p_{S2})^{1/2} / x_S$ are drawn as a function of the molar fraction of sulfur x_s in liquid copper at various temperatures. The free energy of solution of a half mole of sulfur in liquid copper at infinite dilution can be calculated from the slope of the curves at the origin $\exp(\Delta g_{\underline{S}(Cu)(0)}^{(diss)})$, see equation [1.3.51b]. The Henrian activity coefficient f_S can be calculated, see equation [1.3.51b], by:

$$\{(p_{S2})^{1/2} / x_S\} / \{(p_{S2})^{1/2} / x_S\}_{(xS\ =\ 0)} = f_{\underline{S}(Cu)}$$

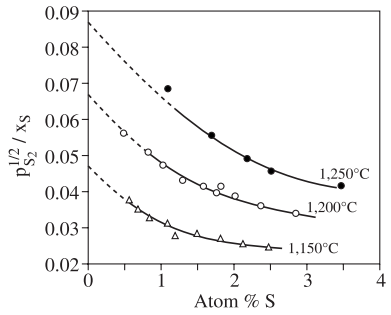

Figure 3.2.12. *Activity coefficient of sulfur in liquid copper, with $a°_{\underline{S}(Cu)} / x_{S(cu)} = p^{1/2}{}_{S2} / x_{S(cu)}$ at 1,150, 1,200 and 1,250°C (see equations [1.3.40] and [1.3.51] in Chapter 1) [BAL 76]*

3.2.2.2. *Sulfur and oxygen in liquid nickel*

The data concerning the activities of oxygen and sulfur in liquid nickel are gathered in Table 3.2.5.

$$1/2\ O_2(g) \rightarrow O_{(Ni)} \qquad [3.2.9a]$$

$$\Delta g_{O(Ni)(1\ \%)}^{(sol)} = -72{,}930 + 3.70\ T\ (J/mole)$$

$$\log f_{O(ni)} = (-1{,}837 / T + 0.782)\ (\%O_{(Ni)})$$

$$1/S_2(g) \rightarrow S_{(Ni)} \qquad [3.2.9b]$$

$$\Delta g_{S(Ni)(1\ \%)}^{(sol)} = -\ 166{,}560 + 34.3\ T\ (J/mole)$$

$$\log f_S^O = (-1{,}083 /T + 0.389)(\%\ S_{(Ni)})$$

with $e_O^S = -540 / T + 0.196$

$$1/2\ H_2(g) \rightarrow H_{(dissolved\ in\ nickel)} \qquad [3.2.9c]$$

$$\Delta g_{H(1\ \%)}^{(sol)} = 4{,}800 - 9.9\ T\ (cal/mole)$$

Table 3.2.5. *Ni-O-S system thermodynamic data [SEE 93]*

3.2.2.3. *Oxygen and sulfur in liquid iron*

Table 3.2.2 presents the Raoultian activity coefficients at infinite dilution $\gamma_{X(Fe)(0)}$, the free energy of solution at infinite dilution and in a solution at 1% for the metalloid elements O_2, P_2, S_2, H_2 and N_2 in liquid iron. Table 3.2.3 presents the interaction coefficients e_j^k, see equation [1.3.44].

The affinity of the reaction:

$$1/2\ O_2(g) \rightarrow O_{(dissolved\ in\ iron)} \qquad [3.2.10a]$$

can be represented by the equation from [KUB 55], seen here in equation [1.3.50]:

$$A = 27{,}930 + 0.62\ T + 4.57\ T \log\{(p_{O2})^{1/2} / f_{\underline{O}}\ .\ [\%O]\}\ (cal) \qquad [3.2.10b]$$

The values of the partial molar free energy ($\Delta G = -A$) of a mole of oxygen solution at 1 atm of pressure in iron at various concentrations are plotted in Figure 3.2.13.

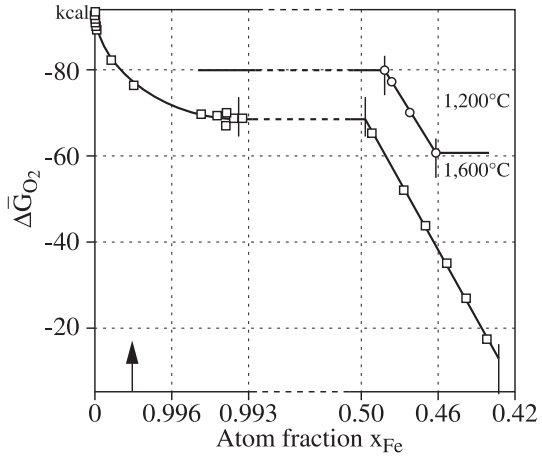

Figure 3.2.13. *Partial molar free energy of a solution of oxygen in liquid and solid iron as a function of the iron concentration [KUB 55]*

$\log f_{\underline{O}(Fe)}$ varies linearly with the oxygen content in liquid iron, almost up to saturation at 1,600°C:

$$\log f_{\underline{O}(Fe)} = -0.20\ (0.10)\ [\%O] \qquad [3.2.11]$$

$\log f_{\underline{O}(Fe)}{}^{k}$ varies linearly with the content of element k dissolved in liquid iron, see Figure 3.2.14. In some publications, the interaction coefficient e^{O}_{O} is equal to zero, which leads to the definition of a new activity coefficient $f'_O = 1$ for %O = 1 and therefore to a new reference potential.

The concentration of oxygen in liquid iron at 1,600°C, as a function of the partial pressure of oxygen, is shown in Figure 3.2.15:

$$\log\{\%\underline{O}_{(Fe)} / (p_{O2})^{1/2}\} = 6{,}127 / T - 0.12 \qquad [3.2.12]$$

The oxygen solubility in liquid iron, in equilibrium with FeO, is equal to 0.23% (in weight) at 1,600°C and increases with temperature:

$$\log \%\underline{O}_{(Fe)(sat)} = -6{,}320 / T + 2.73 \qquad [3.2.13]$$

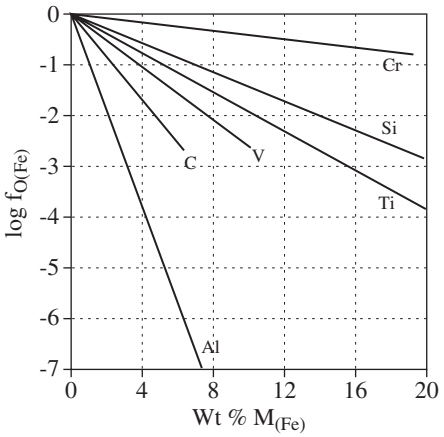

Figure 3.2.14. *Henrian activity coefficient of oxygen $f^k_{O(Fe)}$ in ternary iron alloys, relative to the values in pure iron at 1,600°C, as function of the alloy element concentration ($\log f_C^k = e_C^k$ %k) (see equation [1.3.44]) [BRA 65]*

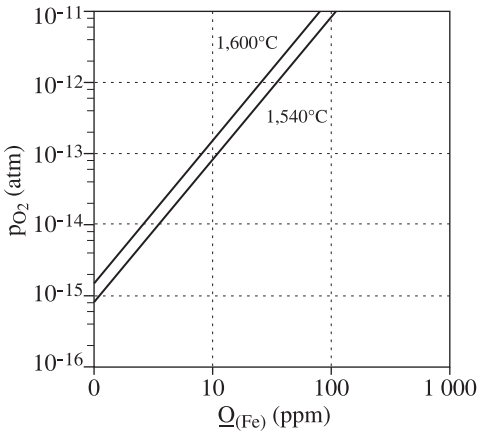

Figure 3.2.15. *Concentration of oxygen in iron at 1,540 and 1,600°C as a function of the oxygen pressure [BRA 65]*

In liquid iron at 1,250 °C, sulfur is miscible up to a content of $x_{S(Fe)} = 50\%$, see Figure 2.2.6. The free energy of solution of a half molecule of sulfur (in the gas state) in liquid iron is given in Table 3.2.2. In Figure 3.2.16, the activity coefficient variations $f_{S(Fe)}^k$ of sulfur are presented as a function of the content of ternary elements in liquid iron.

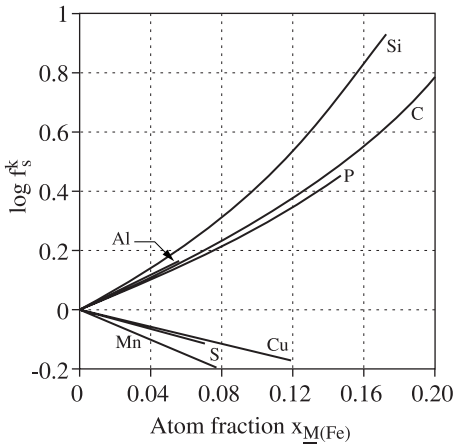

Figure 3.2.16. *Influence of various elements, in liquid iron, on the activity coefficient at 1,600°C of sulfur* $\log f_O^k = e_O^k$ *[%k], see Table 3.2.1 [RIC 74]*

3.2.2.4. *Hydrogen and nitrogen in liquid iron*

The solubilities of both hydrogen and nitrogen in liquid iron at 1,540°C are presented in Figures 3.2.17 and 3.2.18 as a function of their partial pressures. The molar free energies of the solutions are given in Table 3.2.2. The activity coefficients f, f_H and f_N are strongly affected by the presence of alloying elements, as shown in Figures 3.2.19 and 3.2.20.

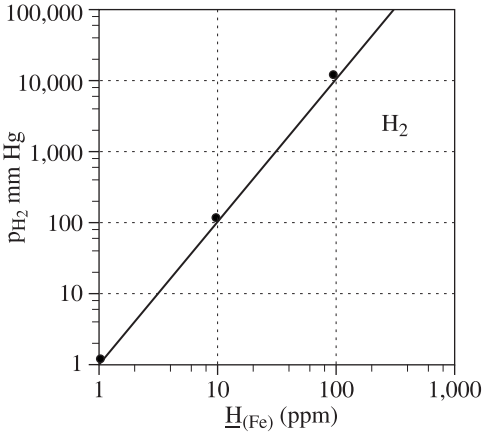

Figure 3.2.17. *Hydrogen concentration in iron at 1,600°C as a function of hydrogen pressure in mmHg [BRA 65]*

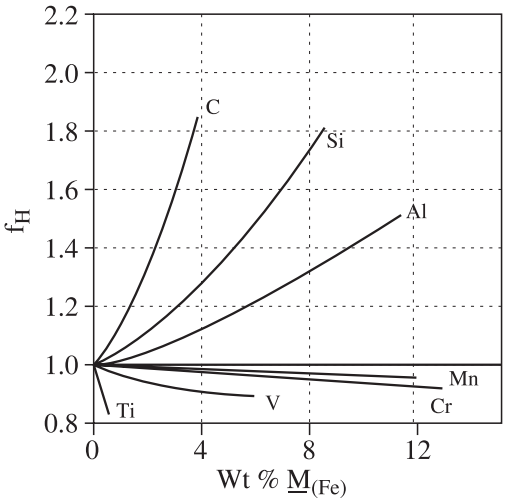

Figure 3.2.18. *Henrian activity coefficient of hydrogen $f_{H(Fe)}$ in ternary iron alloys, relative to the values in pure iron at 1,600°C, as a function of the alloy concentration ($\log f_C^k = e_C^k \%k$), see Table 3.2.3 [BRA 65]*

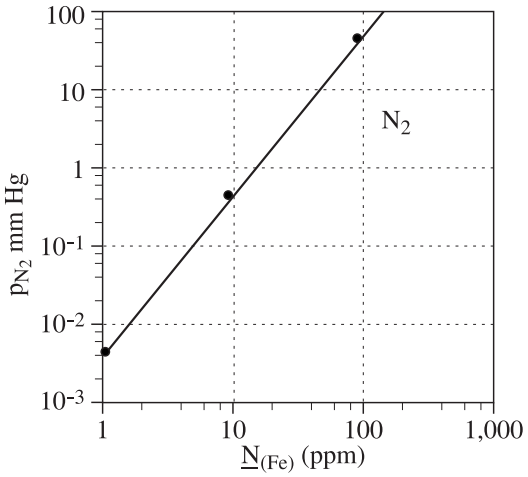

Figure 3.2.19. *Nitrogen concentration in iron at 1,600°C as a function of hydrogen pressure in mmHg [BRA 65]*

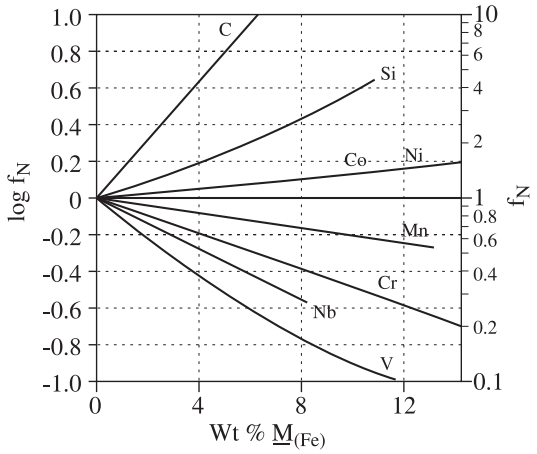

Figure 3.2.20. *Henrian activity coefficient of nitrogen $f_{NFe)}$ in ternary iron alloys relative to the values in pure iron at 1,000°C, as a function of the alloy concentration in wt% ($\log f_C^k = e_C^k$ %k), see Table 3.2.3 [BRA 65]*

3.2.3. *Solubility and precipitation of oxide and sulfide compounds in metals*

The dissolution of elements, such as carbon and oxygen, in liquid iron can lead to the formation of insoluble components by precipitation reactions:

$$\underline{C}_{(Fe)} + \underline{O}_{(Fe)} \rightarrow CO \text{ (gas bubbles)} \qquad [3.2.14]$$

$$\underline{Si}_{(Fe)} + 2\,\underline{O}_{(Fe)} \rightarrow SiO_2(l) \qquad [3.2.15]$$

When the formation of such compounds occurs from the reaction between dissolved elements within the same phase, the transformation is said to be a homogeneous precipitation (see Chapter 5, section 5.3).

Precipitation continues as long as the affinity of the reaction is positive, thus, as long as:

$$\{(a°_A)^{va} \times (a°_B)^{vb}\} > 1/K° \qquad [3.2.16]$$

K° is the equilibrium constant of the reaction whose inverse is called the solubility product (see Chapter 5, equation [5.3.3], and [VIG 11b] Chapter 7, Figures 7.2.2 and 7.2.4).

In Table 3.2.6, the values of the solubility product $K_{ps(1\%)}$ are presented for the oxides, sulfides and nitrides in liquid iron, expressed in terms of the Henrian

activities (f_i . %j; see equation [1.3.41]). For instance, in the case of reaction [3.2.17]:

$$(f_{Si} \,.\, \%\underline{Si}_{(Fe)}) \,.\, (f_O \,.\, \%\underline{O}_{(Fe)})^2 = K_{ps\ (1\%)} \qquad [3.2.17]$$

The solubility product value $K_{(1\%)}$ is obtained from the standard Gibbs free energy of formation of the oxide:

$$-\Delta G^\circ_{f(SiO2)} = 21{,}5400 - 47.73\ T\ (cal/mole)$$

and the standard molar free energies of the solution for both elements:

$$Si(s) \rightarrow Si_{(Fe)} \text{ and } O_2(g) \rightarrow 2O_{(Fe)}$$

Compounds (in the solid state)	*Log $K_{ps(1\%)}$*
Al_2O_3	-62,680 / T + 20.54
MnO	-15,050 / T + 6.70
SiO_2	-31,040 / T + 12
CaO	-25,655 / T + 7.65
MgO	-26,110 / T + 8.24
CaS	-19,980 / T + 5.90
MgS	-13,615 / T + 6.04

Table 3.2.6. *Solubility products for oxides and sulfides in liquid iron [GAT 87]*

3.3. Mattes

3.3.1. *Structure and physical properties of sulfide melts (mattes)*

Mattes are liquid sulfide solutions resulting from the smelting of sulfide ores, concentrates or from different steps of the sulfide conversion (oxidation). Copper and nickel sulfide ores are the most important primary copper and nickel materials. The existence (stability) domain of a matte, at a given temperature, can be more or less expanded around the sulfide stoichiometric compositions.

Mattes are excellent solvents for precious metals: Ag, Au, Pt, etc.

The viscosities of mattes are low – less than or equal to 10 cP.

The specific conductance of mattes range from 150–1,500 ohm^{-1} cm^{-1}. They are higher than those of melted ionic salts (NaCl: 4 ohm^{-1} cm^{-1}) and slags (0.5 ohm^{-1} cm^{-1}). Mattes of FeS, Co_4S_3 and Ni_3S_2 mixtures are electronic conductors. The specific conductance of FeS sulfide is of the same order of magnitude as that of a metal (1,500 ohm^{-1} cm^{-1} at 1,500°C). The specific conductance of Cu_2S sulfide is characteristic of a semiconductor (150 ohm^{-1} cm^{-1} at 1,500°C) and the Cu-S bonds are mainly of covalent character. For some mattes, for instance Sb_2S_3, the conductivity is strongly ionic [RIC 74].

Mattes can dissolve oxygen. The solubility of oxygen in matte Cu_2S is low, see Figure 3.3.9. On the other hand, the solubility of oxygen in a "FeS" matte is high, see Figure 3.3.8.

Mattes can be considered as mixtures of cations embedded in a network of S^{2-} and O^{2-} anions; the anion-cation bond having a certain degree of covalence. Thus, a mixture of Cu_2S,FeS and FeO does not contain the three molecules as such but a mixture of Cu^{+} and Fe^{2+} cations embedded in a network of S^{2-} and O^{2-} anions. The activities of both "sulfides" follow Temkin's law [TEM 45], which assumes a random repartition of both anions and cations on their respective sub-networks.

$$a_{Cu2S} = \{n_{Cu} / (n_{Cu} + n_{Fe})\} \,.\, \{n_S / (n_S + n_O)\} \text{ and}$$

$$a_{FeS} = \{n_{Fe} / (n_{Cu} + n_{Fe})\} \,.\, \{n_S / (n_S + n_O)\}$$

When a matte contains an excess of a metallic species above the stoichiometric composition, this metallic species can be considered as an element in the metallic state. The mattes are made of anions, cations and elements $\{M^{z+}, S^{2-}, M°\}$.

Thermodynamically, mattes can be described by the "standard" activities (see equations [1.3.22] and [1.3.40]) of the "species" of the metals, sulfur and oxygen $a_{\{M\}}°$, $a_{\{S\}}°$ and $a_{\{O\}}°$, in much the same way as the for the oxide (see Chapter 2, section 2.2.1). In a binary M-S matte, both activities can be calculated from the partial pressure of sulfur using the Gibbs-Duhem equation [1.3.52]. The pseudo-activity of sulfide $\hat{a}_{\text{"MexSy"}}$ can be calculated from the species activities by equation [2.3.11]. On either side of the stoichiometric composition, $\hat{a}_{MexSy}$ remains very close to one, see Figure 2.3.3.

For ternary and quaternary Cu-Fe-S and Cu-Fe-S-O mattes, the activities of the {Fe, Cu, S, O} species are calculated by the Gibbs-Duhem equation from the partial pressures of sulfur and oxygen in equilibrium with the matte. These mattes can be also described as being made of "sulfides" and "oxides" (Cu_2S, FeS, FeO, Fe_3O_4), whose activities can be deduced from the activities of the species (Fe, Cu, S, O) thanks to equation [2.3.11].

3.3.2. *Thermodynamic data for the binary Fe-S, Ni-S, Cu-S and Pb-S systems*

Both the Fe-S (see Figure 2.2.6) and Ni-S (see Figure 2.2.8) phase diagrams are similar for the matte liquid state. Between 989 and 1,538°C, the Fe-S matte saturated in iron (point A2) is in equilibrium with γ and the δ iron, in which the solubility of sulfur is low. Below 1,453°C, the Ni-S(l) matte saturated in Ni is in equilibrium with Ni(s). The solubility of sulfur in Ni(s) is close to zero. Above the fusion temperature of iron, sulfur forms a continuous solution with iron in the same manner as with nickel.

Both Fe-S and Ni-S systems present a eutectic at 989°C and 645°C, for a sulfur content of 31.6% and 21.5% (in weight), respectively. The isobar p_{S2} = 1 atm corresponding to a sulfur-saturated matte under a total pressure of 1 atm is drawn on the corresponding phase diagrams. At 1,200°C, under p_{S2} = 1 atm, the FeS matte corresponds to the $Fe_{0,9}S$ composition (point B2).

The Cu-S system (see Figure 2.2.7) presents a miscibility gap between 1,100 and 1,400°C, with a phase rich in copper whose S content varies from 1.33% at 1,200°C to 2% at 1,400°C and a matte phase around the Cu_2S composition. At 1,200°C, under p_{S2} = 1 atm, the matte corresponds to the $Cu_{1,85}S$ composition.

In the Pb-S system (see Figure 2.2.9), between the fusion temperature of lead (327°C) and the fusion temperature of PbS (1,118°C), the solubility of sulfur in the metallic phase strongly increases with temperature. Above 1,118°C, sulfur forms a continuous solution with lead.

In Figures 3.3.1, 3.3.2 and 3.3.3, the curves of variation of the activities of the elements with matte composition (the sulfur's partial pressure log $(p_{S2})^{1/2} = a°_{S(matte)}$) are drawn for the binary systems Fe +S, Cu + S and Pb + S, see equation [1.3.51a] and Figure 2.2.7. The partial pressures of sulfur corresponding to the stoichiometric compositions are $p_{S2} = 10^{-4}$ atm in the case of Cu_2S, $p_{S2} = 10^{-2}$ atm in the case of FeS and $p_{S2} = 10^{-2}$ atm in the case of PbS, respectively.

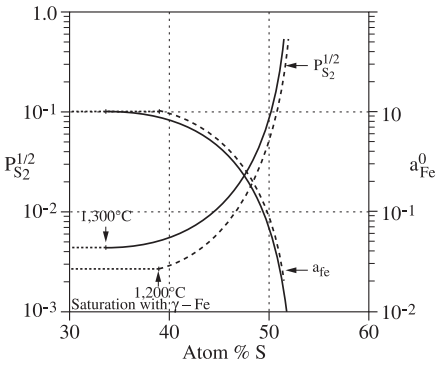

Figure 3.3.1. *Metal and sulfur activities (sulfur partial pressure, see equation [1.3.51a]) for mixtures of Fe+S at 1,200°C (broken lines) and 1,300°C (solid lines), see Table 3.2.2 [RIC 74]*

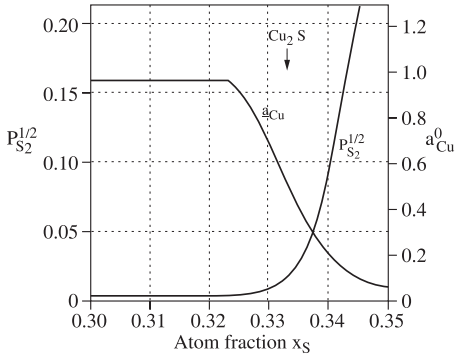

Figure 3.3.2. *Metal and sulfur activities (sulfur partial pressure, see equation [1.3.51a] for mixtures of Cu+S at 1,350°C), see Table 3.2.4 [RIC 74]*

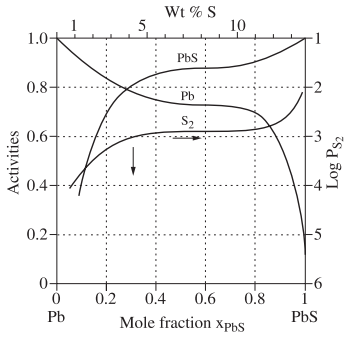

Figure 3.3.3. *Activities of Pb, PbS and sulfur partial pressure p_{S2} for the mixtures of Pb+ S at 1,140°C [WIL 80]*

3.3.3. *Thermodynamic data of ternary mattes*

3.3.3.1. *Fe-Cu-S system*

Figure 3.3.4a shows an isothermal section at 1,200°C of the phase diagram. The presence of three phases has to be noted: the matte, iron and a phase rich in copper, along with two two-phase regions and one three-phase triangle.

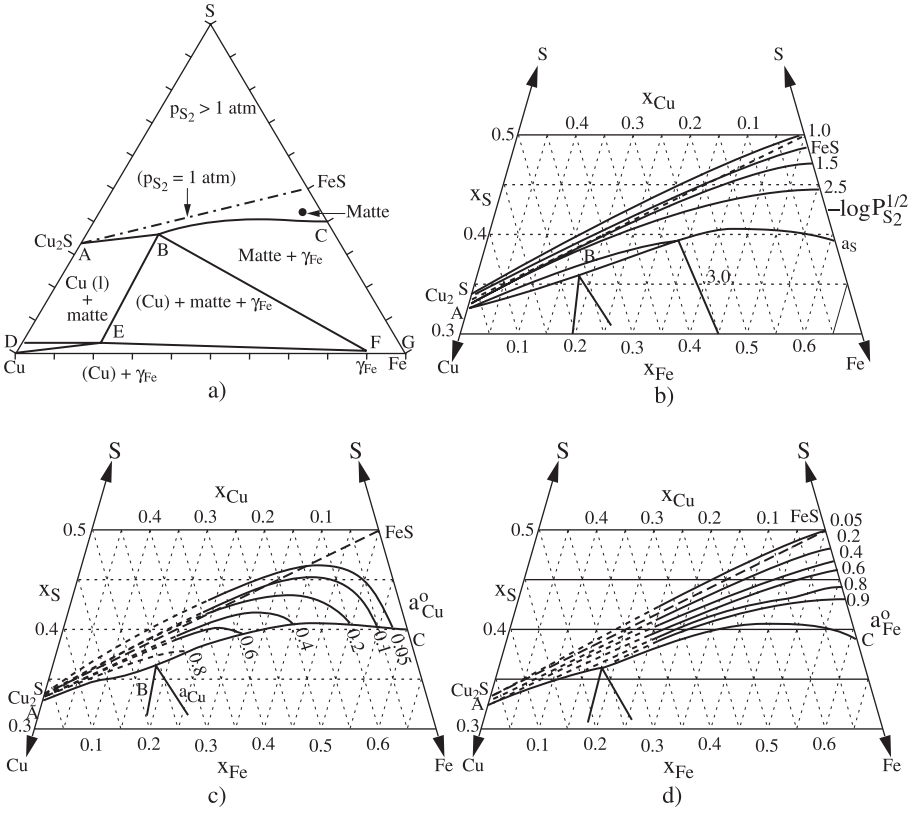

Figure 3.3.4. *Cu-Fe-S system at 1,200°C: a) phase diagram; b, c and d) iso-activity curves of the components [BAL 76]*

The stability region of the matte at 1,200°C is limited by curves AB and BC (matte saturated with {Cu°} and {Fe°}) and by the straight line joining the FeS-Cu_2S compositions (which actually is $Cu_{1.85}S$-$FeS_{1.08}$), which corresponds to the limit of the matte's phase in equilibrium with the gas phase, where the sulfur pressure is equal to 1 atm.

Above this limit, a matte is only stable under pressures $p_{S2} > 1$ atm. The standard isoactivity curves of sulfur, iron and copper are shown in Figures 3.3.4b, c and d.

3.3.3.2. *Fe-Ni-S system*

The stability region of the matte is relatively extended and strongly increases from 1,200–1,400°C (see Figure 3.3.5.a). These mattes can contain high metallic element ({Fe°} and {Ni°}) contents. We can consider that the phase limit, on the sulfur side, corresponds to the line joining the pseudo Ni_3S_2-FeS_1 sulfides, above which a matte is only stable under pressures $p_{S2} > 1$ atm. The iso-activity curves of sulfur, iron and nickle in a matte, at three different temperatures: 1,200, 1,300 and 1,400°C, are shown in Figures 3.3.5b, c and d.

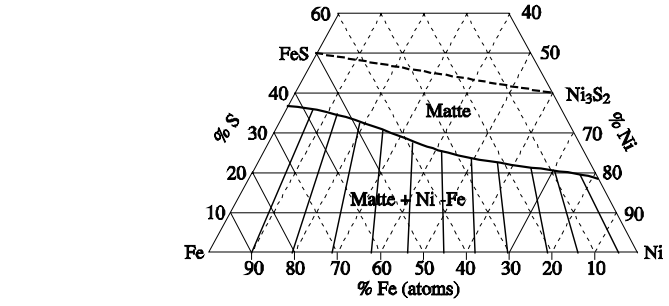

(a)

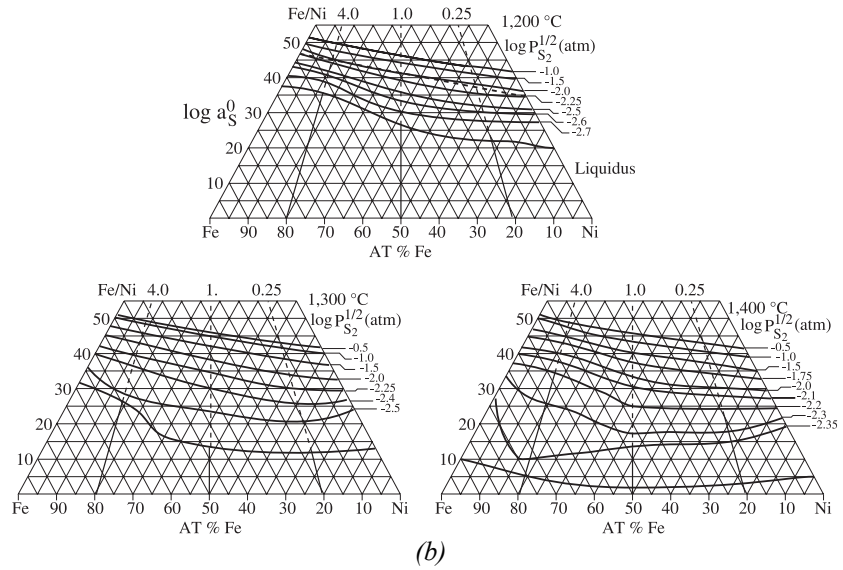

(b)

Figure 3.3.5. *Ni-Fe-S system: a) phase diagram at 1,200°C; and b) sulfur isobars (log a°$_{S(Fe)}$)*

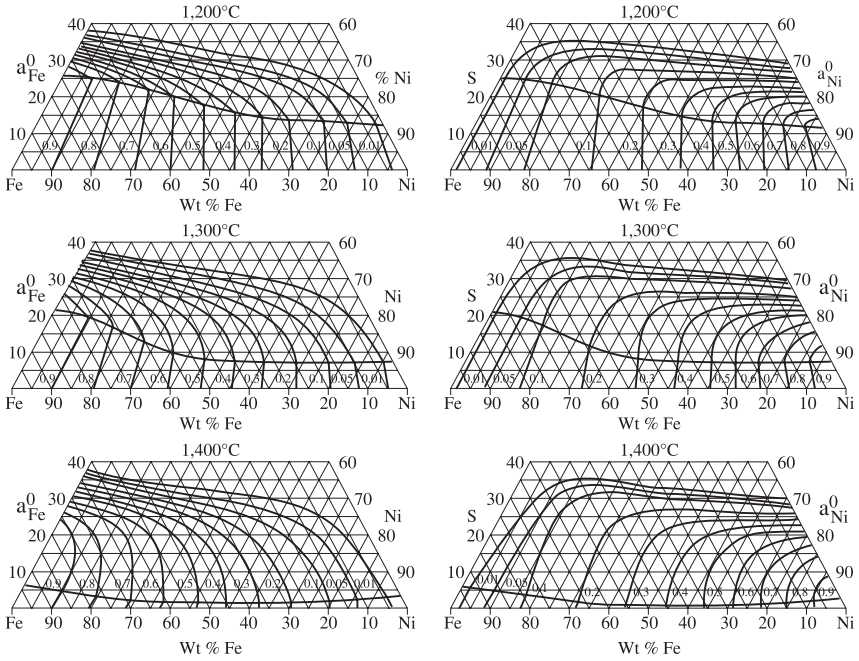

(c)

Figure 3.3.5. *Ni-Fe-S system: c) iso-activity curves of the components at 1,200, 1,300 and 1,400°C [CON 87]*

The mattes produced in the *smelting* processes (see [VIG 11b], Chapter 6, section 6.4, and [VIG 11c], Chapter 7):

– under reducing conditions (in the electric furnace), have compositions close to the saturation limits in metallic elements (*sulfur-deficient matte*);

– under oxidizing conditions (*flash-smelting*), have compositions close to the line joining both $Cu_{1.85}S$-$FeS_{1.08}$ and Ni_3S_2-FeS sulfides.

3.3.4. *Thermodynamic data for M-O-S systems*

In an oxidizing atmosphere during smelting and converting processes (see [VIG 11b], Chapter 6, section 6.4) and when in contact with the oxides produced by these processes, mattes can dissolve a large amount of oxygen. The oxygen content of a binary Fe+S or Cu+S matte or a ternary Cu+Fe+S one, for a given composition, depends on the partial pressures p_{O2} and p_{S2} in the gas phase at equilibrium with the matte.

The thermodynamic data relative to these systems indicating the stability regions of the different phases are graphically represented in the *phase diagrams* as a function of temperature and composition. They are represented in the s*tability diagrams* as a function of partial pressures (p_{O2}-p_{S2}), see Chapter 2, section 2.4.2.

3.3.4.1. *Ni-O-S system*

Three phases coexist in the Ni-O-S system at 1,400°C: the matte (oxisulfide) (l), nickel(s) and the oxide NiO(s), see Figure 3.3.6a. Along the AB line, the matte saturated in oxygen is in equilibrium with the NiO(s) oxide. The oxygen solubility within the matte increases with its sulfur content. Along the AC line, the matte is in equilibrium with Ni(s). At point A, the three phases are in equilibrium. The equilibrium curves of the mattes saturated in oxygen with the NiO oxide (AB) at different temperatures are drawn in Figure 3.3.6b. When the temperature increases, the solubility of oxygen within the matte increases.

The stability diagram (see Figure 3.3.7), shows that at 1,453°C the Ni-S matte forms a continuous solution from the stoichiometric composition Ni_3S_2 to the metal (see Figure 2.2.8). When in contact with an oxidizing gas phase and as long as p_{O2} <10^{-5} atm, the oxidation of sulfide gives metallic Ni (see [VIG 11b], Chapter 6, section 6.6.2):

$$\{Ni_3S_2\} + 2\ O_2(g) \rightarrow 3\ \{Ni°\} + 2\ SO_2 \text{ when } p_{O2} < 10^{-5} \text{ atm}$$

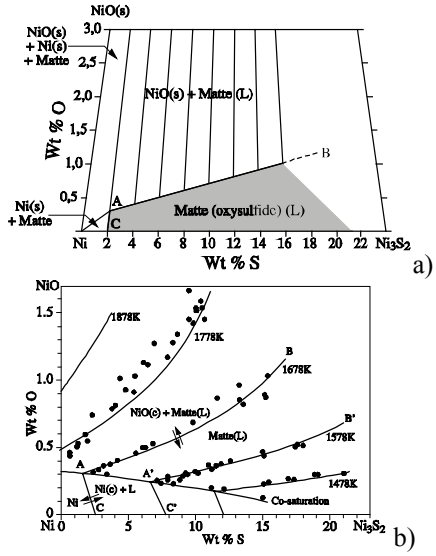

Figure 3.3.6. *Ni-O-S system: a) phase diagram (nickel-rich corner) at 1,400°C [LEN 86]; and b) liquidus projection (isotherms) of the nickel-rich corner [KEL 87]*

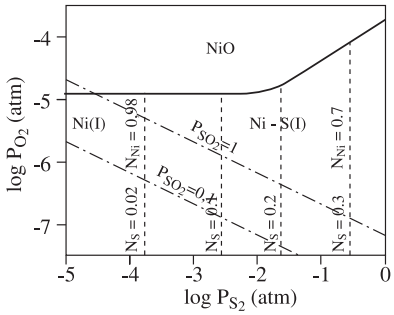

Figure 3.3.7. *Ni-O-S system: predominance diagram at 1,453°C [YAZ 79]*

3.3.4.2. *Fe-O-S system*

The stability region of the Fe-O-S oxisulfide (DEFGH), see Figure 3.3.8a, is totally different from the Ni-O-S oxisulfide one, see Figure 3.3.6. At 1,300°C along the DE curve, the Fe-O-S oxisulfide saturated in {Fe°} is in equilibrium with the Fe_γ. Along EF, the matte is in equilibrium with FeO(s). Along FG, the oxisulfide is in equilibrium with Fe_3O_4(s). The GH line is the phase limit of the matte in equilibrium with a gas phase $p_{SO2} + p_{S2} = 1$ atm. A FeS matte brought into contact with Fe_3O_4(s) will dissolve a certain amount of magnetite. In the oxisulfide in equilibrium with Fe_3O_4(s), along FG, the iron is in the form of Fe^{2+} and Fe^{3+} ions. Depending on the oxygen pressure, when it increases the content in Fe^{3+} ions also increases.

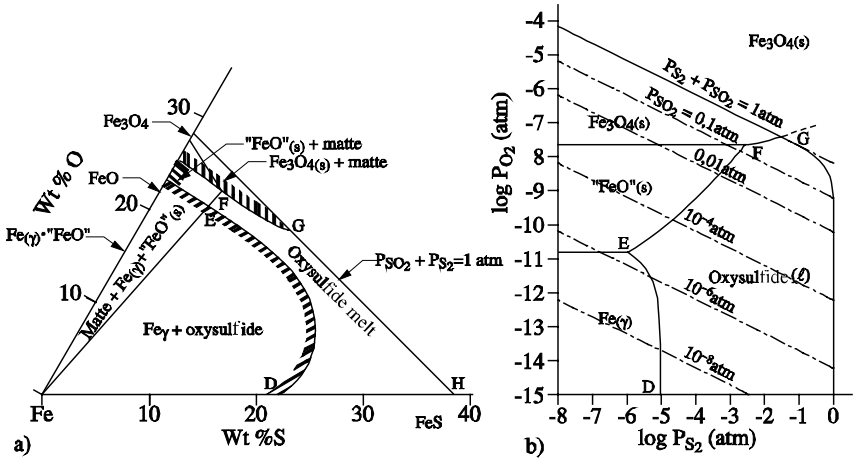

Figures 3.3.8. *Fe-O-S system: a) phase diagram (isotherm); and b) stability diagram at 1,300°C [ELL 76]*

The stability regions of the different phases at 1,300°C as a function of the partial pressures p_{S2} and p_{O2}, are shown in Figure 3.3.8b. Oxisulfide saturated in {Fe°} can only be at equilibrium with the iron γ under an oxygen partial pressure $p_{O2} < 10^{-11}$ atm, corresponding therefore to a highly reducing atmosphere.

3.3.4.3. *Cu-O-S system*

The stability region of the Cu-O-S matte around the Cu_2S composition is very weak (triangle ABC; see Figure 3.3.9a). The maximum solubility of oxygen in the matte in equilibrium with Cu(l) (curve AB) is {%O} =1.35 % (point B). The Cu_2S matte can only coexist with the Cu_2O oxide under partial pressures of $p_{SO2} > 8$ atm. Thus, when a matte Cu_2S is brought into contact with the Cu_2O oxide, an intermediate phase $Cu°_{(metal)}$ will be formed between these two phases, see [VIG 11b], Chapter 6, sections 6.6.1.

The stability diagrams, as a function of p_{S2}-p_{O2} pressures, see Figures 3.2.9 and 3.3.9b, show that at 1,300°C the matte is in equilibrium with the liquid copper when $p_{O2} < 10^{-4}$ atm.

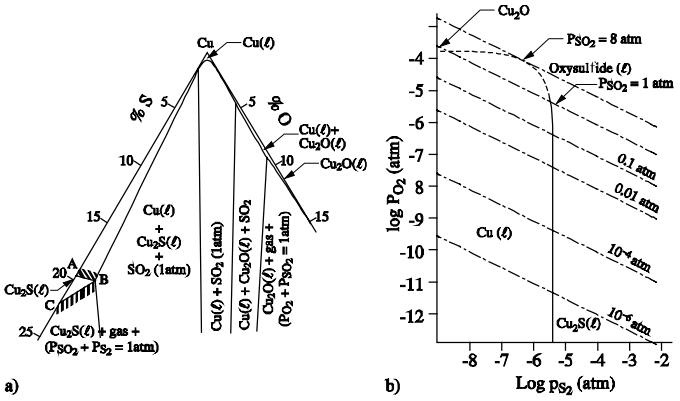

Figure 3.3.9. *Cu-O-S system: a) phase diagram (isotherm); and b) stability diagram at 1,300°C [ELL 76]*

3.3.4.4. *Pb-O-S system*

Above the melting temperature of PbS (1,118°C), the system is composed of two liquid phases: a continuous solution from Pb (metal) to PbS, see Figure 2.2.9, in which the solubility of oxygen is low; and an oxisulfate phase (PbO-$PbSO_4$). The matte at 1,200°C is only stable for oxygen partial pressures at $p_{O2} < 10^{-6}$ atm, see Figure 3.3.10. The sulfur contents, Pb and PbS activities in the matte phase are indicated, see Figure 3.3.3.

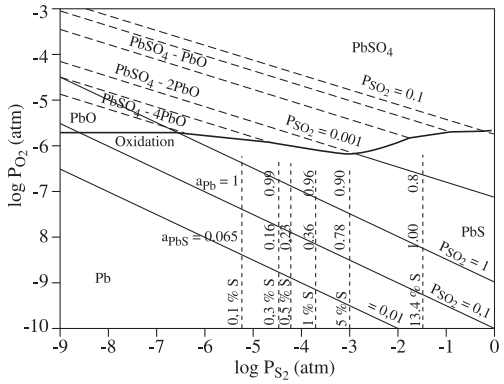

Figure 3.3.10. *Pb-O-S system: stability diagram at 1,200°C [YAZ 79]*

3.3.4.5. *Fe-Cu-O-S system*

The boundaries of the matte field are the saturation surfaces of the matte with various phases: Cu(l), Fe_γ, "FeO"(s) and Fe_3O_4(s) and with a gas phase ($p_{O2} + p_{S2} + p_{SO2} = 1$ atm), see Figure 3.3.11.

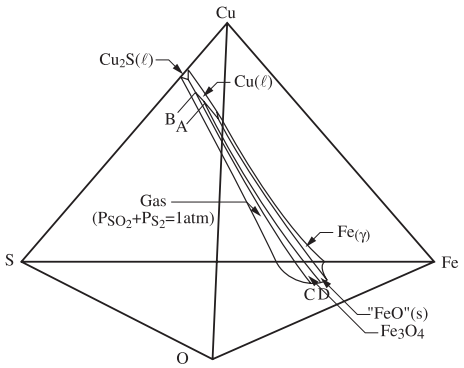

Figure 3.3.11. *The matte phase field at 1,468K. Isothermal tetrahedron of the Fe-Cu-S-O system, 1 atm pressure [KAI 88]*

The oxygen solubility in Cu-Fe-S-O mattes, as a function of the partial pressures p_{O2} and p_{S2} and the relative content in iron, can be represented by the following equations [KAI 86, SOM 95]:

$$\{\%O\} = 2.50\ (p_{O2})^{0.200}\ .\ (p_{S2})^{-0.142}\ (1 + 9.0\ W_{Fe})^{2.19} \text{ at } 1{,}195°C \qquad [3.3.1a]$$

$$\{\%O\} = 2.59\ (p_{O2})^{0.225}\ .\ (p_{S2})^{-0.18}\ (1 + 9.0\ W_{Fe})^{1.86} \text{ at } 1{,}300°C \qquad [3.3.1b]$$

where W_{Fe}: %Fe / (%Fe + %Cu).

These two equations are drawn in Figure 3.3.12 for $p_{O2} = 10^{-8.5}$ and $p_{S2} = 0.0158$ atm. The oxygen content in a Fe-S matte reaches 14% in weight; it strongly decreases as the temperature increases. The oxygen content of mattes saturated in Fe_3O_4 at 1,195°C is function of the iron content of the matte when $p_{S2} < 0.01$ atm, see Figure 3.3.13 [KAI 86]:

$$\%O_{(sat\ Fe3O4)} = 0.14 + 2.39\ W_{Fe} + 12\ W_{Fe}^2 \qquad [3.3.2]$$

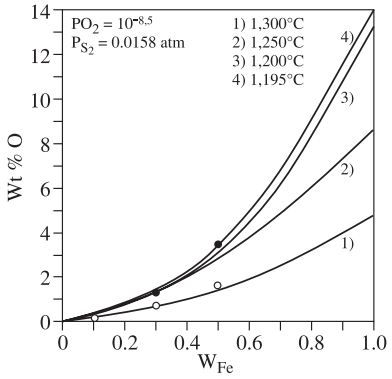

Figure 3.3.12. *Solubility of oxygen in Fe-Cu-S-O mattes at different temperatures under the indicated partial pressures of oxygen and sulfur [SOM 86, SOM 95]*

Both a_{Fe} and a_{Cu} activities have been determined as a function of p_{O2} for different values of $W_{\{Fe\}}$ and of p_{S2}, see Figure 3.3.14. The pseudo-activities of components $\hat{a}_{FeS}$, $\hat{a}_{FeO}$, $\hat{a}_{Fe3O4}$ and $\hat{a}_{Cu2S}$ have been calculated from the activities a_{Fe} and a_{Cu} for different values of $w_{\{Fe\}}$ and of p_{O2}, see Figure 3.3.15.

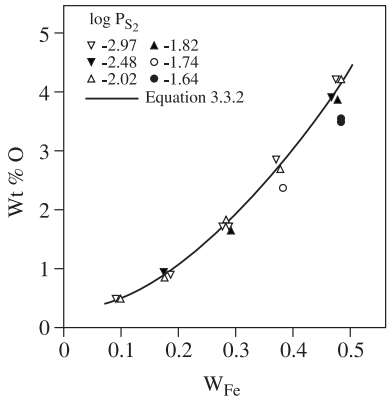

Figure 3.3.13. *Solubility of oxygen within magnetite-saturated Fe-Cu-S-O matte: effect of W_{Fe} and sulfur pressure [KAI 86]*

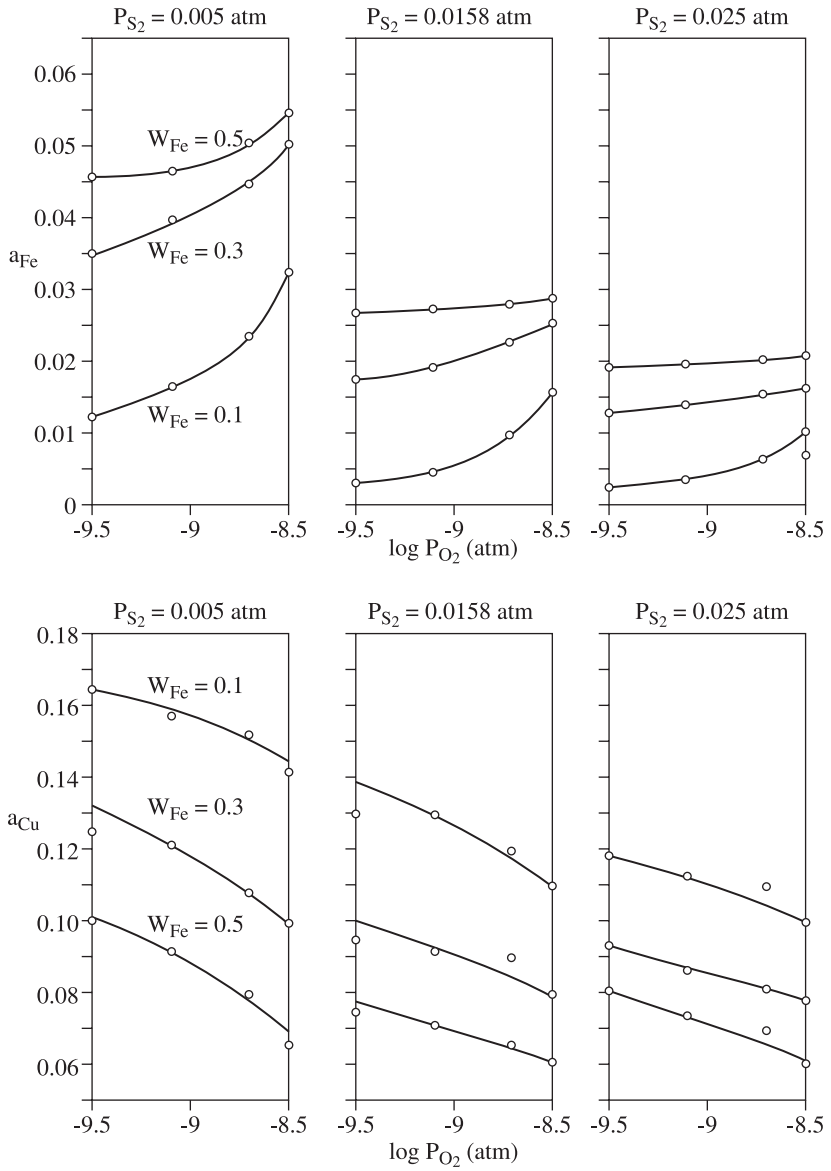

Figure 3.3.14. *Fe-Cu-S-O matte: the Gibbs-Duhem-calculated activities of Fe and Cu as a function of W_{Fe}, p_{O2} and p_{S2} at 1,300°C [SOM 95]*

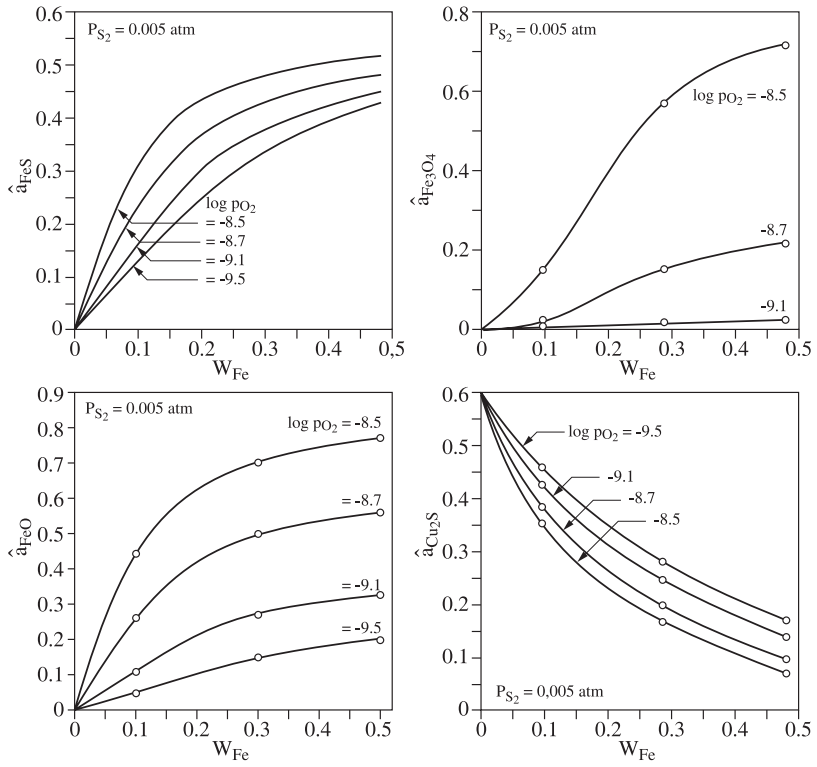

Figure 3.3.15. *Fe-Cu-S-O matte: variations of the pseudo-activities $\hat{a}_{FeS}$, $\hat{a}_{Cu2S}$, $\hat{a}_{FeO}$ and $\hat{a}_{Fe3O4}$ of FeS, FeO, Fe_3O_4 and Cu_2S (see equation [2.3.11]) with W_{Fe} and the oxygen pressure at p_{S2} = 0.005 atm [SOM 95]*

3.4. Slags

3.4.1. *Structure and physical properties*

Slags are molten mixtures of metal oxides and silicates. They are formed in smelting operations where metals are extracted from ores that contain some gangue minerals such as SiO_2, MgO and Al_2O_3. Slags are also formed in matte converting or in the refining of crude metals where they absorb oxidized impurities, such as P_2O_5, MnO or SiO_2. Slags can absorb sulfides (coming from the desulfurization of steels). CaF_2 fluorides are intentionally added to lower the temperature of the slag's liquidus.

Two physical quantities of slags are important for extraction processes: the electric conductibility [PAL 02, RIC 74] and the viscosity [KON 02, SRI 02].

The electric conductibility of slags is important in electro-metallurgical processes: slag reduction in electric furnaces with immerged electrodes, metal refining by the electroslag remelting process (ESR) (see [VIG 11c], Chapter 8, section 8.5.1). The regular composition of an ESR slag is CaF_2 (70%), CaO (15%), Al_2O_3 (15%). There are no industrial electrolysis processes where the electrolyte is a slag.

As slags are always in contact with a second liquid phase − metal or matte − a slag has to be easily separable from this second phase at the end of an operation. The slag at the end of an extraction process must have a low viscosity and low density and remain fluid in a temperature interval that is as extended as possible.

Oxides are compounds whose bonds are partially covalent and partially ionic:

– the oxides SiO_2, GeO_2 and P_2O_5 have bonds with a strongly covalent character, leading to the formation of a three-dimensional network. The viscosity of these oxides is very high, in the order of 10^3–10^5 poises (1 Pa.s = 10 poises), and their specific conductance is very low, in the order of 10^{-5}–10^{-6} ohm^{-1} cm^{-1};

– the oxides CaO, MgO, Al_2O_3 whose bonds have a strongly ionic character, have viscosities of 0.10–0.50 poises and specific conductances >10 ohm^{-1} cm^{-1};

– the FeO, CoO, NiO, Cu_2O, MnO, CuO, V_2O_5 and TiO_2 liquid oxides are electronic conductors (some oxides are semiconductors). The specific conductance of FeO in equilibrium with iron at 1,500°C is equal to 320 ohm^{-1} cm^{-1}.

When oxides such as SiO_2 and CaO are added to oxides such as FeO, the conductibility of the solution decreases and the solution becomes more ionic. For a FeO-SiO_2 mixture where the content of SiO_2 is 10%, the conductibility is 10% ionic and when the SiO_2 content in silica is 34%, the conductibility is 90% ionic. The current efficiency in electrolysis, where the electrolyte would be a mixture of oxides, would thus always be less than one. Electrolytes used for high-temperature electrolysis (alumina electrolysis) are always made of a mixture of alkaline and alkaline earth halides, which ensure total ionic conduction of the current between the electrodes (see Chapter 4, section 4.3).

For slags containing “iron oxide”, “FeO_t”, this “oxide” is present in various oxidation states: FeO and Fe_2O_3; or as ions Fe^{2+}, Fe^{3+}, and O^{2-}. Their respective quantities vary with the partial pressure of oxygen in the gas phase in equilibrium with the liquid phase.

Despite the complexity of the structure of these liquid oxides, following Temkin’s theory [TEM 45] we can consider these solutions as being made up of only charged ions:

– the basic oxides (CaO, MgO, MnO, FeO) are present as cations R^{2+}. They supply O^{2-} ions:

$$CaO \rightarrow Ca^{2+} + O^{2-}$$

– the acid oxides are present as anions, having various coordination numbers for oxygen:

$$SiO_2 \rightarrow [SiO_4]^{4-}, [Si_2O_7]^{6-}; P_2O_5 \rightarrow [PO_4]^{3-}; Al_20_3 \rightarrow [AlO_4]^{5-}$$

They consume O^{2-} ions:

$$(SiO_2) + 2\ (O^{2-}) \rightarrow ([SiO_4]^{4-})$$

They are present in the liquid phase as complex tetrahedral anions, where Si is at the center of the tetrahedron and O on the four summits. These tetrahedrons form long aluminosilicate chains whose length depends on the O^{2-} ion content of the solution. When a basic oxide such as CaO or FeO is added to a silicate melt, the bond between the oxygen atom, common to two tetrahedrons and the two adjacent silicon atoms, is broken to form smaller tetrahedral units, such as, for instance:

$$([Si_2O_7]^{6-}) + (O^{2-}) \rightarrow 2\ ([SiO_4]^{4-})$$

$$([P_2O_7]^{4-}) + (O^{2-}) \rightarrow 2\ ([PO_4]^{3-})$$

The concentration of these different anions depends strongly upon the nature of the cation. In the presence of Ca^{2+}, the previous equilibrium is displaced to the right and the concentration of (O^{2-}) ions is low. In the presence of Fe^{2+}, the equilibrium is displaced to the left and the concentration of (O^{2-}) ions is high (see below), in accordance with the fact that the Ca_2SiO_4 compound is a lot more stable than Fe_2SiO_4.

Some oxides are amphoteric. In the case of Al_2O_3, Al^{3+} is stable in an acid slag and $[AlO_4]^{5-}$ is stable in a basic slag, the predominant species depending on the content in O^{2-} ions in the solution:

$$(Al^{3+}) + 4\ (O^{2-}) \rightarrow ([AlO_4]^{5-}).$$

The basicity is defined as:

$$B = \log a_{O^{2-}} \qquad [3.4.1a]$$

As the activity of the oxygen ion $a_{O^{2-}}$ cannot be measured, the basicity is defined by the ratio:

$$i = (CaO + xMgO) / (SiO_2 + yAl_2O_3 + zP_2O_5) \qquad [3.4.1b]$$

in number of moles, where x varies from 1 to 1.4, y from 0.6 to 1 and z is of the order 0.84.

A high basicity index indicates the presence of free lime available for fixing acid oxides and for a basicity index equal to one. The slag is made of long polymeric chains.

The viscosity of a slag depends on the temperature and on its composition, especially on the length of aluminosilicate chains and thus on the basicity of the slag. In a ternary system such as CaO-Al_2O_3-SiO_2 at 1,450°C (see Figure 3.4.1a), the viscosity varies from 5 poises (1 poise = 0.1 Pa.s) for slags rich in CaO to 10,000 poises for slags rich in SiO_2, even though the existence region of the slag at this temperature is low (see Figure 3.4.2).

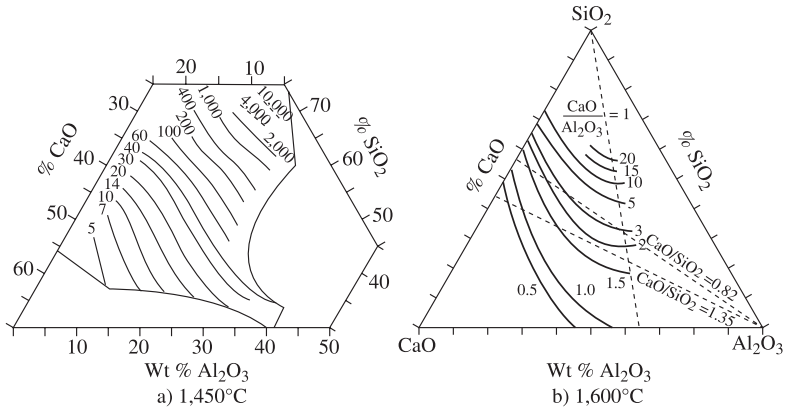

Figures 3.4.1. *Viscosity in poises (1 poise = 0.1Pa.s) for SiO_2-CaO-Al_2O_3 slags: a) at 1,450°C (see the hatched area of Figure 3.4.2); and b) at 1,600°C [MAC 48, ROS 83]*

At 1,600°C, see Figure 3.4.1b, where the liquid phase region is much larger, see Figure 3.4.2, the viscosity varies from 0.5−20 poises.

The viscosity should decrease with the slag's basicity, since the length of the polymeric chains decreases. The variation as a function of the basicity is, however, more complex. The addition of calcium fluoride, CaF_2, to silicate melts, more or less strongly lowers the liquidus temperature and the viscosity of slags, depending on their basicity. The effect of CaF_2 is due to the decrease in the degree of polymerization of the chains by the F^- ion, which presents a similar effect to that involving the O^{2-} ion.

3.4.2. *Phase diagrams and activities*

Phase diagrams (binary, ternary or pseudo-ternary)[1] of oxides [CHA 81, MUA 65, OSB 60, SLA 95] show the existence of a large number of crystalline structures in the solid state, and a liquid phase that often presents a small domain, even at the temperatures of metallurgical processes.

Different models of slags have been developed in order to evaluate the physical (viscosity) and the thermodynamic (phase diagrams and activities) properties of complex slags[2]. Some of these models are based on a structural representation of slags, with anionic and cationic sub-networks.

In the cellular model the structure is described in terms of cells [LEH 98]. A cell is made of a central anion, two peripheral cations and six peripheral anions. This structural representation does not take into account the polymeric structure of these slags. To give an idea of what these models are, we present, in a simplistic manner, a model that was developed in 1945 by Temkin [TEM 45].

This model considers that slags are ideal ionic solutions and defines the activity of the components of a slag as the product of the ionic fractions of these components. For example, the activity of ferrous oxide in a slag is expressed as $a_{(FeO)} = x_{Fe2+} . x_{02-}$, where the ionic fractions of iron and oxygen are the fractions of these ions referred to the total number of ions of the same sign.

The definition of separate cationic and anionic fractions is equivalent to the adoption of a model for the liquid slag of two independent anion and cation lattices on each of which ions of the same sign are randomly arranged. For the activities of the components of a slag, we can define several activities:

– the activities of the elements: oxygen and metal (even though these species are not physically present in the slags)(see equation [2.3.9]);

– the standard activities of the "oxides" referred to their standard potential (see equations [1.3.22] and [1.3.40]) and the pseudo-activities for some oxides (see equations [2.3.11] and [3.4.3]).

Below we present the thermodynamic features of ternary and pseudo-ternary systems that constitute the main slag families. There are two different types of slags: the slags with oxides that cannot easily be reduced (CaO, MgO, SiO_2 and Al_2O_3);

---

1 More information can be obtained from Chapter 1, section 1.4 and Figures 1.4.1, 1.4.2 and 1.4.3 regarding the main features of ternary diagrams.

2 A review of the thermodynamic models can be found in [LI 98]. A synthetic presentation of one of these models – the cellular model – with references quoting other models, can be found in [LEH 98]

and the slags with easily reducible oxides with several oxidation states (FeO-Fe_2O_3/MnO-Mn_3O_4/CrO-Cr_2O_3).

3.4.3. *Phase diagrams and activities of oxide mixtures forming the basis of metallurgical slags CaO-SiO_2-Al_2O_3-MgO*

3.4.3.1. *The CaO-SiO_2-Al_2O_3 system*

Figure 3.4.2 shows, for the ternary system that is the basis of many metallurgical slags, the phase diagram with the *liquidus valleys* and *liquidus isotherms* indicating the liquid phase area at the corresponding temperature. The liquid phase area is small at 1,400°C and relatively large at 1,600°C, see Figure 3.4.3.

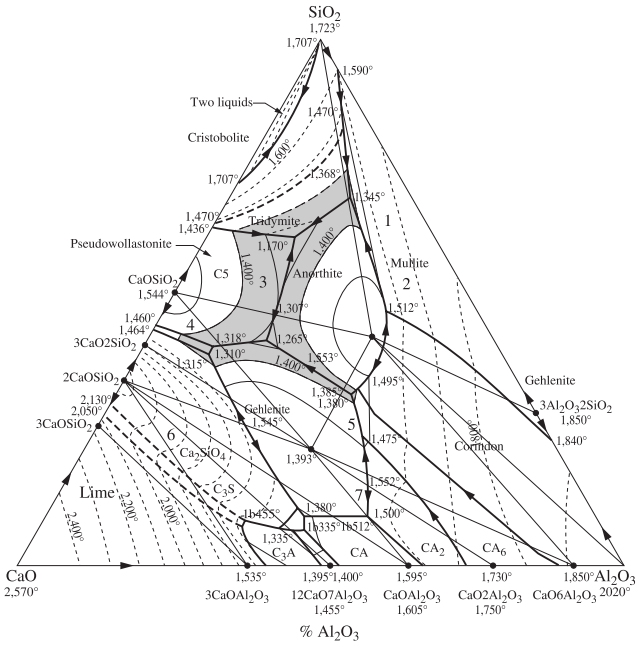

Figure 3.4.2. *SiO_2-CaO-Al_2O_3 system: equilibrium diagram (projection). Continuous lines: valleys (boundary lines that separate the primary phase fields); broken lines: liquidus isotherms (temperature contours of the liquidus surfaces); shadowed area: liquid phase area at 1,400°C [CHA 81, MUA 65]*

As these three oxides present each only one oxidation state, the diagram does not depend on the oxygen pressure (in the gas phase) in contact with the slag. The iso-activities curves of the three oxides in the liquid phase at 1,550°C are shown in

Figures 3.4.3a and b. The silica activity, for low contents in silica, in a CaO-Al_2O_3 mixture is very low (in the order of 5.10^{-5}). The deoxidation of steel by silicon in the presence of this slag according to the reaction $\{Si_{(Fe)} + O_{(Fe)} \rightarrow SiO_2(l)\}$ can be very strong, see equation [3.2.15] and [VIG 11b], Chapter 7, section 7.2.3.

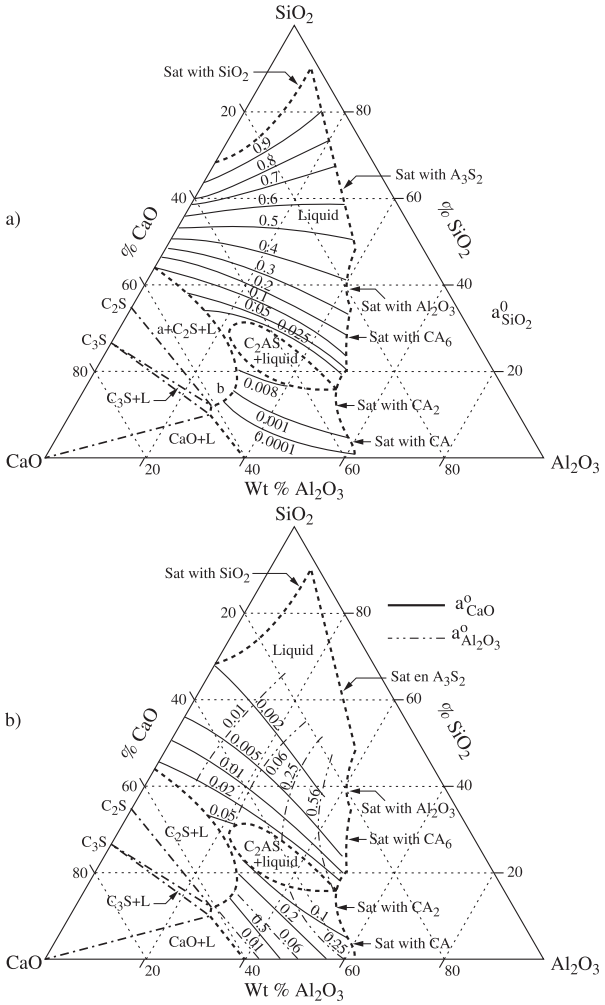

Figure 3.4.3. *SiO_2-CaO-Al_2O_3 system: isoactivity curves (continuous lines) in the liquid phase (broken lines) at 1,550°C: a) $a°_{SiO2}$; and b) $a°_{CaO}$; $a°_{Al2O3}$ (standard states: solid state) [REI 65, RIS 74a]*

3.4.3.2. *MgO-SiO_2-Al_2O_3 system*

This constitutes the base of slags in the smelting reduction of ferrochrome ores in the electric furnace. The small area of the liquid phase at 1,600°C compared to the area of the previous system has to be noted, see Figure 3.4.4. The basic composition of the slag is: SiO_2 (40%), MgO (35%), Al_2O_3 (15%) and CaO (10%) in molar percent, see [VIG 11c], Chapter 8, section 8.4.5.

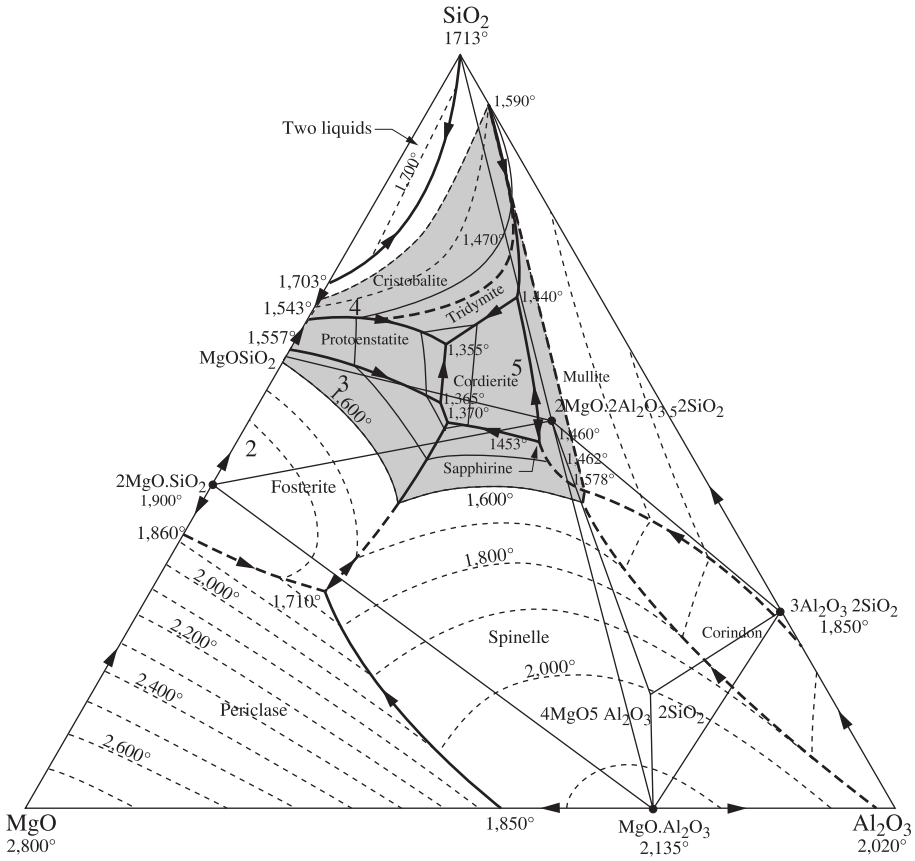

Figure 3.4.4. *MgO-SiO_2-Al_2O_3 system, phase diagram (projection) continuous lines: valleys, broken lines: liquidus isotherms [CHA 81]*

3.4.3.3. *CaO-SiO_2-MgO-Al_2O_3 system*

For slags of the quaternary CaO-SiO_2-MgO-Al_2O_3 system, the liquid phase area at a given temperature are shown in planar projections of the pseudo-ternary CaO-

SiO_2-Al_2O_3 diagram for a given MgO content (see Figure 3.4.5) and of the pseudo-ternary CaO-SiO_2-MgO diagram for Al_2O_3 contents of 10% (see Figure 3.4.6).

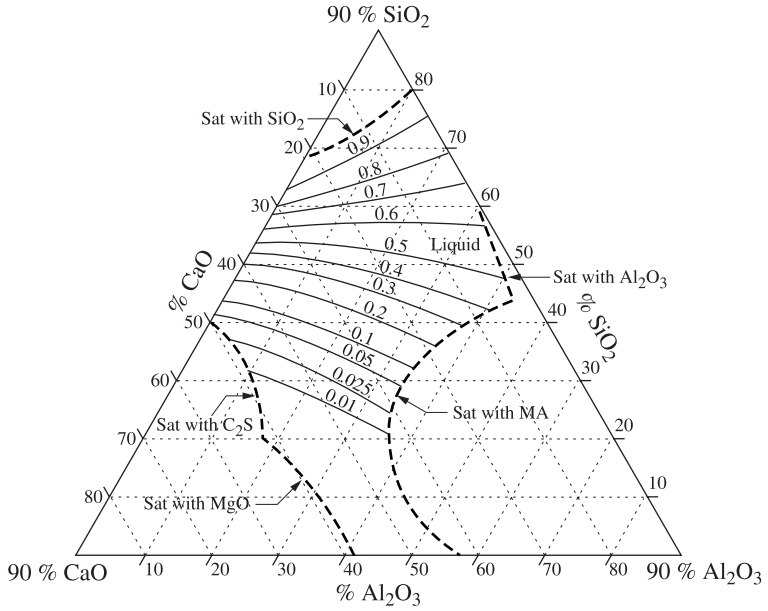

Figure 3.4.5. *Activity of SiO_2 in the system CaO-Al_2O_3-SiO_2-MgO (10%) at 1,600°C [REI 65 p223, RIS 74a]*

The desulfurizing slag in the steel refining operation in a laddle has the composition: CaO (50−60 %), SiO_2 (5−15%), Al_2O_3 (20−30%) and MgO (5−10%) close to saturation in MgO (see Figure 3.4.5). The slag has to be very basic and it should not contain any easily reducible oxide susceptible, by reduction, to enriching the metal in oxygen. Its oxidative power must be very weak. This slag also has to be liquid at the refining temperatures, thus above 1,550°C. For this composition, the sulfur partition coefficient, see [VIG 11b], Chapter 7, Figures 7.2.5 and 7.2.6, can reach 1,000. This supposes perfect control of the composition of the slag during this operation.

The blast furnaces slags have the average composition: CaO (42.5%), SiO_2 (35.5%), Al_2O_3 (10.5%) and MgO (7.5 %), see Figure 3.4.6 and [VIG 11c], Chapter 4, Table 4.2.1a. They absorb the stable oxides (non-reducible by carbon monoxide at these temperatures) coming from the ore's gangue and the combustion ashes of coke. This slag has to be liquid at pouring temperatures of hot metal, thus at 1,400°C. The slag liquid phase area at this temperature is relatively small. Its viscosity is around 100 times higher than the viscosity of hot metal.

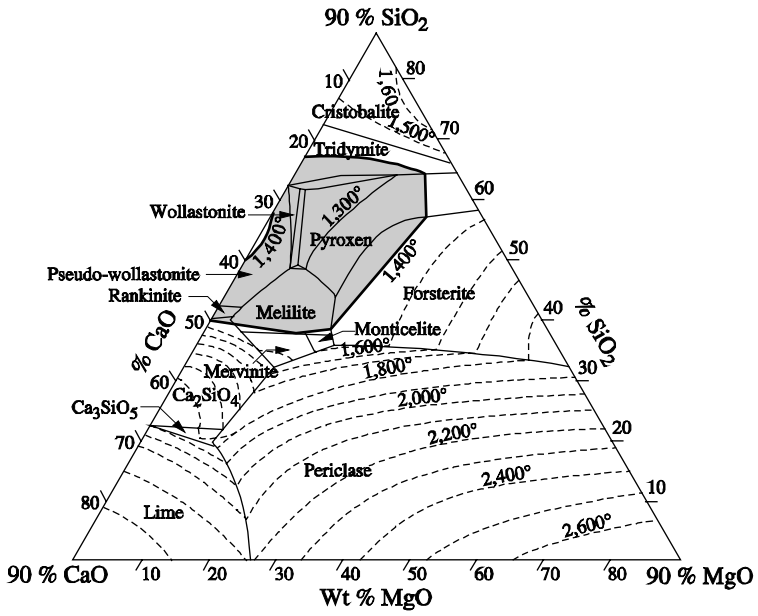

Figure 3.4.6. *SiO_2-CaO-MgO-Al_2O_3 (10%) system phase diagram: valleys – thin continuous lines); liquidus isotherms – broken lines; shadowed area – liquid blast furnace slag at 1,400°C [STE 94]*

During the smelting reduction operation of magnesia by silicon (Magnetherm process, see [VIG 11c], Chapter 5, section 5.4), the slag composition is maintained in a narrow range: CaO (57–60%), SiO_2 (25%), Al_2O_3 (11–15%) and MgO (4–6%). Between 1,550 and 1,650°C the slag is not entirely liquid, with 40% being solid bicalcium silicate (2 CaO-SiO_2). The composition of the liquid phase is located at the limit between the bicalcium silicate and the solid magnesia and is thus saturated in MgO. The magnesia activity in the slag is equal to one.

3.4.4. *Phase diagrams and activities of mixtures of CaO-SiO_2 -Al_2O_3-MgO oxides and reducible (iron, manganese and chrome) oxides*

Iron, manganese, chrome and titanium oxides are present in slags under different oxidation states with variable proportions, depending on the oxidizing or reducing conditions the slags are submitted to and on the basic composition of the slag (SiO_2, CaO, Al_2O_3). These slags can be thermodynamically described, either as being composed of the species CaO, SiO_2, O and Fe, or the species CaO, SiO_2, Fe^{2+}, Fe^{3+} and O^{2-}, or as being composed of compounds CaO-SiO_2-FeO-Fe_2O_3 (or Fe_3O_4), and the same for manganese and chrome oxides.

We remind ourselves here that, in such a slag:

– on the one hand, the contents in $Fe^{2+}$and Fe^{3+} ions can be experimentally determined. For instance, at a given temperature, in the case of a CaO-iron oxide slag in contact with different oxidizing and reducing gas atmospheres or in contact with iron, the variations of the $Fe^{3+}/(Fe^{2+} + Fe^{3+})$ ratio are shown in Figure 3.4.7.

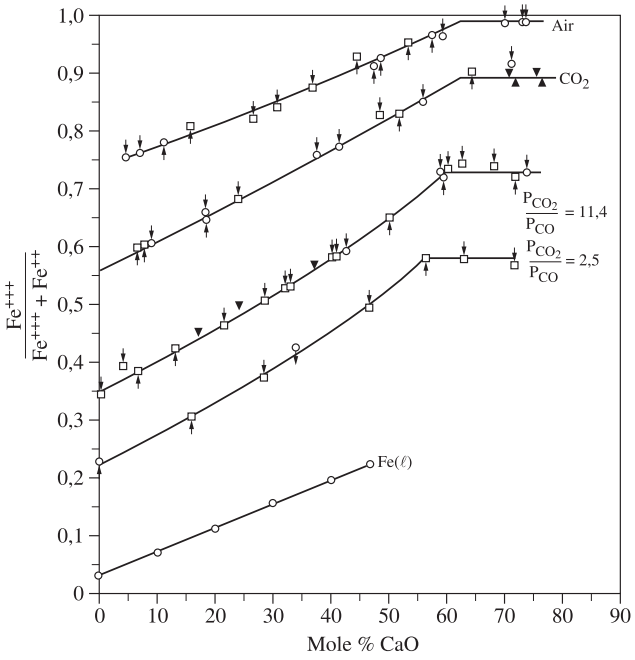

Figure 3.4.7. *Lime-iron oxide slags at 1,550°C: variations of the ratio of ferric iron to total iron $Fe^{3+}/(Fe^{3+}+Fe^{2+})$, with CaO content in the ternary CaO-FeO-Fe_2O_3 system at 1,550°C under the following atmospheres: air, CO_2, CO_2/CO = 11.4 and 2.50 [LAR 54]*

– on the other hand, by considering that slags are composed of the species CaO, SiO_2, O and Fe, the "standard" activity of oxygen $a°_O$ can be determined (see equations [1.3.51a] and [2.2.1])[3] by:

$$a°_O = (p_{O2})^{1/2} \qquad [3.4.2]$$

With the Gibbs-Duhem equation (see equation [1.3.52]), the $a°_{Fe}$ activity is calculated. Following this, the pseudo-activity $\hat{a}_{FeO}$ (see equations [2.3.11] and [2.3.13]) is calculated by:

$$\hat{a}_{FeO} = K°_{(FeO)} \cdot a°_{Fe} \cdot a°_O \qquad [3.4.3a]$$

3 For the calculation of the activities, see Turkdogan [TUR 61] and Larson [LAR 54].

the reference state being the oxide at equilibrium with the liquid iron. Likewise the pseudo-activities $\hat{a}_{Fe2O3}$ or $\hat{a}_{Fe3O4}$ can be calculated by:

$$\hat{a}_{Fe2O3} = K°_{(FexOx)} (a°_O)^3 . (a°_{Fe})^2 \qquad [3.4.3b]$$

the reference state being the stoichiometric oxide Fe_2O_3 (in solid state) where $\Delta G°_{Fe2O3}$ is the Gibbs free energy of formation of the stoichiometric oxide Fe_2O_3.

In the FeO-Fe_2O_3 phase diagram (see Chapter 2, Figure 2.2.10), the oxygen isobars are drawn (oxygen partial pressures in the gas phase in equilibrium with the liquid phase). The variations of the pseudo-activities $\hat{a}_{FeO}$ and $\hat{a}_{Fe2O3}$ at 1,550°C are shown in Figure 3.4.8.

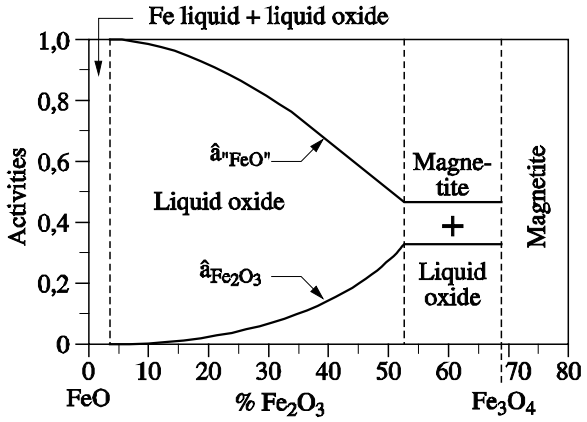

Figure 3.4.8. *Pseudo-activities $\hat{a}_{FeO}$ and $\hat{a}_{Fe2O3}$ in the Fe-O system at 1,550°C (standard states: "FeO" liquid in equilibrium with liquid Fe; solid Fe_2O_3) [RIS 74a]*

3.4.4.1. *SiO_2-iron oxide and CaO-iron oxide systems*

The smelting slags of iron and copper sulfide concentrates and the converting slags of Cu-Fe-S mattes are SiO_2- or CaO-based slags (see [VIG 11b], Chapter 6 and [VIG 11c], Chapter 7). These processes at 1,200–1,300°C produce iron oxides that are absorbed by the slag. In both ternary SiO_2-FeO-Fe_2O_3 and CaO-FeO-Fe_2O_3 phase diagrams, see Figures 3.4.9 and 3.4.10, the liquidus valleys (solid lines), liquidus isotherms, oxygen isobars and oxide activities are plotted[4].

4 Even though these two diagrams are oxide diagrams, the presence of a biphasic domain where one of the phases is the liquid iron saturated in oxygen, and the other one is the oxide "FeO" has to be noted. This comes from the fact that the "FeO" oxide only exists for the ratios where O/Fe > 1, as shown by the binary diagram (see Figure 2.10).

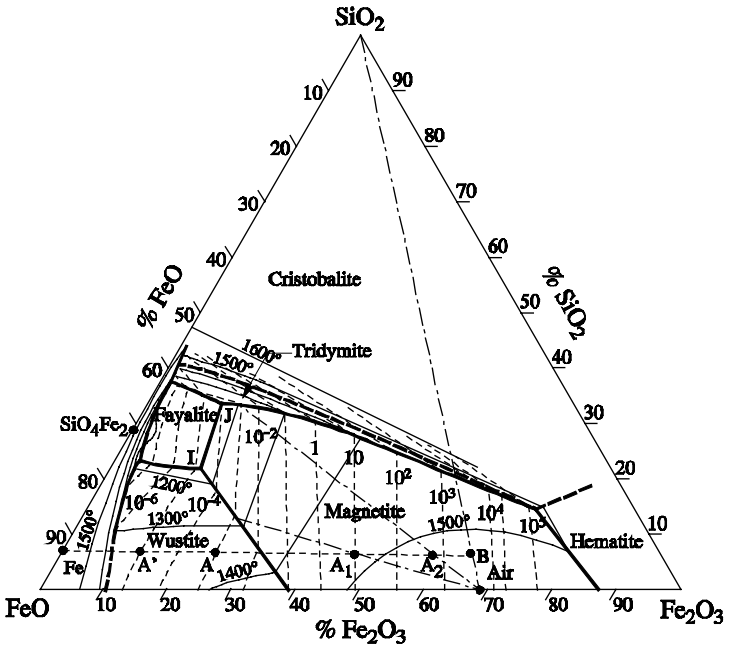

Figure 3.4.9a. *SiO_2-FeO-Fe_2O_3 system: phase diagram (projection), thick continuous lines: valleys; thin continuous lines: liquidus isotherms; broken lines: oxygen isobars p_{O2} [CHA 81,OSB 60]*

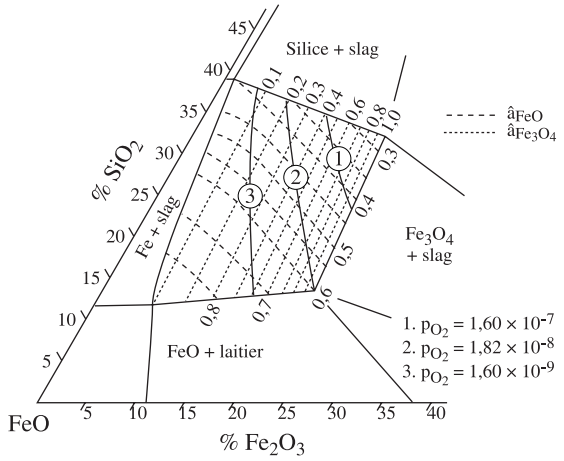

Figure 3.4.9b. *SiO_2-FeO-Fe_2O_3 system: pseudo-activities $\hat{a}_{FeO}$ and $\hat{a}_{Fe3O4}$ and oxygen potentials at 1,300°C. [KOR 62, ROS 83]*

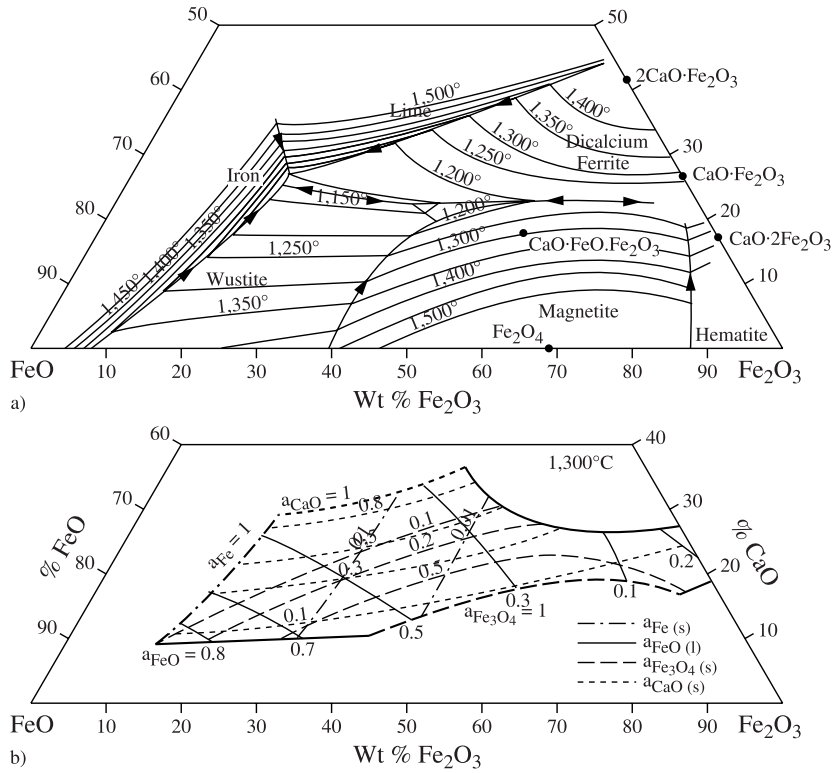

Figure 3.4.10. *CaO-FeO-Fe_2O_3 system: a) phase diagram (projection): valleys – thick continuous lines; and liquidus isotherms – thin continuous lines; and b) activities of Fe, FeO, Fe_3O_4, CaO at 1,300°C [YAZ 81]*

For the SiO_2-Fe_tO-Fe_2O_3 system, the liquid phase region at 1,300 °C is small (see Figure 3.4.11). Near fayalite (FeO-SiO_2), the iron oxide is mainly as $FeO(Fe^{2+})$. Along mc, the slag is saturated with silica, along ci, the slag is saturated with magnetite, along mk, the slag is saturated with iron. As soon as $p_{O2} > 10^{-6}$ atm, solid magnetite is formed.

For the CaO-FeO-Fe_2O_3 system (see Figure 3.4.11), the liquid phase region is larger. Under oxidizing conditions, the iron oxide is mainly as Fe_3O_4. Along OR, the slag is saturated with CaO, along RR', the slag is saturated with 3 CaO-Fe_2O_3, along ZV, the slag is saturated with magnetite and along VP, the slag is saturated with wüstite (FeO), along PO, the slag is saturated with iron.

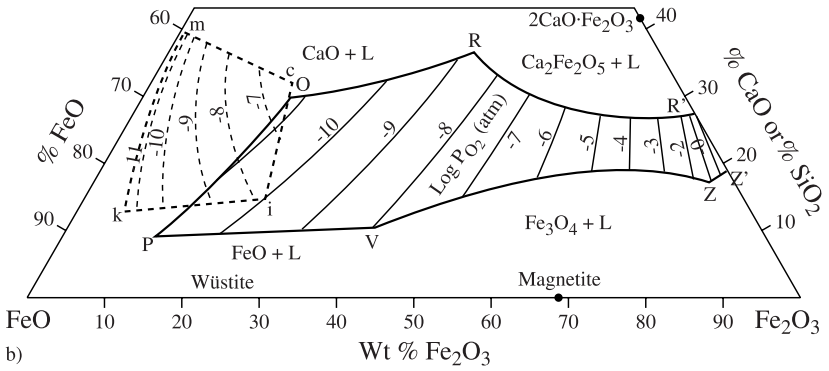

Figure 3.4.11. *Liquidus isotherm (liquid area) and oxygen isobars at 1,300°C for the FeO-Fe_2O_3-CaO (continuous lines) and the FeO-Fe_2O_3-SiO_2 (broken lines) systems [YAZ 81]*

The oxygen isobars and activities $\hat{a}_{"FeO}$ and a_{CaO} of the CaO-FeO-Fe_2O_3 system at 1,550°C are shown in Figures 3.4.12a and b.

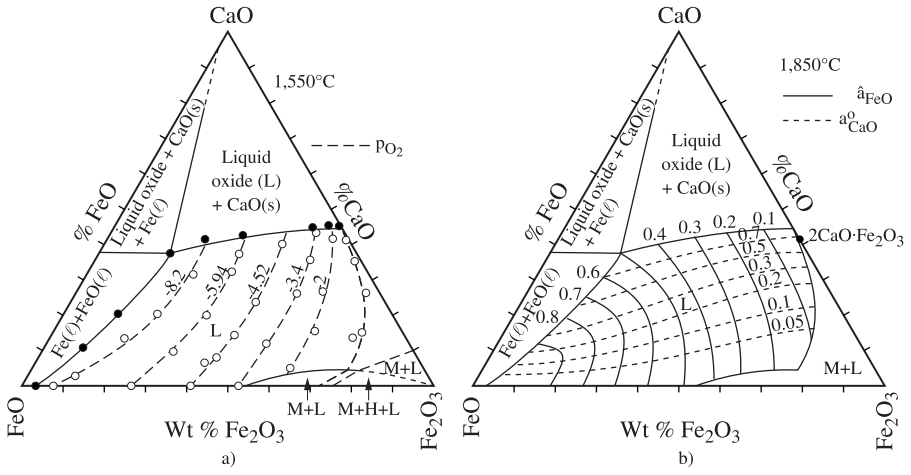

Figure 3.4.12. *CaO-FeO-Fe_2O_3 system: a) isothermal phase diagram and oxygen isobars; and b) activities $\hat{a}_{"FeO"}$ and a_{CaO}. at 1,550°C [TIM 70]*

3.4.4.2. *CaO-SiO_2-iron oxides system*

In steel converting, CaO-SiO_2 basic slags are either in contact with an oxidizing gas phase or with a metallic phase rich in iron. In reduction-smelting processes, the slags are in contact with a reducing gas phase and a metallic phase.

The systems considered to describe the slags are the $CaO\text{-}SiO_2\text{-}Fe_2O_3$ system for slags in contact with an oxidizing gas phase (see Figure 3.4.13) and the $CaO\text{-}SiO_2\text{-}FeO$ system (see Figure 3.4.14) for slags in contact with a metallic phase. For these slags at 1,550°C for low iron oxide contents, the Fe^{3+} content is low (see Figure 3.4.15). The system can thus be considered to mainly be made up of FeO (Fe^{2+}), see Figure 3.4.7.

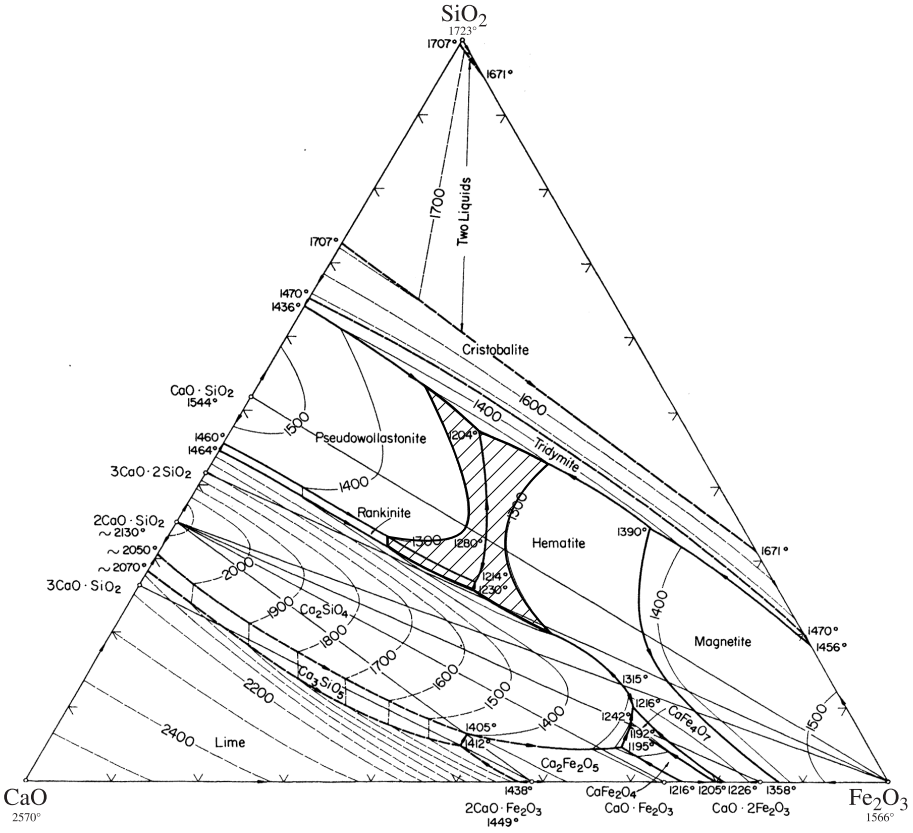

Figure 3.4.13. *SiO_2-CaO-Fe_2O_3 system (condensed phases in equilibrium with air): phase diagram (projection) valleys and liquidus isotherms. Hatched area – liquid area at 1,300°C [OSB 60]*

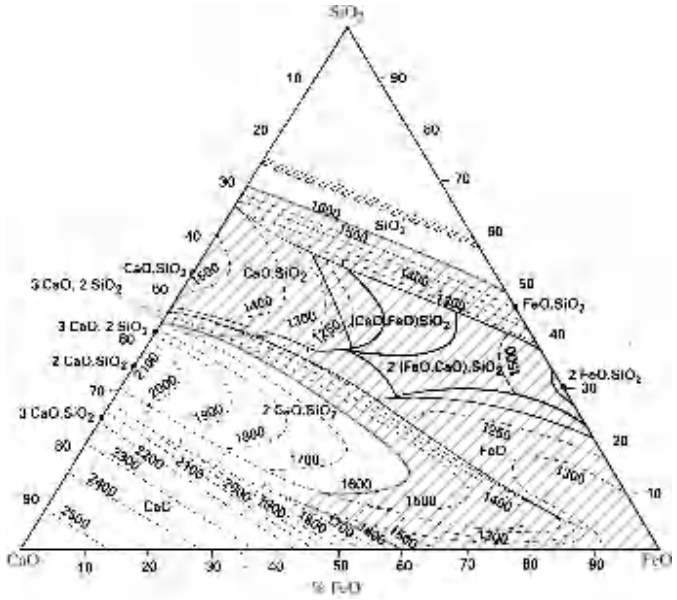

Figure 3.4.14. *SiO_2-CaO-FeO system (oxide phases in equilibrium with metallic iron): phase diagram (projection) valleys and liquidus isotherms. Hatched area – liquid area at 1600°C [OSB 60]*

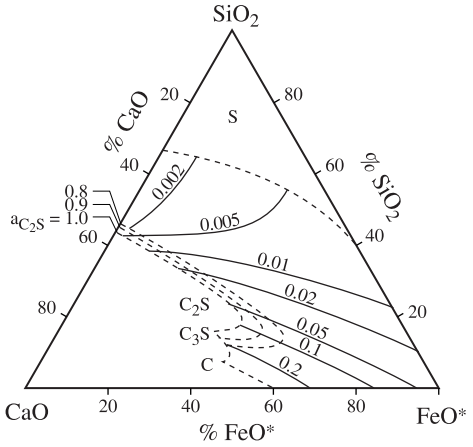

Figure 3.4.15. *Computed lines of iso Fe^{3+}/Fe_t ratio in the SiO_2-CaO-FeO system: in equilibrium with iron at 1,550°C [GAY 84]*

It must be noted that at 1,300 °C the liquid phase area is very small for a slag in contact with the air and is much larger for a slag in contact with the metallic phase. At 1,600°C, the liquid phase areas are similar for both slags.

For a slag in equilibrium with liquid iron, the iron oxide activity $\hat{a}_{(FeO)}$, see equation [2.3.13], is given by:

$$\hat{a}_{(FeO)} = (p_{O2} / p^*_{O2(Fe/FeO)})^{1/2} \qquad [3.4.4]$$

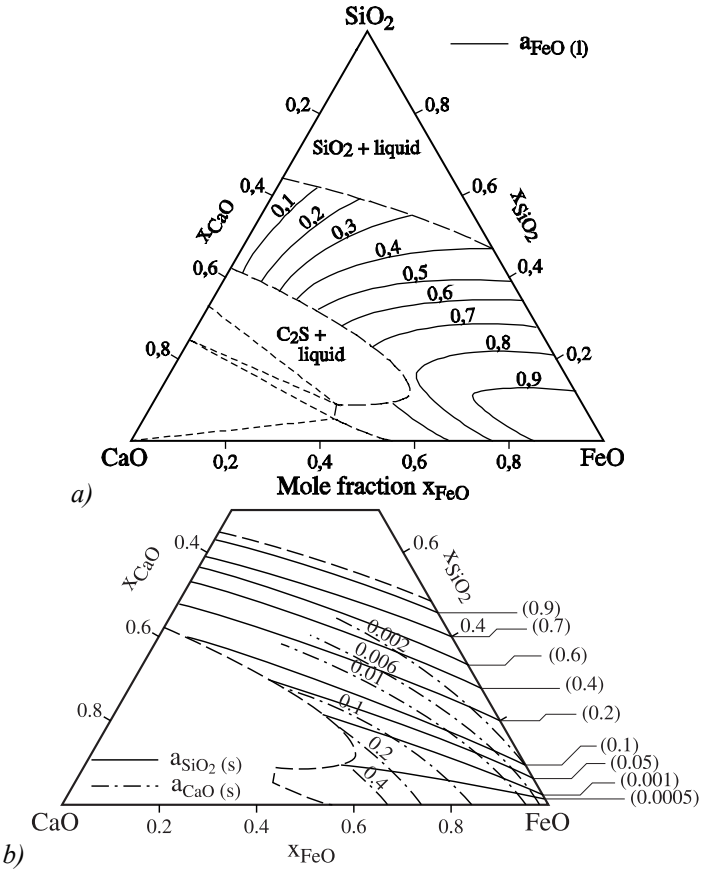

Figure 3.4.16. *Activities: a) of FeO (experimental), $\hat{a}_{\text{"FeO"}}$; and b) of CaO, $a°_{CaO}$. and SiO_2 $a°_{SiO2}$. (by Gibbs-Duhem integration) in CaO-FeO-SiO_2 melts in equilibrium with liquid iron at 1,550°C [TUR 96]*

This activity sets the oxidizing capacity (oxygen potential) of a slag in contact with liquid iron, see [VIG 11b], Chapter 5, section 5.4.3 and reaction [5.4.6]:

$$(FeO)_{(slag)} = Fe(l) + \underline{O}_{(Fe)} \quad [3.4.5]$$

$$a°_{O(Fe)} = \hat{a}_{(FeO)} \cdot (p^*_{O2(Fe/FeO)})^{1/2} \quad [3.4.6]$$

The iso-activity curves of the three components of the slag are drawn in Figures 3.4.16a and b. For a basic slag, $\hat{a}_{(FeO)}$ goes through a maximum for a basicity index of the order of 2, see Figure 3.4.17. For an acidic slag, the FeO activity is roughly proportional to its content.

The composition of the converting slag, at the end of oxygen blowing, is: FeO_x (13–18%), CaO (50–55%), SiO_2 (12–15%), MnO (4%), MgO (5–7%) and Al_2O_3 (2%). The liquid phase area at 1,600°C is much larger than the area of the basic CaO-SiO_2-FeO_x slag. Sections of pseudo-ternary phase diagrams for the CaO, SiO_2, Fe_tO (3%), MnO (3%), MgO (5%), Al_2O_3 (1.5%), P_2O_5 (2%) system (see [VIG 11b], Figures 5.4.7a, b and c) show what the composition of the slags should be at 1,650°C to be fluid (above the lime and magnesia saturation limit – FeO_x < (20–25%)-SiO_2 < 10% – with a ratio of CaO / SiO_2 > 5).

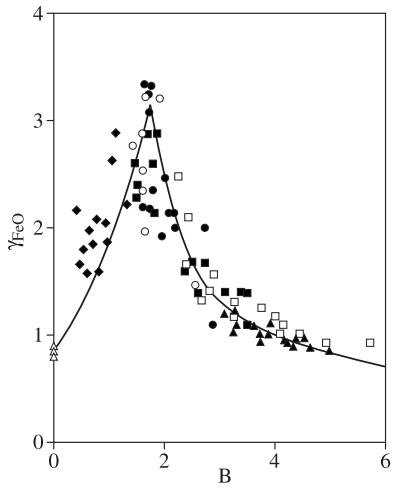

Figure 3.4.17. *Effect of the slag basicity on the activity coefficient of iron oxide in simple and complex slags at 1,600°C [TUR 96]*

In iron ore smelting reduction processes, the typical composition of a slag is FeO (5%), MgO (10–18%), MnO (1–2%), Al_2O_3 (7–12 %), CaO (30%) and SiO_2 (30%) (see [VIG 11c], Chapter 5, Section 5.2.3), with a basicity index (CaO + MgO) / (SiO_2 + Al_2O_3) ranging from 1.7–2.

For these converting and smelting slags, the variation of the activity coefficient $\gamma_{(FeO)}$ with basicity is shown in Figure 3.4.17, where $\gamma_{(FeO)} = a°_{(FeO)} / x_{FeO}$.

3.4.4.3. *CaO-SiO_2 chromium oxides system*

Chromium oxide at high temperature exists as CrO and Cr_2O_3, see Figure 2.2.4. Above 1,650°C, the stable oxide is solid Cr_2O_3 (Cr^{3+}). Above 1,665°C, the liquid oxide phase is an ionic solution (Cr^{2+}, Cr^{3+} and O^{2-}), whose Cr^{2+} and Cr^{3+} contents vary with the partial pressure of oxygen, in a gas phase at equilibrium with the liquid phase. The liquid oxide at equilibrium with the chromium is the divalent oxide CrO (Cr^{2+}).

In the production of stainless steels in the electric furnace, see [VIG 11b], Chapter 5, section 5.5, by refining of scraps rich in chrome and under oxidizing conditions, the chromium dissolved in the metallic phase is oxidized and absorbed by the slag as Cr_2O_3. The CaO-SiO_2-Cr_2O_3 diagram for the slags in contact with the air is shown in Figure 3.4.18. The solubility of Cr_2O_3 in the slags is very low at 1,600°C. The slag is saturated in Cr_2O_3 and thus the Cr_2O_3 activity is equal to one.

In the chromium oxide reduction stage, the slag is in contact with the ferrochrome alloy. Unlike the Cr_2O_3 oxide, the CrO oxide has extensive solubility in slags; the liquid phase region at 1,600°C is much larger (see Figure 3.4.19). The third corner of the ternary diagram corresponds to the total content in chrome oxide (as Cr^{2+} and Cr^{3+} ions) in the slag. In Figures 3.4.20a and b, the pseudo-activities $\hat{a}_{(CrO)}$ and $\hat{a}_{(CrO1,5)}$ are plotted, for the SiO_2,CaO system is in equilibrium with chromium at 1,600°C.

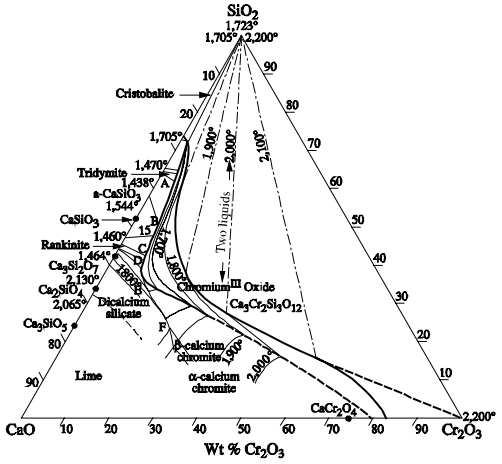

Figure 3.4.18. *SiO_2-CaO-Cr_2O_3 system, phase diagram (projection). Condensed phases in equilibrium with air [VIL92]*

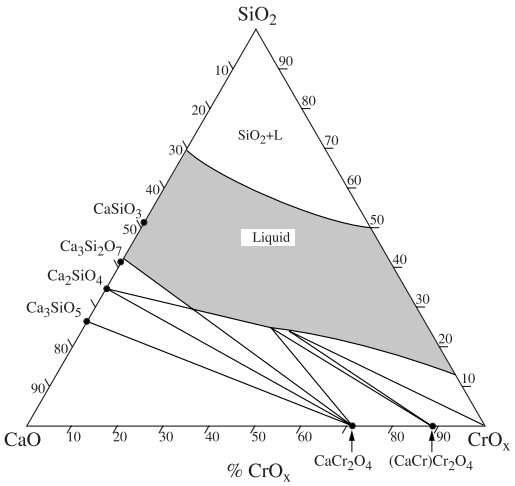

Figure 3.4.19. *SiO_2-CaO-CrO_x system, phase diagram (isothermal section at 1,873K). Condensed phases in equilibrium with metallic chromium [XIA 02]*

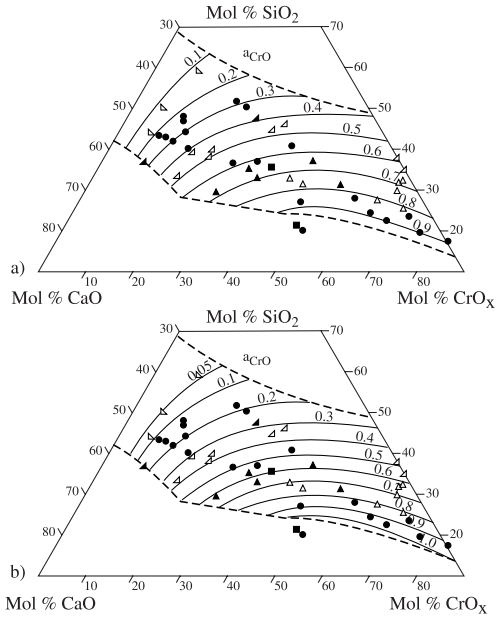

Figure 3.4.20. *SiO_2-CaO-CrO_x system, (isothermal section at 1,873K). Condensed phases in equilibrium with metallic chromium: a) pseudo-activity of CrO), $\hat{a}_{"CrO"}$ (standard state: pure CrO liquid); and b) pseudo-activity of $CrO_{1.5}$, $\hat{a}_{"CrO1.5"}$ (standard state: pure $CrO_{1.5}$ solid) [XIA 02]*

3.4.4.4. *CaO-SiO_2-MnO system*

The manganese oxide MnO, like CrO oxide, has extensive solubility in slags, as shown in Figure 3.4.21.

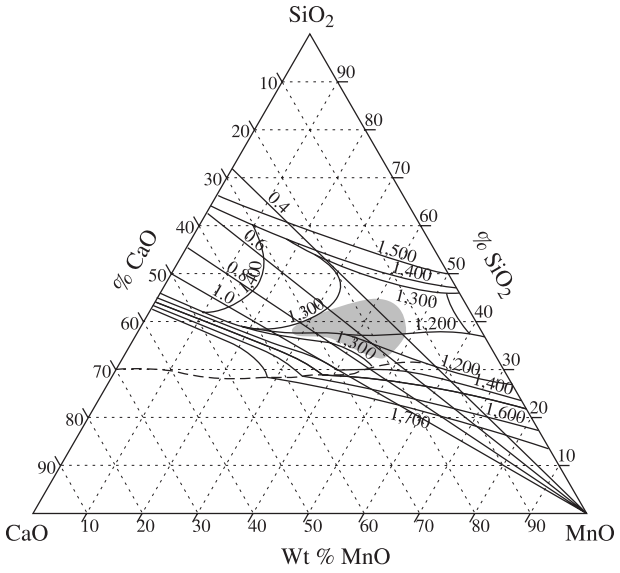

Figure 3.4.21. *SiO_2-CaO-MnO system: phase diagram, liquidus isotherms (slag in equilibrium with Mn-C sat metallic phase) [GLA 62, OLS 98]*

3.5. Bibliography

[BAL 76] C.W. BALE, J.M. TOGURI, *Canadian Metallurgical Quarterly*, Vol. 15, No. 4, pp. 305-318, 1976.

[BOD 63] C. BODSWORTH, *Physical Chemistry of Iron and Steel Manufacture*, Longmans, London, 1963.

[BRA 65] A.V. BRADSHAW, F.D. RICHARDSON, "Thermodynamic and kinetic aspects of vacuum degassing", *Vacuum Degassing of Steel, Report 92*, The Iron and Steel Institute, 1965.

[CHA 81] P. CHAMPION, L. GUILLET, P. POUPEAU, *Diagrammes de Phases des Matériaux Cristallins*, 2nd edition, Masson, Paris, 1981.

[CON 87] B.R. CONARD, G.A. MEYER, *et al.*, *Canadian Metallurgical Quarterly*, Vol. 26, No. 4, pp. 299-307, 1987.

[DAR 53] L.S. DARKEN, R. GURRY, *Physical Chemistry of Metals*, McGraw-Hill, New York, 1953.

[ELL 63] J.F. ELLIOTT, *Thermochemistry for Steelmaking*, Vol II, Addison-Wesley, 1963.

[ELL 76] J.F. ELLIOTT, *Metallurgical Transactions B*, Vol.7B, pp. 17-33, March 1976.

[FRU 69] R.J. FRUEHAN, F.D. RICHARDSON, *Transactions of the Metallurgical Society of AIME*, Vol. 245, pp. 1721-1726, August 1969.

[GAT 87] G. GATELIER, H. GAYE, *Revue de Métallurgie-CIT*, Vol. 760, pp. 25-42, November 1987.

[GAY 84] H. GAYE, J. WELFRINGER, in: *Second International Symposium on Metallurgical Slags and Fluxes*, Ed. H.A. FINE, D.R. GASKELL, TMS-AIME, pp. 357-376, 1984.

[GLA 62] F.P. GLASSER, *J. Am. Ceram. Soc.*, Vol. 45, No. 5, pp. 245, 1962.

[HAN 69] M. HANSEN, *Constitution of Binary Alloys*, 2nd Metallurgy and Metallurgical Engineering Series, McGraw-Hill, 1958.

[HOW 89] S.M. HOWARD, *Metallurgical Transactions B*, Vol. 20B, pp. 849, December 1989.

[JAC 71] K.T. JACOB, J.H.E. JEFFES, *Trans. Inst. Mining. Metall. Sec., C,* Vol. 80, pp. 31-42, 1971.

[KAI 86] Q.L. KAISER, J.F. ELLIOTT, *Metallurgical Transactions B*, Vol. 17B, pp. 147-157, March 1986.

[KAI 88] Q.L. KAISER, J.F. ELLIOTT, *Metallurgical Transactions B*, Vol. 19B, pp. 935-941, December 1988.

[KEL 87] H.H. KELLOG, *Canadian Metallurgical Quarterly*, Vol. 26, No. 4, pp. 285-298, 1987.

[KIM 03] E.J. KIM, B.D. YOU, J.J. PAK, *Metallurgical and Materials Transactions B*, Vol. 34B, pp. 51-59, February 2003.

[KON 02] A. KONDRATIEV, E. JAK, P.C. HAYES, *J. O. M.*, pp. 41-45, November 2002.

[KOR 62] N. Korakas, *Trans. Inst. Min. Metall.*, Vol. 72, No. 35, pp. 1962-1963.

[KUB 55] O. KUBASCHEWSKI, E.L.L. EVANS, *Metallurgical Thermochemistry*, Vol. 66, Pergamon Press, 1955.

[LAR 54] H. LARSON, J. CHIPMAN, "Transactions AIME", *Journal of Metals*, pp. 1089-1096, September 1953, pp. 759-762, June 1954.

[LEH 98] J. LEHMANN, F. BERTRAND, H. GAYE, *Revue de Métallurgie-CIT*, pp. 1131, September 1998.

[LEN 86] J.G. LENZ, B.R. CONARD, *25th Annual Conference of Metallurgists*, CIM, Toronto, August 1986.

[LI 98] H. LI, A.E. MORRIS, D.G.C. ROBERTSON, *Metallurgical and Materials Transactions B*, Vol. 29B, pp. 1181, December 1998.

[LUM 52] LUMSDEN, *Thermodynamics of Alloys*, The Institute of Metals, London, 1952.

[MAC 48] J.S. MACHIN, T.B. YEE, *JACS*, Vol. 3, pp. 200, 1948.

[MAC 65] J. MACKOWIAK, *Physical Chemistry for Metallurgists*, Allen & Unwin, London, 1965.

[MUA 65] A. MUAN, E.F. OSBORN, *Phase Equilibria Among Oxides in Steelmaking*, Addison-Wesley Publishing Co., Reading, M.A, 1965.

[OET 94] F. OETERS, *Metallurgy of Steelmaking*, Stahl and Eisen, 1994.

[OLS 97] S.E. OLSEN, Sintef Report, STEF 24 F 97617, 1997.

[OLS 98] V. OLSO, M. TANGSTAD, S.E. OLSEN, *Infacon 8*, pp. 279-283, 1998.

[OSB 60] E.F. OSBORN, A. MUAN, *Phase Equilibrium Diagrams of Oxide Systems*, ACS, 1960.

[PAL 02] U.B. PAL, *JOM*, pp. 57-61, November 2002.

[REI 65] R.H. REIN, J. CHIPMAN, *Trans. Met. Soc. AIME*, Vol. 223, pp. 415-425, 1965.

[RIC 74] F.D. RICHARDSON, *Physical Chemistry of Melts in Metallurgy*, Vol. 1, Academic Press, 1974.

[RIS 56] A. RIST, J. CHIPMAN, *Revue de Métallurgie*, Vol. 53, No. 10, pp. 796-807, 1956.

[RIS 74a] A. RIST *et al*., *Techniques de l'Ingénieur TI*, M 1730 , Paris, 1974.

[RIS 74b] A. RIST, M.F. ANCEY-MORET, C. GATELLIER, P.V. RIBOUD, *Techniques de l'Ingénieur*, T.I. Form. M1733, pp. 1-8, 1974.

[ROS 83] T. ROSENQUIST, *Principles of Extractive Metallurgy*, McGraw-Hill, 1983.

[SEE 93] S. SEETHARAMAN, K.T. JACOB, *Extractive Metallurgy of Cu*, *Ni and Co*, *TMS*, Vol. 1, pp. 41, 1993.

[VDE 95] VDEH (ed.), *Slag Atlas*, Verlag Stahleisen, Dusseldorf, 1995.

[SOM 86] C. SOMSIRI, D.R GASKELL, *Metallurgical and Materials Transactions B*, Vol. 17B, pp. 147-15, December 1986.

[SOM 95] C. SOMSIRI, D.R GASKELL, *Metallurgical and Materials Transactions B*, Vol. 26B, pp. 1,157-1,164, December 1995.

[SRI 02] S. SRIDHAR, *JOM*, pp. 46-49, November 2002.

[STE 94] J.M. STEILER, M. SCHNEIDER, *Le livre de l'acier*, 187-1228, Lavoisier Tec & Doc, Paris, 1994.

[TEM 45] M. TEMKIN, *Acta Physico-chimica URSS*, pp. 421-440, 1945.

[TIM 70] M. TIMUCIN, A.E. MORRIS, *Metallurgical Transactions*, Vol. 1, pp. 3193-3201, November, 1970.

[TUR 62] E.T. TURKDOGAN, *Transactions AIME*, Vol. 221, pp. 1090-1094, December 1961; and Vol. 224, pp. 294-298, April 1962.

[TUR 96] E.T. TURKDOGAN, *Fundamentals of Steelmaking*, The Institute of Materials, 1996.

[VIG 11b] A. VIGNES, *Extractive Metallurgy 2: Metallurgucal Reaction Processes*, ISTE Ltd, London and John Wiley and Sons, New York, 2011.

[VIG 11c] A. VIGNES, *Extractive Metallurgy 3: Processing Operations and Routes*, ISTE Ltd, London and John Wiley, New York, 2011.

[VIL 92] J.P.R. DE VILLIERS, A. MUAN, *J. Am. Ceram. Soc*., Vol. 75, pp. 1333-41, 1992.

[WAR 62] R.G. WARD, *The Physical Chemistry of Iron and Steel Making*, Edward Arnold, London, 1962.

[WIL 80] G.M. WILLIS, *Lead-Zinc-Tin 80*, *TMS*, pp. 457-476, 1980.

[XIA 02] Y. XIAO, L. HOLAPPA, M.A. REUTER, *Metallurgical and Materials Transactions B*, Vol. 33B, pp. 595-603, August 2002.

[YAZ 69] A. YAZAWA, T. AZAKAMI, *Canadian Metallurgical Quarterly*, Vol. 8, No. 3, p. 257, 1969.

[YAZ 79] A. YAZAWA, *Metallurgical Transactions B*, Vol.10B, pp. 307-321, September 1979.

[YAZ 81] A. YAZAWA, Y. TAKEDA, Y. WASEDA, *Canadian Metallurgical Quarterly*, Vol. 20, No. 2, pp. 129-134, 1981.

Chapter 4

Aqueous Electrolytic Solutions and Salt Melts

4.1. Introduction

In this chapter the basic thermodynamic data is presented:

– on aqueous solutions in hydrometallurgical (see [VIG 11b], Chapter 1) and electrometallurgical (see [VIG 11b, Chapter 2) extraction processes;

– on salt melts (fluxes): solutions of halides of alkaline and alkaline earth metals used as electrolytes in molten salts electrolysis (see [VIG 11c], Chapter 9).

4.2. Thermodynamics of aqueous electrolyte solutions[1]

Water is a polar solvent that plays a dissociating role for an ionic compound ($NaCl(s) \rightarrow Na^{+} + Cl^{-}$), or an ionizing and dissociating role for a polar compound ($HCl(g) \rightarrow H^{+} + Cl^{-}$). In aqueous solutions, a compound M_aA_b (salt, acid or base) dissolved in water is totally or partially dissociated into cations of z^{+} charge and b anions of ζ^{-} charge:

$$M_aA_b\ (s, l \text{ or } g)_{(\text{dissociated molecule})} \rightarrow \alpha\ M^{z+} + b\ A^{z-} \qquad [4.2.1a]$$

$$M_aA_b\ (aq)_{(\text{non-dissociated molecule})} \rightarrow \alpha\ M^{z+} + b\ A^{z-} \qquad [4.2.1b]$$

1 For an introduction, see Prigogine and Defay [PRI 50]

Extractive Metallurgy 1: Basic Thermodynamics and Kinetics Alain Vignes
© 2011 ISTE Ltd. Published 2011 by ISTE Ltd.

with, according to the conservation of electric charges:

$$a\,z^{+} + b\,z^{-} = 0 \qquad [4.2.2]$$

The cations form complex ions with water molecules $(Cu(H_2O)_4)^{2+}$, $(Al(H_2O)_6)^{3+}$ by solvation and ionic hydration. The anions are not solvated (hydrated) [BAT 70]. Furthermore, the cations form complexes with other inorganic and organic ligands. The ligands can be molecules (e.g. NH_3, H_2O) or ions X^{z-} (e.g. OH^-, CN^-, Cl^-, SO_4^{2-}):

$$xM^{z+} + y\,X^{-}(OH^{-}, Cl^{-}, CN^{-}) \rightarrow M_xX_y^{(xz-y)+} \qquad [4.2.3]$$

$$xM^{z+} + y\,(NH_3, H_2O) \rightarrow (M_x(H_2O)_y)^{z+} \qquad [4.2.4]$$

x and y can take several values. Consequently, an aqueous solution contains a great number of complex ions, the content of each complex ion strongly varying with the content of the basic ion and ligand. As these complex ions can have a very high stability, the salts, hydroxides and oxides solubilities depend on the distribution of these complex ions.

4.2.1. *Chemical potentials and activities of the components of electrolyte aqueous solutions*

A chemical potential can be defined for each dissolved species (molecule or ion). The expressions generally used of the chemical potential are those whose activity is referred to the molar concentration, see equation [1.3.46], or for the molality, see equation [1.3.47]:

$$\mu_j = \eta^{\circ}_j + RT \ln \tilde{a}_j = \eta^{\circ}_j + RT \ln f_j \,.\, C_j \qquad [4.2.5]$$

For ions, we define similarly[2]:

$$\mu_{M^{z+}} = \mu^{o}_{M^{z+}} + RT \ln \tilde{a}_{M^{z+}} = \mu^{o}_{M^{z+}} + RT \ln f_{M^{z+}} \,.\, [M^{z+}] \qquad [4.2.6]$$

The Henrian activity coefficient $f \rightarrow 1$ when the concentration of the component or ion $\rightarrow 0$, see equation [1.3.37]. The "standard potentials" of the ions are given in [LAT 38, LAT 64, ZEM 86]. The activities of the ions are estimated from electrochemical measurements.

2 As there is no ambiguity, we will use the notations μ°_j for η°_j and a_j for $\tilde{a}_j$, see equation [1.3.46b].

For an aqueous solution of the compound M_aA_b (salt, acid or base) which, in solution with water, is either totally (see reaction [4.2.1a]) or partially (see reaction [4.2.1b]) dissociated, the chemical potentials of both ions cannot be measured separately. We define a "mean" chemical potential of both ions by:

$$\mu_{\pm} = (a\mu_{+} + b\mu_{-}) / (a + b) \qquad [4.2.7]$$

a mean activity $a_{\pm}$ and a mean activity coefficient $f_{\pm}$:

$$(a_{\pm})^{(a+b)} = (\tilde{a}_{M^{z+}})^{a} \cdot (\tilde{a}_{A^{z-}})^{b} \qquad [4.2.8]$$

$$(f_{\pm})^{(a+b)} = (f_{M^{z+}})^{a} \cdot (f_{A^{z-}})^{b} \qquad [4.2.9]$$

and a "pseudo-activity" $\hat{a}_{(MaAb)}$:

$$\hat{a}_{(MaAb)} = (a_{\pm})^{(a+b)} \qquad [4.2.10]$$

For a totally dissociated component:

$$\hat{a}_{(HCl)} = (a_{\pm(HCl)})^2 = (\tilde{a}_{H^+}) \cdot (\tilde{a}_{Cl^-}) = (f_{\pm})^2 \cdot [H^+] \cdot [Cl^-] \qquad [4.2.10b]$$

$$\hat{a}_{(NiCl2)} = (a_{\pm(NiCl2)})^3 = (\tilde{a}_{Ni^{2+}}) \cdot (\tilde{a}_{Cl^-})^2 = (f_{\pm})^3 \cdot [Ni^{2+}] \cdot [Cl^-]^2 \qquad [4.2.10c]$$

When in a solution, several electrolytes share common ions. The mean activity coefficients, corresponding to the different compounds, are defined in the same way. For instance, for a solution containing the ions Na^+, K^+, Cl^- and NO_3^-, the activity coefficients are defined as previously:

$$f^2_{NaNO3} = f_{Na^+} \cdot f_{NO_3^-} \; ; \; f^2_{KNO3} = f_{K^+} \cdot f_{NO_3^-} \qquad [4.2.11]$$

For a partially dissociated compound, see reaction [4.2.1b], this pseudo-activity is expressed as a function of the equilibrium constant (or dissociation constant) of the reactions and of the Henrian activity of the dissolved non-dissociated compound $\tilde{a}_{(MaXb)}$, see equation [4.2.27], by:

$$\hat{a}_{(MaAb)} = K_D \cdot \tilde{a}_{(MaAb)}$$

4.2.1.1. *Activity of water in aqueous solutions*

Water, a very weak electrical conductor, is weakly dissociated into H^+ (H_3O^+) and OH^- ions:

$$H_2O = H^+ + OH^- \text{ or } (2\ H_2O = H_3O^+ + OH^-) \qquad [4.2.12]$$

The law of mass action, see equation [1.3.54], for this dissociation is written as:

$$K_W = \tilde{a}_{H^+} \,.\, \tilde{a}_{OH^-} / a_{H2O} \qquad [4.2.13a]$$

This reaction is endothermic and dissociation increases with temperature. We define the ionic product as:

$$pK_w = -\log K_w \qquad [4.2.13b]$$

at 0°C: $pK_w = 14.938$; at 25°C: $pK_w = 13.995$; and at 100°C: $pK_w = 12.965$.

The activity of water in equation [4.2.13] ($a_{H2O} = a_w$) is the Raoultian or standard activity, see equations [1.3.21] and [1.3.22]. For aqueous solutions and a high electrolyte content, the water activity $a_{(H2O)}$ decreases with the increase in electrolyte concentration. This is a result of the ion-water interactions (ionic hydration), see equation [4.2.4] and Figure 4.2.1. It can be determined by different measurements: osmotic pressure, lowering of the freezing temperature, raising of the boiling temperature, ratio of the partial pressure of water in the gas phase in equilibrium with the solution and the vapor pressure of pure water: $p_w / p°_w$, see equation [1.3.34].

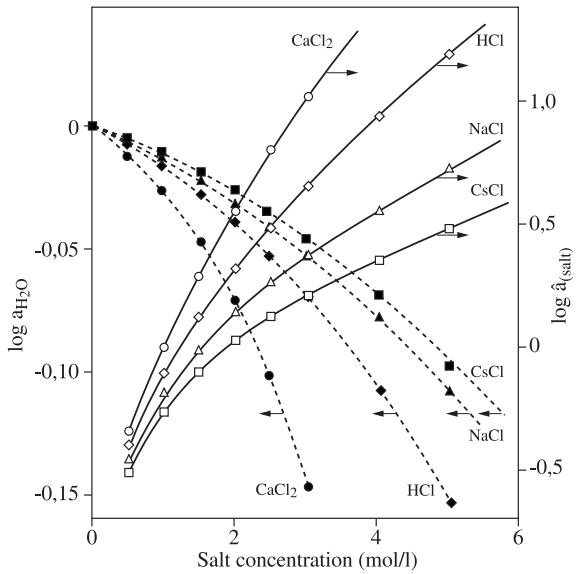

Figure 4.2.1. *Effect of salt concentration on salt activity and water activity in aqueous salts [MUI 85]*

4.2.1.2. *Mean activity of an electrolyte*

The mean activity of strong electrolytes (e.g. HCl, NaOH, H_2SO_4), totally dissociated in solution in water can be directly determined by electrochemical measurements. For most electrolytes, their mean activity in water is calculated from the water activity by the Gibbs-Duhem equation, see equation [1.3.52]:

$$d\ln a_{\pm} = -\left(\frac{55.51}{\langle m \rangle}\right) d\ln a_{H2O} \qquad [4.2.14]$$

where $<m>$ is the molality of the electrolyte. Nonetheless, this equation does not allow us to get accurate values of $f_{\pm}$ at high dilutions. The Debye and Hückel's law, which will be mentioned later, enables the calculation of ions' activities at high dilutions. Several empirical relations have been suggested between the average mean activity coefficient of the electrolyte and the activity of water [STO 48].

4.2.1.3. *Activity of ions and ionic strength: Debye and Hückel law*

The activities of ions can only be estimated from electrochemical measurements. The measurements of the H^+ activity by a pH-meter are only valid for relatively low H^+ contents:

$$pH = -\log \tilde{a}_{H^+} = -\log \tilde{a}_{H3O^+} \qquad [4.2.15]$$

The pH-meter is a battery whose FEM is measured with a reference electrode and a measuring electrode, i.e. a glass electrode. The pH-meters with glass electrodes allow pH measurements between pH = 1 and 11. Above 11, the values are unreliable as the pH-meter indications are not stable.

The ion's activities at high dilution can be calculated with the help of the Debye or Hückel's law [PRI 50]. This was established from a statistical theory, taking into account the long-range electrostatic interactions that occur between the ions of the solution. This theory leads to an expression of the ion's activity as a function of the charge of the ion and the ionic *strength* of the solution.

The ionic *strength* of an aqueous solution of electrolytes is defined by [PRI 50]:

$$I = 1/2 \sum z_j^2 \, . \, C_j \qquad [4.2.16]$$

where z_j is the valence of each ion j present in solution at concentration C_j, or an equivalent expression referred to the molalities:

$$I_m = 1/2 \sum z_j^2 \, . \, <m_j> \qquad [4.2.17]$$

and the expression of activity coefficient of an ion at 25°C is:

$$\ln f_j = -1.1762.z_j^2.\frac{I^{1/2}}{\{\ 1+0.33a\times10^8 I^{1/2}\ \}.} \qquad [4.2.18a]$$

where *a* is the average diameter of the ion (in cm). This equation is valid for I < 0.2. For monovalent ions:

$$\ln f_j = -1.1762.z_j^2.\frac{I^{1/2}}{1+I^{1/2}} \qquad [4.2.18b]$$

Models of electrolytic aqueous solutions have been developed to estimate the thermodynamic properties of these solutions, in particular the activities of the ions for more concentrated solutions. These models lead to expressions of the form:

$$\ln f_j = -\ 1.1762.z_j^2.\frac{I_m^{1/2}}{\{\ 1+b_j.I_m^{1/2}\ \}} + c_j\ .\ I_m \qquad [4.2.19]$$

with very different values for the b and c coefficients depending on the model [PIT 79].

4.2.1.4. *Mean activity of an electrolyte and ionic strength of the solution*

In dilute solutions, the mean activity coefficient of an electrolyte M_aA_b, see equation [4.2.9], can be calculated from the activity coefficients of the ions, see equation [4.2.19]. For more concentrated solutions, we can estimate the mean activity coefficient from the water activity, see equation [4.2.14]. Different models, based on extensions of the Debye and Hückel's law, taking into account the hydration number of the ions h and dissociation degree of the electrolyte, allow a satisfactory calculation of the mean activity of an electrolyte for concentrated solutions. Experimental curves and computed curves of mean activity coefficients of various electrolytes as a function of the molality of the electrolyte are drawn in Figures 4.2.2 to 4.2.6.

For the chloride NaCl, see Figure 4.2.2, the mean activity coefficient $f_\pm$ goes through a minimum of 0.65 for a molality of 1 and increases to values up to 10 in strongly concentrated solutions.

For the sulfate SO_4Na_2, the mean activity coefficient $f_\pm$ strongly decreases when the molality increases and remains low at high molalities, see Figure 4.2.3.

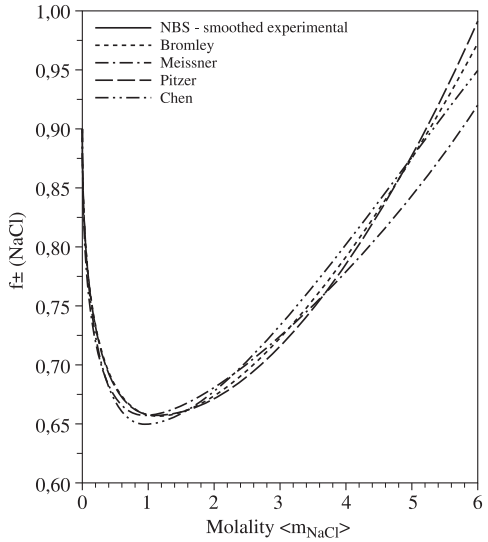

Figure 4.2.2. *Mean activity coefficient of NaCl in aqueous solutions as a function of molality at 25°C. Experimental and computed (various models) values [ZEM 86]*

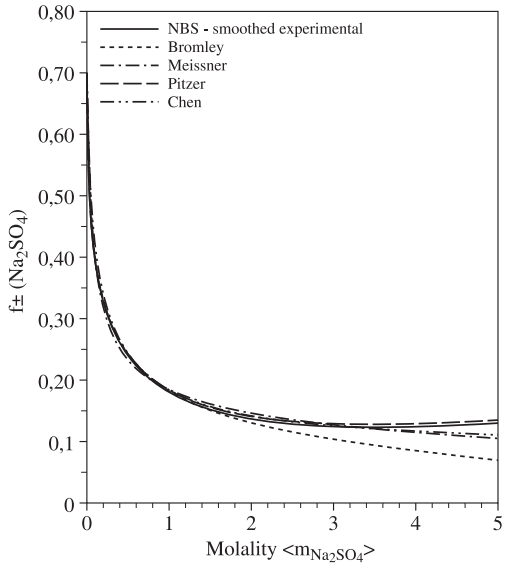

Figure 4.2.3. *Mean activity coefficient of Na_2SO_4 in aqueous solutions as a function of molality at 25°C. Experimental and computed (various models) values [ZEM 86]*

On some curves it is to be noted that for strong electrolyte concentrations, log $f_{\pm}$ varies linearly with the electrolyte molality and therefore with the ionic strength of the solution. Empirical expressions have been established, see equation [4.2.19]:

$$\ln f_{\pm} \approx - A \Delta z^2 \frac{I_m^{1/2}}{\{ 1 + B.I_m^{1/2} \}.} + CI_m \qquad [4.2.20]$$

where: $\Delta z^2 = (az_c^2 + bz_a^2) / (a + b)$.

Expressions have been derived by extending the hydration theory for electrolyte solutions, allowing the estimation of activity coefficients of the ions from the mean activity coefficient of the electrolyte. The Bates equations [BAT 70] are quoted for the activity coefficients of the chloride ions:

$$\log f_{M^+} = \log f_{\pm} + 0.00782\ h\ .\ <m>\ .\ \phi \qquad [4.2.21]$$

$$\log f_{Cl^-} = \log f_{\pm} - 0.00782\ h\ .\ <m>\ .\ \phi \qquad [4.2.22]$$

where h is the hydration number (number of water molecules linked to the cation), <m> is the molality and ϕ is the osmotic coefficient:

$$\phi = -1{,}000 \ln a_{H2O} / (18 \sum n_j\ .\ <m_j>)$$

4.2.2. *Aqueous solutions of acids and bases*

4.2.2.1. *Strong acids or bases*

The strong electrolytes (e.g. ClH, NaOH) at high dilution in water and at low temperature are completely dissociated. At high concentration and temperature, they are partially dissociated. The stronger the concentration and the higher the temperature, however, the less they are dissociated, see section 4.2.2.2, equation [4.2.27].

Dissociation constant $K_D(T)$	*150°C*	*200°C*	*250°C*
HCl	0.51	0.08	-0.54
NaOH	0.34	-0.06	-0.6

The hydrochloric acid HCl, gaseous at room temperature, is soluble in water up to a content of 41% in weight (molality equal to 19.2) at 25°C under a ClH partial

pressure of 1 atm. As it is completely dissociated in water, we consider the equilibrium between the gas phase and the ions of the liquid phase:

$$\mu_{(HCl)}(g) = \mu_{H^+} + \mu_{Cl^-} \qquad [4.2.23]$$

whose equilibrium constant has the following equation:

$$K = \tilde{a}_{H^+} \,.\, \tilde{a}_{Cl^-} / p_{(HCl)} \qquad [4.2.24]$$

thus:

$$p_{(HCl)} = (f_{\pm})^2 [H^+] \,.\, [Cl^-] / K \qquad [4.2.25]$$

When the only electrolyte dissolved in water is hydrochloric acid:

$$p_{(HCl)} = (f_{\pm})^2 [HCl]^2 / K \qquad [4.2.26]$$

At strong dilution $f_{\pm(HCl)} \rightarrow 1$, the partial pressure of HCl is proportional to $[HCl]^2$ in the solution. In Figure 4.2.4a, the variations of the mean activity ($a_{\pm}$) of the mean activity coefficient ($f_{\pm}$) and HCl partial pressures (different scales) as a function of HCl molality are shown.

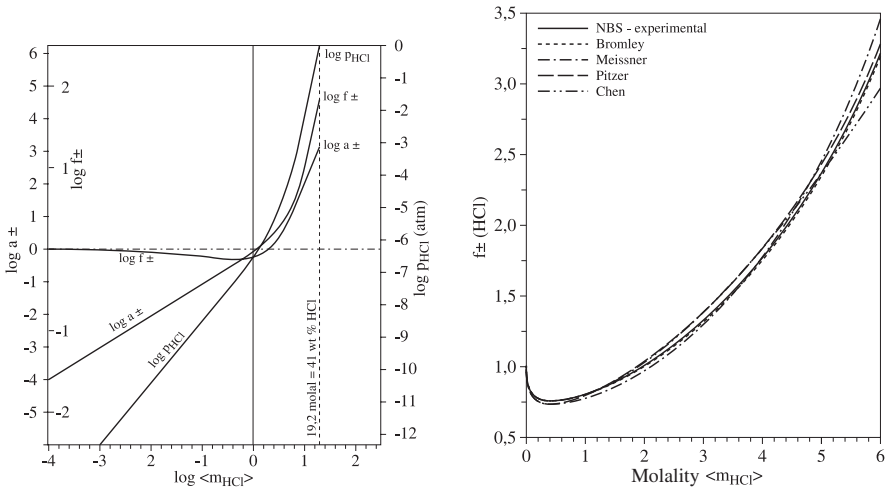

Figure 4.2.4. *Aqueous HCl solutions at 25°C: a) mean activity $a_{\pm}$, mean activity coefficient $f_{\pm}$ and $p_{(HCl)}$ as a function of molality; and b) Experimental and computed (various models) values of the mean activity coefficient [LEW 61, ZEM 86]*

Figure 4.2.4b shows the variations of the mean coefficient activity $f_{\pm}$ at 25°C, experimentally determined as a function of the molality $<m_{HCl}>$ and calculated by different models. The different thermodynamic models provide values in agreement with the experimental values up to a molality of 5, and satisfactory values above. In a concentrated solution at 25°C, $f_{\pm}(HCl)$ can reach 50. Therefore, the concentrated hydrochloric acid solutions present very strong activities. In very concentrated solutions, the equilibrium to be considered is:

$$2\ HCl + H_2O = H_3O^+ + HCl_2^-$$

The addition of NaCl to a ClH aqueous solution increases the mean activity of HCl, see Figure 4.2.5. $â_{(HCl)}$ reaches the values of 100 for a solution containing 3 M of HCl and 3 M of Cl^- ions produced by the addition of NaCl or $CaCl_2$.

The values of the activity coefficients of f_{H^+} and f_{Cl^-} ions in hydrochloric solutions, obtained by equations [4.2.21] and [4.2.22], are presented in Table 4.2.1.

m_{HCl} (mol kg^{-1} H_2O)	f_{H^+}/T (°C)							
	25	40	50	60	70	80	90	100
1	0.91	0.90	0.89	0.88	0.87	0.87	0.86	0.85
2	1.31	1.27	1.24	1.21	1.19	1.16	1.14	1.11
3	2.03	1.92	1.85	1.79	1.72	1.66	1.60	1.54
4	3.29	3.04	2.89	2.74	2.60	2.47	2.34	2.22
5	5.46	4.93	4.60	4.29	4.01	3.74	3.49	3.25
6	9.13	8.03	7.37	6.77	6.21	5.70	5.23	4.80
7	15.30	13.10	11.90	10.70	10.10	8.74	7.89	7.12
8	25.20	21.20	18.90	16.80	14.90	13.30	11.80	10.50

m_{HCl} (mol kg^{-1} H_2O)	f_{Cl^-}/T (°C)							
	25	40	50	60	70	80	90	100
1	0.72	0.71	0.71	0.70	0.69	0.69	0.68	0.68
2	0.78	0.76	0.74	0.73	0.72	0.71	0.69	0.68
3	0.85	0.82	0.80	0.78	0.76	0.74	0.72	0.70
4	0.94	0.89	0.86	0.83	0.81	0.78	0.75	0.73
5	1.04	0.97	0.93	0.89	0.85	0.82	0.78	0.75
6	1.14	1.05	1.00	0.95	0.90	0.85	0.81	0.77
7	1.25	1.14	1.07	1.01	0.95	0.90	0.84	0.80
8	1.38	1.24	1.16	1.08	1.01	0.94	0.88	0.82

Table 4.2.1. *Activity coefficients f_{H^+} and f_{Cl^-} in HCl solutions as a function of molar concentration and temperature. Values selected by Demopoulos [DEM 99, JAN 83]*

Table 4.2.2 lists the values of activity coefficients ã $â_{(HCl)}$, $ã_{H^+}$ and $ã_{Cl^-}$ in hydrochloric solution as a function of the Cl^- content (by additions of NaCl).

HCl (mol/l)	NaCl (mol/l)				
	0.0	0.5	1.0	1.5	2.0
0.5	0.0855	0.205	0.358	0.621	0.91
1.0	0.808	1.35	2.11	2.96	5.76
1.5	1.84	3.45	5.11	7.95	12.7
2.0	3.16	6.73	10.8	18.8	26.8

1. $\hat{a}_{HCl}$

HCl (mol/l)	NaCl (mol/l)				
	0.0	0.5	1.0	1.5	2.0
0.5	0.404	0.468	0.547	0.626	0.738
1.0	1.69	1.89	2.06	2.40	2.92
1.5	2.88	3.33	3.83	4.54	5.31
2.0	4.37	5.14	6.43	7.39	8.57
2.5	6.93				
3.0	9.38				
3.5	15.6				
4.0	17.9				

2. $\tilde{a}_{H^+}$

HCl (mol/l)	NaCl (mol/l)				
	0.0	0.5	1.0	1.5	2.0
0.0		0.316	0.569	0.833	1.17
0.5	0.212	0.439	0.655	0.926	1.23
1.0	0.480	0.711	1.03	1.24	1.97
1.5	0.637	1.04	1.33	1.75	2.39
2.0	0.837	1.31	1.68	2.55	3.13
3.0	2.32				
4.0	4.46				
5.0	11.0				
6.0	15.0				

3. $\tilde{a}_{Cl^-}$

Table 4.2.2. *Activities of $\hat{a}_{(HCl)}$, $\tilde{a}_{H^+}$ and $\tilde{a}_{Cl^-}$ in HCl-NaCl aqueous solutions as functions of the HCl and NaCl contents at 25°C [MAJ 81]*

NOTE.– These values must be taken with caution. Table 4.2.3 contains some values of a_{H^+} and a_{Cl^-} activities in hydrochloric solutions obtained by three models.

[HCl](mole/l)	$\tilde{a}_{H^+}(1)$	$\tilde{a}_{H^+}(2)$	$\tilde{a}_{H^+}(3)$	$\tilde{a}_{Cl^-}(1)$	$\tilde{a}_{Cl^-}(2)$	$\tilde{a}_{Cl^-}(3)$
1 mole/l	0.91	1.69	1.0	0.72	0.48	0.73
2 mole/l	2.62	4.37	3.91	1.56	0.827	1.65
4 mole/l	13.16	17.9	29	3.4	4.46	3.09

Table 4.2.3. *Activities of $\tilde{a}_{H^+}$ and $\tilde{a}_{Cl^-}$ in HCl-NaCl aqueous solutions as functions of HCl content at 25°C, calculated by different models: (1) [JAN 83]; (2) [MAJ 81]; and (3) [SEL 90]*

It is to be noted that the activity coefficients increase with the NaCl content, thus with the ionic strength of the solution, see Figure 4.2.5.

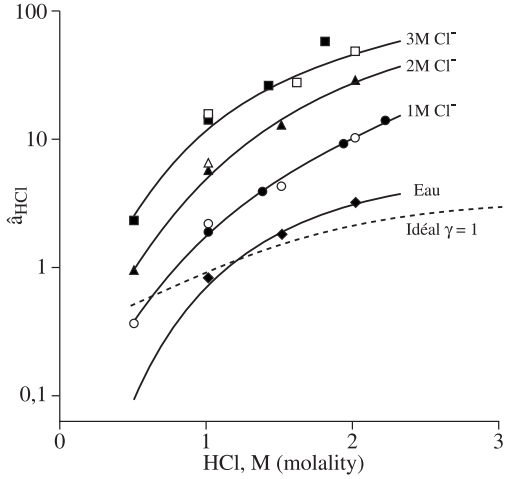

Figure 4.2.5. *Effect of added Cl^- (as NaCl or CaCl2) on the pseudo-activity $\hat{a}_{HCl}$ of HCl (see equation [4.2.10]) [MUI 85]*

The variation of the mean activity coefficient of NaOH dissolved in water with molality is similar to that of the mean activity coefficients of HCl and ClNa, see Figure 4.2.6.

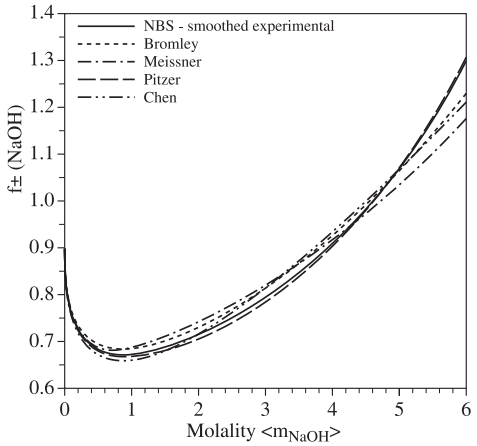

Figure 4.2.6. *Mean activity coefficient of NaOH in aqueous solutions as a function of molality at 25°C. Experimental and computed (various models) values [ZEM 86]*

4.2.2.2. *Weak acids or bases*

Weak electrolytes, acid (e.g. CNH, H_2S) or base (e.g. NH_4OH), dissolved in water are partially dissociated. The law of mass action for the dissociation of component M_aA_b, see reaction [4.2.1b], is written as:

$$K_D(T) = \frac{\left(\tilde{a}_{M^{z+}}\right)^a . \left(\tilde{a}_{A^{z-}}\right)^b}{\tilde{a}_{M_aA_b}} = \left(\frac{(f_\pm)a+b}{f_{(M_aA_b)}}\right)\left(\frac{\left[M^{z+}\right]^a . \left[A^{z-}\right]^b}{\left[M_a . A_b(aq)\right]}\right) \qquad [4.2.27]$$

where $K_D(T)$ is the *dissociation constant* (also called the acidity constant K_a, function of T only) and $\tilde{a}_{(MaXb)}$ is the activity of the $M_aA_b(aq)$ compound present in the solution in a non-dissociated state. The lower the dissociated constant, the less the molecule is dissociated. We often express the dissociation constant by its pK_D:

$$pK_D = -\log K_D \qquad [4.2.28]$$

The *degree of dissociation* α is the ratio of the number of dissociated molecules M_aA_b and the total number of dissolved molecules – whether dissociated or not – in water. If C_t is the total M_aA_b concentration (dissociated or non-dissociated):

$$C_t = [M_aA_b(aq)] + a\,[M^+] \qquad [4.2.29]$$

we have:

$$[M_aA_b(aq)]_{(\text{non-dissociated molecules})} = (1 - \alpha)\, C_T \qquad [4.2.30]$$

The degree of dissociation is determined by the measurement of the electric conductance. The law of mass action written as a function of the degree of dissociation is:

$$K_D = \left(\frac{f_\pm^{(a+b)}}{f_{(M_aA_b)}}\right)\left(\frac{[C_t]^{a+b-1} . \alpha^{a+b}}{(1-\alpha)}\right) \qquad [4.2.31a]$$

in the particular case where $[M^+] = [A^-]$:

$$K_D = \left(\frac{f_\pm^2}{f_{(M_aA_b)}}\right)\left(\frac{[C_t] . \alpha^2}{(1-\alpha)}\right) \qquad [4.2.31b]$$

The concentrations of non-dissociated molecules (equation [4.2.30]) and ions therefore depend on C_T and α. The dissociation coefficient α depends on C_T, K_D and the $\{(f_{\pm})^2 / f_{(MaXb)}\}$ ratio.

When the solution is sufficiently diluted, the activity coefficients tend towards one and K_D is given by the Ostwald's law [PRI 50]:

$$K_D = \alpha^2 C_t / (1 - \alpha) \qquad [4.2.31c]$$

The degree of dissociation $\alpha \rightarrow 1$ when $C_T \rightarrow 0$, the dissociation is complete for strong dilution.

For a weak acid, the dissociation in water is weak, with the formation of a very small quantity of H^+ ions. The resulting solution is therefore very weakly acidic.

For hydrogen cyanide:

$$HCN(aq) \rightarrow CN^- + H^+ \qquad [4.2.32a]$$

This dissociation can be considered to be a hydrolysis:

$$HCN(aq) + H_2O \rightarrow CN^- + H_3O^+ \qquad [4.2.32b]$$

In a dilute solution:

$$\log\{[CN^-] / [CNH]\} = pH - pK_D \qquad [4.2.32c]$$

$pK_D = 9.3$ at 25°C (see Figure 4.2.7)

for $pH = pK_D$: $[HCN] = [CN^-]$.

For $pH < pK_D$, the predominant form is HCN, and for $pH > pK_D$ the predominant form is CN^-. The pH of a hydrogen cyanide solution of total concentration C_0 is given by:

$$pH = 1/2 (pK_D - \log C_o) \qquad [4.2.32d]$$

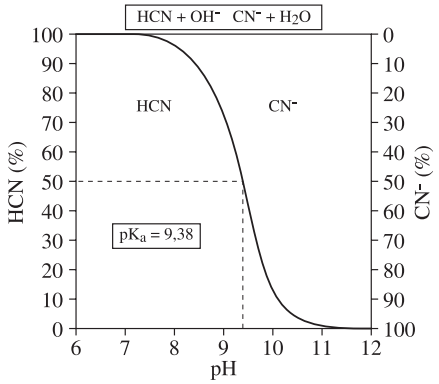

Figure 4.2.7. *Dissociation of CNH as a function of pH*

The acid H_2S undergoes two dissociations:

$$H_2S(aq) + H_2O \rightarrow HS^- + H_3O^+ \qquad pK_{D1} = 7.1\ (8) \text{ at } 25°C \qquad [4.2.33]$$

$$HS^- + H_2O \rightarrow S^{2-} + H_3O^+ \qquad pK_{D2} = 13\ (12) \text{ at } 25°C \qquad [4.2.34]$$

– when $pH < pK_{D1}$; the predominant form is H_2S;

– when $pK_{D1} < pH < pK_{D2}$, the predominant form is HS^-; and

– when $pH > pK_{D2}$, the S^{2-} form is predominant (see the Pourbaix diagram of the S-H_2O system in Figure 8.3.11).

For a concentration $[H_2S(aq)] = 0.1$ mol/L), the pH of a solution is equal to:

$$pH = 1/2\ \{pK1 - \log[H_2S(aq)]\} = 4.05\ (4.5) \qquad [4.2.35]$$

and $[HS^-] = 8.91 \times 10^{-5}$ mol/L and $[S^{2-}] = 10^{-13}$. The acid H_2S can be considered to bea weakly dissociated monoacid.

4.2.2.3. *For sulfuric acid*

The dissociation of H_2SO_4 occurs in two consecutive steps:

$$H_2SO_4(aq) \rightarrow H^+ + HSO_4^- \qquad [4.2.36]$$

$$HSO_4^- \rightarrow H^+ + SO_4^{2-} \qquad [4.2.37]$$

The activity of the H^+ ion in aqueous sulfuric acid solutions is estimated, see equation [4.2.19], by:

$$\ln f_{H^+} = -A.\frac{I_m^{1/2}}{\left\{1+5.66B.I_m^{1/2}\right\}.} + 0.04785\, I_m + \gamma \qquad [4.2.38]$$

where A and B are the temperature-dependent Debye-Hückel coefficients, I_m is the true ionic strength of the solution on a molal basis (see equation [4.2.17]), and γ is a term to convert the activity coefficient from molar fraction scale to molal scale [FIL 95] .

The first dissociation is complete. HSO_4^- is a weak acid, whose dissociation varies strongly with ionic force [DIC 90]:

$$1/K_{D2} = \frac{\tilde{a}_{HSO_4^-}}{\tilde{a}_{H^+}\cdot\tilde{a}_{SO_4^{2-}}} = \frac{f_{HSO_4^-}}{f_{H^+}.f_{SO_4^{2-}}} \times \frac{\left[HSO_4^-\right]}{\left[H^+\right].\left[SO_4^{2-}\right]}$$

at 25°C [DIC 90] and:

$$\frac{f_{H^+}.f_{SO_4^{2-}}}{f_{HSO_4^-}} = 2.036\ \frac{I^{1/2}}{1+0.4I^{1/2}} \qquad [4.2.39]$$

$$\log K_{D2} = -2 \qquad [4.2.40]$$

At 25°C, the HSO_4^- ion is predominant when pH <2. The SO_4^{2-} ion is predominant when pH >2 (see Pourbaix's diagram, Figure 8.3.11).

For dilute solutions, the concentrations of H^+, HSO_4^- and SO_4^{2-} ions can be calculated by the system of three equations:

$$1/K_{D2} = [HSO_4^-] / \{[H^+] \times [SO_4^{2-}]\} \qquad [4.2.41]$$

$$C_a = [SO_4^{2-}]_{(total)} = [SO_4^{2-}] + [HSO_4^-]$$

$$[H^+] = [HSO_4^-] + 2\,[SO_4^{2-}]$$

thus:

$$2\,[H^+] = C_a - K_{D2} + \{(C_a - K_{D2})^2 + 8\,K_2C_a\}^{1/2} \qquad [4.2.42]$$

and it can easily be verified that the sulfuric acid can be considered as a monoprotonic acid.

The values given by the pH-meters are only valid for contents in SO_4H_2 <0.25 mol/L. The pH measurements confirm the semimonoprotonic character of this acid. For $[SO_4H_2] = 0.1$ mo/l, if SO_4H_2 was a diacid the pH should be equal to 0.6. As a monoacid, the pH should be equal to 1. The measured value is equal to 1.01.

The sulfuric solutions present weak activities. The mean activity of the acid is always lower than the unit, between 296 and 423K (see Figure 4.2.8):

$$a_{\pm}^2 = \tilde{a}_{H+} \cdot \tilde{a}_{SO_4H-} = f_{\pm}^2 \cdot [H^+] \cdot [SO_4H^-] \qquad [4.2.43]$$

The activity of the hydrogen ion varies linearly with the SO_4H_2 concentration (see Figure 4.2.8):

$$\tilde{a}_{H+} = f_{H+} \cdot [H^+] = [SO_4H_2] = [SO_4H^-]$$

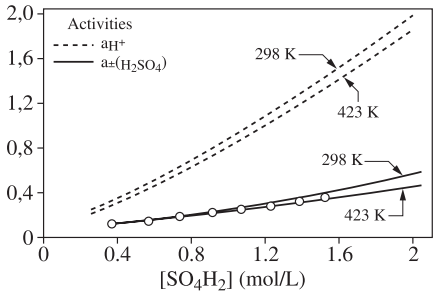

Figure 4.2.8. *Estimated hydrogen ion activity and mean sulfuric acid activity $a_{\pm}$ in H_2SO_4 solutions at 25°C [FIL 95]*

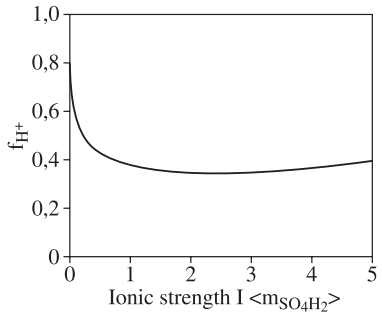

Figure 4.2.9. *Activity coefficient of hydrogen f_{H+} in SO_4H_2 aqueous solutions as a function of the ionic strength (SO_4H_2 molality) at 250°C [BAG 98]*

At 250°C, the activity coefficient of the hydrogen ion $\tilde{a}_{H+}$ in sulfuric solutions is constant and equal to 0.4, when 0.5< I = <m> <5 (see Figure 4.2.9).

Calculated values of activity $\tilde{a}_{H+}$ in sulfuric and sulfate solutions are presented in Table 4.2.4. The very strong influence of the presence of Zn^{2+} and Fe^{3+} ions on the activity of hydrogen in sulfuric solutions is to be noted.

Composition (mol·L^{-1})				a_{H+}		
$[SO_4^{2-}]_{tot}$	$[Zn^{2+}]_{tot}$	$[Fe^{2+}]_{tot}$	$[Fe^{3+}]_{tot}$	298 K	323 K	373 K
0.25	0	0	0	0.220	0.208	0.195
0.50	0	0	0	0.424	0.404	0.382
1.00	0	0	0	0.863	0.831	0.791
1.50	0	0	0	1.367	1.325	1.268
2.00	0	0	0	1.959	1.907	1.834
0.50	0.25	0	0	0.159	0.132	0.087
1.00	0.50	0	0	0.311	0.267	0.195
2.00	1.00	0	0	0.677	0.614	0.514
0.50	0	0.25	0	0.102	0.067	0.027
1.00	0	0	0.25	0.073	0.056	0.022
1.00	0.50	0.10	0	0.198	0.154	0.088
2.00	1.00	0.25	0	0.336	0.270	0.174
3.00	2.00	0.50	0	0.099	0.057	0.017
1.00	0.50	0	0.10	0.185	0.147	0.076
2.00	1.00	0	0.25	0.305	0.245	0.130
3.00	2.00	0	0.50	0.070	0.047	0.018
3.00	2.00	0.10	0.50	0.031	0.019	0.009

Table 4.2.4. *Calculated values of a_{H+} in sulfuric acid solutions [FIL 95]*

4.2.3. *Aqueous solutions of metallic salts: complexation and speciation*

The basic dissolution reaction of a salt in water and aqueous solutions is the dissociation into simple ions, see reaction [4.2.1].

The reaction of the formation of complexes with the salt's anion or with another anion (see reaction [4.2.3]) is:

$$xM^{z+} + yX^{z-} (Cl^-, CN^-, SO_4^{2-}) \rightarrow \left(M_x X_y\right)^{xz^+ + yz^-} \qquad [4.2.44]$$

where x and y can take several values. Formation of several complex ions with the same ligand (the rates at which these complex ions form are very high) can occur.

The equilibrium constant of these complexation reactions is called the *stability coefficient* (or *stability product*), function of T only, and is designated by K_{STxy} or β_{Stxy}:

$$K_{STxy} \text{ or } \beta_{STxy} = \frac{\left(\tilde{a}_{M_x X_y}\right)^{xz^+ + yz^-}}{\left(\tilde{a}_{M^{z+}}\right)^x \cdot \left(\tilde{a}_{X^{z-}}\right)^y} \qquad [4.2.45a]$$

The greater K_{STxy}, the more stable the complex and the less dissociated it is. The quantity of free metallic cations in solution is thus weak.

The stability equilibria is generally expressed directly as a function of the molar concentrations as a stability coefficient, also called stability quotient [BAE 76, FIL 95]:

$$Q_{STxy} = \frac{\left[M_x X_y\right]^{xz^+ + yz^-}}{\left[M^{z+}\right]^x \left[X^{z-}\right]^y} \qquad [4.2.45b]$$

The stability coefficient Q_{STxy}, incorporating the activity coefficients of the ions that depend on the composition of the solution, its variation with the composition of the solution, is often expressed as a function of the ionic strength of the solution (see equation [4.2.16]), such as:

$$\log Q_{STxy} = \log K_{STxy} + A\,\Delta z^2 . \frac{I^{1/2}}{\left\{1 + 1.6 . I^{1/2}\right\}.} + bI \qquad [4.2.46]$$

where: $\Delta z^2 = 1/2 \sum \nu_j z_j^2$, A is the temperature-dependent Debye-Hückel's coefficients, and b is an arbitrary constant [FIL 95]. The literature data allow the calculation of the stability coefficient of these complexes [FIL 95].

For most metallic cations in hydrochloric and sulfuric solutions, complex ions are formed with Cl^- or SO_4^{2-} ions. The formation of these complexes explains the high solubility in water of most sulfates and chlorides at low and medium temperatures.

4.2.3.1. *Chlorocomplexes*

Table 4.2.5 lists some values of stability constants K_{STxY} of chlorocomplexes:

– for the transition metal cations $Fe^{2+} < Co^{2+} < Cu^{2+}$: $\log K_{STxY} < 1$;

– for the $Sn^{2+} < Pb^{2+} < Fe^{3+}$ cations: $\log K_{STxy} = 1–3$;

– for the $Cu^{+} < Ag^{+} < Au^{+} < Zn^{2+} < Cd^{2+} < Hg^{2+} < Pt^{2+} < Pt^{4+}$ cations: $\log K_{STxy} = 3–15$.

The stability constants of these ions are very different and therefore the proportions of the different complexes, for a given solution, for a cation content, a complexing ion content and a pH are very different.

K_{STxy}	*25°C*	*50°C*	*100°C*
$Fe^{3+} + Cl^{-} \rightarrow FeCl^{2+}$	30.2	91.2	871
$Fe^{3+} + 2\ Cl^{-} \rightarrow FeCl_2^{+}$	135	417	4,270
$Fe^{3+} + 3\ Cl^{-} \rightarrow FeCl_3$	13.5	57.5	1,000
$Fe^{3+} + 4\ Cl^{-} \rightarrow FeCl_4^{-}$	0.16	1.12	42.7
$Pb^{2+} + Cl^{-} \rightarrow PbCl^{+}$	39.8	42.7	53
$Pb^{2+} + 2\ Cl^{-} \rightarrow PbCl_2(aq)$	60.3	70.8	109.6
$Pb^{2+} + 3\ Cl^{-} \rightarrow PbCl_3^{-}$	47.9	64.6	134.9
$Pb^{2+} + 4\ Cl^{-} \rightarrow PbCl_4^{2-}$	24	38.9	112
$Pb^{2+} + 2\ Cl^{-} \rightarrow PbCl_2(s)$	6.25×10^4	3.33×10^4	2.12×10^4

Table 4.2.5. *Equilibrium (stability) coefficients for ferric and lead chlorocomplex formation at 25, 50 and 100°C [FUE 86]*

log K_{STxy}	*323K*	*373K*	*423K*
$Cu^{2+} + Cl^{-} \rightarrow CuCl^{+}$	0.53	1.54	2.57
$Cu^{2+} + 2\ Cl^{-} \rightarrow CuCl_2$	-0.06	1.15	2.36
$Cu^{2+} + 3\ Cl^{-} \rightarrow CuCl_3^{-}$	-1.48	0.04	1.52
$Cu^{2+} + 4\ Cl^{-} \rightarrow CuCl_4^{2-}$	-3.54	-1.63	0.018
log K_{Stxy}			
$Cu^{+} + 2\ Cl^{-} \rightarrow CuCl_2^{-}$	4.94	5.06	5.35
$Cu^{+} + 3\ Cl^{-} \rightarrow CuCl_3^{2-}$	5.18	5.39	5.77

Table 4.2.5. (continued) *Equilibrium (stability) coefficients for copper chlorocomplex formation at 25, 50 and 100°C [HIR 87]*

Figures 4.2.10a–d, called *speciation diagrams*, show the distribution curves of hydrochloric complexes of Cu(II), Fe(III), Zn(II), Pb(II) as a function of concentration of chloride ions (the content of chloride ions in the solution is obtained either by addition of a salt NaCl or an acid HCl). By comparing Figure 4.2.10b and Table 4.2.6, it is to be noted that for Fe(III) chlorocomplexes, depending on Fe(III) ion concentration (10^{-3} M in Figure 4.2.10b and 1 M in Table 4.2.6), the dominant chlorocomplexes are very different.

	25 °C NaCl concentration (M)			
	0	1	2	3
Fe^{+3}	5.56×10^{-3}	1.41×10^{-3}	5.94×10^{-4}	3.14×10^{-4}
$FeCl^{+2}$	0.168	0.0849	0.0538	0.0379
$FeCl_2^+$	0.750	0.758	0.721	0.678
$FeCl_3$	0.0751	0.152	0.217	0.271
$FeCl_4^-$	8.90×10^{-4}	3.60×10^{-3}	7.70×10^{-3}	1.29×10^{-2}

Table 4.2.6. *Distribution of the Fe(III)-chloride system at 25°C as a function of NaCl concentration [FUE 86]*

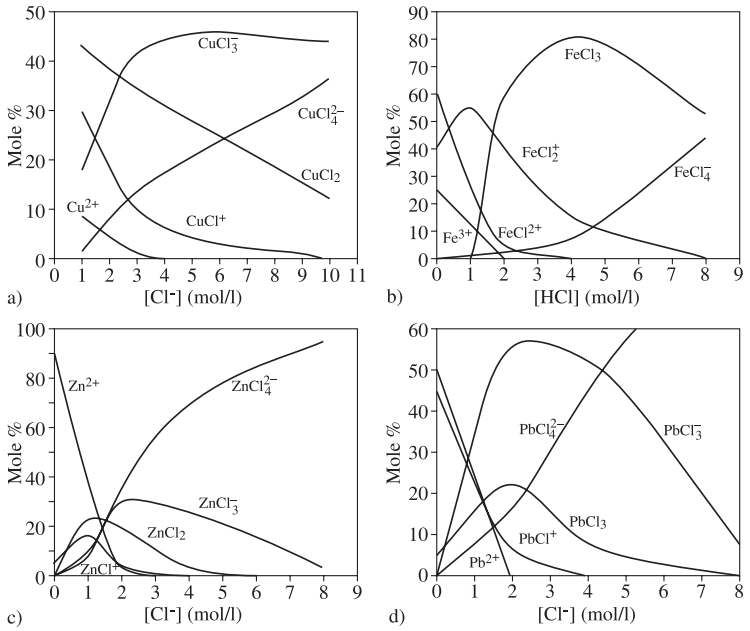

Figure 4.2.10. *Speciation diagrams: a) distribution of cupric chloride complexes as a function of the chloride ion concentration [Cu^{2+}] = 6 × 10^{-3}M; b) distribution of ferric chloride complexes as a function of the HCl concentration ([Fe^{3+}] = 10^{-3}M); c) distribution of zinc chloride complexes as a function of chloride ion concentration [Zn^{2+}] = 0.05 M; and d) distribution of lead chloride complexes as a function of chloride ion concentration [Pb^{2+}] = 0.05 M [DEM 99]*

The predominance domains of these chlorocomplexes are shown in the M-Cl-H_2O Pourbaix diagrams, see Chapter 8, section 8.3.3 and Figures 8.3.6 and 8.3.7.

Nickel chloride, $NiCl_2$, in hydrochloric solutions or in the presence of anions not forming complexes (ClO_4^-) is completely dissociated. The Ni^{2+} ion is the predominant ion for pH values <8 (the most common oxidation state of Ni is +2). Cobalt forms chlorocomplexes in hydrochloric solutions: $CoCl_4^{2-}$ (see [VIG 11b], Chapter 1, sections 1.4.1 and 1.4.4.1).

4.2.3.2. *Sulfuric complexes*

Figure 4.2.11 shows the distribution curves of sulfuric complexes formed with Fe^{2+} as a function of the pH of the solution (the pH is fixed by the addition of sulfuric acid) for a total Fe(II) ion concentration of 0.5 mol/L. The concentration of ferrous sulfate $(FeSO_4)°(aq)$ is practically equal to zero; the sulfate (in solution in water) is completely dissociated. For pH values >2.5, the predominant ion is Fe^{2+}. In a highly acidic solution at 25°C, the predominant ion is $(FeHSO_4)^+$ (the sulfuric acid is monoprotonic and dissociates into HSO_4^- and H^+ ions.). At a higher temperature (373 K), the variations are similar but displaced towards a higher pH.

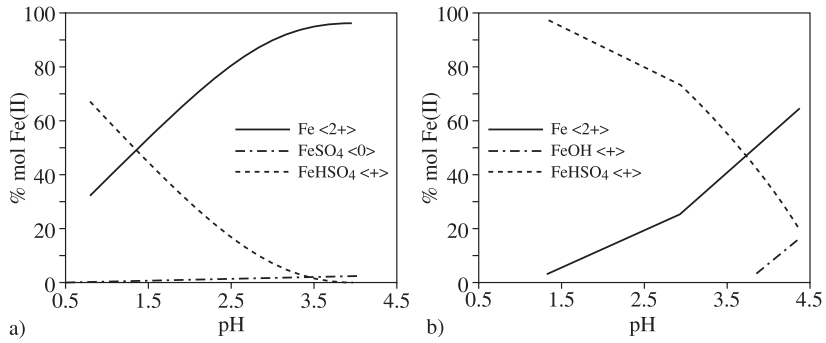

Figure 4.2.11. *Ferrous sulfate speciation diagram: a) at 298K; and b) at 373K. The total ferrous concentration is 0.5 mol/L and the pH value has been adjusted by varying the total sulfate concentration [FIL 95]*

The distributions of ferric complexes as a function of solution pH, for low sulfuric acid concentration, at 298 and 373K, are presented in Figure 4.2.12 for a total ferric ion concentration of 0.5 mol/L. Where $0.5 < pH < 2.5$, the two predominant complexes are $FeSO_4^+$ and $Fe(SO_4)_2^-$. The presence of $Fe_2(OH)_2^{4+}$ ions at 373K is to be noted.

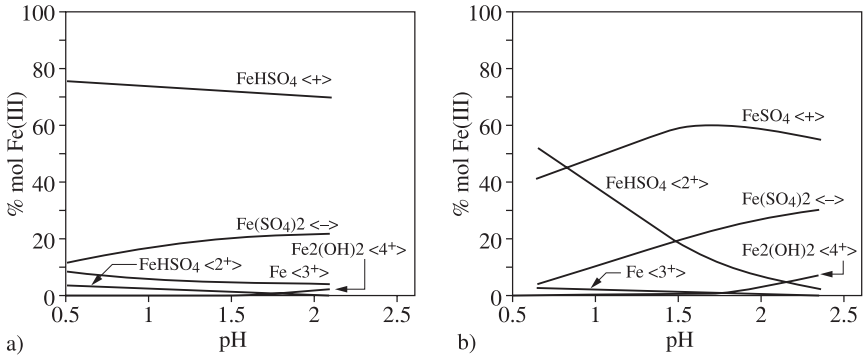

Figure 4.2.12. *Ferric sulfate speciation diagram: a) at 298K; and b) at 373K. The total ferric concentration is 0.5 mol/L and the pH value has been adjusted by varying the total sulfate concentration [FIL 95]*

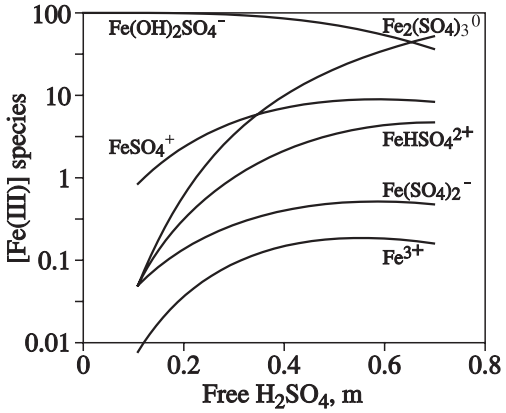

Figure 4.2.13. *Ferric sulfate speciation diagram at 250°C. $[H_2SO_4]_{(free)} = [H_2SO_4]_t - 1.5\ [Fe(III))]_{total}$ [LIU 03]*

At 250°C, the coexisting complexes are $Fe(OH)_2SO_4^-$ and $Fe_2(SO_4)_3°(aq)$, $FeSO_4^+$, $FeHSO_4^{2+}$, $Fe(SO_4)_2^-$, Fe^{3+}, with variable distributions as a function of free acid concentration (see Figure 4.2.13). At strong acidity, the predominant species in solution is $Fe_2(SO_4)_3°$. At 250°C, in the H_2SO_4-$Al_2(SO_4)_3$-$MgSO_4$ system, the soluble species are Al^{3+}, $Al(SO_4)^+$, $Al_2(SO_4)_3(aq)$, Mg^{2+} and $MgSO_4(aq)$.

In Table 4.2.7, some values of stability constants K_{STxY} of Au^+ and Au^{3+} cation complexes are presented with different acids. Gold, platinum and palladium form very stable complexes with these acids.

Complex	Au(+1) β_2	Complex	Au(+3) β_4
$Au(CN)^-_2$	2×10^{38}	$Au(CN)^-_4$	10^{56} to 10^{80}
$Au(S_2O_3)^{3-}_2$	5×10^{28}	$Au\ I^-_4$	5×10^{47}
$Au(CS(NH_2)_2)^+_2$	2×10^{23}	$AuCl^-_4$	10^{26}
$Au(SCN)^-_2$	1.3×10^{17}	$Au\ (SCN)^-_4$	10^{42}

Table 4.2.7. *Stability constants K_{STxY} (or β_2) of some gold complexes [FLE 99]*

4.2.3.3. *Cation complexes formed with the OH^- ion (hydroxocomplexes)*

The reaction of formation of these complexes is:

$$xM^{z+} + y\ OH^- \rightarrow M_x(OH)_y^{(zx-y)} \qquad [4.2.47a]$$

and the expression of the stability coeffcient, see formula [4.2.45], is:

$$Q_{STxy} = \frac{\left[M_x\left(OH\right)_y^{(xz-y)}\right]\cdot}{\left[M^{z+}\right]^x . \left[OH^-\right]^y} \qquad [4.2.47b]$$

These complexes can be considered as being formed by hydrolysis of the cations:

$$xM^{z+} + yH_2O \rightarrow M_x(OH)_y^{(zx-y)} + yH^+ \qquad [4.2.47c]$$

$$Q_{Hxy} = \frac{\left[M_x\left(OH\right)_y^{(xz-y)}\right]\cdot\left[H^+\right]^y}{\left[M^{z+}\right]^x} \qquad [4.2.47d]$$

Q_{Hxy}, the hydrolysis coefficient, is expressed as a function of the ionic strength of the solution by an expression of the equation [4.2.46] type [BAE 76].

The relationship between the stability constants of these complexes, K_{STxy}, and the hydrolysis constant K_{Hxy}, of the cation is:

$$\log K_{STxy} = \log K_{Hxy} + 14\ y \qquad [4.2.48a]$$

or:

$$\log Q_{STxy} = \log Q_{Hxy} + 14\ y \qquad [4.2.48b]$$

The cations of transition metals $Ni^{2+} < Fe^{2+} < Co^{2+}$ are weakly hydrolyzable. Iron (Fe^{2+}) only forms a $Fe(OH)_3^-$ complex for pH values >10 and the ion concentration is very low, see Figure 4.2.15.

The cations Fe^{3+} and Al^{3+} are strongly hydrolyzable (see Figures 4.2.16 and 4.2.17). In aqueous solutions, where the anion (ClO_4^-) does not form complexes with cations, the Al^{3+} ion, for instance, is only predominant for very weak total content and weak pH. For stronger pH, the formation of $Al(OH)^{2+}$(1,1), $Al(OH)_2^+$(1,2), $Al(OH)_3°$(aq)(1,3) and $Al(OH)_4^-$(1,4) ions occurs (see Figure 4.2.17). At high temperature, $Al(OH)_3°$(aq) is the predominant species. For Fe(III), the complexes that are likely to be formed are: Fe^{3+}, $FeOH^{2+}$ ($K_{STxy} = 6.6 \times 10^{11}$), $Fe(OH)_2^+$ (1.34×10^{21}), $Fe_2(OH)_2^{4+}$ (5.4×10^{20}), $Fe(OH)_3°$ and $Fe(OH)_4^-$ (10^{34}).

The chlorocomplexes form complexes with the OH^- ion, for example:

$$FeCl_2^+ + 2\ H_2O \rightarrow Fe(OH)_2^+ + 2\ H^+ + 2\ Cl^- \qquad [4.2.49a]$$

$$\log\{[Fe(OH)_2^+] / [FeCl_2^+]\} = \log Q - 2\log[Cl^-] + 2\ pH \qquad [4.2.49b]$$

The predominance regions of these complex ions are presented in the Pourbaix diagrams of the M-H_2O, M-ClH-H_2O systems (see Chapter 8, section 8.3.2 and Figures 8.3.3, 8.3.6.a, 8.3.6.b and 8.3.7).

4.2.3.4. *Ammoniacal complexes*

In an ammoniacal mixture, the ions of metals such as copper, nickel, cobalt, silver, gold and platinum form soluble complexes:

$$Ni^{2+} + n\ NH_3(aq) \rightarrow Ni(NH_3)_n^{2+} \qquad [4.2.50]$$

where n can vary from 1 to 6 (where the stability coefficent β ($Ni(NH_3)_6^{2+}$) = 5.10^{10}).

Cobalt, in its two oxidation states, forms $Co(II)(NH_3)_n^{2+}$ (n 1 to 6) and $Co(III)(NH_3)_6^{3+}$ ($\beta = 5.10^{35}$) complexes. The formation of these complex ions increases the solubility of Ni and Co salts or reduces the stability domain of the oxide or hydroxide, as shown in the corresponding Pourbaix diagram (see Figures 8.3.8a and b).

4.2.3.5. *Ion stabilization by complexation*

The formation of a complex allows the stabilization of a degree of oxidation. The cuprous ion is unstable in an aqueous mixture; the equilibrium constant for the disproportionation reaction in water is very high:

$$2\ Cu^{+} \rightarrow Cu(s) + Cu^{2+} \quad \text{where} \quad K = 10^{6} \qquad [4.2.51]$$

and therefore only small amounts of Cu^{+} can exist unless stabilized by complexing agents.

In the presence of chloride ions, Cu^{+} gives more stable complexes than Cu^{2+}, in particular $CuCl_2^{-}$ (see Table 4.2.5b):

$$Cu^{+} + 2\ Cl^{-} \rightarrow CuCl_2^{-} \qquad [4.2.52]$$

The Au^{+} ion is not stable. It is very oxidative and cannot exist in an aqueous solution; indeed it oxidizes water according to the following reaction:

$$Au^{+} + H_2O \rightarrow Au + 2\ H^{+} + 1/2\ O_2(g) \qquad [4.2.53]$$

The Au^{+} ion forms a complex with a cyanide ion:

$$Au^{+} + 2\ CN^{-} \rightarrow Au(CN)_2^{-} \qquad [4.2.54]$$

whose stability constant β is very high $2(9.6) \times 10^{38}$ (The complexation stabilizes the Au^{+} ion, see Figure 8.3.10.).

The Co^{3+} ions are very oxidative and cannot exist in an aqueous solution. Indeed they oxidize water (see reaction [8.2.24]) according to the reaction:

$$2\ Co^{3+} + H_2O \rightarrow 2\ Co^{2+} + 2\ H^{+} + 1/2\ O_2(g) \qquad [4.2.55]$$

They form very stable complexes with cyanide ions:

$$Co^{3+} + 6\ CN^{-} \rightarrow Co(CN)_6^{3-} \quad \text{where} \quad \beta = 10^{63} \qquad [4.2.56a]$$

$$Co^{2+} + 6\ CN^{-} \rightarrow Co(CN)_6^{4-} \quad \text{where} \quad \beta = 10^{19} \qquad [4.2.56b]$$

4.2.4. *Solubility of oxides and hydroxides*

Most oxides are practically insoluble in water. Only alkaline and alkaline earth metal oxides react with water giving a strongly basic solution. These are the basic

oxides to which the hydroxides (e.g. NaOH, $Ca(OH)_2$) correspond. The highly oxygenated components of some metals such as CrO_3 and Mn_2O_7, when in contact with water, yield MnO_4H hydrates, giving acid solutions. More generally, a basic oxide that reacts with an acid gives a salt and water and an acid oxide (e.g. SiO_2 and Al_2O_3), which reacts with a strong base (caustic soda or potash) giving an alkaline salt.

The stability domains of the oxides and hydroxides are shown in the Pourbaix diagrams in Figures 8.3.3 to 8.3.5.

When a metal has several oxides, the less oxygenated is always basic and the hydroxide has the following formula: $M(OH)_n$. The most oxygenated oxides are acids and their hydrates are true oxiacids, with more oxygen than hydrogen atoms, e.g. MnO_4H, AlOOH, FeOOH and CoOOH.

The solubility of an oxide or hydroxide in an acid or basic aqueous solution is equal to the sum of the concentrations of all the complex ions:

$$s = \sum[\text{complex ions: hydroxo, chloro or sulfuric complexes}] \qquad [4.2.57]$$

The operating conditions of lixiviation processes (see [VIG 11b], Chapter 1, section 1.2.2) and of precipitation of oxides (section 1.3.1) are determined by the variations in solubility of oxides-hydroxides with pH and temperature.

4.2.4.1. *Effect of pH on the solubility of oxides and hydroxides in aqueous solutions*

4.2.4.1.1. When the anions of the acid or base do not form any complexes with the corresponding cation

– In an acid mixture, the reactions of formation of a hydroxocomplex, from a hydroxide or oxide, are:

$$xM(OH)_z(s) + (xz - y)\ H^+ \rightarrow M_x(OH)_y^{(xz-y)+} + (xz - y)\ H_2O \qquad [4.2.58]$$

$$x/a\ M_aO_b(s) + (xz - y)\ H^+ \rightarrow M_x(OH)_y^{(xz-y)+} + (zx/2 - y)\ H_2O \qquad [4.2.59]$$

where $az = 2\ b$, whose equilibrium coefficient is [FEI 63]:

$$Q_{Sxy} = [M_x(OH)_y^{(xz-y)+}] / [H^+]^{(xz-y)} \qquad [4.2.60]$$

The solubility, the total concentration of [M] as complexes, in the saturated solution is given by:

$$s = [M] = \sum x\ [M_x(OH)_y^{(xz-y)+}] = \sum x\ Q_{Sxy}\ .\ [H^+]^{(xz-y)} \qquad [4.2.61]$$

and (see equation [4.2.47b]:

$$Q_{Sxy} = Q_{Hxy} \cdot (Q_{S10})^{x} \qquad [4.2.62]$$

where Q_{S10} is the equilibrium coefficient of the formation reactions:

$$M(OH)_z(s) + zH^+ \rightarrow M^{z+} + zH_2O \qquad [4.2.63]$$

$$1/a\ M_aO_b(s) + zH^+ \rightarrow M^{z+} + z/2H_2O \qquad [4.2.64]$$

– In a basic mixture, the reaction of formation of a hydroxo complex is:

$$xM(OH)_z(s) + y'OH^- \rightarrow M_x(OH)_{xz+y'}{}^{y'-} \qquad [4.2.65]$$

with:

$$Q'_{Sxy'} = [(M_x(OH)_{xz+y}{}^{y'-}] / [OH^-]^{y'} \qquad [4.2.66]$$

and:

$$\log Q'_{Sxy'} = \log Q_{Sxy} + 14\ y' \text{ where } xz + y' = y \qquad [4.2.67]$$

EXAMPLE.–

$$ZnO(s) + H_2O + OH^- \rightarrow Zn(OH)_3^-$$

$$\log Q'_{s13'} = {}^-3.22 \qquad \log Q_{s13} = {}^-17.22 \text{ at } 25°C$$

The solubility of the oxide and the distribution of the hydroxo complexes in saturated solutions, as a function of pH, are shown below for:

– copper oxide, CuO, see Figure 4.2.14;

– ferrous iron hydroxide, $Fe(OH)_2$, see Figure 4.2.15;

– goethite α-FeOOH, see Figure 4.2.16;

– gibbsite α-$Al(OH)_3$, see Figure 4.2.17; and

– zinc oxide, see Figure 4.2.19.

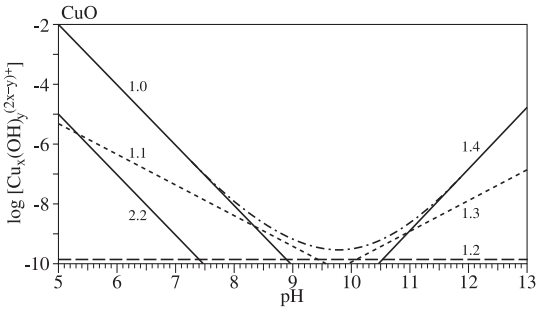

Figure 4.2.14. *Solubility diagram of CuO: solubility of CuO and distribution of hydrolysis products ([$Cu_x(OH)_y^{(2x-y)+}$] complexes) in solutions of ionic strength I = 1 M saturated with CuO at 25°C. The dash-dotted curve is the total concentration of Cu(II) [BAE 76]*

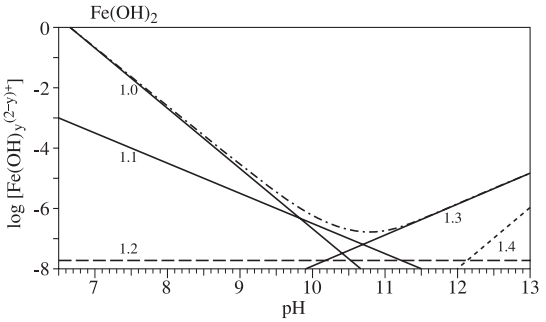

Figure 4.2.15. *Solubility diagram of Fe(II): distribution of hydrolysis products ([$Fe(OH)_y^{(2-y)+}$] complexes) in solutions of ionic strength I = 1 M saturated with $Fe(OH)_2$ at 25°C. The dash-dotted curve is the total concentration of Fe(II) [BAE 76]*

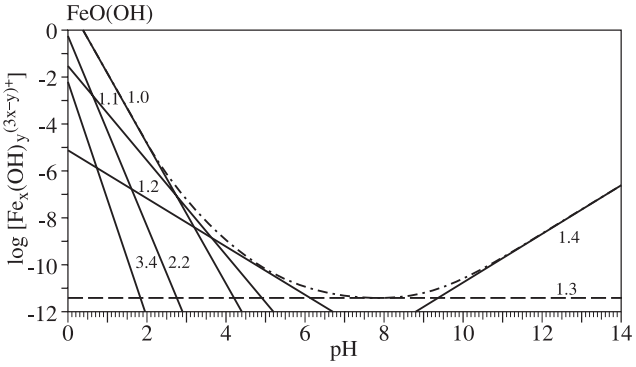

Figure 4.2.16. *Solubility diagram of a-FeOOH (goethite): distribution of hydrolysis products ([$Fe_x(OH)_y^{(3x-y)+}$] complexes) in solutions of ionic strength I = 1 M saturated with a-FeOOH at 25°C. The dash-dotted curve is the total concentration of Fe(III) [BAE 76]*

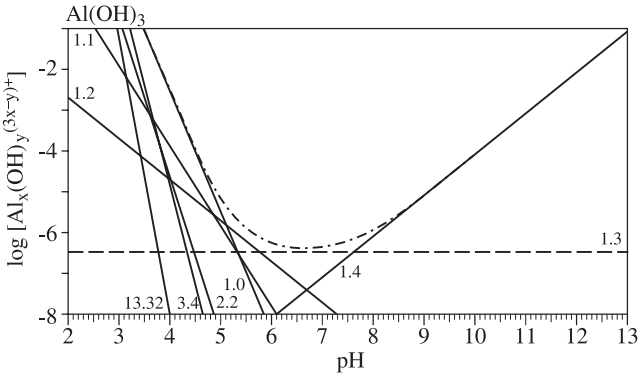

Figure 4.2.17. *Solubility diagram of a-Al(OH)$_3$ (gibbsite): distribution of hydrolysis products ([Al$_x$(OH)$_y^{(3x-y)+}$] complexes) in solutions of ionic strength I = 1 M saturated with a-Al(OH)$_3$ at 25°C. The dash-dotted curve is the total concentration of Al(III) [BAE 76]*

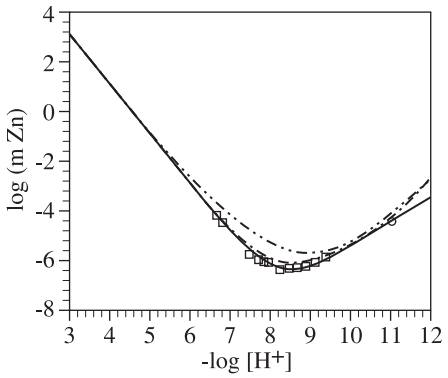

Figure 4.2.18. *ZnO solubility as a function of pH in a solution of ionic strength: I = 0.03 mol/kg at 75°C (solubility expressed as the logarithm of the measured total zinc concentration, in molality) [BEN 99]*

In a strongly acidic solution, the dominant species is the M^{z+} ion and the logarithm of the solubility varies linearly with pH, with a slope equal to the charge of the ion (sign changed):

$$\log s = \log[M^{z+}] = \log Q_{S10} - zpH \qquad [4.2.68]$$

In a strongly basic solution, the dominant species is the hydroxo complex $M(OH)_{z+n}^{-}$: ($Zn(OH)_3^-$, $Ni(OH)_3^-$, $Al(OH)_4^-$) type and the solubility increases with pH:

$$\log s = \log[M(OH)_{z+n}{}^{n-}] = \log Q'_{S1n} + npH \qquad [4.2.69]$$

NOTE.– The dissolution reaction is often written by considering that the ions in solution are ZnO_2^{2-}, $HCuO_2^-$, CuO_2^{2-} and AlO_2^-. The $Fe(OH)_4^-$ and $Al(OH)_4^-$ ions resulting from the total hydrolysis of these ions, are:

$$AlO_2^- + 2\ H_2O \rightarrow Al(OH)_4^-$$

In a basic environment, the soluble oxides in caustic soda and potash are the basic oxides (SiO_2) and the amphoteric oxides (ZnO, Fe_2O_3, Al_2O_3). The dominant ions in solution are in fact $Zn(OH)_3^-$, $Fe(OH)_4^-$ and $Al(OH)_4^-$.

4.2.4.1.2. When there is formation of complexes with anions present in the solution (Cl^-, $SO_4{}^{2-}$, etc.)

The overall reaction for each complex is:

$$(1/a)\ M_aO_b(s) + zH^+ + nX^- \rightarrow MX_n{}^{(z-n)} + z/2\ H_2O \qquad [4.2.70]$$

whose equilibrium constant K:

$$K_{Xn} = \frac{\tilde{a}_{MX_n}{}^{(z-n)}}{\left(\tilde{a}_{H^+}\right)^z \cdot \left(\tilde{a}_{X^-}\right)^n} \qquad [4.2.71]$$

is the product of the equilibrium constant of reaction [4.2.64] with the stability constant of the complex ion (see equation [4.2.45]):

$$K_{Xn} = K_{s10} \times K_{ST} \qquad [4.2.72]$$

The greater the stability constant of the complex, the greater the solubility of the oxide.

EXAMPLE.– Dissolution of ferric oxide in hydrochloric solutions. If the predominant ion is $FeCl_2^+$:

$$Fe_2O_3(s) + 6\ H^+ + 4\ Cl^- \rightarrow 2\ FeCl_2^+ + 3\ H_2O$$

$$\log[FeCl_2^+] = \log s = 1/2 \log K_{Xn} - 3\ pH + 2 \log[Cl^-] \qquad [4.2.73]$$

In more acidic solutions (pH = -1) the predominant ion is $FeCl^{2+}$, see Figure 8.3.7. The solubility of the oxide also increases with the concentration of Cl^- ions.

4.2.4.2. *Effect of temperature*

In Figure 4.2.19 the solubility curves of boehmite (γ-AlOOH) are drawn at three different temperatures. In an acidic solution, the solubility of this oxide decreases as the temperature increases. In a basic solution, the solubility increases with temperature. This result is general, see Figure 4.2.20.

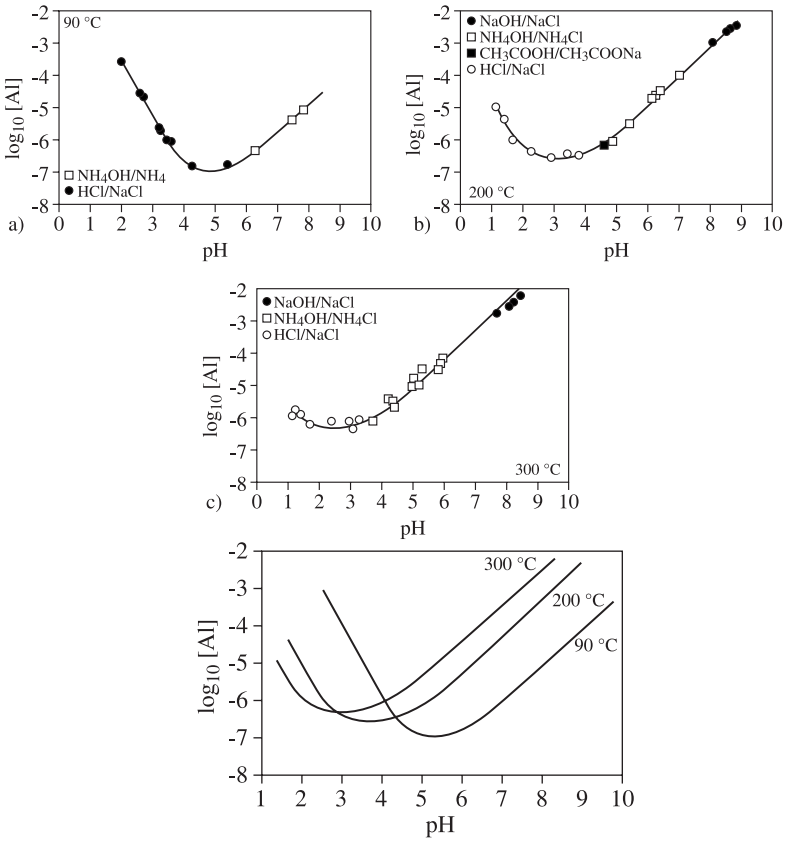

Figure 4.2.19. *Boehmite solubility as a function of pH and temperature at 90, 200 and 300°C in solutions of ionic strength I = 0.01 M [CAS 93]*

4.2.4.3. *Hydroxide solubility product*

In the literature, we find that the values of the solubility product(s) are:

$$K_{sp}\,(T,P)_{(hydroxide)} = \tilde{a}_{Mz+} \,.\, \tilde{a}_{OH-}{}^{z} = f_{\pm}{}^{z+1}\,[M^{z+}] \,.\, [OH^{-}]^{z} \qquad [4.2.74]$$

equilibrium constant corresponding to the dissociation:

$$M(OH)_z(s) \rightarrow M^{z+} + zOH^- \qquad [4.2.75]$$

where for the weakly soluble hydroxide, in acidic media (see equation [4.2.60]):

$$\log K_{sp}(T,P)_{(hydroxide)} = \log Q_{S10} + (z+1)\log f_{\pm} - 14\,z \qquad [4.2.76]$$

where $f_{\pm}$ is a function of the ionic force, see equation [4.2.20].

The solubility product only depends on the temperature.

Ca(OH)₂	*Mg(OH₂*	*Fe(OH)₂*	*Co(OH)₂*	*Zn(OH)₂*	*Cu(OH)₂*	*Al(OH)₃*	*amorphous Fe(OH)₃*	*Co(OH)₃*
$3.5 \cdot 10^{-6}$	$1.8 \cdot 10^{-11}$	10^{-15}	5.10^{-15}	$1.2 \cdot 10^{-17}$	$2.2 \cdot 10^{-20}$	$4.6 \cdot 10^{-33}$	4.10^{-38}	$1.6 \cdot 10^{-44}$

Table 4.2.8a. *Hydroxide solubility products at 20°C [FUG 00]*

As these reactions are endothermic, the equilibrium constants increase with temperature.

NOTE.– The solubility product of a complex hydroxide can be difficult to estimate. Thus, for jarosite, the solubility in water is due to the dissociation reaction:

$$Na\,[Fe_3(SO_4)_2(OH)_6]\,(s) \rightarrow 3\,Fe^{3+} + 6\,OH^- + Na^+ + 2\,SO_4^{2-} \qquad [4.2.77]$$

$$K_{sp} = [Fe^{3+}]^3\,[OH^-]^6\,[Na^+]\,[SO_4^{2-}]^2$$

$$K_{sp}(298°C) = 10^{-91}\,(mol/L)^{12}$$

and the solubility (concentration of $[Fe^{3+}]$ ions) not only depends on the pH, but also on the Na^+ ion and sulfate ion contents.

4.2.4.4. *Solubilities of iron and aluminum oxides and hydroxides*

4.2.4.4.1. Solubility of $Al(OH)_3$ amorph, boehmite (γ-AlOOH) and gibbsite ($Al_2O_3 \cdot 3\,H_2O = Al(OH)_3$)

Alumina is an amphoteric oxide that can be dissolved in acidic and basic solutions. The lixiviation operation of aluminum oxides is carried out in a basic solution. The dissolved species is the complex ion ($Al(OH)_4^-$), see Figure 4.2.17. The solubility of the hydroxide depends on the pH at 25°C, see equation [4.2.69].

$Al(OH)_3$ amorph	*γ-AlOOH boehmite*	*$Al(OH)_3$ gibbsite*
$\log K_{sp} = -31.2$	$\log K_{sp} = -31.7$	$\log K_{sp} = -33.8$
$\log[Al(OH)^{4-}] = -12.2 + pH$	$\log[Al(OH)^{4-}] = -13.2 + pH$	$\log[Al(OH)^{4-}] = -14.5 + pH$

Table 4.2.8b. *Solubility product and solubility of aluminum hydroxides at 25°C [FEI 63]*

It is necessary to reach a temperature of 150°C to completely dissolve gibbsite γ-$Al(OH)_3$; 250°C to dissolve boehmite γ-AlOOH(s); and 300°C for the diaspora α-AlOOH(s), see Figure 1.2.1 in [VIG 11b], Chapter 1.

4.2.4.4.2. Solubility of ferric oxides and hydroxides

The solubility products of the three ferric oxides are given in Table 4.2.8c at 25°C:

$Fe(OH)_3$ (amorph)	*α-FeOOH*	*1/2 Fe_2O_3*
$\log K_{sp} = -37.2$ to 37.9	$\log K_{sp} = -38.7$ to – 41.3	$\log K_{sp} = -42.7$

Table 4.2.8c. *Iron hydroxides and oxides solubility products [FEI 63]*

The iron oxides FeOOH and Fe_2O_3 are practically insoluble in an alkaline mixture, see Figure 4.2.16. The dissolved species is the ion $Fe(OH)_4^-$ at 25°C, see equation [4.2.68]:

$$\log[Fe(OH)_4^-] = -18.5 + pH \qquad [4.2.78]$$

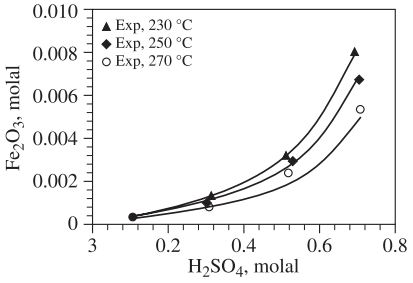

Figure 4.2.20. *Solubility of Fe_2O_3 in H_2SO_4 solutions at 230-270°C [LIU 03]*

The solubility of hematite $Fe_2O_3(s)$ in sulfuric solutions at high temperatures is shown in Figure 4.2.20. Solubility increases with increasing concentration of H_2SO_4 and decreases with increasing temperatures. The dominant species is ferric sulfate ($Fe_2(SO_4)_3$, see Figure 4.2.13.

4.2.5. *Solubility of salts*

The basic reaction of dissolution of a transition metal salt *in water* is a dissociation into its ions (see reaction [4.2.1]):

$$M_a \,.\, A_b(s) \rightarrow aM^{z+} + bA^{z-} \qquad [4.2.79]$$

whose *solubility product* K_{sp} (see equation [4.2.74]) increases with temperature:

$$K_{sp}(T,P) = a_{\pm}^{(a+b)} = (f_{\pm})^{(a+b)} \,.\, [M^{z+}]^a \,.\, [A^{z-}]^b \qquad [4.2.80]$$

The solubility of a weakly soluble salt in water is:

$$s = a\,[M^{z+}] = b\,[A^{z-}] \qquad [4.2.81]$$

$$s^{(a+b)} = a^a \,.\, b^b \,.K_{ps} /(f_{\pm})^{(a+b)} \qquad [4.2.82]$$

The solubility of most metallic salts *in water* increases with increasing temperatures up to 120–150°C, then decreases with increasing temperatures to become zero at temperatures approaching water's critical temperature of 373°C (see Figure 4.2.21). The decrease in solubility as the temperature increases above 120–150°C, is due to the formation of a hydroxide by a hydrolysis reaction, see reaction [4.2.47a].

When there is formation of complexes, reaction [4.2.79] must be associated with the reaction of formation of complexes with OH^-, Cl^-,SO_4H^- or SO_4^{2-}), see reaction [4.2.44], for instance:

$$M^{z+} + nX^{—} = MX_n^{(z-n)} \qquad [4.2.83]$$

thus:

$$M_aA_b(s) + anX^- \rightarrow aMX_n^{(z-n)} + bA^{z-} \qquad [4.2.84]$$

and the equilibrium constant of this reaction is the product of the solubility product and the stability constant of the complex ion (see equation [4.2.45a]):

$$K_n = K_{sp} \,.\, K_{ST} \qquad [4.2.85]$$

The concentration of each complex depends on the concentration of complexing ions, pH and temperature.

When there is formation of several complex ions, n = 1,2,3,4, the solubility is the sum of the concentration of all the complexes formed (see equation [4.2.57]):

$$s = [M^{z+}] + \sum[MX_n^{z-n}] \qquad [4.2.86]$$

The solubility is determined as a function of the concentration C of the complexing ion:

$$C = [X^-] + \sum n\,[MX_n^{z-n}] \qquad [4.2.87]$$

In the case where there is only one complex formed:

$$s = [MX_n^{z-n}] + [M^{z+}] \approx [MX_n^{z-n}] = [X^{z-}] \qquad [4.2.88]$$

The expression of the solubility of the compound (assuming that the concentration of the complexing ion or molecule is high and the stability constant is high) is:

$$(f_{\pm})^{(a+b)} \,.\, s^{(a+b)} = K_{ps} \,.\, (K_{ST})^a \,.\, (C)^{na} \qquad [4.2.89]$$

4.2.5.1. *Solubility of sulfates*

Metals form numerous salts with sulfuric acid: $FeSO_4$, $H_3OFe_3(SO_4)_2$, $Fe(SO_4)OH$ (basic sulfate), $Fe_2(SO_4)_3$ and $Fe_4(SO_4)(OH)_{10}$.

In water at low temperatures, sulfates such as $SO_4M(II)$ are soluble, except those of Ba ($BaSO_4$: $K_{ps} = 1 \times 10^{-10}$ at 25°C), Sr and Pb ($K_{ps} = 2.1 \times 10^{-8}$ at 20°C). Calcium sulfate $CaSO_4$ is slightly soluble ($K_{ps} = 2.4 \times 10^{-5}$). The variations of the solubility of transition metal sulfates with temperature are shown in Figure 4.2.21.

The solubility increases up to a certain temperature then decreases above that. The solubility of $CuSO_4.5H_2O$ in water (1.43 mol/L at 25°C) is at its maximum between 100 and 200°C (8.47 mol/L at 100°C), then it becomes weak at 300°C.

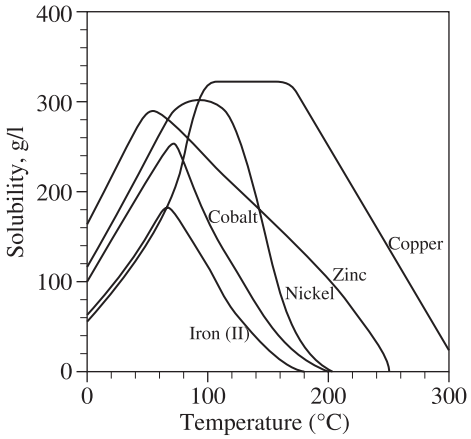

Figure 4.2.21. *Solubility of metal sulfates in water [DEM 99]*

The solubility of ferrous sulfate SO_4Fe (see Figure 4.2.22), is very weak in pure water at high temperatures >160°C. It increases with SO_4H_2 content in the solution. Similarly, the solubility of ferric sulfate $Fe_2(SO_4)_3$ at high temperatures >150°C increases with the acid content and decreases with temperature (see Figure 4.2.23). Ferric sulfate $Fe_2(SO_4)_3$ is soluble in water. Its solubility increases up to 140°C then decreases between 150 and 270°C. $Al_2(SO_4)_3$ is soluble in water: s = 0.91 M at 0°C and 2.90 M at 100°C.

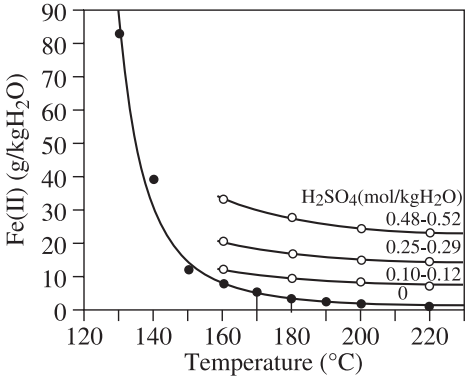

Figure 4.2.22. *Solubility of ferrous sulfate in sulfuric acid solutions as a function of temperature [DEM 99]*

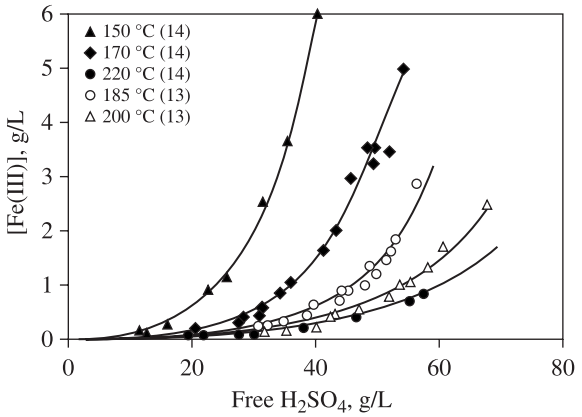

Figure 4.2.23. *Solubility of $(SO_4)_3Fe_2$ at various temperatures in sulfuric acid solutions as a function of $[H_2SO_4]_{(free)} = [H_2SO_4]_t - 1.5\ [Fe(III)]_{total}$ [LIU 03]*

4.2.5.2. *Solubility of chlorides*

Metals form hydrochloric acid with a number of salts. In general, chlorides are very soluble in water and their solubilities increase with temperature ($FeCl_3$: 4.59 mol/L at 0°C and 33 mol/L at 100°C). The exceptions are silver chloride (AgCl: 10^{-5} mol/L, $K_{ps} = 1.6 \times 10^{-10}$), lead chloride $PbCl_2$ (4×10^{-2} mol/L, $K_{ps} = 1.7 \times 10^{-5}$ at 20°C) and copper chloride (CuCl: 10^{-3} mol/L). These become soluble in concentrated Cl^- solutions owing to the formation of chlorocomplexes $CuCl_2^-$, $PbCl_3^-$ and $PbCl_4^{2-}$, whose stability increases with temperature [WIN 91].

Silver chloride is very poorly soluble in water but dissolves in an ammoniac solution by the formation of a silver-ammoniacal (diammine) complex:

$$AgCl(s) \rightarrow Ag^+ + Cl^-$$

$$Ag^+ + 2\ NH_3(aq) \rightarrow Ag(NH_3)_2^+$$

K_{sp} is the solubility product of silver chloride in water ($K_{sp} = 1.6 \times 10^{-10}$) and K_D the dissociation constant ($K_D = 6 \times 10^{-8}$). For the overall reaction:

$$AgCl(s) + 2\ NH_3 \rightarrow Ag(NH_3)_2^+ + Cl^- \qquad [4.2.90a]$$

the equilibrium constant is equal to:

$$K = \{[Ag(NH_3)_2^+] \,.\, [Cl^-]\} / [NH_3]^2 = K_{ps} / K_D = 2.6 \times 10^{-3} \qquad [4.2.90b]$$

The solubility s of silver chloride in an ammoniac solution of concentration c, with excess ammonia, is given by:

$$s = [Ag+] + [Ag(NH_3)_2^+] \approx [Ag(NH_3)_2^+]$$

$$c = [NH_3] + 2\,[Ag(NH_3)_2^+] \qquad [4.2.91]$$

As the complex is stable ($K_D = 6 \times 10^{-8}$), the concentration in $[Ag^+]$ is very low and the solubility of silver chloride in an ammoniacal solution is given by:

$$(f_\pm)\ s = c\,(K_{ps} / K_D)^{1/2} = c \times 0.05 \qquad [4.2.92]$$

In an ammoniacal solution, metals such as copper, nickel, cobalt, gold, silver, platinum and zinc give soluble polyatomic complex ions in water, for instance $Cu(NH_3)_4^{2+}$, $Zn(NH_3)_2Cl_2$ complexes. These complexes increase the solubility of the metallic ions (Ni^{2+}, etc.), and thus reduce the stability domain of the corresponding oxide or hydroxide to allow the dissolution of sulfides or oxides at high pH.

4.2.5.3. *Solubility of sulfides*

Metallic sulfides are very weakly soluble in water:

$$MS(s) \rightarrow M^{2+} + S^{2-} \qquad [4.2.93a]$$

$$K_{sp} = a_{M}2+ .\ a_{S}2- = f_\pm^{MS} .\ [M^{2+}] .\ [S^{2-}] \qquad [4.2.93b]$$

Ag_2S	*CdS*	*CuS*	*FeS*	*MnS*	*NiS*	*CoS*	*PbS*	*SnS*	*ZnS*
6.10^{-51}	8.10^{-27}	6.10^{-37}	6.10^{-19}	2.10^{-13}	3.10^{-19}	4.10^{-21}	3.10^{-29}	10^{-26}	2.10^{-25}

Table 4.2.9. *Sulfide solubility products at 20°C [SIM 63]*

If a very strong, and therefore completely dissociated, acid (e.g. HCl) is added to a sulfide's aqueous solution, the S^{2-} ions are captured by the H^+ ions, by the reactions:

$$S^{2-} + H^+ \rightarrow HS^- \qquad [4.2.94a]$$

$$HS^- + H^+ \rightarrow H_2S_{(\text{in solution})} \qquad [4.2.94b]$$

with dissociation constants K_1 ($pK_1 = 7.1$) and K_2 ($pK_2 = 13$), see equations [4.2.33] and [4.2.34]. As the concentrations of $[HS^-]$, $[S^{2-}]$ and $[H_2S_{(aq)}]$ ions are low, their activities are taken as equal to their concentrations. The sulfide's solubility:

$$s = [M^{2+}] = [H_2S_{(aq)}] + [HS^-] + [S^{2-}] \qquad [4.2.95a]$$

is therefore expressed as a function of three constants, K_1, K_2 and K_{ps}, and on the activity a_{H+} by:

$$s = (K_{ps} / f_{\pm})^{1/2} \{1 + a_{H+} / K_2 + a_{H+}^2 / K_1K_2\}^{1/2} \qquad [4.2.95b]$$

The more acidic the solution, the bigger its dissolution capacity and the more the solubility increases.

4.2.5.4. *Summary: factors controlling salt solubility*

Apart from the temperature, we can displace the equilibrium and so increase or decrease the solubility of a salt:

– by adding another salt or an acid from another anion;

– by decreasing or increasing the pH of the salt of a weak acid and poorly soluble weak base; or

– by adding a complexing agent to the salt of strong acid and weak base.

The addition of a strong acid from a different anion (e.g. NO_3H) produces an increase in the solubility of ClAg, owing to the increase in ionic strength of the solution (see equation [4.2.16]):

$$I = 1/2 \{[Ag^+] + [Cl^-] + [NO_3^-] + [H^+] + [OH^-]\} \approx [NO_3H]$$

which produces a variation in the average activity coefficient of compound $f_{\pm}$ (see equation [4.2.20]), and therefore the electrolyte's solubility (see equations [4.2.46], [4.2.61], [4.2.68] and [4.2.89]):

$$(a + b) \log s \approx \log K_{ps} + \alpha I^{1/2} \qquad [4.2.96a]$$

Experimentally, the logarithm of the solubility of AgCl (in mol/L) linearly varies with the square root of the concentration of nitric acid, and therefore of the ionic strength I [PRI 50]:

$$\log s = 0.5\, I^{1/2} - 4{,}9 \qquad [4.2.96b]$$

$(I \approx [NO_3H])$

as the concentration of OH^- ions can be neglected in an acid environment compared to H^+ ions and as the solubility of silver chloride is very weak ($1/2 \log K_{ps} = -4.9$).

Silver cyanide is insoluble in water:

$$CNAg(s) \rightarrow CN^- + Ag^+$$

$$K_{ps} = 1.6 \times 10^{-14} \text{ at } 20°C$$

and:

$$s = [Ag^+] = K_{ps}^{1/2}.$$

If we add H^+ ions, the following reaction occurs (see reaction [4.2.32a]):

$$CN^- + H^+ \rightarrow CNH \text{ (pK = 9.3), see Figure 4.2.7.}$$

which displaces the equilibrium, and thus the solubility increases:

$$s = \{K_{ps} (1 + [H^+] / K_D)\}^{1/2} \qquad [4.2.97]$$

4.2.6. *Solubility of gases in an aqueous solution*

A large number of lixiviation reactions occur under oxygen pressure. The variation of oxygen and hydrogen content in water as a function of temperature and partial pressure of the gas are shown in Figures 4.2.24, 4.2.25 and 4.2.26. For oxygen, the following correlations have been established:

1. (Zoss) [ZOS 54]

$$[O_2(aq)](kg/m^3) = K_h \,.\, p_{O2} \text{ (in kPa)} \qquad [4.2.98]$$

$$K_h = (3.418 \times 10^{-3} - 3.738 \times 10^{-5} T + 1.95 \times 10^{-7} T^2) \times 0.145 \text{ where T in °C}$$

2. (Baldwin) [BAL 95]

$$P_{O2} \text{ (in atm)} = H\,[O_2(aq)] \text{ in mol/L}$$

$$H \times 10^{-3} = -3.8 \times 10^{-5} T^2 + 0.02 T + 0.24 [Fe^{3+}] + 0.81 [Zn^{2+}]$$

$$+ 0.074 [H_2SO_4] - 0.70 \text{ atm/mol/L} \qquad [4.2.99]$$

In a solution of zinc and iron sulfates at 50°C (0.330 mol/L acid, 0.106 mol/L Fe_t and 2.78 mol/L Zn^{2+}), the Henrian constant is H = 4395.5 atm/mol/L, and in pure water at this temperature, H = 1,067 atm/mol/L.

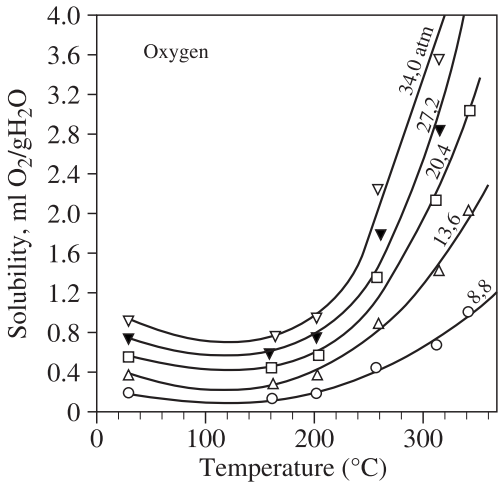

Figure 4.2.24. *Solubility of oxygen in water as a function of temperature and pressure [DEM 99]*

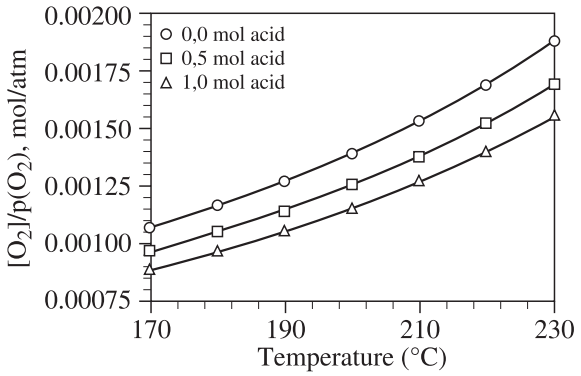

Figure 4.2.25. *Oxygen solubility as a function of temperature and [H_2SO_4] concentration (Tromans' model) [LON 04, TRO 98]*

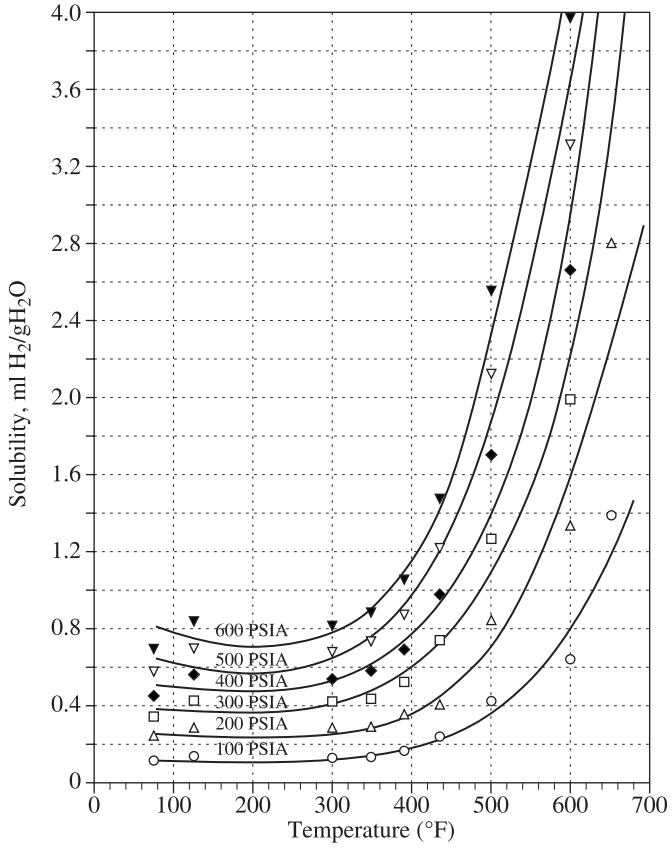

Figure 4.2.26. *Solubility of hydrogen (in moles H_2/gH_2O) in water at varying temperatures and pressures [SCH 56]*

4.3. Thermodynamics of salt melts (fluxes)

Fluxes are mixtures of halides (chlorides and fluorides) of alkaline and alkaline earth metals. They are used:

– as electrolytes in molten salt electrolysis: LiCl, $MgCl_2$, $CaCl_2$, $AlCl_3$ and $ZrCl_4$ or for the reduction of oxides (e.g. Al_2O_3) by electrolysis of aluminum fluoride (AlF_6Na_3) and for the reduction of oxide TiO_2 in $CaCl_2$;

– as a cover for liquid metals (aluminum) during their melting or remelting to protect them from the oxidative atmosphere. A typical composition is 47.5% NaCl, 47.5% KCl and 5% NaF, whose fusion temperature for the eutectic composition is 607°C;

– as refining fluxes, playing the same role as slags by absorbing the chlorides of Mg, Li, Na and K formed during the refining of aluminum. Elements Li, Na, K, Ca and Mg are thus eliminated from liquid aluminum by injection of chlorine gas (see [VIG 11b], Chapter 7, section 7.3.2.1):

$$Mg_{(\text{dissolved in Al})} + Cl_2 \rightarrow (MgCl_2)_{(\text{dissolved in a flux})} \quad [4.3.1]$$

– as fluxes in the metal refining process by electroslag remelting (ESR). Composition fluxes 50-50 ($MgF_2 + CaF_2$) or Na_3AlF_6 and 70 CaF_2 + 30 Al_2O_3 (mass) at 1,400 and 1,500°C are used for the ESR of copper scraps [UTI 98, UTI 01].

4.3.1. *Compositions and physical properties of fluxes*

Fluxes are ionic solutions whose conductance, which increases by a factor of 10^2–10^4 at fusion, is entirely ionic in the molten state and of the order 1–5 ohm^{-1} cm^{-1} (the metals' conductance is of the order of 10^5 ohm^{-1} cm^{-1}). This explains their use as electrolytes. The current efficiency for the reduction is equal to one.

$AlCl_3$, an ionic compound in solid state, is composed of covalent Al_2Cl_6 molecules in the liquid state whose conductance decreases at fusion. For magnesium chloride, $MgCl_2$, the Mg-Cl bond has a strong covalent contribution, with the formation of a complex $(MgCl_4)^{2-}$ ion. The molten KCl-$MgCl_2$ mixture is therefore made of K^+, Cl^-, Mg^{2+} and $(MgCl_4)^{2-}$ ions.

Their melting temperature is low (NaCl 800°C, $MgCl_2$ 714°C and CaF_2 858°C) and they form eutectics whose melting temperatures are even lower. The NaCl-KCl eutectic melts at 665°C. The $MgCl_2$-KCl eutectic melts at 424°C.

Their viscosity is low (NaCl becomes viscous at 900°C: 1 cP, and $PbCl_2$ at 650°C: 2 cP) [RIC 74].

4.3.2. *Thermodynamic properties*

The Gibbs free energy of formation of chlorides and fluorides was presented in Chapter 2 (see Figure 2.4.3).

In a molten salt or in a mixture of molten salts, the entities are ions and their thermodynamic functions cannot be measured. We can only determine the thermodynamic functions of electrically neutral groups such as ionic pairs. The reference states are therefore the standard states of the corresponding pure salts at the given temperature.

The great stability of alkaline and alkaline earth fluorides and chlorides (see Figure 2.4.5) or their high, reversible decomposition tension voltage (see [VIG 11c], Chapter 9, Figure 9.1.1) explain their use as electrolytes in the electrolysis of chlorides and metal oxides in molten salts.

4.3.2.1. *$MgCl_2$-NaCl-KCl system*

Figure 4.3.1 shows that the variation of the activity coefficient of $MgCl_2$ in NaCl and KCl melts between 723 and 823°C. The strong negative deviation from ideality is caused by the formation of $(MgCl_4)_2^-$ complexes. In a 50-50 mix of NaCl-KCl, the activity coefficient $\gamma_{MgCl2} = 0.009$ at 800°C.

The low value of the activity of magnesium chloride has a very strong effect in the refining of aluminum. In the refining process, represented by reaction [4.3.1], the lower the activity of $MgCl_2$ in the flux, the greater the affinity of reaction will be and therefore the extraction of magnesium from the liquid aluminum. By adding 1% in the weight of NaF to the 50-50 mix of NaCl-KCl, the activity coefficient of $MgCl_2$ is furthermore divided by a factor of 10.

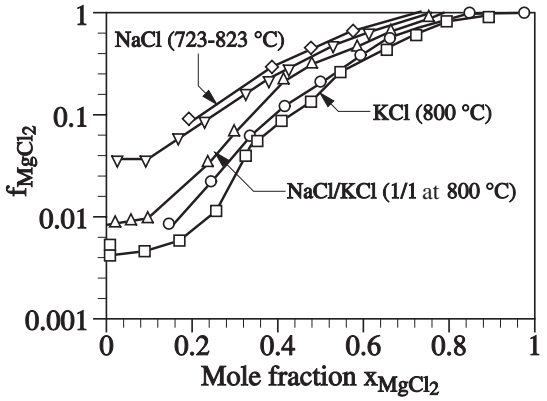

Figure 4.3.1. *The activity coefficient of $MgCl_2$ in NaCl-KCl melts at 723 and 823°C [UTI 98]*

4.3.2.2. *NaF-AlF_3 system*

Aluminum is produced by the reduction of alumina via electrolysis in molten salts (see [VIG 11c, Chapter 9, section 9.3). The electrolytic bath is composed of cryolite (AlF_6Na_3), aluminum (AlF_3) and calcium (CaF_2) fluorides. Figure 4.3.2 shows the phase diagram of the NaF-AlF_3 system.

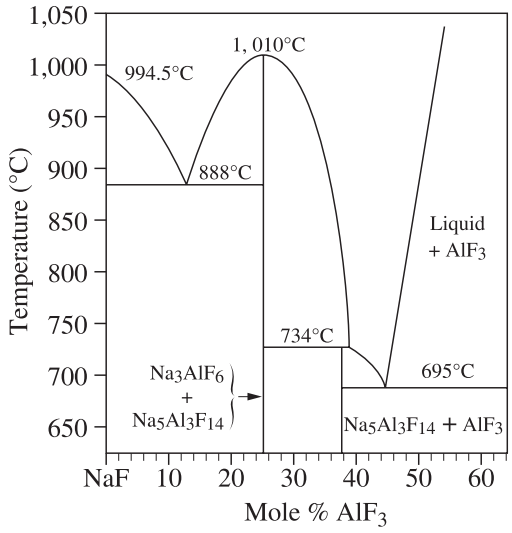

Figure 4.3.2. *NaF-AlF_3 phase diagram [RIC 74]*

The molten flux is considered to be acidic, for ratio is < 3 ($r = x_{NaF} / x_{AlF3}$), and is considered to be basic for a ratio r > 3.

The standard Gibbs free energy of formation of compound AlF_6Na_3 is given by:

$$3\ NaF(l) + AlF_3(s) \rightarrow Na_3\ AlF_6 \qquad [4.3.2]$$

$$\Delta G°_{1,293} = -44\ 684 - 53{,}544\ T(J)$$

The activities of both components NaF and AlF_3, just above the melting point of cryolite at the stoichiometric composition, have the following values [DEW 90, ZHA 02]:

at 1,293K, $x_{AlF3} = 0.25$, $a_{NaF} = 0.37$ and $a_{AlF3} = 5 \cdot 10^{-4}$

where (see equation [2.3.11]):

$$\Delta G°_{1,293} = RT \ln (a_{NaF})^3 \cdot (a_{AlF3}) \qquad [4.3.3]$$

The very low value of activity a_{AlF3} is due to the formation of the $(AlF_6)^{3-}$ ion.

These components are present in the electrolytic bath as partially dissociated (Na_3AlF_6, Na_2AlF_5, $NaAlF_4$) species, see Figure 4.3.3 [GIL 95]:

$$Na_3AlF_6 \rightarrow 3\ Na^+ + (AlF_6)^{3-} \quad [4.3.4a]$$

$$(AlF_6)^{3-} \rightarrow (AlF_5)^{2-} + F^- \quad [4.3.4b]$$

$$(AlF_5)^{2-} \rightarrow (AlF_4)^- + F^- \quad [4.3.4c]$$

Thus the majority of the ions present in the electrolyte are Na^+, $(AlF_5)^{2-}$, $(AlF_4)^-$ and F^- whose contents evolve with that of AlF_3 in the electrolyte.

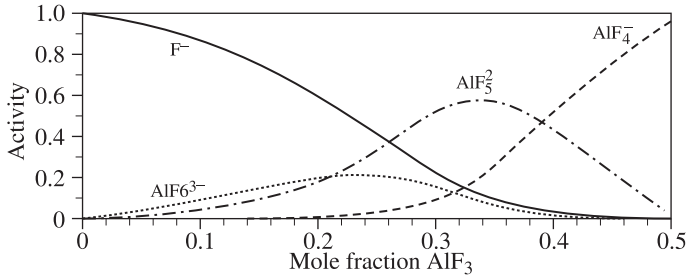

Figure 4.3.3. *Variations of the distribution of chemical species in the NaF-AlF_3 melt as a function of the AlF_3 molar fraction at 1,000°C [ZHA 02]*

4.3.3. *Solubility of oxides in halides*

Oxides are practically insoluble in the chlorides of their metal (MgO is insoluble in $MgCl_2$), with the exception of Ba, Ca, Sr oxides which have a great solubility in their chlorides (see [VIG 11c], Chapter 9, section 9.1). However, the alkaline earth chlorides and especially the fluorides are good solvents for oxides and they strongly lower their viscosity.

TiO_2 is practically insoluble in the molten chlorides of alkaline and alkaline earth metals. However, it is soluble in sodium (up to 8%) and potassium fluorides and in titanium hexafluoride (up to 14%).

4.3.3.1. *Solubility of alumina in the NaF-AlF_3 system*

The Na_3AlF_6-Al_2O_3 phase diagram (see Figure 4.3.4) shows the extent of the alumina solubility in cryolite, with formation of a eutectic for a content of 10% in weight of alumina.

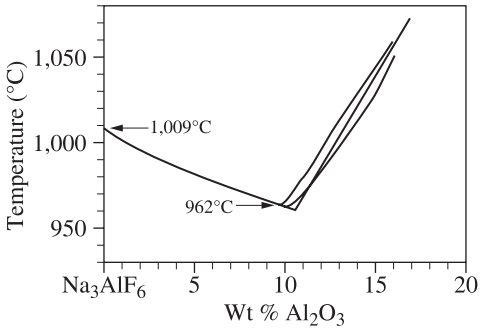

Figure 4.3.4. *Na_3AlF_6-Al_2O_3 phase diagram [FOS 60]*

In the electrolytic bath there is the formation of $(Al_2OF_6)^{2-}$ and $(Al_2O_2F_4)^{2-}$ ions. The mechanism by which the alumina dissolution occurs is unknown. Depending on the content in alumina and the acidity of the bath, formation of either $(Al_2OF_6)^{2-}$ or $(Al_2O_2F_4)^{2-}$ ions may occur. Their molecular structures respectively are:

$(Al_2OF_6)^{2-}$

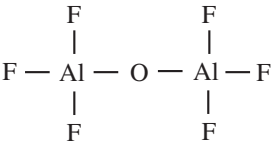

$(Al_2O_2F_4)^{2-}$

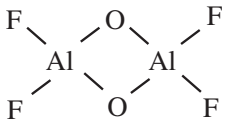

These complexes are formed [GIL 95]:

– for low concentrations of alumina (general case) in the electrolytic bath, in a neutral or acidic environment, by the reaction:

$$Al_2O_3(s) + 4\ (AlF_5)^{2-} + 4\ F^- \rightarrow 3\ (Al_2OF_6)^{2-} \qquad [4.3.5]$$

– for higher concentrations of alumina, by the reaction:

$$Al_2O_3(s) + (AlF_5)^{2-} + F^- \rightarrow 3/2\ (Al_2OF_4)^{2-} \qquad [4.3.6]$$

For a molten acidic bath, r = 1.5 saturated in alumina at 1,300K, the dominant ion is $(Al_2OF_6)^{2-}$. Near the stoichiometry r = 3, the dominant ion is $(Al_2O_2F_4)^{2-}$, see Figure 4.3.5.

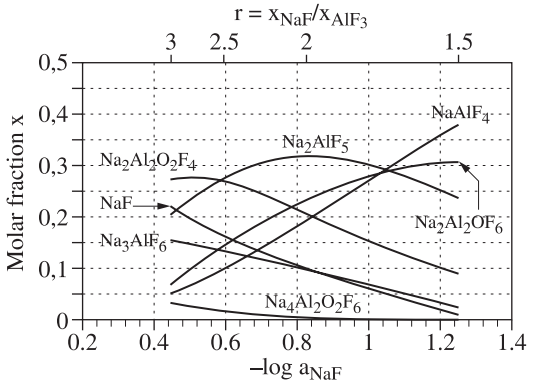

Figure 4.3.5. *Calculated concentrations of all the solutes for the alumina-saturated cryolite melt at 1,300K [ZHA 02]*

In alumina electrolysis, the content of the electrolyte is in the order of 2–4% and the electrolyte has a AlF_3 content such that the ratio is r > 3.

4.4. Bibliography

[BAE 76] C.F. BAES, R.E. MESMER, *The Hydrolysis of Cations*, John Wiley & Sons, New York, 1976.

[BAG 98] M. BAGHALHA, V.G. PAPANGELAKIS, *Metallurgical and Materials Transactions B*, Vol. 29B, pp. 945-957, October 1998.

[BAL 95] S.A. BALDWIN, G.P. DEMOPOULOS, V.G. PAPANGELAKIS, *Metallurgical and Materials Transactions B*, Vol. 26B, pp. 1035-1047, October 1995.

[BAT 70] R. BATES, B.R. STAPLES, R.A. ROBINSON, *Anal. Chem.*, Vol. 42, pp. 867-871, 1970.

[BEN 99] P. BENEZETH *et al.*, *Geochimica and Cosmochimica Acta*, Vol. 63, No. 10, pp. 1571-1586, 1999.

[CAS 93] S. CASTET, J.L. DANDURAND, J. SCHOTT, R. GOULT, *Geochimica and Cosmochimica Acta*, Vol. 57, pp. 4869-4884, 1993.

[DEM 99] G.P. DEMOPOULOS, *Leaching Fundamentals and Industrial Practice*, TMS Short Course, San Diego, February 1999.

[DEW 90] E.W. DEWING, *Metallurgical Transactions B*, Vol. 21B, pp. 285-294, April 1990.

[DIC 90] A.G. DICKSON, D.J. WESOLOWSKI, D.A. PALMER, R.E. MESMER, *Jour. Phys. Chem.*, Vol. 94, pp. 7978-85, 1990.

[FEI 63] W. FEITKNECHT, P. SCHINDLER, *Solubility Constants of Metal Oxides, Metal Hydroxides and Metalhydroxide salts in Aqueous Solutions*, Butterworths, 1963.

[FLE 99] C.A. FLEMING, *Leaching of Gold Ores, Leaching Fundamentals and Industrial Practice*, TMS Short Course San Diego, February 1999.

[FIL 95] D. FILIPPOU, G.P. DEMOPOULOS, V.G. PAPANGELAKIS, *AICHE Journal*, Vol. 41, No. 1, pp. 171-184, January 1995.

[FUE 86] M.C. FUERSTENAU *et al*., *Metallurgical Transactions B*, Vol. 17B, pp. 416, September 1986.

[FUG 00] S. FUGLEBERG, *Lead-Zinc*, TMS, Short Course, 2000.

[GIL 95] B. GILBERT, E. ROBERT, E. TIXHON, J.E. OLSEN, T. OSTVOLD, *Light Metals*, J. Evans (ed.), TMS, pp. 181-194, 1995.

[HIR 87] T. HIRATO, H. MAJIMA, Y. AWAKURA, *Metallurgical Transactions B*, Vol. 18B, pp. 31-33, March 1987.

[JAN 83] J.J.C. JANSZ, *Hydrometallurgy*, Vol. 11, pp. 13-31, 1983.

[LAT 38] W.M. LATIMER, *Oxidations States of the Elements and their Potentials in Aqueous Solutions*, Prentice Hall, 1938.

[LAT 51] W.M. LATIMER, *Oxidation Potentials*, Prentice Hall, 1951.

[LEW 61] G.N. LEWIS, M. RANDALL, *Thermodynamics*, McGraw-Hill, New York, 1961.

[LIU 03] H. LIU, V.G. PAPANGELAKIS, M.S. ALAM, G. SINGH, *Canadian Metallurgical Quarterly*, Vol. 42, No. 2, pp. 199-208, 1993.

[LON 04] H. LONG, D.G. DIXON, *Hydrometallurgy*, Vol. 73, pp. 335-349, 2004.

[MAJ 81] H. MAJIMA, Y. AWAKURA, *Metallurgical Transactions B*, Vol. 12B, pp. 141-145, March 1981.

[MUI 85] D.M. MUIR, G. SENANAYAKE, *Extractive Metallurgy 1985*, The Institution of Mining and Metallurgy, London, pp. 65-83, 1985.

[PIT 73] K.S. PITZER, "Thermodynamics of electrolytes: theoretical basis and general equations", *J. Phys. Chem.*, Vol. 77, pp. 268, 1973.

[PIT 79] K.S. PITZER, (dir.), *Activity Coefficients in Electrolyte Solutions*, CRC Press, Boca Raton (Fl.), pp. 75-153, 1979.

[PRA 52] H.A. PRAY *et al*., *Industrial and Engineering Chemistry IEC*, Vol. 44, pp. 1147, 1952.

[PRI 50] I. PRIGOGINE, R. DEFAY, *Thermodynamique chimique*, Desoer, Liege, Chapter 27, 1950.

[RIC 74] F.D. RICHARDSON, *Physical Chemistry of Melts in Metallurgy*, Vol. 1, Academic Press, London and New York, Chapter 6, 1974.

[ROS 83] T. ROSENQUIST, *Principles of Extractive Metallurgy*, McGraw-Hill, New York, 1983.

[SCH 56] F.A. SCHAUFELBERGER, *Transaction AIME*, *Journal of Metals*, pp. 695-704, May 1956.

[SEL 90] C. SELLA, D. BAUER, *Hydrometallurgy*, Vol. 23, pp. 353-364, 1990.

[SEN 03] S. SENANAYAKE, D.M. MUIR, *Hydrometallurgy*, Vol. 1, pp. 517-531, 2003.

[SIM 63] C. S. SIMONS, *Unit processes in Hydrometallurgy*, New York, Gordon & Breach, pp. 592-615, 1963.

[SOR 99] S. SORENSEN, S. KJELSTRUP, *Aluminum Transactions*, Vol. 1, No. 1, pp. 179-185, 1999.

[STO 48] R.H. STOKES, R.A. ROBINSON, *J. Am. Chem. Soc.*, Vol. 70, pp. 1870-1878, 1948.

[TRO 98] D. TROMAN, *Hydrometallurgy*, Vol. 50, pp. 279, 1998.

[UTI 98] T.A. UTIGARD *et al*., *JOM*, pp. 38-43, November 1998.

[UTI 01] T.A. UTIGARD *et al*., *Canadian Metallurgical Quarterly*, Vol. 4, No. 3, pp. 327-334, 2001.

[VIG 11b] A. VIGNES, *Extractive Metallurgy 2: Metallurgical Reaction Processes*, ISTE Ltd, London and John Wiley and Sons, New York, 2011.

[VIG 11c] A. VIGNES, *Extractive Metallurgy 3: Processing Operations and Routes*, ISTE Ltd, London and John Wiley and Sons, New York, 2011.

[WIN 91] R. WINAND, *Hydrometallurgy*, Vol. 27, pp. 285-316, 1991.

[ZEM 86] J.F. ZEMAITIS, D.M. CLARK, M. RAFAL, N.C. SCRIVENER, *Handbook of Aqueous Electrolyte Thermodynamics. The Art and Applications*, DIPPR, AIChE, New York, 1986.

[ZHA 02] Y. ZHANG *et al*., *Metallurgical and Materials Transactions B*, Vol. 33B, pp. 315-319, April 2002.

[ZOS 54] L.M. ZOSS *et al*., *Trans. ASME*, Vol. 76, 69-71, 1954 (see H.K. LIN, H.Y. SOHN, *Metallurgical Transactions B*, Vol. 18, pp. 497-503, September 1987).

Chapter 5

Reaction Kinetics

5.1. Introduction

Thermodynamics does not provide any information on the mechanism of a chemical reaction or its rate. Chemical kinetics studies the factors that control the rate of the chemical reaction and works out its mechanism.

The conversion and extraction processes occur in multiphase systems. They involve:

– homogeneous and heterogeneous chemical reactions; and

– mass and heat intraphase transport and interphase transfer across phase boundaries.

The rates of these processes are determined either by chemical reaction or by transport phenomena.

The mechanisms and kinetics of chemical reactions are dealt with in this chapter. The mechanisms and kinetics of electrochemical reactions are dealt with in Chapter 8. Transport and transfer phenomena are examined in Chapter 6.

In many multiphase processes, contact between the phases is achieved by the dispersion of one phase into another. The particle kinetic laws (between a particle and a continuous phase) for various processes, e.g. conversion, precipitation or solvent extraction, are dealt with in Chapter 7.

Extractive Metallurgy 1: Basic Thermodynamics and Kinetics Alain Vignes
© 2011 ISTE Ltd. Published 2011 by ISTE Ltd.

The overall kinetics of these processes in operations are dealt with, in terms of engineering processes, in Chapters 2 to 7 of [VIG 11c].

The majority of these processes involve "heterogeneous" reactions between the reactants present in both phases. The only processes involving homogeneous reactions are complexation reactions (see Chapter 4, section 4.2.3) and "homogeneous precipitations" (see section 5.3), with formation and growth of particles, globules or bubbles in a homogeneous phase.

This chapter analyzes the mechanisms and rates of these chemical reactions.

5.2. Rate of a chemical reaction

5.2.1. *Definitions*

5.2.1.1. *Homogeneous reaction*

This is a single phase reaction system in a closed container, perfectly mixed, thus of uniform composition and temperature. At a given instant in volume V, there are $n_A(t)$, $n_B(t)$, $n_R(t)$ and $n_S(t)$ moles of each component and, between reactants A and B dissolved in the same (α) phase, one or other of the following reactions occurs:

$$\nu_A A(\alpha) + \nu_B B(\alpha) \rightarrow \nu_R R(\alpha) + \nu_S S(\alpha) \qquad [5.2.1a]$$

$$\nu_A A(\alpha) + \nu_B B(\alpha) \rightarrow \nu_S S(\beta)\downarrow \qquad [5.2.1b]$$

giving either products dissolved in the initial α phase or a product forming a new phase S(β) (homogeneous precipitation).

The rate of consumption r_A of reactant A is defined as the variation of the number of moles of A per time unit and volume of the reaction mixture:

$$dn_A / dt = V.\, r_A \qquad [5.2.2]$$

The variation of the fractional conversion χ_A of reactant A, see Chapter 1, equation [1.2.7], is expressed by:

$$d\chi_A / dt = -(V / n_{Ai}) r_A \qquad [5.2.3]$$

In the same way, the rate of consumption of reactant B and formation of products R and S are in accordance with the law of definite proportions (see equation [1.2.5]):

$$r_A / -\nu_A = r_B / -\nu_B = r_R / \nu_R = r_S / \nu_S = r_v \qquad [5.2.4]$$

$$r_v = (1 / V) \cdot d\xi / dt = -(1 / \nu_A \cdot V) \cdot dn_A / dt = -(1 / \nu_B \cdot V) \cdot dn_B / dt \quad [5.2.5]$$

where r is the rate of the reaction in moles or in *mass* per unit volume and time.

If the composition and temperature in the system are not uniform, the rate will vary from one point to the next.

5.2.1.2. *Heterogeneous reaction*

A heterogeneous reaction occurs on the surface (at the interface) between two phases (α and β). The reaction can involve:

– two reactants, respectively, in each phase:

$$\nu_A A(\alpha) + \nu_B B(\beta) \rightarrow \nu_R R(\alpha) + \nu_S S(\beta) \quad [5.2.6]$$

with a special case where component B is a solid (oxide or sulfide) that undergoes a complete *conversion* (oxide reduction or conversion of a sulfide into oxide) with formation or not of another solid S(β);

– one or two reactants in the same phase reacting on a surface S' to form a deposit S on this surface (heterogeneous precipitation):

$$\nu_A A(\alpha) + \nu_B B(\alpha) \rightarrow \nu_R R(\alpha) + \nu_S S(s)\downarrow \text{ (deposit on S')} \quad [5.2.7a]$$

EXAMPLE.– Thermal decomposition of gaseous nickel carbonyl ($Ni(CO)_4$) on nickel particles:

$$Ni(CO)_4(g) / Ni(s)_{(particles)} \rightarrow Ni(s)_{(deposit\ on\ particles)} + 4\ CO(g) \quad [5.2.7b]$$

– the "transfer" of a component from phase α into a second phase β across the interface, with a change in the chemical state of this component:

$$\nu_A A(\alpha) \rightarrow \nu_R R(\beta) \quad [5.2.8]$$

EXAMPLES.– Transfer of sulfur in metal-slag reactions, gas-liquid extraction (hydrogen removal of liquid metals), solvent extraction in hydrometallurgy with the formation of some complexes.

The rate of consumption of reactant A, r_{As}, is defined by the number of moles of component A in phase α converted or transferred per unit time and surface $S_{\alpha\beta}$ between phases α and β:

$$dn_A / dt = S_{\alpha\beta}\, r_{As} \quad [5.2.9]$$

from which the reaction rate, r_s, is defined as:

$$r_S = 1 / S_{\alpha\beta} \cdot d\xi / dt = -(1 / \nu_A) \cdot r_{As} = -(1 / \nu_B) \cdot r_{Bs} \qquad [5.2.10]$$

where r_s is expressed in moles (mass) per (contact) unit surface and time.

5.2.2. *Expressions of the rate of a chemical reaction*

The rate of a reaction, per unit volume, r_v (see equation [5.2.5]) or unit surface r_s (see equation [5.2.10]), is usually a complex function that depends on the composition of a reacting mixture in the elementary volume or in the immediate vicinity of the surface on which the reaction is occurring. The kinetic law is written as a difference between the rates of both "forward and reverse" reactions. Each of these rates is expressed as a product of a temperature-dependent term (*rate constant*) and a composition-dependent term:

$$r = k_{rc}^{+}(T,P)\ f\{C_A(t \text{ or } z), C_B(t \text{ or } z)\} - k_{rc}^{-}\ f\{C_r(t \text{ or } z), C_s(t \text{ or } z)\} \qquad [5.2.11]$$

The composition-dependent term can often be expressed by:

$$r^{+} = k_{rc}^{+}(T) \cdot C_A^{\,a} \cdot C_B^{\,b} \text{ (in mol/cm}^3\text{.sec or mol/cm}^2\text{.sec)} \qquad [5.2.12]$$

depending on whether the reaction is homogeneous or heterogeneous, or for a reaction in a gas phase:

$$r^{-} = k_{rp}(T, P) \cdot p_A^{\,a} \cdot p_B^{\,b} \qquad [5.2.13]$$

where C_A and C_B are the concentrations, and p_A. p_B, the partial pressures of reactants in the elementary volume or in the immediate vicinity of the interface between both phases: $C_{A(\alpha)s}$ or $p_{A(\alpha)s}$. Thus:

$$r = r^{+} - r^{-} = k_{rc}^{+}(T) \cdot C_A^{\,a} \cdot C_B^{\,b} - k_{rc}^{-}(T) \cdot C_R^{\,r} \cdot C_S^{\,s} \qquad [5.2.14]$$

In most cases, the kinetic coefficients or orders of reactions a and b are not related to the stoichiometric coefficients ν_A and ν_B.

The units of the rate constants, k, depend on the rate expression.

5.2.2.1. *Elementary reactions*

When the orders of reaction a and/or b are equal to 1 or 2, the reaction is usually an elementary reaction occurring:

– by dissociation of a molecule:

$$MX \rightarrow M + X \qquad [5.2.15]$$

$$r = k_{rc}\, C_{MX} \text{ or } k_{rp} \,.\, p_{MX} \qquad [5.2.16]$$

– by collision between two molecules:

$$A + B \rightarrow R + S \qquad [5.2.17]$$

$$r = k_{rc} \,.\, C_A \,.\, C_B \text{ or } k_{rp} \,.\, p_A \,.\, p_B \qquad [5.2.18]$$

Conversely, when the kinetics of a reaction has a simple form it means that an elementary reaction is the limiting step of the overall reaction and the rate of overall reaction is the rate of this step. In other cases, the overall reaction occurs via a series of elementary reactions.

5.2.2.2. *Reversible and irreversible reactions*

For an elementary reversible reaction (see reaction [5.2.17]), whose kinetics of the forward and reverse reactions are given by equation [5.2.18], at equilibrium, the ratio of the rate constants is equal to the equilibrium coefficient of the reaction (see Chapter 1, equation [1.3.54]):

$$K_C = C_R \,.\, C_S / C_A \,.\, C_B = k_{rc}^{+} / k_{rc}^{-} \qquad [5.2.19]$$

The rate of the reaction can be expressed (see equations [5.2.16] and [5.2.18]) as:

$$r = r^{+} - r^{-} = k_{rc}^{+}(T) \,.\, \{C_A \,.\, C_B - C_R \,.\, C_S / K_c\} \qquad [5.2.20]$$

– when the equilibrium constant is very low, the reaction in the forward direction in fact does not occur;

– when the equilibrium constant of the elementary reaction is high, the reaction is irreversible. The rate is that of the forward reaction.

From the *de Donder equation* [1.3.18], between the affinity (see Chapter 1, equations [1.3.14] and [1.3.53]) and rate of a reaction:

$$A \,.\, r \geq 0 \qquad [5.2.21]$$

the thermodynamics of irreversible phenomena states that at near equilibrium, the rate of the reaction is proportional to its affinity:

$$r = \alpha \,.\, A \qquad [5.2.22]$$

EXAMPLE.– Reduction of iron oxide particles by CO is represented by the reaction:

$$FeO(s) + CO(g) \rightarrow Fe(s) + CO_2(g) \qquad [5.2.23]$$

whose affinity can be expressed, near equilibrium, by:

$$A = RT \ln K_p (p_{CO} / p_{CO2}) \approx RT (K_p / p_{CO2}) / (p_{CO} - p_{CO2} / K_p)$$

where K_p is the equilibrium constant = $(p_{CO2} / p_{CO})^*$ at equilibrium.

When the rate-controlling step is the chemical reaction, the experimental rate of the chemical reaction is correctly represented by the following expressions:

$$r_s = k_{rp}(p_{CO} - p_{CO2} / K_p) = k_{rp} (1+ 1/K_p) (p_{CO} - p^*_{CO}) \qquad [5.2.24]$$

where r_s is the reduction rate, expressed in oxygen mass or moles removed per unit surface (cm^2) and unit time (second), and k_{rp} is the rate constant in $molO/cm^2.sec.atm$ and p_{CO} in atm. The values of the partial pressures are those in the immediate vicinity of the interface. p^*_{CO} is the partial pressure of CO in a gas phase of composition $p_{CO2} + p^*_{CO}$ in equilibrium with FeO/Fe.

Under a constant total pressure P, $p^*_{CO} = P/(1+Kp)$ when the rate is referred to the concentrations and is of the first order with respect to the concentrations:

$$r_s = (k_{rc}) \{C_{CO} - C_{CO2} / K_C\} \qquad [5.2.25]$$

$$k_{rc} (cm/sec) = k_{rp} . RT = k_{rp} . 82{,}1\ T \qquad [5.2.26]$$

NOTE.– The rate is generally referred to the concentrations or partial pressures. The most rigorous form of the kinetic law is referred to the activities, in accordance with equation [5.2.22]. Some examples of this will be shown later on.

Even for a reversible reaction, the rates of the forward and reverse reactions can be determined in operating conditions where one or the other of the reactions does not occur thus far from the equilibrium. For example, in a closed reactor when the initial composition of the reaction mixture only has reactants, the initial rate will be that of the forward reaction. Or, by removing one of the products of the reaction, the reaction will occur far from the equilibrium and therefore the rate will be that of the forward reaction. For example, for the nitrogen removal of liquid steel:

$$2\ \underline{N}_{(Fe\ liquid)} \rightarrow N_2(g)$$

under vacuum, the rate will be that of the forward reaction (see equation [5.4.44b]).

5.2.2.3. *The effect of temperature on chemical reaction rates*

Most elementary reactions are thermo-activated processes. The reaction rate constant has been found to be correctly represented by Arrhenius' law and therefore varies exponentially with temperature:

$$k_{rc}(T) \text{ or } k_{rp} = k_o \exp(-E_a / RT) \qquad [5.2.27]$$

where E_a is the activation energy of the reaction[1].

For an overall reaction, it is often noted that Arrhenius' law can be applied but in a relatively large temperature range. In fact, by drawing the logarithm of the rate constant as a function of 1/T, we can observe that the curve can often be decomposed into two or three straight line segments. This indicates that the mechanism governing the reaction varies.

NOTE.– The activation energy of a chemical reaction is usually high ≥ 20 kCal/mol. The activation energy of a (diffusional) transport process in a gas or liquid phase is generally low, except for the diffusion in very viscous slags. High activation energy is often considered to indicate that the process controlling the transformation is a chemical reaction. This is not always true [SOH 04], see Chapter 6, section 6.3.2.1, equation [6.3.14b] and corresponding note.

5.3. Homogeneous precipitation

"Homogeneous" precipitation occurs by a homogeneous reaction between reactants dissolved in the same phase α, with formation of S molecules in supersaturation in this phase, then the formation of particles of a second phase β, by the formation and growth of nuclei:

$$\nu_A A(\alpha) + \nu_B B(\alpha) \rightarrow S(\alpha)_{(\text{in supersaturation})} \rightarrow S(\beta)(s, l, \text{or } g)\downarrow \qquad [5.3.1]$$

The precipitation is "heterogeneous" when the chemical reaction occurs on the surface of a substrate or at a phase boundary, with formation and growth of a deposit of S on this surface.

EXAMPLES.– Formation of CO bubbles in the decarburization of steel or in the deoxidation of steel by carbon under vacuum represented by the reaction:

$$\underline{C}_{(Fe)} + \underline{O}_{(Fe)} \rightarrow CO \text{ (gas bubbles)}\downarrow$$

1 E in cal/mol and R = 1.986 cal/mol.°K, E in joules/mol and R = 8.32 joules/mol = 0.0821 liter-atm/mol.°K.

Formation of SO_2 bubbles in the desulfurization of liquid copper by blowing oxygen through a liquid metallic bath:

$$\underline{S}_{(Cu)} + 2\,\underline{O}_{(Cu)} \rightarrow SO_2(g)\downarrow$$

Formation of oxide inclusions (particles) during deoxidation of liquid steel by aluminum or silicon, see Chapter 7 of [VIG 11b], section 7.2.3:

$$\underline{Si}_{(Fe)} + \underline{O}_{(Fe)} \rightarrow SiO_2 \text{ (globules)}\downarrow$$

Hydroxide precipitation from a salt by hydrolysis in an aqueous solution: hydroxylation of an anion by lowering the pH (see Chapter 1 of [VIG 11b], section 1.3.1.2):

$$Al(OH)_4\,Na \rightarrow Al(OH)_3(s)\downarrow + NaOH$$

The precipitation of alumina hydroxide is one of the operations of the processing of bauxites.

The homogeneous precipitation, with formation of particles by primary nucleation (spontaneous formation of nuclei of phase β in phase α), proceeds according to the following steps:

– homogeneous chemical reaction producing a chemical species $\underline{S}$ dissolved in the solution and in supersaturation;

– condensation (coagulation) of these molecules into nuclei: primary nucleation step;

– formation of primary particles by collision of nuclei and coagulation;

– growth of the primary particles by diffusional transport processes;

– formation of secondary particles by agglomeration (aggregate formation) of primary particles, i.e. is collision in turbulent eddies and sticking. These aggregates can undergo breakage by shocks.

5.3.1. *Thermodynamics of primary nucleation*

The affinity of reaction [5.3.1] has the following expression (see Chapter 1, equation [1.3.53]):

$$A = (-\Delta G_r) = -RT \ln K_{sp} + RT \ln \tilde{a}_A^{\nu A} \,.\, \tilde{a}_B^{\nu B} \qquad [5.3.2]$$

where K_{sp} is the solubility product (see equations [3.2.17], [4.2.74] and [4.2.80])[2]. For precipitation to occur, the species $S(\alpha)$ must be in supersaturation in the initial phase (α), thus $\tilde{a}_{\underline{S(\alpha)}} > 1$. The precipitation continues as long as the affinity of the reaction is positive, thus as long as:

$$\{\tilde{a}_A^{va} . \tilde{a}_B^{vb}\} > K_{sp} \qquad [5.3.3]$$

The formation of a nucleus β leads to the creation of an interface $S_{\alpha\beta}$. The energy that must be supplied to create the surface $S_{\alpha\beta}$ is $\sigma_{\alpha\beta}.S_{\alpha\beta}$, where $\sigma_{\alpha\beta}$ is the interfacial energy per unit area of the α/β interface. Thermodynamic analysis shows the existence of an energy barrier to the formation of a stable nucleus ΔG_g and allows the calculation of the size of these stable nuclei, which will be spontaneously formed for a given supersaturation. A nucleus of radius R_g will be stable, if:

$$R_{nuclei} > R_{gc} = 2\ \sigma_{\alpha\beta} / (-\Delta G_v) \qquad [5.3.4]$$

where ΔG_v is the standard free energy of reaction [5.3.2] per unit volume of β. The Gibbs free energy of formation of a stable nucleus is:

$$\Delta G_{nucleus} = (16\ \pi / 3) . \{\sigma^3 / (-\Delta G_v)^2\} \qquad [5.3.5]$$

At low supersaturation (low $-\Delta G_v$), the energy barrier $\Delta G_{nucleus}$ is high and the critical radius R_{gc} is large. As the formation of a nucleus is a thermo-activated process, the probability of nucleus formation is low and thus the number of stable nuclei that appear per unit volume of phase α is small. At high supersaturation (high $-\Delta G_v$), R_{gc} is small and the probability of nucleus formation is high.

5.3.2. *Nucleation and primary particle formation processes*

The nucleation phenomenon occurs for a well defined value of this supersaturation. When this critical supersaturation is reached, a "burst" of nuclei occurs almost instantaneously.

For a nucleus to be formed, the chemical reaction must have sufficiently progressed and reached a sufficient concentration (supersaturation) of molecules S. The first nucleus will appear after a time termed the *incubation time*, which depends on the rate of the homogeneous reaction.

---

2 The values of the solubility product K_{sp} of oxides, sulfides and nitrites in the liquid iron are given in Chapter 3, section 3.2.3 and Table 3.2.6. Values of solubility products of hydroxides, sulfides, sulfates and chlorides in aqueous solutions are given in Chapter 4, sections 4.2.4. and 4.2.5.

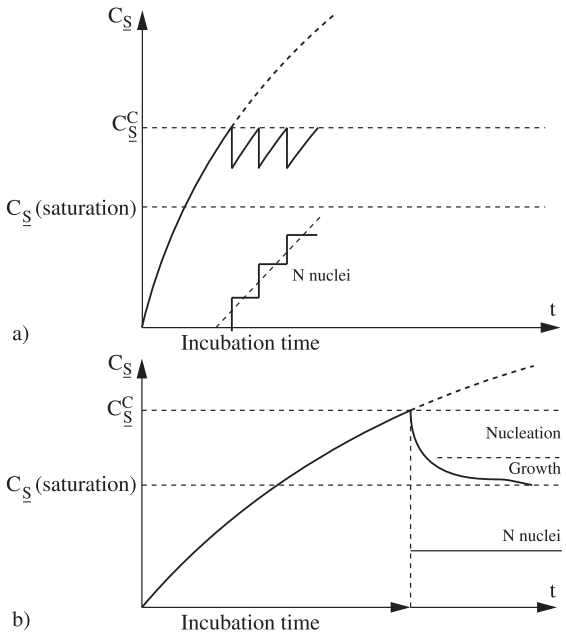

Figure 5.3.1. *Kinetics of homogeneous precipitation. Schematic presentation of the concentration change with time of a particle forming solute species generated in situ before and after homogeneous nucleation: a) fast homogeneous chemical reaction–continuous nucleation; and b) slow homogeneous chemical reaction–discontinuous nucleation. C_S^C is the critical supersaturation of the nuclei forming solute species [MAT 81]*

Figure 5.3.1 presents both extreme cases of homogeneous nucleation:

– For a fast reaction (the concentrations of the reactants in the mother phase are high), when the concentration of the species S(α) reaches a critical value, there is almost instantaneous formation of a "burst" of nuclei, with a correlative lowering of the concentration of the species S. As the chemical reaction proceeds, as soon as the concentration of the species S has re-reached the critical value, a new burst of nuclei occurs and so on. The nucleation process appears to be continuous, with the formation of "successive bursts" of nuclei and the formation of nuclei with a constant rate N(t) = It.

– For a slow reaction, after the first burst of nuclei leading to a decrease in the concentration of species S(α) where the rate of new species $\underline{S}(\alpha)$ production is low, the new $\underline{S}(\alpha)$ molecules are removed from the solution by adsorption onto the first nuclei. In this instance, the critical concentration will not be reached and no secondary nucleation can take place. There is thus an instantaneous formation of a number N of nuclei.

Two different quantities are involved: the *critical supersaturation of the particle-forming species* S(α), which is necessary for nucleation to occur; and the *incubation time* at which the first "burst" of nuclei occurs, which depends on the reaction's kinetics.

Primary particles are formed by *coagulation*, which is the *collision and aggregation (coalescence) of* nuclei, the *collisions, being produced by the Brownian motion*. An extended distribution of the sizes of the primary particles is obtained.

These primary particles can then grow via two processes:

– incorporation of $\underline{S}(\alpha)$ molecules in supersaturation, the process being controlled by the diffusion of these molecules. Around each particle, a concentration gradient of $\underline{S}(\alpha)$ occurs (see Figure 5.3.2); or

– agglomeration of primary particles.

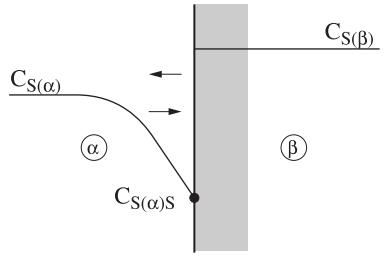

Figure 5.3.2. *Diffusion-controlled growth of a precipitate by diffusion of a supersaturated species S*

The formation step of the primary particles is very important in the production of fine and ultra-fine powders of metals, oxides and carbides.

5.3.3. *Secondary nucleation*

Primary nucleation requires high supersaturation. The industrial operations of precipitation, when the supersaturation necessary for the *in situ* formation of nuclei (homogeneous nucleation) is very high, are performed in the presence of *seed particles* produced during a previous operation and added to the solution. Secondary nucleation is the nucleation process due to the presence of these seeds.

In the mechanically agitated reactors, these seeds undergo shocks with the surface of the reactor or impellers and break down into fragments. The number and size of these fragments depends on the impact energy communicated to the particles

via the shocks. These fragments constitute the primary particles. On the surface of these fragments, the S molecules are adsorbed and incorporated to the crystalline fragment structure. The fragments subsequently grow by a diffusion process.

Secondary nucleation can occur according to a second mechanism. If the supersaturation is high, the flux of S molecules on the primary particles is high, the rate of deposit of S molecules on these primary particles is high, and excrescences (dendrites) grow. In a reactor, whose reactive mixture is strongly agitated, these dendrites are detached by particle shocks. They therefore constitute new primary particles, growing via a diffusion process of S molecules or via agglomeration. The secondary nucleation rate may be considered constant.

5.4. Kinetics and mechanism of heterogeneous reactions

5.4.1. *Mechanism of heterogeneous chemical reactions*

As the chemical reaction must occur at the interface of the two phases in contact, the generally accepted reaction mechanism presents three steps:

– adsorption of the reactants on the contact surface or interface;

– reaction between the adsorbed reactants; and

– desorption of the product(s) or *in situ* formation of nuclei of a new phase at the surface or interface of the fluid phases, then growth of these nuclei.

This mechanism was postulated by Langmuir [LAN 48] for catalytic reactions. It is based on the following model: on the catalyst's surface there are a certain number of vacant "active" sites on which the reacting species are temporarily adsorbed. The chemical reaction occurs on the surface between the species temporarily adsorbed, with desorption of the reaction's products. Desorption of products from the reaction sets some active sites free. Some sites can be blocked by adsorption of the species that do not participate in the reaction and the adsorption of these species can lead to a notable decrease in the reaction rate. This explains the poisoning of the catalysts.

In the case of heterogeneous non-catalytic reactions, the reactants being temporarily adsorbed react at the surface of fluid-solid systems or at the interface of fluid-fluid systems. On the other hand, the adsorption on the surface or interface of species blocking a relatively important fraction of the active sites also has a notable effect on the rate of certain reactions.

Here, we successively consider gas-solid reaction systems, fluid-fluid reaction systems and heterogeneous reactions with formation of a new phase (*in situ* conversion and heterogeneous precipitation).

5.4.2. *Rates of heterogeneous reactions in fluid-solid systems*

5.4.2.1. *Rate of the adsorption step*

The adsorption of some species (reactants) at the surface of a solid has been experimentally observed and particularly thoroughly studied in metal oxidation phenomena and electrolytic deposits. Thus, when a metal such as silver is exposed to air at about 300 °C, a certain amount of oxygen is adsorbed at its surface in an irreversible manner. This oxygen adsorption is linked to the unsaturated bonds of the surface atoms and is due to a very strong metal-oxygen energy bond. The saturation state of the surface corresponds to the association of an oxygen atom with a superficial metal atom according to the reaction:

$$M_{(\text{naked surface})} + O_{(\text{adsorbed})} \rightarrow (M\text{-}O)_{(\text{adsorption complex})}$$

The energy of adsorption, thus of formation of the (M-O) complex, is actually greater than that of oxide formation. At temperatures lower than that of reversible dissociation of the oxide, an oxide film will form.

When the chemical adsorption of a species (molecule or atom) on vacant sites of the surface is the only process occurring, a monomolecular layer will form at the surface of the solid. The covering rate of the surface θ_S is a function of the concentration or partial pressure of the adsordable species in the immediate vicinity of the surface.

For the adsorption process on a vacant site:

$$A(\alpha) \rightarrow A_{(ads)} \qquad [5.4.1]$$

the adsorption rate of species A is proportional to the concentration $C_{A(\alpha)S}$ or partial pressure $p_{A(\alpha)S}$ in the immediate vicinity of the surface and to the fraction of vacant sites at the surface (per unit surface) θ_V:

$$r_{(ads)} = k^+ C_{A(\alpha)s} \,.\, \theta_v \text{ or } k^+ p_{A(\alpha)s} \,.\, \theta_v \qquad [5.4.2]$$

and the desorption rate of the reactant is proportional to the amount adsorbed:

$$r_{des} = k^- \,.\, \theta_T \qquad [5.4.3]$$

with $\theta_v + \theta_T = 1$ and $K_{ads} = k^+ / k^-$.

If the adsorption is reversible, at equilibrium the rates of adsorption and desorption are equal. The expression of the fraction of sites occupied by species A, and therefore the superficial concentration of A, is:

$$\theta_T = C_{A(ads)} = K_{ads}\, C_{A(\alpha)s} / (1 + K_{ads}\, C_{A(\alpha)s}) \quad [5.4.4]$$

and the fraction of the free surface available for other reaction processes is:

$$1 - \theta_T = 1 / (1 + K_{ads}\, C_{A(\alpha)s}) \text{ or } 1 / (1 + K_{ads}\, p_{A(\alpha)s}) \quad [5.4.5]$$

For the dissociative adsorption of a molecule, such as:

$$O_2(g) \rightarrow 2\, O_{(ads)} \quad [5.4.6a]$$

where each atom occupies a site, the fraction of the occupied sites is then given by:

$$\theta_s = C_{O(ads)} = (K_{(ads)} \cdot p_{O2(\alpha)s})^{1/2} / \{1 + (K_{(ads)} \cdot P_{O2(\alpha)s})^{1/2}\} \quad [5.4.6b]$$

5.4.2.2. *Rate of heterogeneous reaction: approximation of the steady state of adsorbed species*

In the case of a process involving first-order reactions for the steps of the overall reaction:

$$\underline{A}(g) + \beta B(s) \rightarrow \underline{R}(g) \quad [5.4.7]$$

– adsorption of reactant A: $A(g)_s \rightarrow (A_{(ads)})$; (1)

– chemical reaction: $A_{(ads)} + \beta B(s) \rightarrow R_{(ads)}$; (2)

– desorption of product R: $R_{(ads)} \rightarrow R(g)_s$. (3) [5.4.8]

The equation for the overall rate is derived by applying the steady state approximation for the adsorbed species. The number of active surface sites being much lower than the number of molecules of reactant converted via these sites, the superficial concentrations of the adsorbed species can be considered constant and very low compared to the concentrations of the reactants and products. A steady state for the adsorbed species will thus be established, which allows us to consider both steps as being fast (adsorption of the reactants and desorption of one or more product(s)) and that an equilibrium for each step is established:

$$dA_{(ads)} / dt = k_1\, p_A\, \theta_v - k_{-1}\, \theta_{A(ads)} = 0 \quad \text{with } K_1 = k_1 / k_{-1} \quad [5.4.9]$$

$$dR_{(ads)} / dt = k_{-3}\theta_{R(ads)} - k_3\, p_R\, \theta_v = 0 \quad \text{with } K_3 = k_3 / k_{-3} \quad [5.4.10]$$

the rate of reaction (2) therefore being:

$$r_s = r_2 = k_2\,\theta_{A(ads)} - k_{-2}\,\theta_{R(ads)} \qquad [5.4.11]$$

with:

$$K_2 = k_2 / k_{-2}\ ; \quad \theta_v + \theta_{A(ads)} + \theta_{R(ads)} = 1 \text{ and } \quad K = K_1 K_2 / K_3 \qquad [5.4.12]$$

where K is the equilibrium constant of the overall reaction, θ_v the fraction of vacant sites on the surface, $\theta_{A(ads)}$ the fraction of sites on the surface occupied by adsorbed species A, and $\theta_{R(ads)}$ the fraction of sites occupied by species R.

From these equations, we obtain:

$$\theta_v = 1 / (1 + K_A p_A + K_R p_R) \qquad [5.4.13]$$

and:

$$r_s = k_2\,K_1(p_{A(\alpha)s} - p_{R(\alpha)s} / K) / (1 + K_1 p_A + K_3 p_R) \qquad [5.4.14]$$

For a first-order reversible chemical reaction, not taking into account the adsorption and desorption processes, the experimental rate is given by (see reaction [5.2.24]):

$$r_s = k_{rp}(p_{A(\alpha)s} - p_{R(\alpha)s} / K) \qquad [5.4.15]$$

The role of the adsorption and desorption processes of the reactant and product can clearly be seen. At low temperature, where the adsorption constants are high, the adsorption and desorption processes can have a notable effect on the overall reaction rate (see equation [5.4.14]). At high temperature, the equilibrium constants decrease and therefore the reaction rate can be expressed by equation [5.4.15].

If a fraction of the surface is occupied by surface-active molecules, the constant k_{rp} will be replaced by $k_{rp}(1 - \theta_T)$ where θ_T is given by equation [5.4.5].

5.4.3. *Experimental rates of gasification reactions*

All results presented are obtained in operating conditions where the rate-controlling step is the heterogeneous chemical reaction. The experimental rates of heterogeneous chemical reactions are often simple expressions, indicating that an elementary reaction is the limiting step.

5.4.3.1. *Reduction of a dense particle of zinc oxide*

$$ZnO(s) + CO(g) \rightarrow Zn(g) + CO_2(g) \quad [5.4.16a]$$

$$A(T) = A°(RT \ln K_p(T)) + RT \ln p_{CO} / p_{Zn} \cdot p_{CO2} \quad [5.4.16b]$$

As the product of the reduction of dense zinc oxide is a gas, the contact between the oxide particle and CO gas is constantly maintained. The oxide/CO reaction can continue on the residual surfaces of the oxide. The rate of the heterogeneous reaction, see equation [5.2.22], is given by:

$$r_s = k_{rp} (p_{CO} - p_{Zn} \cdot p_{CO2} / K_p) \quad [5.4.17]$$

By operating with a strong flow rate of reducing gas around the particle, we can minimize the resistance in the boundary layer around the particle and maintain low Zn and CO_2 partial pressures in the gas stream. The rate of the heterogeneous reaction is therefore the rate of the forward reaction.

Between 1,000 and 1,300°C, for dense ZnO of high purity [GUG 71]:

$$k_{rc} \text{ (cm/sec)} = 10^6 \exp(-37{,}900 \text{ (cal/mole)} / RT)$$

The complete reduction time of a particle of ϕ = 1 cm is of 40 minutes at 1,200°C, 22 minutes at 1,300°C and 10 minutes at 1,500°C.

5.4.3.2. *Direct chlorination of zirconium oxide*

$$ZrO_2(s) + 2\ Cl_2(g) \rightarrow ZrCl_4(g) + O_2(g) \quad [5.4.18a]$$

Even though the equilibrium constant of this reaction is very low: 2×10^{-4} at 1,000°C, by operating under a very strong chlorine gas flow rate to prevent the accumulation of chloride in the immediate vicinity of the zirconium particles, the forward reaction can proceed until complete gasification of the oxide particle. In these conditions, the forward reaction rate is determined. The rate is first-order with respect to chlorine pressure (see Figure 5.4.1) although the stoichiometric coefficient is two, which indicates that an elementary reaction must be the limiting step of the overall reaction:

$$\log(r / p_{Cl2}) = -39{,}700 / RT + 4.2 \quad [5.4.18b]$$

where r is in mg/cm^2, hr/p_{Cl2}, p_{Cl2} in torr and E in cal/mole of $ZrCl_4$.

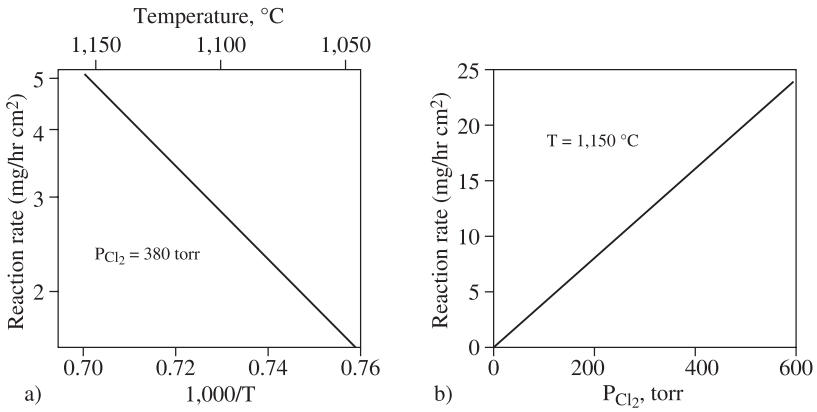

Figure 5.4.1. *Chlorination kinetics of ZrO_2 single crystals: a) Arrhenius plot; and b) effect of chlorine pressure at 1,150°C [LAN 72]*

The fact that the rate is proportional to the chlorine pressure indicates that the limiting step must be the formation of an intermediate compound, such as oxychloride. But this is only a hypothesis. No further study to provide a mechanism for this has been performed.

Results of chlorination rates of porous particles by $Cl_2 + CO$ and $Cl_2 + C(s)$ (carbochlorination) are presented in Chapter 3 of [VIG 11b], Figures 3.2.6, 3.2.7 and 3.2.8.

5.4.3.3. *Carbon and coal combustion*

The combustion of coal occurs in two steps: a devolatilization and subsequent combustion of volatile products, then a combustion of the semi-coke (*char*) product.

With pulverized coal and high particle heating rates of 10^4–10^5 K/s, the volatile material is released in 10 ms. The combustion of semi-coke thus produced is much slower, at 50–100 ms [PAL 03, SMO 85].

The primary reaction that occurs at the surface of the particle is the formation of CO, see Chapter 2, section 2.6.1 and reaction [2.6.2]. This occurs by the following mechanism dissociative adsorption of oxygen on the coal reaction producing CO, and desorption of CO:

$$O_2(g) \rightarrow 2\ O_{ads} \qquad [5.4.19a]$$

$$C(s) + O_{ads} \rightarrow CO(g) \qquad [5.4.19b]$$

In the presence of excess oxygen and for long contact times $>10^{-3}$ sec, CO is oxidized into CO_2 (see reaction [2.6.3]):

$$CO(g) + 1/2\ O_2(g) \rightarrow CO_2(g) \qquad [5.4.20]$$

As the coals and semi-coke are porous at temperatures up to 700°C, the combustion rate is controlled by the heterogeneous reaction as it is very slow and the specific carbon surface does not vary greatly. We can thus determine a combustion rate per specific surface unit and activation energy E. It varies significantly with the nature of the carbon, see Figure 5.4.2.

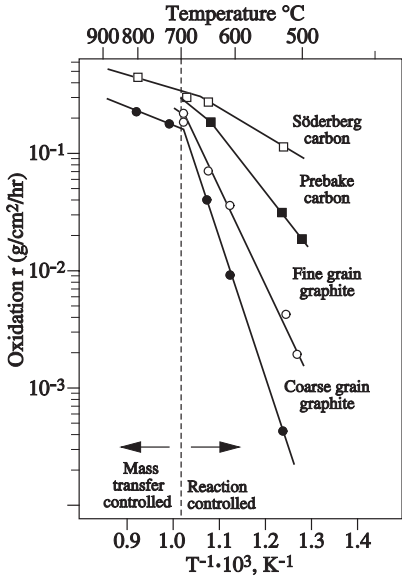

Figure 5.4.2. *Oxidation (combustion) rates of various carbon grades*

5.4.3.4. *Boudouard reaction or gasification of carbon by CO_2*

$$CO_2(g) + C(s) \rightarrow 2\ CO(g) \qquad [5.4.21]$$

This reaction (see Chapter 2, section 2.6.2) occurs in three steps:

– dissociative adsorption of CO_2 (1):

$$CO_{2(ads)} \rightarrow O_{(ads)} + CO(g)\ (k_1 \text{ and } k_{-1}) \qquad [5.4.22a]$$

– chemical reaction (2):

$$O_{(ads)} + C(s) \rightarrow CO_{(ads)}(2)\ (k_2 \text{ and } k_{-2}) \qquad [5.4.22b]$$

– desorption-gasification (3):

$$CO_{(ads)} \rightarrow CO(g) \qquad [5.4.22c]$$

with $K = k_{-2}\, k_{-1} / k_1 k_2$.

Depending on whether step (3) is considered irreversible (only occurring in the indicated direction) or reversible, the reaction rates respectively are:

$$r = k_1 k_2\, p_{CO2} / \{k_2 + k_1\, p_{CO2} + k_{-1}\, p_{CO}\} \qquad [5.4.23a]$$

$$r = k_1 k_2\, \{p_{CO2} - p_{CO}^2 / K\} / / \{k_2 + k_1\, p_{CO2} + (k_{-1} + k_{-2})\, p_{CO}\} \qquad [5.4.23b]$$

The experimental law determined by Turkdogan and Vinters in a gas phase with more than 10% of CO is [TUR 70]:

$$r_S = -k_r\, \{(p_{CO2} - p^*_{CO2})\} / \{1 + \alpha\, p_{CO}\} \qquad [5.4.24]$$

where:

$$p^*_{CO2} = (p_{CO})^2 / K_p$$

p^*_{CO2} is the partial pressure of CO_2 in a gaseous phase in equilibrium with carbon for a particular value of p_{CO} in this gaseous phase, and α is related to the fraction of the sites occupied by CO:

$$p_{CO} = \alpha \times \{\theta_{CO} / (1 - \theta_{CO})\}$$

In operating conditions where the diffusion of gas molecules in the pores is not the limiting process, and in the presence of more than 10% of CO in the gaseous phase, the overall kinetics between 800 and 1,200°C is controlled by the chemical reaction [5.4.21] and the conversion rate of the particles (see Chapter 7, equation [7.2.18]) is given by:

$$\ln (1 - X) / t = -k^{app}\, \{(p_{CO2} - p_{CO2}^*)\} / \{1 + \alpha\, p_{CO}\} \qquad [5.4.25]$$

where X is the fraction of carbon consumed (fractional conversion), with k^{app} in $atm^{-1}.min^{-1} = k_r \,.\, s_m$ (internal surface per unit carbon mass) [TUR 70]:

$$\log k^{app} = -13{,}200 / T + 9.68 \text{ for wood carbon (*coconut charcoal*)} \qquad [5.4.26a]$$

$$\log k^{app} = -13{,}200 / T + 8.60 \text{ for metallurgic coke}$$

$$\log k^{app} = -13{,}200 / T + 7.68 \text{ for (electrode) graphite.}$$

The activation energy is 60 kcal where 800°C < T < 1,200°C. A number of studies confirm this activation energy between 800 and 1,400°C for the different types of carbon and:

$$\log \alpha = 5{,}940 / T - 3.46 \qquad [5.4.26b]$$

The high value of this activation energy (27 kcal/mol) of CO is due to the very strong chemisorption of CO on graphite and coke.

5.4.4. *Experimental rates of oxide and sulfide dissolution by acid-base reactions*

The leaching of oxides and sulfides can be performed by two types of reaction: acid-base reaction or redox chemical reaction, with or without complexation. Redox reactions are dealt with in Chapter 8, section 8.5.

The thermodynamic data on the solubility of oxides and hydroxides (Chapter 4, section 4.2.4 and equations [4.2.68] and [4.2.69]) as a function of the nature of the oxide, of the lixiviant, of pH and T, set the basic operating conditions of a leaching operation.

It is common to write these dissolution reactions in the form (see Chapter 4, reaction [4.2.59]):

$$\text{oxide (or sulfide)} + H^+ \rightarrow \text{cation} + H_2O \text{ (or } H_2S) \qquad [5.4.27]$$

but the anion of the acid or salt added to the solution can also have a strong effect:

– because the anions are adsorbed and block the H^+ ion adsorption sites and thus actually control the dissolution rates of the particles; or

– by being adsorbed they lower the bond between the metallic atoms and oxygen (for CuO); or

– because they form stable complexes, increasing the oxide or sulfide solubility (see Chapter 4, section 4.2.3). The leaching rates of Fe_2O_3 and CuO by HCl are 10 times higher than those by ClO_4H for the same the H^+ ion activity (the ClO_4^- ions are very poor complexing ions; see Figures 5.4.4 and 5.4.5).

The elementary reactions involved in these transformations, see reaction [5.4.8], are:

– adsorption of the H^+ ion at the surface of the oxide or sulfide:

$$MO + H^+ \rightarrow MO \,.\, H^+$$

– dissociative desorption:

$$MO \,.\, H^+ \rightarrow M^{2+} + OH^- \text{ (or } HS^-)_{(aq)}$$

These two steps can be considered as an anion-transfer reaction:

$$O^{2-}(S^{2-}) + H^+_{(aq)} \rightarrow OH^-_{(aq)} \text{ or } (HS^-_{(aq)})$$

followed by the homogeneous reaction (in the aqueous phase):

$$OH^-_{(aq)} \text{ or } (HS^-_{(aq)}) + H^+_{(aq)} \rightarrow H_2O \text{ or } H_2S \text{ (high-speed reaction)}$$

The limiting step is the anion-transfer reaction.

According to studies, the dissolution rates are referred to the concentration of the acid, the average activity of the acid $a_{\pm}$ or to the concentration of H^+ ions, or the activity of the H^+ ion: $\tilde{a}_{H+}$ (see Chapter 4, equation [4.2.15]):

– when the rate is referred to the molar concentration of the acid:

$$r = k\,[\text{acid}]^{\,n} \qquad [5.4.28]$$

- $n > 1$ for the acids ClH, ClO_4H, NO_3H;

- $n \approx 0.5$–0.7 for SO_4H_2 (this acid is practically monoprotonic, $[SO_4H_2] = [H^+]$ when pH < 2, see Figures 5.4.3a and b);

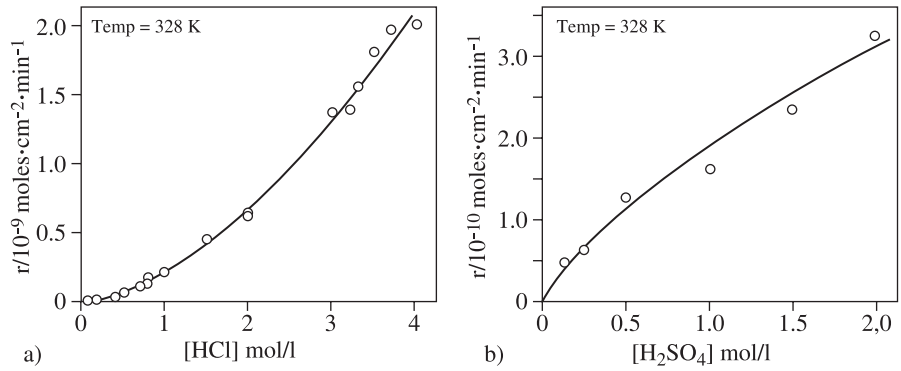

Figure 5.4.3. *Rate of dissolution of hematite in acidic solutions: a) effect of hydrochloric acid concentration; and b) effect of sulfuric acid concentration [MAJ 85a]*

– when the rate is referred to the activity of the H^+ ion:

$$r = k'(\tilde{a}_{H+})^{n'} \qquad [5.4.29]$$

- n' ≈ 1 for the acids ClH, ClO_4H and NO_3H, and for a pH varying from 0.05–5 at 303°K, see Figure 5.4.4a. The addition of ClNa, which increases the activity of HCl (see Chapter 4, Figure 4.2.5, Table 4.2.2 and Figure 4.2.5), and therefore that of a_{H+}, increases the rate;

- n' ≈ 1/2 for sulfuric aqueous solutions, see Table 4.2.4 and Figures 4.2.8 and 5.4.4b.

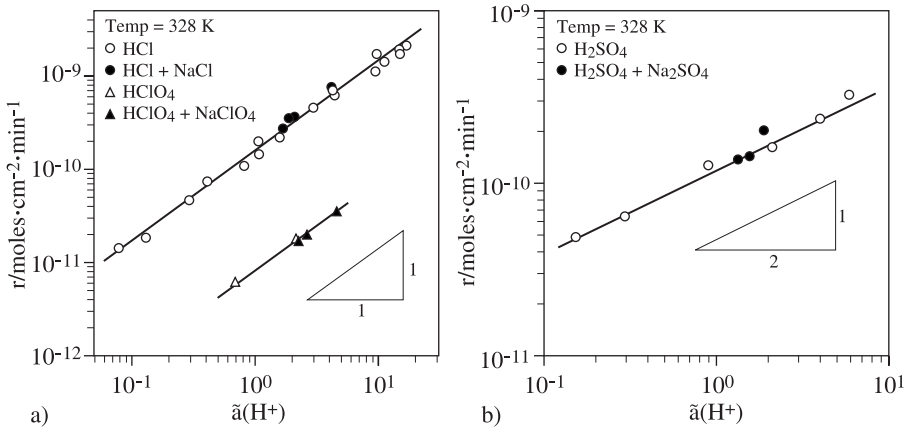

Figure 5.4.4a and b. *Rate of dissolution of hematite in various acid solutions: effect of hydrogen ion activity* $\tilde{a}_{H+}$ *[MAJ 85a]*

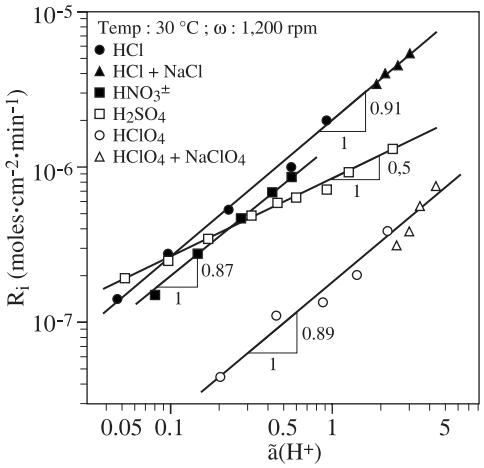

Figure 5.4.5. *Rate of leaching of cupric oxide disks in various acid solutions: effect of hydrogen ion activity* $\tilde{a}_{H+}$ *[MAJ 80a]*

It is to be noted that the dissolution rate of the Fe_2O_3 hematite in different acids is extremely slow, whereas the dissolution rate of the CuO oxide is a lot faster (see Figure 5.4.5).

Metallic sulfides are very poorly soluble in water, in acidic or basic solutions (see Chapter 4, section 4.2.5.3). At 55°C, for the sulfides ZnS, PbS and NiS in a hydrochloric acid solution, the dissolution rate is very slow, but strongly varies with the concentration of hydrochloric acid (see Figures 5.4.6 and 5.4.7).

Referred to H^+ ion activity, the variation of dissolution rate is linear. Actually, the higher is the sulfide solubility in a hydrochloric solution, the higher the rate of dissolution. This is due to the formation of complexes, see Chapter 4, equation [4.2.44].

The dissolution rate of ZnS and PbS in hydrochloric solutions is strongly increased by the addition of NaCl and $MgCl_2$ salts. On the other hand, the dissolution rate of NiS does not depend on the chloride ion content as the Ni^{2+} ion has a very low tendency to form chlorocomplexes, see Chapter 4, section 4.2.3.1.

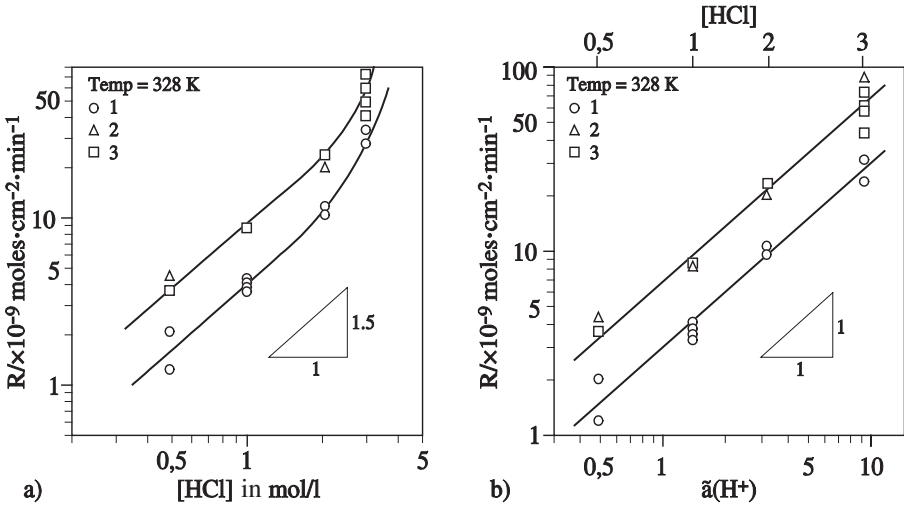

Figure 5.4.6. *Dissolution rate of sphalerite (ZnS): a) effect of acid concentration; b) effect of hydrogen ion activity* $\tilde{a}_{H^+}$ *[MAJ 85b]*

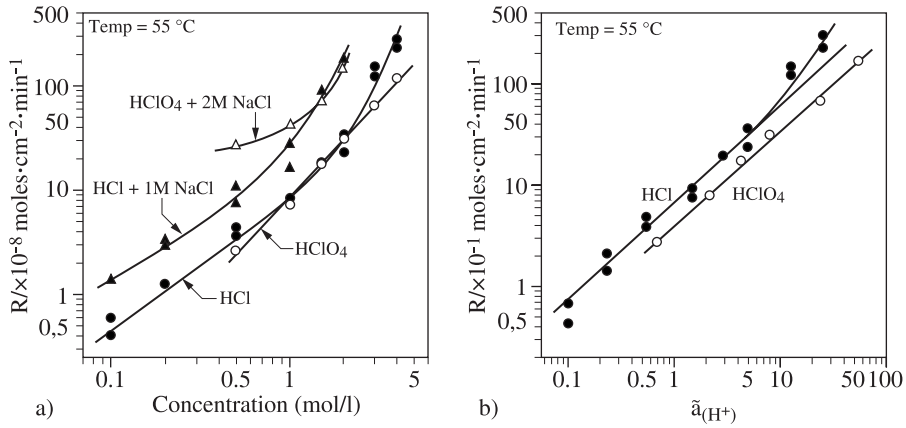

Figure 5.4.7. *Dissolution rate of galena (PbS) in various acids: a) effect of acid concentration; b) effect of hydrogen ion activity $\tilde{a}_{H+}$ [MAJ 80b]*

5.4.5. *Rates of heterogeneous chemical reactions in fluid-fluid systems*

In a fluid-fluid system, the two fluid phases in contact are separated by an interfacial layer whose thickness is low but not equal to zero. In this layer, the composition progressively varies from that of the first phase to that of the second phase. Langmuir and Harkins [LAN 17] consider it as a monomolecular layer in which some species are selectively adsorbed. Defay and Prigogine [DEF 52] have derived an expression of the chemical potential of a component in this monomolecular interfacial layer as a function of the surface or interfacial tension.

The adsorption of the species in the interfacial layer between both fluid phases (gas-liquid or liquid-liquid) is a very real physical phenomenon. It is revealed and followed by the variation of the surface or interfacial tension as a function of species concentration.

In gas-liquid and liquid-liquid reactions, the adsorption of surface-active species in the interfacial layer decreases the transfer rate of a reactant from one phase to the other. We can interpret this effect in terms of sites blocked by surface-active species. The phenomenon is well known for water evaporation, which is strongly slowed down by the presence of surface-active agents in water, which as adsorbed “block the active sites of the water’s surface”. A number of studies have shown that the adsorption or desorption kinetics of nitrogen in liquid metals (e.g. Fe, Ni-Cr) is strongly decreased when the metal contains important quantities of surface-active elements, such as sulfur, oxygen (see reaction [5.4.30]). Similarly, the dissociation

kinetics of CO_2 during the decarburizing of steel (see reaction [5.4.48]), are significantly lowered when the metal contains sulfur.

5.4.6. *Experimental rates of transfer processes*

$$\nu_{\underline{A}} A(\alpha) \rightarrow \nu_{\underline{R}} R(\beta) \qquad [5.4.30]$$

The mechanism of these reactions is identical to that presented in the previous section: adsorption of a reactant, chemical reaction in the interface, desorption of the product.

5.4.6.1. *Nitrogen absorption by a liquid metal [BEL 93, FRU 00]*

$$N_2(g) \rightarrow 2\ \underline{N}_{(\text{dissolved in liquid metal})} \qquad [5.4.31]$$

The steps of the overall reaction are:

– dissociative adsorption of nitrogen: the *limiting step*:

$$N_2(g) \rightarrow 2\ N_{(ads)} \qquad [5.4.32]$$

$$r_1 = k_1 \,.\, p_{N2} \,.\, \theta_v^{\,2} - k_{-1} \,.\, \theta_s^{\,2} \qquad [5.4.33]$$

– rapid desorption (whose equilibrium is instantaneous):

$$N_{ads} \rightarrow \underline{N}_{(\Phi\varepsilon)} \qquad [5.4.34]$$

$$\theta_S = K_{2dés} \,.\, C_{N(Fe)s} \,.\, \theta_v \qquad [5.4.35]$$

and the reaction rate is given by:

$$r = r_1 = k_1 \{p_{N2} - (K_{2des} / K_{1ads}) \,.\, C_{N(\alpha)s}^{\,2}\} / \{1 + K_{2des}\, C_{N(Fe)s}^{\,2}\} \qquad [5.4.36]$$

The expression of the experimental rate is:

$$r = k_{r1} \{p_{N2} - C_{N(Fe)s}^{\,2} / K\} \qquad [5.4.37]$$

which can also be written:

$$r = k_{r1} (p_{N2} - p^*_{N2}) \qquad [5.4.38]$$

where p^*_{N2} is the partial pressure of nitrogen in the gaseous phase in equilibrium with the solution whose nitrogen content is $C_{\underline{N(\alpha)}}$:

$$K_1 = C_{\underline{N}(Fe)}^{\,2} / p^*_{N2} \qquad [5.4.39]$$

For partial pressures $0.25 < p_{N2} < 1$ atm:

$$r = k_{r1}\, p_{N2} \qquad [5.4.40]$$

(Under this form, the reaction appears to be of the first order.)

In the presence of adsorbed surface-active species (e.g. sulfur, oxygen):

$$r = k_{r1}\, (1 - \theta)\, (p_{N2} - p^*_{N2}) \qquad [5.4.41]$$

where:

$$1 - \theta = 1 / \{1 + K_{ads}\, f_S[\%S]\} \qquad [5.4.42]$$

where 0.01%S in the liquid iron blocks at 90% of sites, which lowers the nitriding rate by a factor of 10.

At 1,600°C: $k_{r1}\, (1 - \theta) = 2 \times 10^{-6}$ (moles/cm^2.sec.atm) for $\%\underline{S}_{(Fe)} = 0.05$

$= 0.5 \times 10^{-6}$ (moles/cm^2.sec.atm) for $\%\underline{S}_{(Fe)} = 0.2$

5.4.6.2. *Oxygen absorption by a liquid metal*

The same process is active in oxygen dissolution in liquid iron. Oxygen is a surface-active element for iron. A lowering of the surface tension of liquid iron indicates a very strong oxygen adsorption. At 1,550°C for an oxygen content of 0.05% mass, 95% of the surface of the liquid iron bath is covered by a monomolecular layer of oxygen (see Chapter 5 of [VIG 11b], section 5.2.1).

5.4.6.3. *Nitrogen removal of a liquid metal*

$$2\underline{N}_{(\text{dissolved in a liquid metal})} \rightarrow N_{2(\text{dissolved in a gas phase})} \qquad [5.4.43]$$

Industrially, nitrogen removal of a liquid metal is carried out by injection of neutral gas bubbles into the liquid metal bath under vacuum, see Chapter 7 of [VIG 11b], Figure 7.2.8, for the effect of sulfur on nitrogen removal of steel.

At high temperatures the experimental rate of the reaction, see equation [5.4.37], is represented by:

$$r_2 = k_{r2}.\ \{(C_{N(Fe)})^2 - p_{N2} / K_2\} \qquad [5.4.44a]$$

If the partial pressure p_{N2} is kept very low by a strong vacuum, the reaction rate is given by:

$$r_2 = k_{r2}.\ (C_{N(Fe)})^2 \qquad [5.4.44b]$$

It has been verified that $k_{r2} = k_{r1} / K_1$, see equation [5.4.40].

For the removal of hydrogen from liquid iron or liquid aluminum, the rate of the transfer is compatible with the approximation of equilibrium at the interface (the transfer is controlled by the transport of hydrogen in liquid iron):

$$C^*_{H(\Phi\varepsilon)s} = K(p_{H2})^{1/2} \qquad [5.4.45]$$

5.4.7. *Experimental rates of gas-liquid reactions*

5.4.7.1. *Reduction of liquid iron oxide by a reducing gas*

$$FeO(l) + CO(g) \rightarrow Fe(l) + CO_2(g) \qquad [5.4.46a]$$

of which the affinity has the following expression:

$$A = RT \ln K_p (p_{CO} / p_{CO2}) \qquad [5.4.46b]$$

The kinetics is studied by blowing a gas jet over the surface of a liquid iron bath, see Chapter 6, section 6.4.3 and Figure 6.4.5a. Reduction occurs and continues by a repetitive process of metallic drop formation at the bath surface, which on reaching a certain size no longer stay at the surface of the liquid bath (this has been observed), therefore leaving the surface of the oxide in direct contact with the reducing gas. The limiting process of the reduction of liquid iron oxide "FeO" can only be a heterogeneous reaction and the experimental rate is represented by the following equation (see Figure 5.4.8):

$$r = k_{rp} . \{p_{CO} - p_{CO2} / K_p\} \text{ (molO/cm}^2\text{.s)} \qquad [5.4.47]$$

when $0 < \{p_{CO} - p_{CO2} / K_p\} < 0.2$ (atm) at 1,400°C, $k_{rp} = 1.13 \times 10^{-5}$ [NAG 86] and 1.8×10^{-5} molO/cm^2.s. atm [LI 00] and between 1,300–1,600°C[1]:

$$k_{rp} = 1.4 \times 10^{-2} . \exp(-14{,}500 \text{ (cal/mole)} / RT) \text{ (mole/cm}^2\text{.s.atm)}$$

For the reduction of iron oxide dissolved in a slag by CO, the heterogeneous reaction is only the limiting step at very low pressures p_{CO}. For example, at 1,400°C, for a FeO-SiO_2 slag whose silica content is 33% (molar fraction), transport by diffusion of the oxide in the slag becomes the limiting step for $p_{CO} > 0.01$ atm.

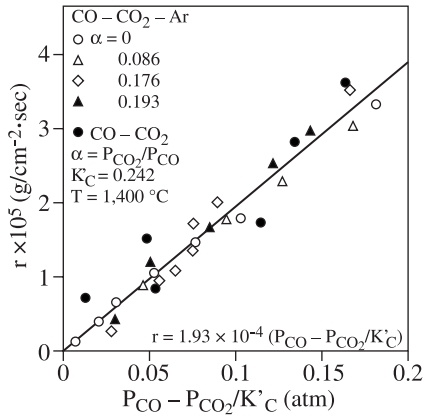

Figure 5.4.8. *Reduction rate of pure liquid Fe_tO as a function of the driving force $p_{CO} - p_{CO2}/K'_C$ for various operating conditions [NAG 86]*

5.4.7.2. *Decarburization of carbon-saturated liquid iron by CO_2 gas*

$$CO_2(g) + \underline{C}_{(\text{dissolved in liquid iron})} \rightarrow 2\ CO(g) \qquad [5.4.48a]$$

The experimental rate is represented by the following expression:

$$r_{CO2} = A\ k_r\ (p_{CO2} - p^*_{CO2}) \qquad [5.4.48b]$$

The overall reaction proceeds by the following steps:

– dissociative adsorption of CO_2:

$$CO_2(g) \rightarrow CO(g) + O_{(ads)} \qquad [5.4.49]$$

– desorption:

$$O_{(ads)} + C_{(\text{at the surface})} \rightarrow CO(g) \qquad [5.4.50]$$

In operating conditions, where the CO_2 gas is blown over a liquid bath with a sulfur content higher than 0.05%wt, the rate of decarburization is almost independent of the gas flow rate. Being of first order with respect to the pressure of CO_2, it is controlled by the dissociative adsorption step with pure iron [PET 97]:

$$k_r = k^\circ_r / (1 + K_S\ a_S) + k'_r \qquad [5.4.51]$$

where a_S is the sulfur's activity in the liquid iron ($0.002 < a_s < 0.01$).

At 1,600°C with:

$$k°_r = 1.8 \,.\, 10^{-3} \text{ (mole/cm}^2\text{.s.atm)}, \quad k'_r = 6.1 \,.\, 10^{-5} \text{ (mole/cm}^2\text{.s.atm)}$$

where k'_r is the rate constant for high sulfur contents and $K_S = 330 \pm 20$.

At low sulfur contents, [S] < 0.05%, the chemical reaction rate is fast and, even with the operating conditions of these experiments (see Figure 6.4.5), the effect of the gas phase mass transfer is not negligible. For very low sulfur contents or for pure iron, the decarburization rate is controlled by the gas phase mass transfer (see Chapter 6, sections 6.3.2.1.3 and 6.4.3).

5.5. Reaction rates for *in situ* conversion of a solid particle

I will now discuss heterogeneous reactions with *in situ* formation of a new phase.

5.5.1. *Reduction of an oxide in solid state by carbon monoxide or hydrogen*

A new phase (a metal) is formed as a growing layer surrounding the oxide core, see reaction [5.2.23] and Chapter 4 of [VIG 11b], section 4.2.3. For the reduction and growth of this layer to proceed, direct contact with the reducing gas must be maintained; the metallic layer must be porous for the gas to gain access to the oxide surface.

This metallic layer grows by the following process: first step "extraction" of oxygen atoms (ions) from the oxide, leaving *in situ* the metal atoms in an imperfect crystalline state, which via a recrystallization process form new crystalline grains whose size increases with temperature, forming a more or less porous layer at the surface of the oxide. For the reduction of the FeO oxide, the recrystallization of reduced iron occurs above 600–650°C. The microstructure of this external metallic layer can evolve during its growth by progressive sintering, forming a progressively dense layer [BEN 51].

Thus, depending on the operating conditions, this layer is either dense or porous. The reduction of dense wüstite (FeO) by pure hydrogen between 600 and 1,100°C, as well as by H_2-H_2O and CO-CO_2 mixtures at 1,000 and 1,100°C, yields the formation of a porous iron layer. Reduction by H_2-H_2O mixtures between 700 and 900°C leads to the formation of a dense iron layer. The presence of impurities such as Mn, Mg and Ca dissolved in the iron oxides has a very strong influence on the structure of the oxide layer. The operating conditions to obtain a layer of porous metal can only be determined by specific experimental tests.

As this metallic layer becomes dense by sintering, the reduction of a particle almost stops for a small degree of reduction at high temperatures where sintering is more rapid. For example, the higher the temperature, the smaller the degree of reduction, as shown in Figure 5.5.1, for the reduction of nickel oxide by hydrogen. The reduction of iron oxides is studied in Chapter 4 of [VIG 11b], section 4.2.3.1.

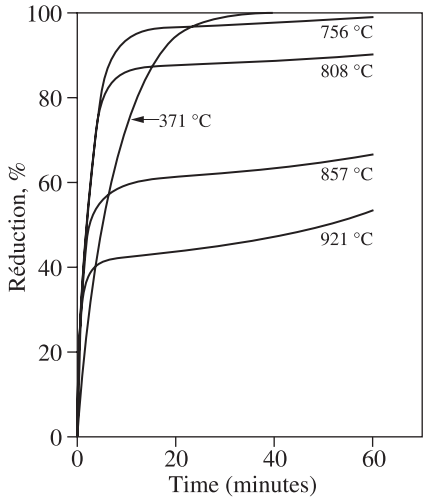

Figure 5.5.1. *Reduction of micronic dense particles of NiO with hydrogen at various temperatures [SZE 71]*

When this layer remains porous, the reducing gas molecules can reach the underlying oxide by the pores of this metallic layer. At the back of these pores, the reduction process with formation of metallic grains occurs again with the release of CO_2, which maintains the porosity of the layer (see Chapter 4 of [VIG 11b] Figure 4.2.1).

The experimental rate at high temperatures is represented by the following expression, in accordance with equations [5.2.24] and [5.4.15]:

$$r = k_{rp} (p_{CO} - p_{CO2} / K_p) = k_{rp} (p_{CO} - p_{CO}^*) \qquad [5.5.1a]$$

The reduction of dense hematite particles (Fe_2O_3 monocrystals or sintered balls) by H_2-H_2O-N_2 mixtures between 700 and 1,000°C follows the kinetic law [5.4.15], see Figure 5.5.2:

$$r_r = k_{rp} (p_{H2} - p_{H2O} / K_p) \qquad [5.5.1b]$$

where r in moles/cm^2.sec and k_{rp} in moles A (mass of A)/cm^2.sec.atm. The variation of the conversion rate of a particle as a function of time is given by equation [7.2.7] for a process controlled by a chemical reaction. The equilibrium constant K_p is that of the FeO-Fe equilibrium. The limiting step is therefore the reduction of wüstite into iron. The activation energy is 13,800 cal/mol. The results of different studies are in good agreement [DUT 64].

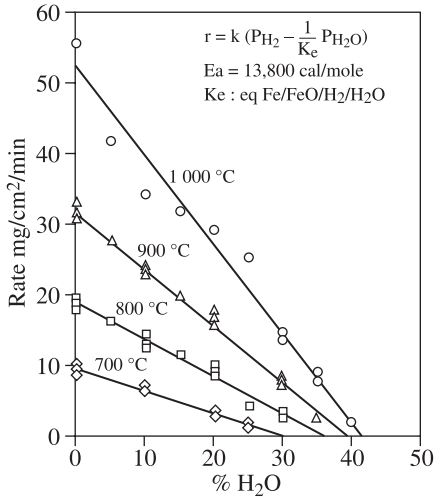

Figure 5.5.2. *Reduction rates of hematite pellets in H_2-H_2O [MCK 62]*

The reduction of dense magnetite particles by H_2-H_2O-N_2 mixtures follows the same kinetic law. The value of the rate constant between 400 and 1,000 °C is of the same magnitude order as that of the reduction of hematite. The first-order rate constant for hydrogen reduction of magnetite to iron (0.86 atm) is given by [QUE 61]:

$$k = 2.0 \times 10^{-2} \exp(-14{,}600/RT) \text{ in moles } O_2/cm^2 sec.atm.$$

The wüstite layer, which forms by reduction of both oxides (magnetite or hematite) by hydrogen, is porous and the iron layer form on the pores of the wüstite pores via kinetics controlled by the chemical reaction. The kinetics are therefore those of the reduction of a porous wüstite particle.

At low temperatures, the rate varies as a function of the pressure p_{H2} according to equation [5.4.14], indicating that the hydrogen adsorption on the oxide controls the reaction (see Figure 5.5.3).

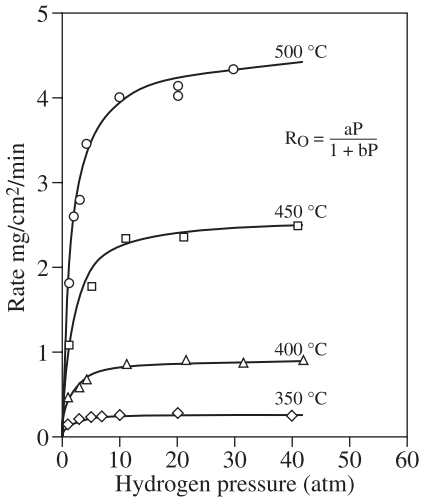

Figure 5.5.3. *Reduction rates of magnetite pellets at various temperatures. Effect of hydrogen pressure [MCK 62]*

5.5.2. *Roasting of a zinc sulfide particle*

$$ZnS(s) + 3/2\ O_2(g) \rightarrow ZnO(s) + SO_2(g) \qquad [5.5.2]$$

Oxidation of dense particles topologically occurs with formation and growth of an external porous layer of ZnO. The oxidation proceeds at the sulfide-oxide interface, oxygen penetration through the porous external layer being possible, see Chapter 6 of [VIG 11b], section 6.2.2.

On the (110) surfaces of monocrystals, under oxygen pressures varying from 0.014–0.5 atm between 680 and 830°C after an initial short period of ZnO crystal nucleation, the growth of the external oxide layer is linear with time. This indicates that the heterogeneous reaction (which occurs at the ZnS unreacted core/ZnO external layer interface) is the limiting step. The initial rate is given by [CAN 57]:

$$r\ (cm/sec) = 8 \times 10^4 \exp(-E / RT)\ (p_{O2})^{1/2} \qquad [5.5.3]$$

If r is expressed in moles/cm^2.sec, we get $k = 3.2 \times 10^3$ moles/cm^2/sec and E = 50 kcal/mol.

We can interpret this rate expression as the dissociative adsorption of oxygen (see reaction [5.4.6]) molecules on the free surface of the sulfide core. The formation and growth of oxide particles giving a continuous layer simultaneously

occurs due to sulfur oxidation at the surface of the particles. The SO_2 gas being released prevents the formation of a dense oxide layer.

5.6. Heterogeneous precipitation

Heterogeneous precipitation is a process where the formation and growth of a new phase occurs as gas bubbles or liquid drops at the interface between two liquid phases, or as a solid layer (continuous or not) on the surface of a substrate (particular or continuous), via a heterogeneous chemical reaction between adsorbed reactants:

$$\nu_a A(\alpha) + \nu_\beta B(\alpha \text{ or } \beta) \rightarrow \nu_a A_{(ads)} + \nu_\beta B_{(ads)} \rightarrow M(g, l, \text{or } s) \downarrow \quad [5.6.1]$$

EXAMPLES.–

– In hydrometallurgy:

- production of metallic powders by reduction of nickel salts in aqueous solution by hydrogen under pressure on nickel particles (see Chapter 1 of [VIG 11b], section 1.3.3):

$$\{\underline{Ni}^{2+}_{(aq)} + H_{2(aq)}\} / Ni_{(particles)} \rightarrow Ni(s)\downarrow + 2\ H^+ \quad [5.6.2]$$

- reduction of a salt by a less electronegative metal transformation called *cementation*: copper in diluted solutions of copper sulfate with iron that acts as a reducing agent is thus recovered (see Chapter 1 of [VIG 11b], section 1.3.4).

$$\underline{Cu}^{2+}_{(aq)} + Fe(s) \rightarrow Cu(s)\downarrow + \underline{Fe}^{\ 2+}_{(aq)} \quad [5.6.3]$$

– In pyrometallurgy; *chemical vapor deposition* (CVD):

- thermal decomposition of gas nickel carbonyl on nickel particles (see Chapter 3 of [VIG 11b], section 3.4.2):

$$Ni(CO)_4(g) / Ni_{(particles)} \rightarrow Ni(s)_{(particles)} + 4\ CO(g) \quad [5.6.4]$$

- reduction of gas chromium chlorides on chrome particles (see Chapter 3 of [VIG 11b], section 3.3.1):

$$\{CrCl_2(g) + H_2(g)\} / Cr_{(particles)} \rightarrow Cr(s)\downarrow + 2\ HCl(g) \quad [5.6.5]$$

- deposition of silicon by heterogeneous thermal decomposition of silane on silicon particles (in a fluidized bed):

$$SiH_4(g) / Si_{(particles)} \rightarrow Si(s)\downarrow + 2\ H_2(g) \quad [5.6.6]$$

5.6.1. *Deposition mechanism*

For deposition of a metal on a substrate of the same metal there is no nucleation step and therefore no nucleation barrier. However, the growth and morphology of the deposit depends on the kinetics of the reaction.

If the reaction rate is slow, the supersaturation is low. There is incorporation of the atoms, atom-by-atom, in the crystal lattice of the substrate (of Ni in the Ni substrate, of Si on the Si substrate, etc.) and epitaxial growth.

If the reaction rate is fast, the supersaturation is high. The adsorbed "atoms" gather into clusters which grow, yielding primary particles without any epitaxial relationship with the substrate. The higher the supersaturation, the higher the superficial density of these particles. These primary particles grow, yielding columnar crystals as fine as the primary particles. Like in the homogeneous precipitation process, see Figure 5.3.1, for very high supersaturations the formation process of primary particles can repeat itself yielding a polycrystalline (equiaxed) layer.

When the deposited metal is different to the substrate metal, in a first step, by adsorption and atom migration, there is the formation of embryos on the substrate defects, like dislocation emergences. The embryos stick to the substrate by a coherent interface. Due to the difference in crystalline structure between the substrate and deposited metal, and the difference of lattice parameters, this coherence can only be realized by an elastic distortion of the lattice of the embryos. When these "coherent" islands have reached a certain size, the stored elastic energy spontaneously transforms these coherent embryos into nuclei with the crystalline structure of the deposited element. The nucleation is therefore a *crystallographic transformation* analogous to a recrystallization and it produces nuclei whose number and size depend on the number of active sites, such as emergent lattice defects (dislocation steps), and on the rate of the heterogeneous reaction. As the rates of these reactions are generally very fast the operating conditions, substrate temperature, etc., are set so that the nucleation step is very rapid. The growth from these primary particles continues as described previously.

5.6.2. *Silicon deposition by heterogeneous thermal decomposition of silane*

The decomposition of silane occurs in the gas phase at high temperature, yielding nuclei and then silicon particles by homogeneous precipitation (see section 5.3). At relatively low temperatures and for relatively low supersaturations, the silane molecules in contact with the substrate undergo decomposition (dissociative

adsorption). The adsorbed silicon atoms gather into clusters that grow into primary particles and the process repeats itself, yielding a continuous deposit.

On silicon particles (in a fluidized bed) between 500 and 700°C under atmospheric pressure and silane partial pressures $p_{(SiH4)}$ of 0.1 atm, the reaction rate [5.6.6] is given by [CLA 81]:

$$R = k_1 \, p_{SiH4} \, / \, \{1 + k_2 \, p_{H2} + k_3 \, p_{SiH4}\} \text{ in Si mol/m}^2\text{/sec} \qquad [5.6.7]$$

with:

k_1 (Si mol/m^2.sec.atm) = $1.25 \, . \, 10^9 \exp(-18{,}500 / T)$

k_2 (atm^{-1}) = $1.75 \, . \, 10^3$ and k_3 (atm^{-1}) = 10^4.

5.7. Bibliography

[BEL 93] G.R. BELTON, *Metallurgical Transactions B*, Vol. 24B, pp. 241-258, April 1993.

[BEN 51] J. BENARD, *Revue de Métallurgie*, Vol. 48, pp. 486, 1951.

[CAN 57] K.J. CANNON, K.G. DENBIGH, *Chemical Engineering Science*, Vol. 6, No. 4/5, pp. 145, 1957.

[CLA 81] W.A.P. CLAASSEN, J. BLOEM, *Journal of Crystal Growth*, Vol. 51, pp. 443-452, 1981.

[DEF 52] R. DEFAY, I. PROGOGINE, *Tension Superficielle et Absorption*, Désoer, Liege, 1952.

[DUT 64] P. DUTILLOY, P.C. GHOSH, A. RIST, *Revue de Métallurgie*, Vol. 61, No. 12, pp. 1013-1060, December 1964.

[FRU 00] R.J. FRUEHAN *et al.*, *Metallurgical and Materials Transactions B*, Vol. 31B, pp. 891-898, October 2000.

[GUG 71] C.E. GUGER, F.S. MANNING, *Metallurgical Transactions*, Vol. 2, pp. 3083-3090, November 1971.

[HAR 52] W.D. HARKINS, *Physical Chemistry of Surface Films*, New York, 1952.

[LAN 48] I. LANGMUIR, *J. Amer. Chem. Soc.,* (1917), Vol. 39, 1848.

[LAN 72] A. LANDSBERG, C.L. HOATSON, F.E. BLOCK, *Metallurgical Transactions*, Vol. 3, pp. 517-523, February 1972.

[LI 00] Y. LI, I.P. RATCHEV *et al.*, *Metallurgical and Materials Transactions B*, Vol. 31B, pp. 1049-1057, October 2000.

[MAJ 80a] H. MAJIMA, Y. AWAKURA, *Metallurgical Transactions B*, Vol. 11B, pp. 209-214, June 1980.

[MAJ 08b] H. MAJIMA *et al*., *Metallurgical Transactions B*, Vol. 11B, p. 379, September 1980.

[MAJ 85a] H. MAJIMA, Y. AWAKURA, *Metallurgical Transactions B*, Vol. 16B, p. 23, March 1985.

[MAJ 85b] H. MAJIMA, Y. AWAKURA, *Extraction Metallurgy*, Vol. 85, pp. 607-627, IMM, London, 1985.

[MAT 81] E. MATIJEVIC, *Acc. Chem. Res*, Vol. 14, pp. 22-29, 1981.

[MCK 62] W.M. MCKEWAN, *Transactions Metallurgical Society*, Vol. 224, pp. 2-5, February 1962.

[NAG 86] T. NAGASAKA, Y. IGUCHI, S. BAN-YAN, *5th Int. Iron and Steel Congress*, Vol. 6, pp. 669-678, 1986.

[PAL 03] S. PAL, A.K. LAHIRI, *Metallurgical and Materials Transactions B*, Vol. 34B, pp. 103-114, February 2003.

[PET 97] C.P. PETIT, R.J. FRUEHAN, *Metallurgical and Materials Transactions B*, Vol. 28B, pp. 639-645, August 1997.

[QUE 61] M.J. QUETS, M.E. WADWORTH, J.R. LEWIS, *Transactions AIME*, Vol. 218, No. 545 and 221, 1960; p. 1186, 1961.

[SMO 85] L.D. SMOOT, P.J. SMITH, *Coal Combustion and Gasification*, Plenum Press, New York, 1985.

[SON 04] H.Y. SOHN, *Metallurgical and Materials Transactions B*, Vol. 35B, 121-131, February 2004.

[SZE 71] J. SZEKELY, J.W. EVANS, *Chem. Eng. Sci*., Vol. 26, p. 1901, 1971.

[TUR 70] E.T. TURKDOGAN, J.V. VINTERS, *Carbon*, Vol. 8, pp. 39-53, 1970.

[VIG 11b] A. VIGNES, *Extractive Metallurgy 2:Metallurgical Reaction Processes*, ISTE Ltd, London and John Wiley and Sons, New York, 2011.

[VIG 11c] A. VIGNES, *Extractive Metallurgy 3: Processing Operations and Routes*, ISTE Ltd, London, John Wiley and Sons, New York, 2011.

Chapter 6

Transport Kinetics

6.1. Introduction

In the previous chapter, the rates of heterogeneous (interfacial) chemical reactions of various extraction processes were studied.

For extraction processes between two phases (fluids), between reactant A dissolved in phase α and reactant B dissolved in phase β (see Chapter 5, section 5.4.5), represented by the chemical reaction occurring at the contact surface (interface) between both phases (see reaction [5.2.6]):

$$\nu_A A(\alpha) + \nu_B B(\beta) \rightarrow \nu_R R(\alpha) + \nu_S S(\beta) \qquad [6.1.1]$$

both reactants A and B are consumed at the interface. Their concentrations close to the interface decrease as soon as the reaction starts and they become lower than those in the bulk of each phase (in which they are located), far from the interface (see Figure 6.1.1). For the reaction to proceed, the reactants have to "diffuse" from the bulk of the phase in which they are present and where their concentrations are high, up to the interface. Concentration gradients normal to the interface are then established, generating fluxes normal to the interface of both reactants and products (number of moles of the considered species crossing a surface parallel to the interface of both phases per unit surface and time[1]). The fluid phases are extensive enough (*semi-infinite phases*) to consider that the bulk concentrations of the reactants and products, during contact time, remain equal to the initial concentrations.

1 Accurately speaking these are flux densities, but they are traditionally called fluxes, as they are here.

Extractive Metallurgy 1: Basic Thermodynamics and Kinetics Alain Vignes
© 2011 ISTE Ltd. Published 2011 by ISTE Ltd.

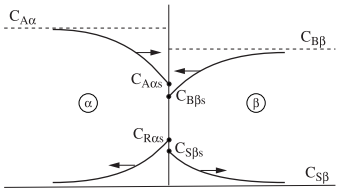

Figure 6.1.1. *Concentration profiles and diffusion fluxes of the reactants and products at a given time between two semi-infinite fluid phases resulting from a heterogeneous reaction [6.1.1]*

The various types of extraction processes have been presented in Chapter 5, sections 5.4.2 to 5.4.5. Further information can also be found in Chapter 7, section 7.1. With respect to the transport processes that can control the *overall rate of the process*, these extraction processes can be classified into three main families:

– *First family*: processes for which transport of reactant A and product R are localized in the same phase, such as:

- solid-fluid conversion,
- gasification, see section 5.4.3,
- leaching/dissolution, see section 5.4.4, or
- heterogeneous precipitation (chemical vapor deposition), see section 5.6,

which can be represented by the following overall reaction:

$$\nu_A A(\alpha) + \nu_B B(\beta) \rightarrow \nu_R R(\alpha) \qquad [6.1.2]$$

Figure 6.1.2 shows the changes in the concentration profiles of both reactant A and product R in the gas phase α as the process proceeds. The concentrations right next to the interface, $C_{A\alpha s}$, of reactant A (which is consumed at the interface) and $C_{R\alpha s}$, of product R evolve towards the asymptotic concentrations $C^*_{A\alpha s}$ and $C^*_{R\alpha s}$ corresponding to thermodynamic equilibrium.

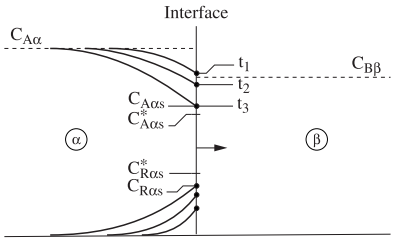

Figure 6.1.2. *Solid-fluid process resulting from heterogeneous reaction [6.1.2]. Concentration profiles of the reactant and product in the fluid phase at various times*

– *Second family*: transfer processes for which transport in both phases must be taken into account, such as extraction (removal)/absorption of a component in phase α by/in phase β (see section 5.4.6), for instance sulfur removal from metal to slag (see [VIG 11b], chapter 7, section 7.2.4) or nitrogen removal from a metal (see Chapter 5, reaction 5.4.43) represented by the following reaction:

$$\nu_A A(\alpha) \rightarrow \nu_R R(\beta) \qquad [6.1.3]$$

Figure 6.1.3a represents the changes in concentration profiles on either side of the interface of both components over time. Concentrations $C_{A\alpha s}$ and $C_{R\beta s}$ at both ends of the interface evolve and tend towards asymptotic values corresponding to the thermodynamic equilibrium (see equation [6.3.7]).

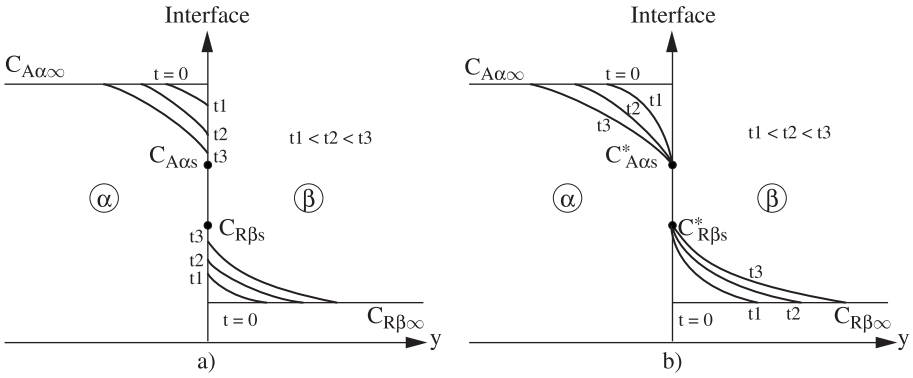

Figure 6.1.3. *Transfer process as represented by reaction [6.1.3]. Concentration profiles at various times: a) for a chemically controlled process; and b) for a diffusion-controlled process – fast interfacial reaction and interfacial reaction at virtual equilibrium*

– *Third family*: fluid-fluid process represented by reaction [6.1.1], such as the decarburizing of hot metal (Fe-c) by CO_2 (see Chapter 5, reaction [5.4.48a]) for which transport of the two reactants in both phases must be taken into account.

For each reactant and product, these extraction processes involve two or three successive elementary steps:

– the transport of each reactant within the phase, where it is present, from the bulk of the phase up to the interface of both phases;

– an interfacial chemical reaction that occurs at the interface of both phases;

– the transport process of each product R or S from the interface up to the bulk/core of the corresponding phase.

Two limiting cases − chemical reaction control and mass transport control – are considered:

– when the interfacial chemical reaction is the rate-limiting step, called the *chemical reaction control*;

– when one or other reactant transport is the rate-limiting step, either called the *diffusion controlled process* or *mass transport control.*

When the overall rate is controlled by the heterogeneous chemical reaction, the transport of the reactants by diffusion from the bulk of the phase up to the interface is faster than their consumption at the interface. Therefore, there is no reactant concentration gradient and the concentrations close to the interface are equal to the concentration in the bulk of the phases. Both phases remain homogeneous. The kinetics of the processes under chemical reaction control have been studied in Chapter 5, sections 5.4−5.6.

When the rate of the heterogeneous chemical reaction is high, the concentrations of the reactants on either side of the interface rapidly reach values close to the concentrations corresponding to the thermodynamic equilibrium (see Figure 6.1.3b). The concentration gradients of the species within the phases still evolve and the overall rate is then controlled by the *transport* of these species within the phases.

To get the expression of the overall process rate as a function of the components concentrations within each phase, the fluxes of the components on either side of the interface have to be expressed (see equation [6.3.4]). To do so, the equations giving the material balances for each component in each phase have to be resolved, taking into account the contacting patterns of the system, for instance a solid particle or droplet (finite dimension phase) in contact with a semi-infinite fluid phase.

As the reactions occur with heat absorption or release (endo- or exothermic reaction), these mass transport processes have to be connected to heat transport (within the same phase) and transfer (from one phase to the other) processes.

6.1.1. *Identification of the rate-limiting step*

The diffusion coefficients in a gas or liquid phase vary more slowly as a function of temperature compared to the constant rate of a chemical reaction, whose variation with temperature is given by an Arrhenius law (see Chapter 5, section 5.2.2.3). It is then quite often observed that at low temperature the chemical reaction with strong activation energy (a few dozens of kcal/mol) is the limiting process. At high temperature, one of the other transport processes with a low activation energy is the

limiting step. However, the value of the activation energy does not always lead to the identification of the limiting step of the process (see equation [6.3.14b]).

6.2. Equations of change and relationships between diffusion fluxes and driving forces

The basic laws of mass, heat and momentum transport in phases in contact are ruled by the equations of change and by the relations between diffusion fluxes and driving forces.

These differential equations, together with the relations between diffusion fluxes and driving forces with the initial and boundary conditions, lead to the establishment of the expressions of material and heat fluxes in each phase on either side of the interface. An exhaustive presentation of these equations can be found in *Transport Phenomena* [ABL 05, BIR 60].

6.2.1. *Equations of change (in terms of the fluxes)*

6.2.1.1. *The equation of continuity or law of mass conservation (over a stationary volume element through which the fluid is flowing)*

The equation of continuity or law of mass conservation is:

$$\delta\rho / \delta t + \text{div}\,(\rho\mathbf{u}) = 0 \qquad [6.2.1]$$

where ρ is the local mass density of the phase and $\mathbf{u}$ is the barycentric velocity i.e.: the local mass average velocity (of the fluid flow) with respect to stationary coordinate. $\boldsymbol{\rho u}$ is the *mass flux* that passes through a unit surface per unit time.

For an extraction process, the velocity $\mathbf{u}$ is defined with respect to a reference frame tied to the interface (phase boundary) between both phases and the normal component of the velocity at the interface is equal to zero ($u_n = 0$).

6.2.1.2. *Equation of continuity (differential material balance) of a component j in a mixture (phase or solution)*

$$\frac{\delta C_j}{\delta t} + \text{div}\,\boldsymbol{\Phi}_j\,(x, t) = r_j \qquad [6.2.2]$$

where C_j is the molar concentration, $\mathbf{\Phi_j\ (x, t)}$[2] is the molar flux of component **j** (that passes through a unit surface per unit time) with respect to stationary coordinates and r_j is a volumetric source term : r_j is the rate of production (or consumption) of component j by a homogeneous chemical reaction (see Chapter 5, section 5.2.11).

For an extraction process, where an heterogeneous chemical reaction occurs, the reaction rate r_s will appear in the boundary conditions (at the surface on which the reaction occurs) and not in the continuity equation. The local conservation equation of a component in a phase can then be written as:

$$\frac{\delta C_j}{\delta t} + \text{div } \mathbf{\Phi}_j\ (x, t) = 0 \qquad [6.2.3]$$

The molar flux, $\mathbf{\Phi_j}$, is split into a *convection flux*, which is the molar flux of component j resulting from the bulk motion of the fluid (bulk flow) and a *molar (barycentric) diffusion flux J_j relative to the mass-average velocity* ***u***:

$$\mathbf{\Phi}_j\ (x, t) = C_j\ .\ \mathbf{u} + \mathbf{J}_j \qquad [6.2.4]$$

with, according to the law of mass conservation:

$$\sum M_j\ .\ \mathbf{\Phi}_j = \rho\mathbf{u} \qquad [6.2.5]$$

with the following relationship between the molar (barycentric) diffusion fluxes $\mathbf{J}_j$:

$$\sum M_j\ .\ \mathbf{J}_j = 0 \qquad [6.2.6]$$

In addition, *a molar diffusion flux* $\boldsymbol{j_j}$ *relative to a local molar-average velocity* is defined as [BIR 60]:

$$\mathbf{\Phi}_j\ (x, t) = x_j\ .\ \sum\mathbf{\Phi}_j + \mathbf{j}_j \qquad [6.2.7]$$

The sum of the molar diffusion fluxes relative to the molar-average velocity is equal to zero:

$$\sum\mathbf{j}_j = 0 \qquad [6.2.8]$$

6.2.1.3. *The differential enthalpy balance for a reacting system*

$$\frac{\delta(\rho H)}{\delta t} + \text{div } (\rho H\mathbf{u}) + \text{div } \mathbf{J}_T = r\ .\ (-\Delta H_r) \qquad [6.2.9]$$

2. Fluxes are vectors, which explains the use of bold symbols: **F**, **J**, etc.

where H is the enthalpy per unit mass of the phase ($\rho H = \sum \rho_j \, . \, C_{pj}$) and $\mathbf{J_T}$ is the *heat conduction flux* tied to the temperature gradient (see equation [6.2.10a]). ($-\Delta H_r$) is the enthalpy of the homogeneous reaction, if it occurs. In the case of an extraction process where the chemical reaction is heterogeneous, the enthalpy of this reaction will appear in the boundary conditions.

The equation for the energy balance is quite complex and will not be used.

6.2.2. *Relationships between diffusion fluxes, driving forces and transport properties*

A exhaustive presentation of these relations for the different cases is provided by *Transport Phenomena* [BIR 60]. Only the main results will be presented in this section.

In a multi-component system, according to the thermodynamics of irreversible processes, there will be a contribution to each flux owing to each driving force in the system (linear phenomenological relations):

$$J_i = \sum L_{ij} . X_j$$

Furthermore, the (phenomenological) coefficients L_{ij} are those such as $L_{ij} = L_{ji}$ (Onsager reciprocal relations).

For the processes studied, the diffusion fluxes are only a function only of the corresponding forces. Fourier's and Fick's laws will then be used.

6.2.2.1. *Fourier's heat conduction law*

The expression of the heat conduction flux:

$$\mathbf{J}_T (x, t) = -\lambda_T \, . \, \nabla T \qquad [6.2.10a]$$

which is often written as:

$$\mathbf{J}_T (x, t) = -\alpha_T \, . \, \nabla (\rho C_p T) \qquad [6.2.10b]$$

where λ_T is the thermal conductivity in cal(joule)/cm.sec.K and α_T is the thermal diffusivity in cm^2/sec of the considered phase.

The local heat balance [6.2.9], in the absence of convection, $\mathbf{u} = 0$, can then be written as:

$$\rho C_p \frac{\delta T}{\delta t} = \lambda_T \,.\, \nabla^2 T \qquad [6.2.11a]$$

or as:

$$\frac{\delta T}{\delta t} = \alpha_T \,.\, \nabla^2 T \qquad [6.2.11b]$$

6.2.2.2. *Fick's diffusion laws*

The expressions of the molar diffusion fluxes for each component are given for two cases: binary solutions and diluted solutions (reactants and products in each phase, α and β, are diluted in some solvents or in inert gases).

For a monophase binary system, (A + R), see Figure 6.1.2, the expressions of both diffusion fluxes $\mathbf{J}_A$ and j_A, for each component, are respectively [BIR 60]:

$$\mathbf{M_A J_A} = -\rho D_{AR} \,.\, \mathbf{grad}\ w_A \qquad [6.2.12]$$

$$\mathbf{j_A} = -C D_{AR} \,.\, \mathbf{grad}\ x_A \qquad [6.2.13]$$

where D_{AR} is the inter-diffusion coefficient (*mass diffusivity*, see equation [6.2.10b]) expressed in cm^2/sec, which is identical in equations [6.2.12] and [6.2.13]. $C = C_A + C_B$ is the total molar density, ρ is the total mass density, x_A is the molar fraction, and w_A is the mass fraction of component A at the considered location and time (see Chapter 1, equations [1.2.29] and [1.2.30]).

These are the only expressions of the molar diffusion fluxes for which the diffusion fluxes satisfy equations [6.2.6] and [6.2.8] respectively.

They can be rewritten:

– *For a phase with a constant density ρ,* where expression [6.2.12] becomes:

$$\mathbf{J_A} = -D_{AR} \,.\, \nabla C_A \text{ and } \mathbf{J_R} = -D_{AR} \,.\, \nabla C_R \qquad [6.2.14]$$

and is known as Fick's first law. This leads to the equation giving the change of component A, see equation [6.2.3]:

$$\frac{\delta C_A}{\delta t} + \mathbf{u} \,.\, \nabla C_A = D_{AR}\, \nabla^2 C_A \qquad [6.2.15]$$

When the velocity **u** is equal to zero, $u = 0$, $\Phi_A = J_A$, Fick's second law is then obtained for each component:

$$\frac{\delta C_A}{\delta t} = D_{AR} \nabla^2 C_A \text{ and } \frac{\delta C_R}{\delta t} = D_{AR} \nabla^2 C_R \qquad [6.2.16]$$

– *For a phase, with constant total molar density C* or under a constant global pressure ($P = p_A + p_R = cste$), expression [6.2.13] of flux $\mathbf{j_A}$ becomes:

$$\mathbf{j_A} = -D_{AR} \nabla C_A = -D_{AR} / RT \,.\, \nabla p_A = -\mathbf{j_R} \qquad [6.2.17]$$

The equation of continuity of component A [6.2.3] in a binary solution reduces to Fick's second law [6.2.16] only when $\Phi_A(\alpha) + \Phi_R(\alpha) = 0$, owing to equation [6.2.7].

In a multicomponent solution, where the components are present in low concentration in a solvent, a diffusion coefficient is defined for each component by [BIR 60]:

$$\mathbf{M_j J_j} = -\rho D_j \,.\, \nabla w_j \qquad [6.2.18]$$

$$\mathbf{j_j} = -C \,.\, D_j \,.\, \nabla x_j \qquad [6.2.19]$$

Equations [6.2.6] and [6.2.8] are no longer satisfied. Local molar or mass balances [6.2.3] will have to be solved for each reactant and product.

NOTE.– Many analytical solutions of the continuity equations [6.2.11] and [6.2.16] have been established for various particular cases [CAR 59, CRA 56]. They are useful, however, as they show the influence of some factors or parameters on the process kinetics. They lead to some quite useful dimensionless equations (see section 6.4).

The numerical methods for resolving these equations based on partial derivates are presented in various studies: FDM (*finite difference method*) [DEB 05, ZIE 00], FVM (*finite volume method*) [FER 02, JAR 05, PAT 80] and FEM (*finite element method*) [RAP 98].

6.3. Interphase mass or heat transport (mass and heat transfer)

6.3.1. *Definitions of heat and mass transfer coefficients*

Section 6.4.1.1 presents the analytical solution of the local heat balance (see equation [6.2.11]) in the simple case of heat transfer between a plane hot wall and a

stagnant cooler fluid (see Figure 6.4.1a). The expression of the heat flux transferred from the solid to the fluid (across the solid-fluid interface) $\Psi_{T(s \rightarrow \alpha)}$ (equation [6.4.3]) is the product of a "conductance" h_T and the difference between the temperature of the bulk fluid and the solid (assumed constant):

$$\Psi_{T(\beta \rightarrow \alpha)} = h_T \, (T_\beta - T_{\alpha\infty}) \qquad [6.3.1a]$$

Newton's law of heat transfer is based on this expression. It is not really a law but rather an equation that defines the *heat transfer coefficient*.

As $T_\beta = T_{\alpha s}$ and as the fluid is stagnant (see equation [6.2.4]), the resistance to the transfer is located in the fluid phase:

$$\psi_{T(\beta \rightarrow \alpha)} = \Phi_{T\alpha s} = J_{T\alpha s} = h_{T\alpha s} \, \{T_{\alpha S} - T_{\alpha\infty}\} \qquad [6.3.1b]$$

and the heat transfer coefficient is in fact a heat conductance in the α phase.

For extraction processes, such as the evaporation of a liquid, the gasification of a solid, or a transfer process (see Figures 6.1.2 and 6.1.3) for each component, the *molar diffusion flux* $j_{A\alpha s}$ resulting from a concentration gradient is normal to the interface (see equation [6.2.7]) at the interface of both phases in contact. This is expressed by a similar equation:

$$j_{A\alpha s} = h_{A\alpha} \, (C_{A\alpha\infty} - C_{A\alpha s}) \qquad [6.3.2]$$

where $C_{A\alpha\infty}$ is the concentration of component A in the bulk of the phase, outside the diffusion zone; $C_{A\alpha s}$ is the concentration of the component right next to the surface (or interface); and $\mathbf{h_{A\alpha}}$ is an (intraphase) *mass transport conductance* that is also called the *mass transfer coefficient* (in one phase) [BIR 60].

In the absence of convection *with a reference frame tied to the interface* (supposed plane), the flux $\Phi_{A\alpha s}$ of each component in phase α at the interface (and normal to the interface, see equations [6.2.7] and [6.4.7]), is given by:

$$\Phi_{A\alpha s} = h_{A\alpha} \, (C_{A\alpha\infty} - C_{A\alpha s}) + x_{A\alpha s} \sum(\Phi_{j\alpha s}) \qquad [6.3.3]$$

As the reactants are stoichiometrically consumed and the products R and S, are stoichiometrically produced at the interface of both phases, by the heterogeneous reaction, the molar fluxes of both reactants and products in their respective phases at the interface are proportional to the stoichiometric coefficients of the reaction [6.1.1] (see Chapter 1 , equation [1.2.5]):

$$\Phi_{A\alpha s} / -\nu_A = \Phi_{R\alpha s} / \nu_R = \Phi_{B\beta s} / -\nu_B = \Phi_{S\beta s} / \nu_S \qquad [6.3.4]$$

NOTE.– We could have defined a mass transfer coefficient $h'_{A\alpha}$ with respect to the (barycentric) diffusion flux J_j (see Equation [6.2.4]) but the expression of the flux $\Phi_{A\alpha s}$ corresponding to [6.3.3] would have been more complex.

NOTE.– In some studies, a *mass transfer coefficient* is defined by:

$$\Phi_{A\alpha s} = h_{A\alpha} (C_{A\alpha\infty} - C_{A\alpha s}) \qquad [6.3.5]$$

Both definitions are equivalent in the case of reactant A is present in phase α in low concentration, or when $\nu_A = \nu_R$ (see section below).

The expressions of the mass transfer coefficients for different contact patterns between two phases are established in section 6.4, and the expressions of the overall kinetics under a mixed regime (kinetics controlled by the transport processes and the interfacial chemical reaction) are presented in section 6.5 for some processes.

6.3.2. *Kinetics of diffusion-controlled processes*

In many heterogeneous systems with fast chemical reactions, the overall rate is found to be controlled by mass transport of a component between the reaction surface and the bulk fluid.

Under mass transport control, as the rate of the heterogeneous chemical reaction rate is high compared to the rate of the mass transport, the concentrations near the interface of the reactants and of the products rapidly reach the concentrations corresponding to the thermodynamic equilibrium (see Figures 6.1.2 and 6.1.3), and for a process represented by reaction [6.1.2]:

$$\left(C^*_{A\alpha s}\right)^{\nu_A} \Big/ \left(C^*_{R\alpha s}\right)^{\nu_R} = K_C \qquad [6.3.6]$$

and for a transfer process (see reaction [6.1.3]), to:

$$\left(C^*_{A\alpha s}\right)^{\nu_A} \Big/ \left(C^*_{R\beta s}\right)^{\nu_R} = K_C \qquad [6.3.7]$$

6.3.2.1. *Extraction processes controlled by mass transport in one phase*

For a gas-solid process such as the gasification of a solid particle (see reaction [6.1.2] and Figure 6.1.2), the fluxes of reactant A and product R in phase α at the interface (see equation [6.3.3]), owing to relations [6.3.4], can be written as:

$$\Phi_{A\alpha s} = h_{A\alpha} (C_{A\alpha\infty} - C_{A\alpha s}) / \{1 + \varepsilon_A . x_{A\alpha s}\} \quad [6.3.8]$$

and:

$$\Phi_{R\alpha s} = h_{R\alpha} (C_{R\alpha s} - C_{R\alpha\infty}) / \{1 - \varepsilon_A . x_{R\alpha s} . \nu_A / \nu_R\} \quad [6.3.9]$$

where:

$$\varepsilon_A = (\nu_R - \nu_A) / \nu_A \quad [6.3.10]$$

When the equilibrium relationship [6.3.6] can be approximated (within a given concentration range) by a linear relation between the concentrations close to the interface of reactant A and product R:

$$C^*_{A\alpha s} = C^*_{R\alpha s} / K'_C \quad [6.3.11]$$

the conversion rate of particle B per unit surface can be expressed as (see Chapter 7, equation [7.2.3]):

$$\frac{1}{\nu_B}\frac{dn_B}{dt} = h_{AR\alpha}\left(C_{A\alpha\infty} - \frac{C_{R\alpha\infty}}{K'_c}\right). \quad [6.3.12]$$

a product of a transport conductance in phase α, $h_{AR\alpha}$ and a "driving force" ($C_{A\alpha\infty} - C_{R\alpha\infty} / K_C$). $h_{AR\alpha}$ is a complex expression.

In the case where $\nu_A = \nu_R$, then $\varepsilon_A = 0$, and the conversion rate of B can be written as:

$$\frac{1}{\nu_B}\frac{dn_B}{dt} = \frac{C_{A\alpha\infty} - \frac{C_{R\alpha\infty}}{K'_c}}{\frac{1}{h_{A\alpha}} + \frac{1}{K'_c . h_{R\alpha}}} \quad [6.3.13]$$

and with a new approximation: $h_{A\alpha} = h_{R\alpha}$, which is often implicitly made, the following expression is obtained [SZE 76]:

$$\frac{1}{\nu_B}\frac{dn_B}{dt} = h_{A\alpha}\left(C_{A\alpha\infty} - \frac{C_{R\alpha\infty}}{K'_c}\right)\frac{K'_c}{(1+K'_c)} \qquad [6.3.14a]$$

In practice, $C_{R\alpha\infty} = O$ and:

– for a reaction where the equilibrium constant K'_c is low:

$$\frac{1}{\nu_B}\frac{dn_B}{dt} = h_{R\alpha}.K'_c.C_{A\alpha\infty} \qquad [6.3.14b]$$

– for an irreversible reaction (high K'_C):

$$\frac{1}{\nu_B}\frac{dn_B}{dt} = h_{A\alpha}.C_{A\alpha\infty} \qquad [6.3.14c]$$

NOTE.– The activation energy of the process [6.3.4b] includes the variation d (ln K'_C / d (1 / T), see Chapter 1, equation [1.3.56]. This can be very high if the reaction enthalpy is high for an endothermic reaction.

In this section, some examples of extraction processes controlled by mass transport in one phase are presented. Some other cases are presented in other chapters, for instance *sulfur transfer from metal to slag*, i.e. *steel desulfurization* (see [VIG 11b], Chapter 7, section 7.2.4) controlled by the transport process of sulfur in the metallic phase; and *steel dephosphorization* (see [VIG 11b], Chapter 5, section 5.3.7) controlled by the transport process of (PO_4^{3-}) phosphorous in the slag.

6.3.2.1.1. Gas-solid reaction type: *in situ* conversion of a particle

$$ZnS(s) + 3/2\ O_2(g) \rightarrow ZnO(s) + SO_2(g) \qquad [6.3.15a]$$

At high temperatures, the roasting rate of a ZnS particle is controlled by the transport process of oxygen in the pores of the growing ZnO layer (see [VIG 11b], Chapter 6, Figure 6.2.5). The oxygen flux at the surface of the unreacted core of the particle can be written as:

$$2/3\ \frac{dn_{ZnS}}{dt} = \Phi_{O2s} = \frac{\left(\frac{h_{O_{2g}}}{RT}\right).\left(p_{O_2} - p^*_{O_{2s}}\right)}{\left(1 - \frac{p^*_{O_{2s}}}{3P}\right)} \qquad [6.3.15b]$$

with: $p^*_{SO2s} / (p^*_{O2s})^{3/2} = K_p(T)$ and $p^*_{SO2s} + p^*_{O2s} = P$.

As the equilibrium constant K_p of the reaction is quite high at the operating temperatures, $p^*_{O2s} = 0$ and the rate can be written as:

$$\Phi_{O2\alpha s} = (h_{O2g} / RT) \,.\, p_{O2} \qquad [6.3.15c]$$

This expression can be compared to the rate of particle conversion term in the chemical regime (rate controlled by the heterogeneous chemical reaction, see Chapter 5, section 5.5.2 and equation [5.5.3]). This reaction is dealt with in [VIG 11b], Chapter 6, sections 6.2.1 and 6.2.2.

6.3.2.1.2. Gas-solid reaction-type gasification: reduction of ZnO by CO gas

$$ZnO(s) + CO(g) \rightarrow Zn(g) + CO_2(g) \qquad [6.3.16a]$$

The rate of zinc oxide particle reduction when it is controlled by the transport of CO gas molecules in the gas boundary layer surrounding the particle, see equation [6.3.3], can be written as:

$$\frac{dn_{ZnO}}{dt} = \Phi_{CO(g)s} = \left(\frac{h_{CO}}{RT}\right).\left(p_{CO} - p^*_{CO}\right) + \left(\frac{p_{CO}}{P}\right) \,.\, \{\Phi_{CO} + \Phi_{Zn} + \Phi_{CO2}\}$$

which, thanks to equation [6.3.4], can also be written as:

$$\frac{dn_{ZnO}}{dt} = \frac{(h_{CO}/RT).\left(p_{CO} - p^*_{CO}\right)}{\left(1 + p_{CO}/P\right)} \qquad [6.3.16b]$$

$p^*_{CO(s)}$ can be obtained from the mass action law $K_p(T) = p^*_{Zn} \,.\, p^*_{CO2} / p^*_{CO}$,

with $p^*_{Zn} + p^*_{CO2} + p^*_{CO} = P$ and $p^*_{Zn} = p^*_{CO2}$.

The rate of this process, when controlled by the heterogeneous reaction, is presented in Chapter 5, section 5.4.3.1. The process is studied in [VIG 11b,] Chapter 4, section 4.2.2.3 (see equation [4.2.13]).

6.3.2.1.3. Fluid-fluid reaction: decarburization of liquid iron by O_2 gas

$$\underline{C}_{(\text{dissolved in liquid Fe})} + 1/2\ O_2(g) \rightarrow CO(g) \qquad [6.3.17a]$$

The decarburization rate of a "hot metal" (Fe-c) by various oxidizing gases – O_2, CO_2, H_2O – has been studied under various experimental contacting patterns: either a steady gaseous atmosphere over the liquid bath (see Figure 6.3.1); or with the liquid droplets under levitation in an O_2 gas stream, see Figure 6.3.2, and [VIG 11b], Chapter 5, section 5.3.3 and Figure 5.3.3.

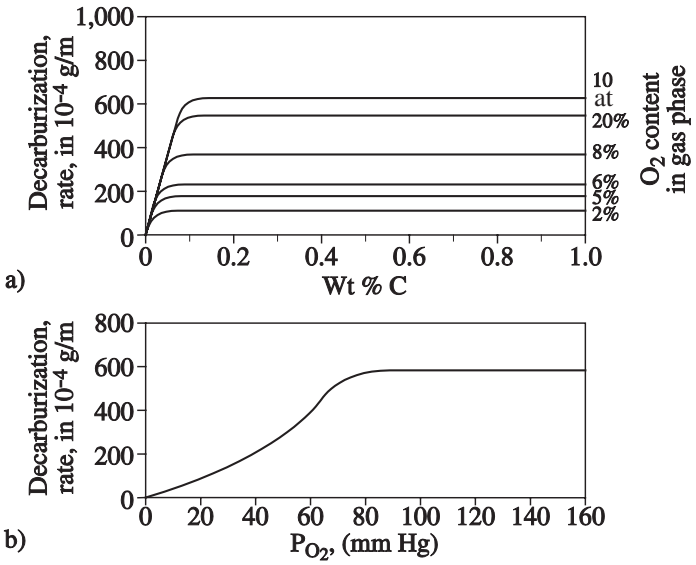

Figure 6.3.1. *Decarburization rate of a liquid carbon-iron bath by steady O_2 gas atmosphere at 1,600°C: a) as a function of the carbon content of liquid iron and of the O_2 content in the gas phase; and b) as a function of the partial pressure of oxygen for a bath with a carbon content of 0.40% [FUJ 67]*

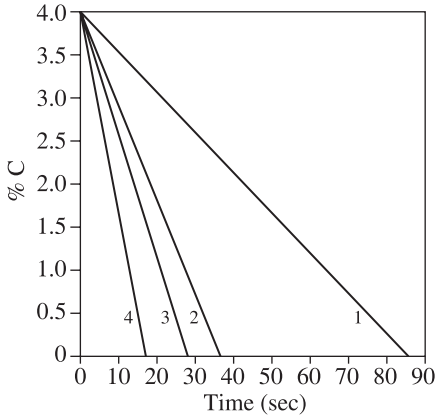

Figure 6.3.2. *Decarburization of carbon-saturated liquid iron droplets under levitation conditions exposed to O_2 at various flow rates – 100, 300, 500 and 1,200 cm^3/min (see [VIG 11b], Chapter 5, Figure 5.3.3) and at 1,600°C [DIS 68]*

In these tests, for carbon concentrations C ≥ 0.15-0.20%, the decarburization rate does not depend on the C concentration in the "hot metal" (see Figures 6.3.1a and 6.3.2). As the liquid phase is strongly mixed up (by induction), the transport of carbon in the liquid phase is very fast and the carbon diffusion flux in the liquid phase is quite high. The decarburization rate is then controlled by the diffusion of oxygen in the gaseous phase and can be written:

$$V_{Fe}\frac{d\left[\underline{C}_{(Fe)}\right]}{dt} = S.\Phi_{O2s} = S.\ \frac{\left(h_{O_2}/RT\right).\left(p_{O_2} - p^*_{O_2}\right)}{\left(1 + p_{O_2}/P\right)} \qquad [6.3.17b]$$

where $\underline{C}_{(Fe)}$ is the average concentration of carbon in the liquid phase and p^*_{O2s} can be obtained thanks to the mass action law (for a carbon saturated iron $a_{\underline{C}} = 1$):

$$p^*_{O2s} = (p_{CO} / K_p)^{1/2}$$

with $p^*_{CO} + p^*_{O2} = P$.

For an iron bath in contact with a steady gas phase, the decarburization rate depends on p_{O2} (see Figure 6.3.1b), (the mass transfer coefficient h_{O2g} being constant).

For iron droplets in contact with an oxygen gas stream, the decarburization rate depends on the gas flow rate (see Figure 6.3.2), its variation being due to the variation of the mass transfer coefficient h_{O2} with the oxygen flow rate (variation of the thickness of the outer boundary layer surrounding the droplet) (see Figures 6.4.5 and 6.4.7).

When the carbon concentration in the iron becomes < 0.15 in a bath in contact with a steady gas phase (see Figure 6.3.1a), the decarburization rate depends on the carbon concentration. The transport resistance is localized in the liquid phase (diffusion of the carbon in liquid iron):

$$1/2\ (V/S)_g\ .\ \frac{d\left[\underline{C}_{(Fe)}\right]}{dt} = h_{(\text{metallic phase})}\ \{[\underline{C}_{(Fe)}] - [\underline{C}_{(Fe)s}]\} \qquad [6.3.17c]$$

The rate of this process, when controlled by the heterogeneous reaction, is presented in Chapter 5, section 5.4.5, equation [5.4.50].

6.3.2.2. *Transfer processes*

We consider the transfer process between two semi-infinite phases (see Figure 6.1.3) represented by reaction [6.1.3]:

$$\nu_A A(\alpha) \rightarrow \nu_R R(\beta) \qquad [6.3.18]$$

and assume that the equilibrium at the interface (see Figure 6.1.3b and Equation [6.3.7]) can be represented by the partition coefficient H (see [VIG 11b], Chapter 1, equation [1.4.6]):

$$C^*_{A\alpha s} = C^*_{R\beta s} / K_C \qquad [6.3.19]$$

In addition, we assume that the concentrations of reactant A to be extracted from phase α and product R in their respective phases are low (see equation [6.3.3]). The the flux of A in phase α at the interface is therefore given by:

$$\Phi_{A(\alpha)s} = h_{A\alpha} (C_{A\alpha\infty} - C_{A\alpha s}) \qquad [6.3.20]$$

and the same expression for the flux of R in phase β, $\Phi_{R(\beta)s}$. The transfer flux Ψ_A ($\alpha \rightarrow \beta$) of component A from phase α towards phase β can then be written as the product of a transfer driving force by an *overall (interphase) mass transfer coefficient* h_A:

$$\Psi_A (\alpha \rightarrow \beta) = h_A \{C_{A\alpha\infty} - C_{R\beta\infty} / K_C\} \qquad [6.3.21]$$

where:

$$\frac{1}{h_A} = \frac{1}{h_{A\alpha}} + \frac{\nu_R}{\nu_A} \frac{1}{K_c h_{R\beta}} \qquad [6.3.22]$$

The overall mass transfer resistance is the "sum" of the two transport resistances. The rule of addition of the resistances acting in series is satisfied as both processes are of the same vectorial nature.

If K_C is *a priori* high, the limiting process is the transport towards phase α:

$$h = h_{A\alpha} \qquad [6.3.23a]$$

If K_C is low, the limiting process is the transport in phase β, and:

$$h = h_{R(\beta)} \, . \, K_C \qquad [6.3.23b]$$

6.3.2.2.1. Example: hydrogen extraction from liquid iron

$$\underline{H}_{(Fe)} \rightarrow 1/2\ H_2(g) \qquad [6.3.24a]$$

The interfacial chemical reaction is fast so an equilibrium is established at the interface very quickly, see Chapter 5, section 5.4.6.3 and equation [5.4.45]. The transport of hydrogen in the metallic liquid phase is the limiting step and the expression of the transfer flux is:

$$\Phi_H = h_{H(Fe)} ([\underline{H}_{(Fe)}] - K_p\ (p_{H2})^{1/2}) \qquad [6.3.24b]$$

where p_{H2} is the hydrogen pressure in the gas phase. This expression can be compared to that of the removal rate of nitrogen from liquid iron where the heterogeneous reaction is the limiting process, see Chapter 5, equation [5.4.44].

In practice, dehydrogenation occurs under a vacuum and $p_{H2} = 0$, so:

$$\Phi_H = h_{H(Fe)}\ [\underline{H}_{(Fe)}] \qquad [6.3.25]$$

6.4. Mass and heat transfer coefficients

The kinetic laws of extraction processes, when the interfacial chemical reaction is fast compared to the transport processes in each phase, can be obtained by resolving the equations of continuity for each component (see equation [6.2.3]), with the boundary conditions at the interface corresponding to the thermodynamic equilibrium. Thus, the expressions of the fluxes of each constituent are obtained in each phase at the interface (or contact surface) between both phases and the corresponding mass and heat transport conductance, also called transfer coefficients.

In practice, the available analytical solutions regarding the processes where mass transports are the controlling processes are transpositions of the solutions obtained for heat transfer [CAR 59, CRA 56]. Therefore, they are only valid for low (molar) mass fluxes. The flux $\Phi_{A\alpha s}$ in phase α at the interface of component A will be almost equal to the diffusion fluxes $J_{A\alpha s}$, see equations [6.2.7] and [6.4.6].

The analytical solutions depend on the initial and boundary conditions. Two main types of configurations have to be considered. Figures 6.1.1–6.1.3 present a configuration where both phases are semi-infinite on either side of the interface. The other configuration corresponds to a phase of finite dimension (solid particle, droplet or bubble) in contact with another fluid phase that can be considered semi-infinite (see Figure 6.4.5).

6.4.1. *Mass and heat transfer (across a phase boundary) between two semi-infinite and stagnant phases*

6.4.1.1. *Heat transfer between a plane wall and a fluid*

We consider a semi-infinite fluid phase, initially at a temperature of $T_{\alpha\infty}$, brought into contact at time t = 0 with a solid phase (plane wall) at a higher temperature T_β (see Figure 6.4.1a). The contact between both phases being considered "ideal", the temperature of the fluid in contact with the plane wall $T_{\alpha s}$ is instantaneously raised to the temperature of the wall $T_{\beta s}$. The temperature of the wall is considered constant during the contact time, thus the temperature of the fluid at the surface remains constant during this same contact time.

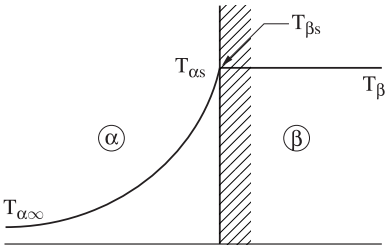

Figure 6.4.1a. *Heat transfer between a wall at temperature T_S and a semi-infinite stagnant fluid. Temperature profile at time t*

When z = 0, at any time t: $T_{\alpha s} = T_S$ = constant.

The temperature profile is obtained in the fluid phase by solving equation [6.2.11], whose solution is:

$$\frac{\left(T_\alpha - T_{\alpha\infty}\right)}{\left(T_{\alpha S} - T_{\alpha\infty}\right)} = 1 - \text{erf}\ \{z / 2\ (\alpha_T\ t)^{1/2}\} \qquad [6.4.1]$$

where erf is the error function: $\text{erf}(z) = \int_0^\pi e^{-z^2} dz$.

The heat conduction flux (see equation [6.2.10a]) in the fluid phase at the interface is given by:

$$J_{T\alpha s} = -\lambda_T \cdot \left(\frac{\delta T}{\delta z}\right) = \frac{\lambda_T}{\left(\alpha_T \pi t\right)^{1/2}} \cdot \{T_{\alpha S} - T_{\alpha\infty}\} \qquad [6.4.2]$$

The heat being transferred from the solid to the stagnant fluid, this heat conduction flux J_{Tfs} is equal to the rate of heat transfer across the solid-fluid interface (see equation [6.3.1b]):

$$\psi_{T\alpha s} = \Phi_{T\alpha s} = J_{T\alpha s} = h_{Ts} \{T_{aS} - T_{\alpha\infty}\} \qquad [6.4.3]$$

and the *heat transfer coefficient*, $h_{T\sigma}$, is given:

$$h_{T\alpha} = \frac{\lambda_T}{(\alpha_T \pi t)^{1/2}} = \rho C_p \,.\, (\alpha_T / \pi t)^{1/2} \qquad [6.4.4]$$

The average transfer flux for the contact time τ is:

$$\Phi_{Ts}(\tau) = \rho C_p \left(\frac{4\alpha_T}{\pi\tau}\right)^{1/2} . \{T_S - T_{\alpha\infty}\} = 2\, h_{T\alpha s}(\tau)\, \{T_S - T_{\alpha\infty}\} \qquad [6.4.5]$$

This expression is only valid when T_β and $T_{\alpha\infty}$ are constant.

6.4.1.2. *Mass transfer: evaporation of a liquid into a gas phase*

Let us consider an elementary mass transfer process like the evaporation of a pure liquid A in a gas phase α whose component B is insoluble in the liquid phase (the system being maintained at constant temperature and pressure), see Figure 6.4.1b.

The transport of component A in gas phase α is the only process to be considered.

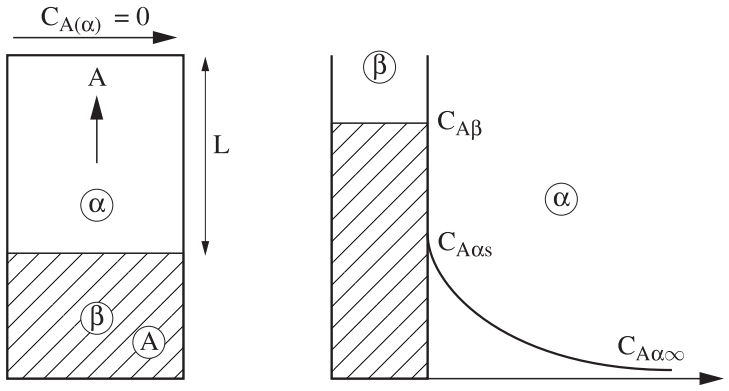

Figure 6.4.1b. *Evaporation of a liquid*

Under a mass transport regime, the concentration (or partial pressure) of constituent A in gas phase α at the liquid-gas interface is the concentration corresponding to equilibrium with the liquid $C_{A\alpha s}$*. The evaporation of a liquid leads to a decrease in the liquid mass level. We can then easily imagine some liquid phase device that maintains the level of the liquid phase constant. At the top of the tube, a gas stream B flows past slowly so the concentration of component A is maintained at a value equal to zero. For z = 0 at any time t (interface), $C_{A\alpha} = C_{A\alpha s}$ (constant) = $C^*_{A\alpha s}$ and for x = ∞, $C_{A\alpha} = C_{A\alpha\infty} = 0$.

The evaporation rate (per surface unit) Ψ_A is then equal to the flux of component A in phase α, at the interface $\Phi_{A\alpha s}$ (see equations [6.2.25] and [6.3.13]).

When the flux of component A in gas phase α is low, the flux $\Phi_{A\alpha z}$ is nearly equal to the diffusion flux $j_{A\alpha z}$ (see equation [6.3.3]). The concentration profile of constituent A in phase α is then obtained by the resolution of Fick's second law (see equation [6.2.16]), whose solution is similar to the heat transfer profile expression (see equation [6.4.1]):

$$\{C_{A\alpha} - C_{A\alpha s}\} / \{C_{A\alpha\infty} - C_{A\alpha s}\} = 1 - \text{erf}\,\{z / (4\, D_{A\alpha} \,.\, t)^{1/2}\} \qquad [6.4.6]$$

The expression of the flux of component A transferred into phase α, i.e. the evaporation rate is:

$$\Psi_{A\alpha} = \Phi_{A\alpha s} = J_{A\alpha s} = -\, D_{A\alpha} \left(\frac{\delta C_A}{\delta z}\right)_s = (C_{A\alpha s} - C_{A\alpha\infty}) \left(\frac{D_{A\alpha}}{\pi t}\right)^{1/2} \qquad [6.4.7]$$

This flux can be written as the product of a conductance $h_{A\alpha}$ (a mass transfer coefficient), see equation [6.3.2], by a force $(C_{A\alpha s} - C_{A\alpha\infty}) = C_{A\alpha s}$:

$$h_{A\alpha} = \left(\frac{D_{A\alpha}}{\pi t}\right)^{1/2} \qquad [6.4.8]$$

This expression is only valid when the component is present at a low concentration in the phase.

6.4.2. *Heat and mass transfer between a flat wall and a fluid flowing along the flat surface in forced convection: boundary layer theory*

Mass and heat transports mainly depend on the contact patterns between both phases and on the relative flow of these phases. Boundary layer theory leads to a

satisfactory expression of the transport conductance (heat and mass transfer coefficient) in a phase flowing around a submerged object, see Figure 6.4.2.

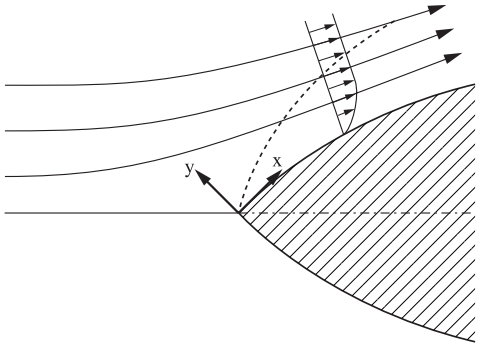

Figure 6.4.2. *2D flow around a submerged object [BIR 60]*

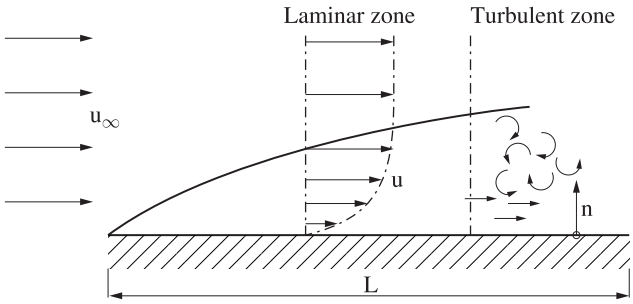

Figure 6.4.3. *Boundary-layer development near a flat plate [RAP 98]*

Figure 6.4.2 shows the 2D flow pattern of a fluid under forced convection conditions around a submerged object. The fluid immediately adjacent to the object surface is brought to rest. The velocity of the fluid is equal to zero at the surface and increases in a layer, called the boundary layer, whose thickness grows. The flow pattern near the leading edge of a flat plate immersed in a fluid stream is shown in Figure 6.4.3. The laminar-turbulent transition usually occurs at a distance x down the plate so that (u_∞ x / ν) is of the order 10^5. For this configuration, the Nevier-Stokes equation that describes the flow field has been solved and the solution yields the variation of the boundary layer thickness with distance along the plate (see equation [6.4.9]) [BIR 60].

The thickness of the viscous boundary layer increases with distance x along the plate, as shown in Figure 6.4.3, according to a parabolic law:

$$\delta_\nu = 5.2 \sqrt{\frac{\nu . x}{u_\infty}} \qquad [6.4.9]$$

where ν is the kinematic viscosity of the fluid (μ / ρ).

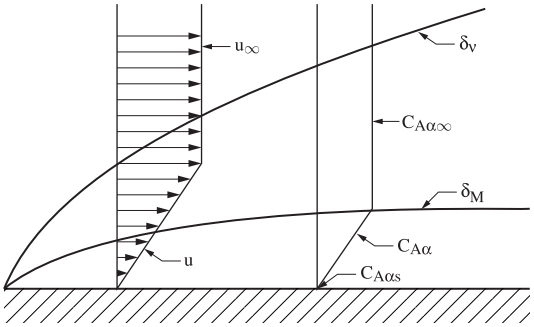

Figure 6.4.4. *Velocity and concentration profiles in the laminar boundary layer for a chemical vapor deposition process (with an interfacial chemical reaction)*

For the heat transfer between a hot flat plate and a cooler viscous fluid with constants ρ, ν and α in forced convection laminar flow past the flat plate (problem analogous to the one presented in section 6.4.1.1), the boundary-layer solution yields the expression of the local heat flux normal to the surface along the plate [BIR 60]:

$$\Phi_{T\alpha s}(x) = -\rho\, C_p\, \alpha_{T\alpha} \left(\frac{\delta T}{\delta y}\right)_s = 0.332\, Pr^{-2/3} \left(\frac{\nu u_\infty}{x}\right)^{1/2} . \{ T_{\alpha s} - T_{\alpha\infty} \} \qquad [6.4.10]$$

which defines a local heat conductance (heat-transfer coefficient) that varies along the contact surface.

Figure 6.4.4 shows the velocity and concentration profiles in the boundary layer for a chemical vapor deposition (CVD) process where a gaseous reactant A in a gas phase in forced convection flows along a hot substrate, undergoing thermal decomposition at the surface of the substrate (see Chapter 5, reactions [5.6.4] to [5.6.6]) giving a deposit whose thickness grows along the substrate:

$$A(g) \rightarrow \nu_S S(s)\downarrow + \nu_R R(g)$$

Reactant A being consumed at the surface, a concentration gradient forms: the concentration of reactant A varies from $C_{A\alpha\infty}$ in the gas stream to $C_{A\alpha s} = 0$ at the surface where the reaction occurs. When the interfacial chemical reaction is fast, the process is controlled by the diffusion of the reactant in the boundary layer. The flux of reactant A normal to the surface of the substrate is given by the same expression as the heat flux (see equation [6.4.9]) [BIR 60]:

$$\Phi_{A\alpha s}(x) = - D_{A\alpha} \left(\frac{\delta C_{A\alpha}}{\delta y} \right)_s = 0.332\ Sc^{-2/3} \left(\frac{\nu u_\infty}{x} \right)^{1/2} . \{C_{A\alpha\infty} - C_{A\alpha s}\} \quad [6.4.11]$$

This expression, being a transposition of the expression for a heat flux, is only correct when the concentration of the diffusing species in the gas stream is very small.

The temperature and concentration gradients are usually smaller than that of the velocity boundary layer and it is assumed that they vary similarly. The thickness ratio between the thermal or mass diffusion boundary layer and the velocity boundary layer being a function of two dimensionless numbers:

$$\delta_M / \delta_\nu = Sc^{-1/3} \text{ where } Sc = \nu_\alpha / D_{A\alpha} \quad [6.4.12a]$$

and:

$$\delta_T / \delta_\nu = Pr^{-1/3} \text{ where } Pr = \nu_\alpha / \alpha_{T\alpha} \quad [6.4.12b]$$

For a contact surface of length L, an average heat or mass flux per unit surface can be calculated:

$$\Phi_{A\alpha} . (L) = h_{A\alpha}(L) (C_{A\alpha\infty} - C_{A\alpha s}) \quad [6.4.13]$$

where $h_{A\alpha}(L) . L = \int h(x) . dx$. The average mass-transport conductance or heat-transfer coefficient for this contact surface of length L [BIR 60] is:

$$h_{A\alpha}(L) = 0.664\ (Sc)^{-1/6} \left(\frac{D_{A\alpha} u_\infty}{L} \right)^{1/2} \quad [6.4.14a]$$

$$h_{T\alpha}(L) = 0.664\ (Pr)^{-1/6} \left(\frac{\alpha_{T\alpha} u_\infty}{L} \right)^{1/2} \quad [6.4.14b]$$

6.4.3. *Heat and mass transfer between particles, drops or bubbles and a continuous fluid phase*

In extraction operations, the main contacting pattern between the phases is a dispersion of one phase into another – the fluid (either gas or liquid) flowing around particles, droplets or gas bubbles by forced convection. Under mass transport control, transport resistance can be localized in the dispersed or continuous phase, depending on how the dispersed phase behaves; it can either behave as a (solid) particle or a particle undergoing internal circulation.

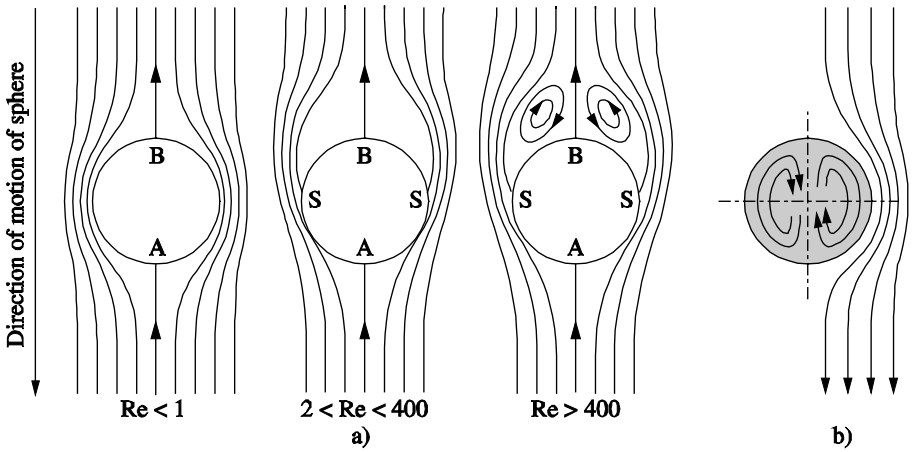

Figure 6.4.5. *a) Streamlines about rigid spheres in a lighter continuous phase as a function of Reynolds number (with a vortex ring behind the sphere for Re>400). A and B: forward and rear stagnation points; S: separation of flow [GAR 59]; and b) flow pattern inside and outside a falling drop or gas bubble in the absence of adsorption*

When the viscosity of the dispersed phase is higher than the viscosity of the continuous phase ($\mu_D > \mu_C$), the droplet behaves as a rigid particle, see Figure 6.4.5a. Conversely, when the viscosity of the dispersed phase is lower than the viscosity of the continuous phase (μ_C / μ_D) > 1, both droplets and bubbles present an internal circulation movement, the continuous phase being liquid (see Figure 6.4.5b).

6.4.3.1. *Heat and mass transfer between a solid particle or rigid drop ($\mu_D > \mu_C$) and a fluid phase*

6.4.3.1.1. Rate controlling process = heat or mass transport in the continuous phase

The streamlines of the fluid flow under forced convection around a solid sphere are shown in Figure 6.4.5a for various Reynolds numbers. At the front of the particle, which is supposed to be spherical, a boundary layer is formed and the

conductance is correctly given by the boundary layer model. The following correlations have been experimentally established for mass and heat transport phenomenon [BIR 60]:

$$2\,h_{Tf}\,.\,R_p\,/\,\alpha_T = 2.0 + 0.60\left(\frac{2R_p u_\infty \rho_f}{\mu_f}\right)^{1/2}.\,(Pr)_f^{1/3} \qquad [6.4.15a]$$

or expressed in dimensionless numbers (Nusselt number for heat transfer and Sherwood number for mass transport):

$$Nu_c = 2\,h_{T\alpha}\,R_p/\,\alpha_{T\alpha} = 2.0 + 0.60\,(Re)^{1/2}\,.\,(Pr_f)^{1/3} \qquad [6.4.15b]$$

or:

$$Sh_c = 2\,h_{A\alpha}\,R_p/\,D_{A\alpha} = 2.0 + 0.60\,(Re)^{1/2}\,.\,(Sc_f)^{1/3} \qquad [6.4.15c]$$

where R_p is the particle radius and $Re = 2R_p u_\infty \rho_f/\mu_f$ is the Reynolds number of the flow related to the particle (see Figure 6.4.6).

A more complex expression has been proposed [LEE 68]: the average Sherwood number over the front half of the sphere, where the boundary layer will be formed, is correlated by the equation:

$$Nu(Sh)\ (\text{front zone}) = 1.02\,Re^{1/2}\,.\,Sc^{1/3} \qquad [6.4.16]$$

and for the turbulent zone (wake region) over the rear of the particle:

$$Nu\ (\text{rear zone}) = 0.0447\,Re^{0.78}\,Sc^{1/3} \qquad [6.4.17]$$

and the detachment of the boundary limit occurs when $\theta = 90°$. The correlation for the entire sphere can then be written as:

$$Nu\,.\,Sc^{-1/3} = 0.51\,Re^{1/2} + 0.02235\,Re^{0.78} \qquad [6.4.18]$$

This equation is shown in Figure 6.4.7 together with various other recommended correlations and experimental data for heat and mass transfer. It correctly represents various experimental results over the Reynolds number range $200 < Re < 20{,}000$.

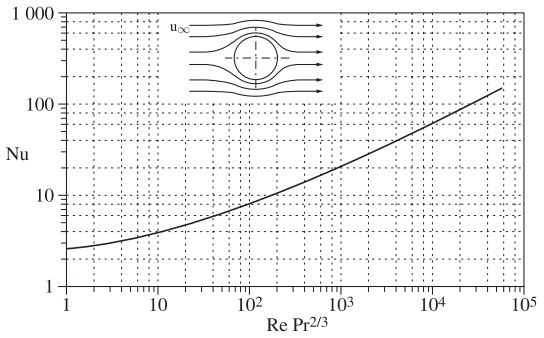

Figure 6.4.6. *Forced convection heat transfer from a single sphere (see equation [6.4.15a]) [MAR 52]*

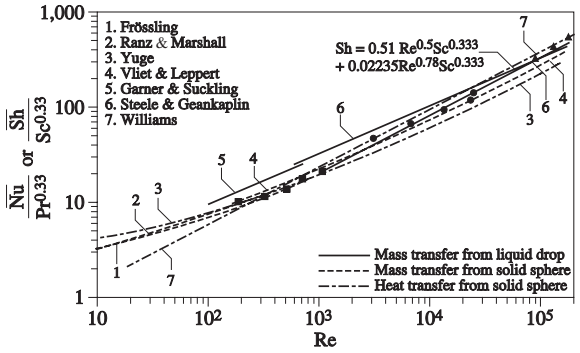

Figure 6.4.7. *Overhall heat- and mass-transfer coefficient from a single sphere (see equation [6.4.18]) [LEE 68]*

6.4.3.1.2. Rate controlling process: heat or mass transport in a rigid drop

For a rigid drop and when heat or mass transport in the drop is rate determining, the concentration or temperature profile within the droplet is obtained by the solution of Fick's or Fourier's second law (see equation [6.2.11] and [6.2.16]). The fraction X of solute A extracted from the drop or adsorbed by the drop for a contact time t is given by:

$$X = \left\{1 - \exp\left(\frac{-2\pi^2 D_{Ad} t}{R_d^2}\right)\right\}^{1/2} \qquad [6.4.19a]$$

where D_{ad} is the diffusion coefficient of component A, in the rigid drop, and:

$$X = (C_{Ad} - C_{Ad0}) / (C_{Ads} - C_{Ad0}) \qquad [6.4.19b]$$

where, for absorption $C_{Ad0} = 0$ and extraction $C_{Ads} = 0$. For short times equation [6.4.19] reduces to:

$$X = 3.385 \left(\frac{D_{Ad} t}{R_d^2} \right)^{1/2} \qquad [6.4.19c]$$

and the average mass transfer coefficient over the surface of the drop and for a contact time τ (see equations [6.4.4] and [6.4.8]) is given by:

$$h_{Ad} = 1.7 (D_{Ad} / \tau)^{1/2} \qquad [6.4.20]$$

6.4.3.2. *Mass transfer between a drop or bubble undergoing internal circulation and a continuous phase: Higbie's model*

The circulation pattern within drop A moving (due to gravity) within a second liquid phase is shown in Figure 6.4.5b. The internal circulation is induced by friction with the continuous phase and a boundary layer is formed on either side of the interface in the continuous phase and within the droplet. While the droplets move around, due to its internal circulation there is a continuous renewal of the phases adjacent to the interface. A new surface is always produced at the top of the droplet and removed at its lower end. If a point M of the interface of the phases describes a semi-circumference, two points M_1 and M_2 respectively in each phase and right next to this semi-circumference will remain in contact during the time needed for point M to pass from the front to the rear of the drop (or bubble). This is the contact time between the phases. The whirling movement within the droplet is such that the drop can be considered perfectly mixed. Resistance to mass or heat transfer is then localized in the continuous phase and, the contact time being quite short, the mass or heat transport conductance at the interface during this contact time τ can be approximated by equation [6.4.7]:

$$h_{Ac} = (D_{Ac} / \pi\tau_{(contact)})^{1/2} \qquad [6.4.21]$$

The velocity of the surface of the droplet being of the same order of magnitude as the velocity of the droplet, the average conductance can be expressed as a function of droplet velocity by [HIG 35]:

$$h_{Ac} = \left(\frac{D_{Ac} u_\infty}{2\pi R_d} \right)^{1/2} \qquad [6.4.22a]$$

or, in dimensionless terms:

$$Nu_c = 2\, h_{Ac}\, R_d / D_{Ac} = 1.13\, Re^{1/2} \,.\, Sc^{1/2} \qquad [6.4.22b]$$

This expression gives a correct order of magnitude of the mass transfer coefficient in the continuous (liquid) phase for the absorption of a gas by water, for gas bubbles 0.3–0.5 cm in diameter. Small amounts of surfactants lead to a significant decrease in transport flux and therefore in transfer kinetics due to the formation of a film that prevents circulation occurring within the droplet; the droplet then behaves as a solid particle in contact with a fluid.

6.5. Overall kinetics of extraction processes under mixed control

When the heterogeneous chemical (interfacial) reaction and mass transport processes occur in series and present resistances of the same order of magnitude, the contributions of these processes must be taken into account.

Analytical solutions have been established for a few contacting patterns between the phases. Here, as an example, we present two solutions for stagnant and semi-infinite phases in contact along a plane surface in order to show that the overall rate of the processes do not follow the "rule" of addition of resistances in series, which is generally assumed.

6.5.1. *Extraction process-type gasification*

Let us consider a process such as gasification (see reaction [6.1.2]) between reactant A present in low concentration in a stagnant and semi-infinite gas phase and a semi-infinite solid. The concentration profiles of reactant A and product R vary in time, as shown in Figure 6.1.2. In the gas phase, the transport of reactant A is governed by Fick's second law (see equation [6.2.16]). The resolution of this differential equation, with the following condition at the interface:

$$\Phi_{A\alpha s} = r_s \qquad [6.5.1]$$

where the rate of reaction is supposed to be of the first order with respect to the concentration of reactant A in phase α right at the interface:

$$r_s = k_r \,.\, C_{A\alpha s}$$

and the diffusion flux at the interface given by:

$$\Phi_{A\alpha s} = - D_{A\alpha} \frac{\delta C_{A\alpha}}{\delta x} \qquad [6.5.2]$$

leads to the following expression of the variation of the reactant concentration in the phase (α) right next to the interface [CRA 56]:

$$C_{A\alpha s} / C_{A\alpha\infty} = \exp\left(\frac{k_r^2.t}{D_{A\alpha}}\right)^{1/2} \operatorname{erfc}\left(\frac{k_r^2.t}{D_{A\alpha}}\right)^{1/2} = \Psi\ \{k_r\left(\frac{t}{D_{A\alpha}}\right)^{1/2}\} \qquad [6.5.3]$$

Tables directly give the value of function $\psi(z) = \exp z^2 . \operatorname{erfc} z$ as a function of z. The overall rate can be written as:

$$r = k_r . C_{A\alpha\infty} . \Psi\ \{k_r\left(\frac{t}{D_{A\alpha}}\right)^{1/2}\} \qquad [6.5.4]$$

For "short" times, equation [6.5.3] can be written:

$$C_{A\alpha s} / C_{A\alpha\infty} = 1 - \left(\frac{k_r^2.t}{D_{A\alpha}}\right)^{1/2} \qquad [6.5.5]$$

and the rate can be written:

$$r = k_r . C_{A\alpha\infty}\ \{1 - k_r\left(\frac{t}{D_{A\alpha}}\right)^{1/2}\} \qquad [6.5.6]$$

For longer times, the rate is given by:

$$r = C_{A\alpha\infty}\left(\frac{D_{A\alpha}}{\pi t}\right)^{1/2}\ (1 - \frac{D_{A\alpha}}{2k_r^2 t}) \qquad [6.5.7]$$

For $\tau_1 < 25 . 10^{-4} (D_{A\alpha} / k_r^2)$, the overall rate is almost equal to the rate of the heterogeneous reaction and the process is controlled by it.

For $\tau_2 > 10\ (D_{A\alpha} / k_r^2)$, the overall rate becomes:

$$r = C_{A\alpha\infty}\left(\frac{D_{A\alpha}}{\pi t}\right)^{1/2} = \Phi_{A\alpha s} \qquad [6.5.8]$$

which is the expression of the reactant flux right to the interface for a process controlled by the transport process in phase α (see equation [6.4.7]), with the boundary conditions for x = 0, $C_{A\alpha s} = 0$ and for x = ∞, $C_{A\alpha} = C_{A\alpha\infty}$.

6.5.2. *Transfer process-type solvent extraction*

Let us consider a system made of two phases in contact (two liquid phases or a liquid phase in contact with a gas phase) along a plane surface and a transfer process (extraction, absorption) of solute A from phase α to phase β (see equation [6.1.3]). Both phases are considered semi-infinite. At a given time, the concentration profiles of solute A in phase α and product R in phase β are shown in Figure 6.1.3a.

Diffusion in each phase and interfacial chemical reaction occur in series, leading to the following boundary conditions:

$$\Phi_{A\alpha s} / -\nu_A = r_s = \Phi_{R\beta s} / \nu_R \qquad [6.5.9]$$

In what follows, we assume that $\nu_A = \nu_R$ and that the expression of the reaction rate is given by:

$$r = k_r (C_{A\alpha s} — C_{R\beta s}/K_c)$$

which comes down to assuming a chemical reaction that is near equilibrium, see Chapter 5, equation [5.2.22].

In each phase, the transport of the solute is governed by Fick's second law (see equation [6.2.16]), and the resolution of the differential equations system with the boundary conditions [6.5.9] leads to the following equation for the overall rate r:

$$r = k_t \left(C_{A\alpha\infty} - \frac{C_{A\beta\infty}}{K_c} \right) . \psi \{ k_r (\frac{1}{h_{A\alpha}} + \frac{1}{K_c h_{R\beta}}) \ t^{1/2} \} \qquad [6.5.10]$$

where the mass transfer coefficients $h_{A\alpha}$ and $h_{R\beta}$ are given by equation [6.4.8] and the function Ψ is defined by equation [6.5.3].

For short contact times, expression [6.5.10] is reduced to:

$$r = k_t \left(C_{A\alpha\infty} - \frac{C_{A\beta\infty}}{K_c} \right) \{ 1 - k_r (\frac{1}{h_{A\alpha}} + \frac{1}{K_c h_{R\beta}}) \ t^{1/2} \} \qquad [6.5.11]$$

For long contact times, expression [6.5.10] can be approximated by:

$$r_s = \frac{\left(C_{A\alpha\infty} - \frac{C_{A\beta\infty}}{K_c} \right)}{\frac{1}{h_{A\alpha}} + \frac{1}{K_c h_{R\beta}}} \qquad [6.5.12]$$

which is equation [6.3.22] where only the transport processes are acting, so the overall resistance obeys the rule of addition of resistances acting in series.

6.5.3. *Note on the rule of addition of resistances acting in series*

In an extraction process, interfacial chemical reaction and transfer processes act in series. In the case of a transfer between two phases, where the process is controlled by transport processes in each phase and even in an unsteady state, the overall transfer rate is the product of a driving force by a transfer coefficient that obeys the rule of addition of the resistances acting in series (see section 6.3.2.2 and equation [6.3.22]).

As we could observe in the two examples given above, when the overall rate depends on the transport processes in the phases and the interfacial chemical reaction under an unsteady state, the rule of addition of the resistances acting in series is not satisfied (see equations [6.5.4] and [6.5.10]).

The rule of addition of the resistances acting in series is often presented as a consequence of processes acting in series. This rule is only correct in two cases:

– when the phenomena in series are of the same nature: vectorial (a flux is a vectorial variable, i.e. a gradient of the chemical potential) or scalar (reaction rate);

– when the process is in a steady state, i.e. when the rate does not depend on the contact time.

These processes acting in series, they will only proceed at the same rate at steady state. It is therefore generally assumed [LEV 72, SZE 76] that for extraction processes, such as gasification of particles, the process is in a *pseudo-steady state* with the following rate expressions of the two individual steps:

$$r = k_r(C_{A\alpha s}{}^{a} - C_{R\alpha s}{}^{r} / K_C) = h_r (C_{A\alpha\infty} - C_{A\alpha s})$$

In a pseudosteady state, the rates of each step being constant during the progress of the process, the mass transfer coefficient is assumed to be constant. Even with these assumptions, it is not possible to obtain a simple expression for the overall

rate, when the reaction rate is not of the first order with respect to the concentration of the reactant A.

So, only for a steady state and for the simple case of a first order interfacial reaction, can we obtain an overall rate as a function of the concentration of the reactant $C_{A\alpha\infty}$, the rate constant k, the mass transfer coefficient and an overall resistance satisfying the rule of addition of resistances

The most commonly quoted theory to explain and justify the use of the stationary state approximation and then to justify use of the rule of addition of resistances acting in series is the one related to the "two films" model that was developed by Lewis and Whitman [BIR 60]. This theory assumes that when two fluids are in contact in laminar flowing conditions, the two laminar boundary films have a constant and thin width so there is a linear concentration of the reactants and a steady diffusion regime is occurring.

This assumption or approximation of a pseudo-steady state cannot, however, be considered valid. As will be seen in Chapter 7, the conversion of a solid particle or the transfer of a component from a continuous phase to a dispersed phase and *vice versa* are unsteady processes. In this case, when the rates of the elementary processes have to be taken into account, the overall resistance of the process cannot be expressed by the rule of addition of the resistances acting in series.

6.6. Bibliography

[BIR 60] R.B. BIRD, W.E. STEWART, E.N. LIGHTFOOT, *Transport Phenomena*, John Wiley & Sons, New York, 1960.

[CAR 59] H.S. CARSLAW, J.C. JAEGER, *Heat Conduction in Solids*, Oxford University Press, Oxford, 1959.

[CRA 56] J. CRANK, *The Mathematics of Diffusion*, Oxford University Press, Oxford, 1956.

[DIS 68] P.A.O. DISTIN *et al*, *JISI*, pp. 821-833, August 1968.

[FER 02] J.H. FERZIGER, M. PERIC, *Computational Methods for Fluid Dynamics*, 3rd edition, Springer-Verlag, Berlin, 2002.

[FUJ 67] T. FUJI, T. ARAKI, *Revue de Métallurgie*, CIT, Vol. 1, pp. 3-30, 1967.

[GAR 59] F.H. GARNER, *Trans. Instn. Chem. Eng*., Vol. 28, p. 88, 1959.

[HIG 35] R. HIGBIE, *A. I. Ch. E. Journal*, Vol. 31, pp. 365-389, 1935.

[KIK 82] A. KIKUCHI *et al.*, *Proc. Symp. of the International Union of Theoretical and Applied Mechanics*, Metal Society, London, p. 79, 1982.

[LEA 07] L.G. LEAL, *Advanced Transport Phenomena*, Cambridge University Press, 2007.

[LEE 68] K. LEE, H. BARROW, *International Journal Heat Mass Transfer*, Vol.11, pp. 1013-1026, 1968.

[MAR 52] W.R. MARSHALL Jr., *Chem. Eng. Progr.*, Vol. 48, pp. 141-146 and pp. 173-180, 1952.

[PAT 80] S.V. PATANKAR, *Numerical Heat Transfer and Fluid Flow*, Hemisphere Publishing, Washington DC, 1980.

[RAP 98] M. RAPPAZ, M. BELLET, M. DEVILLE, "Modélisation numérique en science et génie des matériaux", *Traité des Matériaux*, Volume 10, Presses Polytechniques et Universitaires Romandes, Lausanne, 1998.

[SZE 76] J. SZEKELY, J.W. EVANS, H.Y. SOHN, *Gas-Solid Reactions*, Academic Press, New York, 1976.

[VIG 11b] A. VIGNES, *Extractive Metallurgy 2: Metallurgical Reaction Processes*, ISTE Ltd, London and John Wiley and Sons, New York, 2011.

[VIG 11c] A. VIGNES, *Extractive Metallurgy 3: Processing Operations and Routes*, ISTE Ltd, London, John Wiley and Sons, New York, 2011.

[ZIE 00] O.C. ZIENKIEWICZ, R.L. TAYLOR, *Finite Element Method, Basic Formulation and Linear Problems*, 5th edition, Butterworth-Heineman, Oxford, 2000.

Chapter 7

Particulate Kinetics

7.1. Introduction

A large number of extraction processes involve particulates: solid particles, drops or bubbles, dispersed in a continuous phase. In this chapter are presented:

– the kinetic laws of conversion (growth or shrinkage) of solid particles in the following processes:

- gasification or leaching of a particle,

- *in situ* conversion of a particle into a new solid phase,

- heterogeneous precipitation: growth of solid particles on seeds or deposit on a substrate (chemical vapor deposition (CVD) process);

– the kinetic laws of mass and heat transfer between a droplet or a bubble and a continuous fluid phase.

These "laws" are presented in two reference books: [LEV 89, SZE 76].

The overall kinetic laws of conversion of multiparticle systems are established in [VIG 11b], Chapter 6 and [VIG 11c], Chapter 3. They are directly deduced from "single particle conversion kinetics".

These "kinetic "laws" identify the factors the particle conversion rate depends on: size and shape, structure (dense or porous) of the solid particles, exo- or endothermic reactions. They are established for the different regimes controlling the kinetics: chemical regime, mass transport regime or mixed regime.

Extractive Metallurgy 1: Basic Thermodynamics and Kinetics Alain Vignes
© 2011 ISTE Ltd. Published 2011 by ISTE Ltd.

The identification of the step controlling the kinetics of conversion of a particle or transfer of a component between two phases is, however, extremely difficult.

The establishment of these kinetics starts from "macroscopic" balances and not from local balances (equations of change) by using the expressions of the chemical reaction rates or diffusion fluxes established in Chapter 6.

7.2. Gasification/leaching of a particle

These processes involve the shrinking of solid particles (see Figure 7.2.1):

– by a liquid phase (in hydrometallurgy: leaching or dissolution), e.g.:

$$Al_2O_3 \text{ (particles)} + 2 \text{ (NaOH)} \rightarrow 2\ AlO_2Na \text{ (aq)} + H_2O$$

– by a gas phase (in pyrometallurgy: gasification for instance, the Boudouard reaction [5.4.21] or the reduction of zinc oxide (see Chapter 5, reaction [5.4.16]).

The chemical reaction occurs at the surface of the particles, between reactant A, present in the fluid phase (α), and component B of a particle (β). The conversion can be controlled by the reaction (see Chapter 5, section 5.4.2) or the transport of the gaseous reactant A in the fluid phase surrounding the particle (see Chapter 6, section 6.3.1):

$$\nu_A A(\alpha) + \nu_B B(\beta) \rightarrow \nu_R R(\alpha) \qquad [7.2.1]$$

with: $b = \nu_B / \nu_A$.

7.2.1. *Non-porous particles*

Let us consider a spherical particle (for the presentation to be simple) located within an infinite fluid phase (we can thus assume that the concentration of the reactant $\mathbf{C}_{A\alpha\infty}$ in the fluid phase outside the boundary layer remains constant during the entire conversion of the particle). Let $n_B(t)$ be the number of moles of constituent B with a molar volume of v_{MB}, in a particle of radius $R_p(t)$ at a given time, which decreases along with the conversion of the particle (see Figure 7.2.1):

$$n_B(t) = (4\pi / 3v_{MB}) \,.\, R_p^3 \qquad [7.2.2]$$

The variation of the number of moles of B, dn_B / dt, is proportional to the surface of the residual particle and to the overall r rate, i.e. reaction rate r_s (see Chapter 5, equation [5.2.10]) or flux of the reactant at the interface, $\Phi_{A\alpha s}$ (see Chapter 6, equation [6.3.3]):

$$-dn_B / dt = -S \,.\, b \,.\, r_s = -4\pi R_p^{\,2} \,.\, b \,.\, (r_s \text{ or } \Phi_{A\alpha s}) \qquad [7.2.3]$$

With equation [7.2.2], this leads to the expression of the linear rate at which radius of particle g_p decreases:

$$g_p = dR_p / dt = -v_{MB} \,.\, b \,.\, r_s \text{ (or } \Phi_{A\alpha s}) \qquad [7.2.4]$$

The extent of conversion of particle B, i.e. the fractional volumetric conversion X_B, i.e. the ratio of volume of the unreacted core to the initial volume of the particle, varies according to:

$$1 - X_B(t) = (R_p(t) / R_{po})^3 \qquad [7.2.5]$$

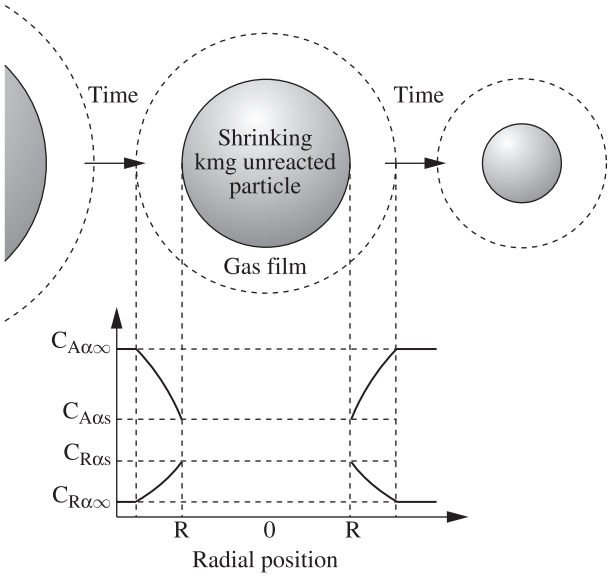

Figure 7.2.1. *Gasification or dissolution (leaching) of a dense particle. Concentration profiles of reactant A and product R in the fluid phase for reaction [7.2.1] between a shrinking solid particle and a fluid [LEV 72]*

7.2.1.1. *Rate-controlling step: heterogeneous chemical reaction*

When the process is controlled by the interfacial chemical reaction, the concentration of reactant A close to the surface is equal to the concentration within the core of the fluid phase. As the latter is considered to be constant, the second term of equation [7.2.4] is a constant, which leads to expression of the variation in the particle radius during the reaction:

$$R_{po} - R_p(t) = b \,.\, v_{MB} \,.\, r_s \,.\, t = -g_p t \qquad [7.2.6]$$

the fractional conversion X_B of particle B varies with time, according to:

$$1 - (1 - X_B)^{1/3} = R_B t \qquad [7.2.7]$$

The time for complete conversion τ of the particle can be obtained for $R_p(t) = 0$, leading to:

$$\tau = \frac{R_{p0}}{b v_{MB} r_s} = \frac{R_{p0}}{g_p} \qquad [7.2.8]$$

NOTE.– The slope at the origin of X(t) curves directly gives τ ($dX / dt = 3 / \tau$).

7.2.1.2. *Rate-controlling process: diffusion through the fluid boundary layer*

The flux of the gaseous reactant $\Phi_{A(\alpha)s}$ at the interface is given by equation [6.3.2] or [6.3.4], and the mass transfer coefficient $h_{A\alpha}$ depends on the conditions of fluid phase flow around the particle. When the fluid flow produces a boundary layer around the particle, the mass transfer coefficient depends on the size of the particles and is given by equation [6.4.15a].

In the case of small-sized particles, Nu = 2, the reciprocal shrinkage is given by:

$$dR_p / dt \approx (\text{const})\ 1 / R_p \qquad [7.2.9]$$

The time for complete conversion is given by:

$$\tau \approx (\text{const})\ R_{po}^{\,2} \qquad [7.2.10a]$$

where (see equations [6.3.2], [6.3.3] and [6.3.4]):

$$(\text{const}) = - v_{MB} b \,.\, h_{A\alpha} [C_{A\alpha\infty} - C_{R\alpha\infty} / K_C] \qquad [7.2.10b]$$

The fractional conversion X_B varies with time, according to:

$$1 - (1 - X_B)^{2/3} = t / \tau \qquad [7.2.11]$$

In the case of larger particles, $Sh = 0.6\ Re^{1/2}\ .\ Sc^{1/3}$ (see equation [6.4.15]), the conductance $h_{A\alpha}$ varies according to:

$$h_{A\alpha} \approx (\text{const})\ R_p(t)^{-1/2} \qquad [7.2.12]$$

The time for a complete conversion is given by:

$$\tau = (\text{const})\ (R_{po})^{3/2} \qquad [7.2.13]$$

and the fractional conversion varies with time, according to:

$$t / \tau = 1 - (1 - X_B)^{1/2} \qquad [7.2.14]$$

NOTE.– Identification of the rate-controlling step. The rate-controlling step can be determined by the variations of the fractional conversion, with the normalized time (see equations [7.2.7], [7.2.11] and [7.2.14]). In addition, the variations in fractional conversion with initial particle size allows identification of the limiting process.

7.2.1.3. *Examples*

The leaching of dense zinc ferrite particles with hydrochloric acid HCl has been studied on dense particles, significantly recrystallized with a thermal treatment at 1,300°C [NUN 84]:

$$ZnFe_2O_4(s) + 8\ HCl \rightarrow ZnCl_2 + FeCl_3 + 4H_2O \qquad [7.2.15]$$

for HCl molalities ranging from 2–7 and particle sizes ranging from r = 0.088 to 0.189 cm, at 90–100°C. The conversion of a particle occurs under chemical reaction control (see equations [7.2.7] and [7.2.8]). The reaction rate linearly varies as a function of activity $\hat{a}_{(HCl)}$ (see Chapters 4 and 5, equations [4.2.10] and [5.4.28]). At 90°C:

$$r = 1.26 \times 10^{-6}\ \hat{a}_{HCl}\ \text{mole/cm}^2\text{.min} \qquad [7.2.16]$$

$$1 - (1 - X)^{1/3} = k_a t = (k v_{MB} / R_{po})\ .\ \hat{a}_{(HCl)}\ .\ \exp(-\ 83\ (\text{kJ/mol}) / RT)\ .\ t$$

where v_{MB} is the molar volume (47.9 cm^3/mol), $k_a = 1 / \tau = 4 \times 10^{-3}\ min^{-1}$ when R_{po} = 0.189 cm.

The *dissolution of dense ilmenite $FeTiO_3$ particles* is industrially performed with sulfuric and hydrochloric attacks. At temperatures close to 100°C, for concentrated sulfuric solutions (from 5–20 M), the conversion of a particle occurs under chemical reaction control (see equation [7.2.7] and [VIG 11b], Chapter 1, Figures 1.2.5a and b).

The *leaching of dense sphalerite (Zn-Fe)S particles with ferric sulfate* (0.3 M $(SO_4)_{1,5}$ Fe, 0.3 M H_2SO_4) solution, between 40 and 100°C, for particles with sizes ranging from 5–60 μm, occurs under chemical reaction control. The fractional conversion is given by equation [7.2.7], see Figures 7.2.2a and c. The variation of the time for complete conversion as a function of particle size is linear, see equation [7.2.8] and Figure 7.2.2b, with an activation energy of 44 kJ/mol, see Figure 7.2.2d.

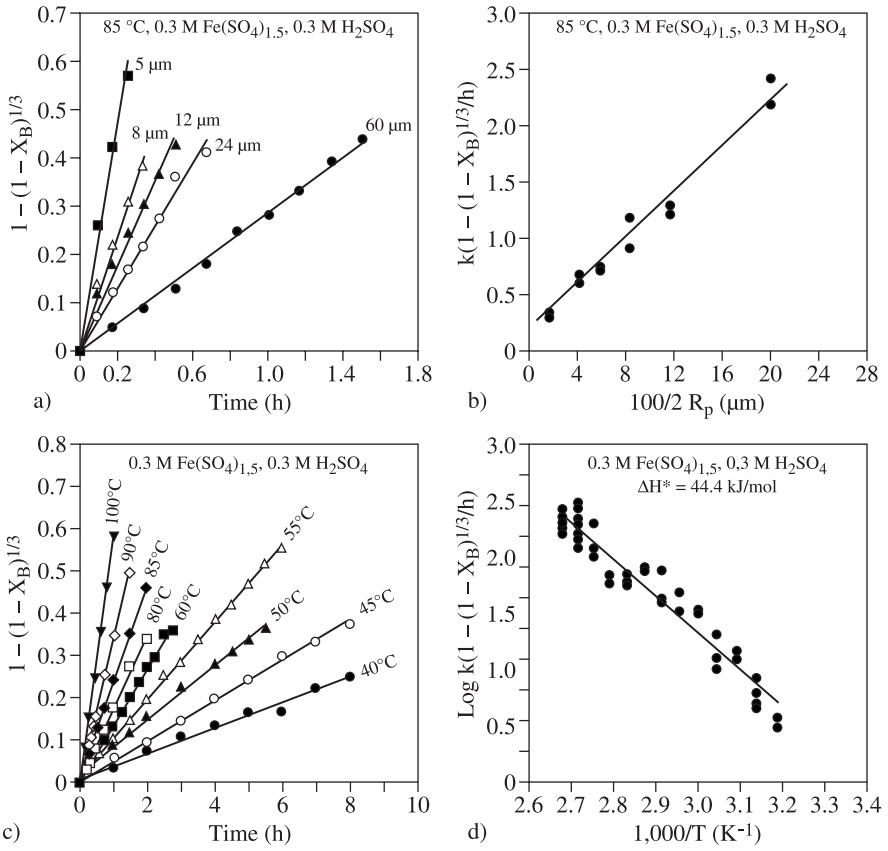

Figure 7.2.2. *Leaching (dissolution) of a non-porous particle of sphalerite (Zn-Fe)S with ferric sulfate under chemical control conditions (see equation [7.2.7]); variation of the fractional conversion X: a) as a function of time for different particle sizes at 85°C; b) variation of the leaching rate constant with the average diameter of the particles ($k = 1/\tau$); c) for particles -75 +45μm size as a function of time for different temperatures; and d) Arrhenius plot for the dissolution of zinc from the sphalerite [DUT 06]*

Table 7.2.2 summarizes the conversion-time expressions for various shapes of particles and controlling steps [LEV 72].

7.2.2. *Porous particles (pellets)*[1]

7.2.2.1. *Rate-controlling step: heterogeneous chemical reaction*

For some particles presenting a strong porosity, where diffusion of the gaseous reactant in the pores is not a limiting step, the concentration of fluid reactant A is uniform throughout the porous particle and equal to that in the bulk gas stream. The entire surface of the pores is therefore available for the reaction to occur and continue by enlarging the pores. Thus, the solid reactant is continuously and progressively converted throughout the particle. The variation of the particle mass can be expressed by:

$$dm_B / dt = m_B(t) \,.\, s_m \,.\, b \,.\, r_s \qquad [7.2.17]$$

where s_m is the surface per mass unit of the particle.

If the gasification occurs by enlarging the pores, s_m increases during the process. A model of a porous solid with cylindrical pores and random intersections leading to an expression of the variation of fractional conversion with time can be found in [SZE 76]. By assuming that the surface per unit mass does not vary during the gasification process, the variation of the fractional conversion can be obtained by simple integration of equation [7.2.17]:

$$\ln(1 - X_B) = s_m \,.\, b \,.\, r_s \,.\, t \qquad [7.2.18]$$

An estimation of the complete gasification time of a porous particle can also be obtained by another model: that of a porous particle made of dense grains of size R_{go} (the "grain model"), see Figure 7.4.4. Where each grain undergoes gasification according to the kinetics given by equations [7.2.7] and [7.2.8], and the complete gasification time is a function of the grain size (and not of pellet size):

$$\tau = \frac{R_{g0}}{b v_{MB} r_s} \qquad [7.2.19]$$

7.2.2.2. *Rate determined by both chemical reaction and diffusion*

At a higher temperature, where both processes are involved, the gaseous reactant cannot get deeply into the particle and most of the process occurs in a zone near the external surface of the pellet. This surface is relatively thin, which leads to continuous shrinking of the porous particle. The conversion kinetics are modeled by considering that, in this external layer, a homogeneous reaction occurs, whose rate per volume unit can be expressed by the product $s_v \,.\, r_s$ where s_v is the specific

1 The case of porous particles is extensively studied in *Gas-solid Reactions* written by Szekely [SZE 76].

surface per unit volume of the grains the particle is made of ($s_v = \rho_B.s_m$ where ρ is the density of the particle). A mass balance (see Chapter 6, equation [6.2.2]) within the pellet, for an irreversible reaction, gives the following equation:

$$D_A d^2C_A / dr^2 - k_r . \rho_B . s_m . C_A^n = 0 \qquad [7.2.20]$$

where C_A is the concentration of the fluid reactant and D_A is the effective diffusion coefficient of gaseous reactant A in the porous particle. The solution of this equation gives the expression of the overall rate (see expression [7.2.3]):

$$r_S = \left(\frac{2}{(n+1)}\right) \{k_r . \rho_B . s_m . D_A\}^{1/2} . C_A^{(n+1)/2} \qquad [7.2.21]$$

which leads to the expression of the fractional conversion, similar to expression [7.2.7] and to the time of complete conversion given by equation [7.2.8].

NOTE.– These expressions are valid only up to high fractional conversion if the concentration of the reactant in the bulk gas stream remains constant during the entire conversion. Most dissolution experiments are carried out in closed reactors, however, where the reactant is consumed during the conversion. The time of complete conversion of particles is therefore longer than that of a system where the concentration of the reactant is constant.

7.2.2.3. *Examples*

7.2.2.3.1. Leaching of zinc ferrite porous particles

For leaching at low temperature, $65 < T < 95°C$, with an acidic medium (pH 1.7) of porous zinc ferrite $ZnOFe_2O_3$, particles according to the chemical reaction:

$$ZnOFe_2O_3(s) + 4\ H_2SO_4 \rightarrow ZnSO_4 + Fe_2(SO_4)_3 + 4\ H_2O \qquad [7.2.22]$$

and for the operating conditions: $[H_2SO_4]$ range from 0.25−1.5 mole/L, and for particles from residues of the neutral leaching of calcine sphalerite range from 9–20 μm in size with porous specific surfaces s_m: 2.90 m^2/g (corresponding to 0.5 μm grains), the leaching process is controlled by the heterogeneous reaction. The variation in fractional conversion does not depend on the size of the particles and, up to conversion ratios greater than 85%, as predicted by the grain model (see equations [7.2.7] and [7.2.19] and Figure 7.2.3) is given by:

$$1 - (1 - X)^{1/3} = (1/3)\ k . s_m [H_2SO_4]^n . t \qquad [7.2.23]$$

$n = 0.60$; $A = 29{,}465 \pm 591\ mol^{0.4}/m^2.min$; $Ea = 63$ kJ/mol.

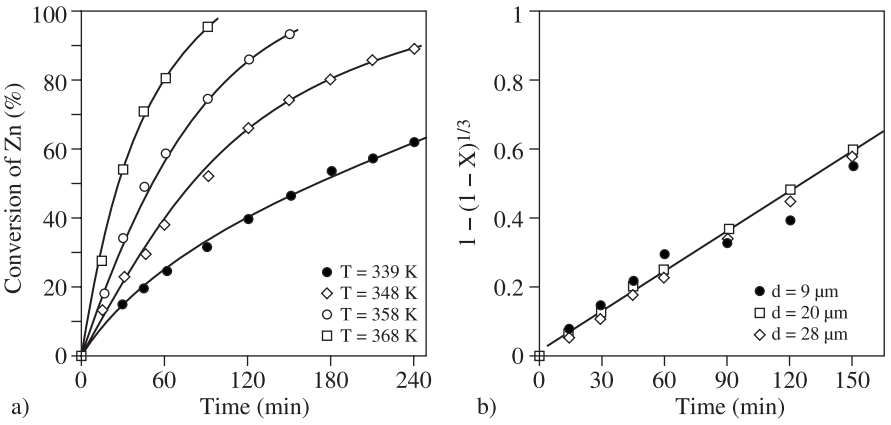

Figure 7.2.3. *Leaching of zinc ferrite porous particles with sulfuric acid [H_2SO_4] = 1.0 mol/L. Variation of the fractional conversion X as a function of time: a) (Zn%) for a 20mm particle at different temperatures; and b) for different particles sizes at 85°C (see equations [7.2.7] and [7.2.19]) [FIL 92]*

7.2.2.3.2. Carbon combustion

This topic is covered in Chapter 2, section 2.6.1 and Chapter 5, section 5.4.3.3, reactions [5.4.19] and [5.4.20]. The main reaction that occurs at the surface of the carbon particle is the formation of CO. In the presence of excess oxygen and for long contact times $>10^{-3}$ sec, CO is oxidized into CO_2. The carbon combustion is highly exothermic (see section 7.5.1) as charcoals and semi-coke are porous, three different regimes can be distinguished:

– At low temperatures, up to 700°C, the combustion rate is controlled by the heterogeneous reaction. As it is very slow, the specific carbon surface varies slightly and a combustion rate per specific unit surface as well as an activation energy E can be determined. The combustion rate significantly varies with the nature of carbon (see Chapter 5, Figure 5.4.2).

– At intermediate temperatures, ranging from 700–1,200°C, combustion occurs under a mixed regime (see equation [7.2.21]). The specific surface varies significantly during the combustion of a particle. The variations, at different temperatures, of the fractional conversion X (burnoff) with time determined in a drop-tube furnace (see section 7.5.1) are shown in Figure 7.2.4a.

– At a higher temperature, the combustion process is controlled by the diffusion of the gaseous species in the pores of the particle with an activation energy that is almost equal to zero.

The combustion reactivity of char is the rate of carbon consumption per unit mass of carbon remaining in the char (see equation [7.2.17]):

$$\rho_{mC} = -\frac{1}{m_C} . \frac{dm_C}{dt} \qquad [7.2.24]$$

where m_C is the residual carbon mass at time t. Figure 7.2.4 represents the variation in reactivity of a semi-coke over time for different operating conditions. Although the specific surface of the particles increases during the combustion process, the reactivity decreases during that time due to a modification of the structure of the charcoal during this combustion process.

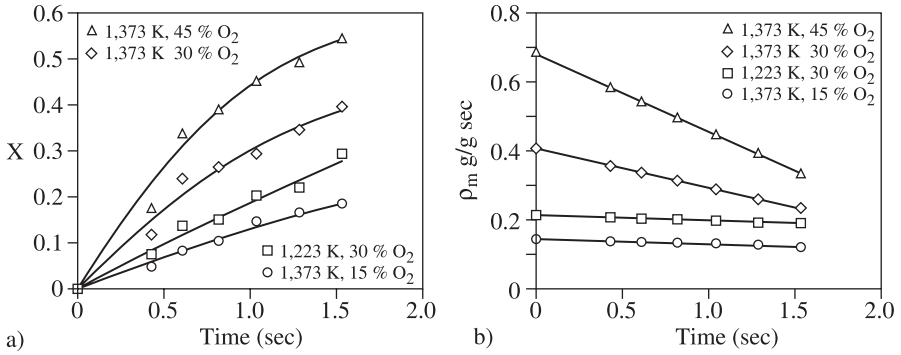

Figure 7.2.4. *Combustion of carbon (coal char) for different operating conditions: a) fractional conversion (burnoff) as a function of time; and b) combustion reactivity (see equation [7.2.24]) [LU 01]*

7.2.2.3.3. Boudouard reaction

Between 800 and 1,200°C the rate of the Boudouard reaction (see Chapter 2, section 2.6.2, reaction [2.6.6]) is quite slow and is controlled by the chemical reaction (see Chapter 5, section 5.4.3.4). In these conditions, where the diffusion of gaseous molecules in the pores is not the limiting step, the variation in fractional conversion of the carbon particles is given by equation [7.2.18] (see Chapter 5, equation [5.4.25]).

At higher temperatures, depending on the size of the particles (T > 1,200°C), the gasification process occurs under a mixed regime (see section 7.2.2.2). The variation of fractional conversion with time is given by equation [7.2.7]. The rate, with respect to the external surface of the particle, is given by equation [7.2.21]:

$$r_C = k_{Gc} . C_{CO2} = k_{Gp} . p_{CO2} / RT = (D_e . \rho . s_m . k_{rp})^{1/2} . p_{CO2} / RT \qquad [7.2.25]$$

where k_{Gc} is expressed in cm/s, k_{Gp} and k_{rp} in mol/cm^2.s.atm (see Chapter 5, equation [5.2.26]), D_e is the effective diffusivity of CO_2 in the pores, ρ is the density, S_m is the surface of the pores per unit mass unit, and p_{CO_2} is the pressure of the gaseous reactant surrounding the particle. The values of the rate constant of the Boudouard reaction for different types of carbons are presented in Table 7.2.1.

	Temperature °C	k_{GC}^{Ar} *cm/s*	k_{GC}^{He} *cm/s*
CP graphite	1,500	48.8	83.5
UHP graphite	1,500	28.9	26.6
Coke A	1,400	13.4	21
Coke B	1,400	16.9	28
Coke C	1,400	12.7	22.9
Coke D	1,400	6.9	-

Table 7.2.1. *Rate constants for the gasification of various types of carbon in 10% CO_2-Ar or He gas mixtures [STO 00]*

These results do not seem coherent with those presented in Chapter 5, section 5.4.3 and equation [5.4.25]. The values of the mixed rate constant k_G, are significantly higher for graphite than for coke. This is due to a significant increase in the internal surface of the graphite at this temperature during its gasification.

The salts of alkaline metals (e.g. Na_2CO_3, K_2CO_3, Li_2CO_3) when present in low concentrations (2%) are powerful catalysts of the Boudouard reaction, due to the following mechanism:

$$M_2CO_3(s) + 2\ C(s) \rightarrow 2\ M + 3\ CO(g)$$

$$2\ M + 2\ CO_2 \rightarrow M_2CO_3(s) + CO(g)$$

Some metals, such as Mn, Ni and Sn, also catalyze the Boudouard reaction, but their influence decreases with temperature.

7.3. Heterogeneous precipitation: growth rate of the particles

The heterogeneous precipitation process is studied in Chapter 5, section 5.6.1. The growth of particles from the primary particles by heterogeneous precipitation according to equation [5.6.1] is the result of two successive processes:

– the transport(s) of one or several reactants in phase α up to the particle;

– a heterogeneous reaction occurring at the surface of the growing particles S.

At high temperature the transport process is the limiting step, and at a lower temperature the chemical reaction is the limiting step.

For the growth of a particle from primary particles with an initial radius of R_{po}, equations [7.2.4], [7.2.7] and [7.2.11] describe the growth (with a sign change):

$$dR_p / dt = + v_{MB} b \, . \, r_s \text{ (or } \Phi_{A\alpha s}) \qquad [7.3.1]$$

– when the rate-limiting step is the chemical reaction (for a reaction whose rate is of the first order with respect to the concentration of reactant A), the growth law of the precipitates is linear (see equation [7.2.6]):

$$R_p(t) - R_{po} = b v_{MB} \, . \, r_s t = g_p t \qquad [7.3.2]$$

where R_{po} is the initial radius of the primary particle;

– when the limiting step is the mass transport of reactant A in phase α, right next to the precipitate, the growth of the precipitates will vary (see equation [7.2.10]) according to:

$$R^2_p(t) - R^2_{po} = (\text{const}) \, . \, t \qquad [7.3.3]$$

The reactions involving heterogeneous precipitations are studied in [VIG 11b] Chapter 1, section 1.3.

7.4. *In situ* conversion of a solid particle

These are processes where the product is a new solid phase, see Figure 7.4.1.

EXAMPLE.– Reduction of an oxide by a reducing gas to give a metal:

$$FeO\,(s) + CO(g) \rightarrow Fe(s) + CO_2(g)$$

or the roasting of sulfides:

$$ZnS\,(s) + 3/2\ O_2(g) \rightarrow ZnO(s) + SO_2(g)$$

7.4.1. *Non-porous particle: the shrinking unreacted core model*

The progress of the conversion of particle B(s) → S(s) is shown schematically in Figure 7.4.1. It occurs on a reaction front that moves towards the core of the particle (R_C is the radius of the reaction front or of the shrinking core and R_{p0} is the radius of the initial particle). It is assumed that the overall size of the particle does not change.

The reaction occurs at a sharp interface or within a narrow region between the unreacted core and the product layer, which may or may not be porous. In either case, the gaseous reactant must be able to penetrate through the product layer in order for the reaction to proceed to completion. The product layer is usually porous. When the product layer is dense, the reaction does not proceed or is slow, controlled by diffusion of the reactant through a dense solid. As the reaction proceeds, the unreacted core diminishes in size. The reaction is usually performed with operating conditions where the nucleation of the solid "product" S on the initial particle "B" can easily occur. The conversion rate is therefore the growth rate, towards the center of the particle, of the external layer of the product.

Figure 7.4.1b presents the concentration profiles of reactant A and product R. The concentration of reactant A decreases from its value in the bulk fluid stream, $C_{A\alpha}$, to its values C_{As} on the reaction front (at the surface of the shrinking core). The concentration of R varies in reverse order. The limiting step can be one of three processes: the diffusion within the fluid boundary layer surrounding the particle; the diffusion within the porous layer of product S; and the chemical reaction at the interface.

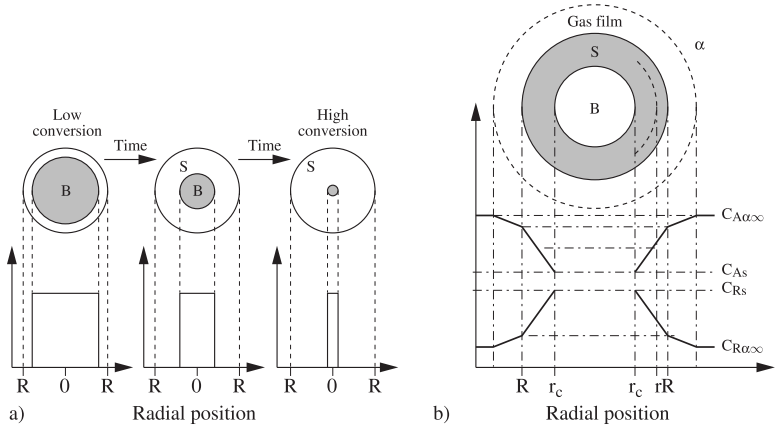

Figure 7.4.1. *In situ conversion of a dense particle with formation of a product layer around the shrinking core B: a) the reaction proceeds at a narrow front that moves into the solid particle; and b) concentration profiles of the gaseous reactant A and gaseous product R in the gas film and the product layer [LEV 72]*

7.4.1.1. *Rate-controlling step: gas diffusion in the fluid boundary layer*

As the external radius of the particle R_{p0} does not vary, the mass transfer coefficient $h_{A\alpha}$ and the flux of the gaseous reactant remain constant as the conversion proceeds, and so (see equations [7.2.3] and [6.3.12] or [6.3.14]):

$$dn_B / dt = -4\pi R_{p0}^2 . b . \Phi_{A\alpha s} \qquad [7.4.1]$$

The fractional conversion of a particle varies linearly with time:

$$X_B = t / \tau \qquad [7.4.2]$$

and the time for a complete conversion varies according to:

$$\tau = \frac{R_{p0}}{b v_{MB} \Phi_{A\alpha s}} \qquad [7.4.3]$$

7.4.1.2. *Rate-controlling step: diffusion through the product layer*

The mass transfer coefficient for reactant A varies according to:

$$h_{As} = D_{As} / e_s \qquad [7.4.4]$$

where D_{As} is the diffusion coefficient of reactant A in the pores of the layer of product S. The thickness of the external layer e_s increases with time. For a spherical particle, the fractional conversion varies with time according to:

$$t / \tau_{diff} = 1 - 3 (1 - X_B)^{2/3} + 2 (1 - X_B) \qquad [7.4.5a]$$

with:

$$\tau_{diff} = (const) R_{p0}^2 \qquad [7.4.5b]$$

where (const) is given by equation [7.2.10b].

EXAMPLE.– *Galena leaching*. Between 50 and 90 C, the leaching process of galena occurs with the formation of a thin $PbCl_2$(s) layer between the PbS and an external layer made of sulfur S°(s). The $PbCl_2$ thus formed reacts with the Cl^- ions and gives

a hydrochloric complex (see [VIG 11b], Chapter 1, section 1.2.3.3, reactions [1.2.36] and [1.2.37] and Figure 1.2.14a):

$$PbCl_2(s) + 2\ Cl^- \rightarrow PbCl_4^{2-} \qquad [7.4.6]$$

The dissolution rate of galena is controlled by the diffusion of the $PbCl_4^{2-}$ ion through the growing S°(s) layer towards the aqueous phase. The fractional conversion varies according to equations [7.4.5a] and [7.4.5b] (see Figure 7.4.2). The time for complete leaching of a particle τ varies with the initial size of the particle, as given by equation [7.4.5b].

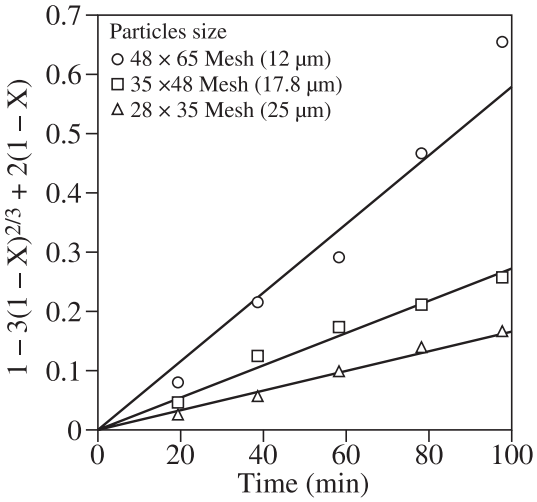

Figure 7.4.2. *Leaching of PbS galena in ferric chloride solutions ($FeCl_3$) at 50°C. Fractional conversion* versus *leaching times for different particle sizes (product layer diffusion control), see equation [7.4.5] [FUE 86]*

7.4.1.3. *Rate-controlling step: surface (heterogeneous) reaction*

The chemical reaction occurs at the unreacted core surface. The conversion rate is referred to the surface of this unreacted core. The real available surface for the reaction depends on the porosity of the product layer. The variation of the fractional conversion with time follows equation [7.2.7] and the time of the complete conversion is given by equation [7.2.8].

EXAMPLE.– *Reduction of a non-porous magnetite pellet*. The fractional conversion of a dense particle is given by equation [7.2.7], see Figure 7.4.3.

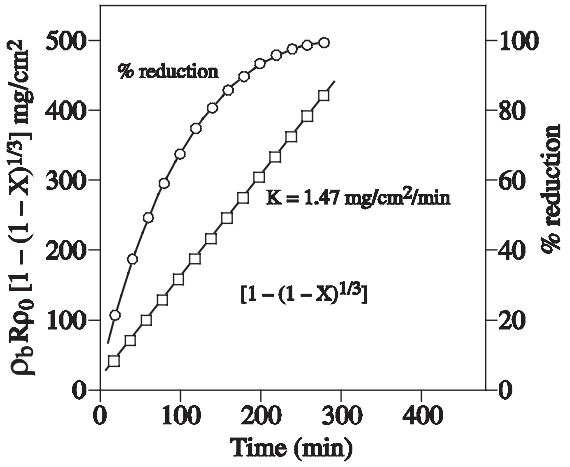

Figure 7.4.3. *Reduction of a non-porous magnetite pellet at 470°C in hydrogen (with formation of a porous iron layer, see equation [7.2.7]). K is the rate constant [MCK 61]*

NOTE.– From the variations of the fractional conversion with time it appears to be very difficult to identify the rate-controlling process. Identification of the limiting step is, however, possible by the time of complete conversion of a particle τ that is a function of particle size with different exponents depending on the limiting step and by the activation energy. In addition, the identification process is much harder because the limiting step may vary during the progress of conversion. As long as the external porous layer is thin, the limiting process is the heterogeneous reaction, and then once the external layer has become large enough or its porosity low, diffusion in this layer becomes the limiting process.

Table 7.2.2 summarizes the corresponding conversion-time expressions for different shapes of dense particles.

7.4.1.4. *Multiple conversions*

The reduction of a hematite particle gives rise to the formation of successive layers of some sub-oxides $Fe_3O_4 \rightarrow Fe_2O_3 \rightarrow FeO$ and an external metal layer. The reduction can only proceed if the layers are porous, allowing the reducing gas to reach the hematite core. The reaction occurs topologically and the model of the shrinking core is applied. A complete modeling of this process has been performed [TSA 76].

7.4.2. *In situ conversion of a porous particle: the grain pellet model*

A pellet is formed by compacting fine grains of size R_g. In the grain model, the pellet is made up of individual spherical grains of equal size (R_g), see Figure 7.4.4.

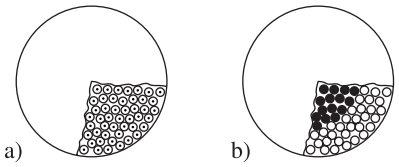

Figure 7.4.4. *In situ conversion of a porous particle – the grain model: a) for a solid undergoing a conversion under chemical control s conditions; and b) for a solid undergoing conversion under pore diffusion control [SZE 76]*

7.4.2.1. *Rate-limiting step: chemical heterogeneous reaction*

The gaseous reactant is present in the pores under a concentration equal to that of the surrounding gas stream $C_{A(\alpha)}$ and therefore the reaction uniformly occurs across the particle: all the grains forming the particle react simultaneously (see Figure 7.4.4a) and the reaction time of the particle only depends on the size of the grains. The fractional conversion X_B and time of complete reaction are respectively given by equations similar to [7.2.7] and [7.2.8]. The time of complete reaction varies linearly with the size of the grain R_g:

$$\tau = \frac{R_{g0}}{b v_{MB} r_s} \qquad [7.4.7]$$

If the diffusion of the gaseous reactant in the external layer of each grain is or becomes the limiting step (as soon as an external layer of a given thickness is reached), then equations [7.4.5a] and [7.4.5b] are obtained and the time of complete reaction varies with the square of the dimension of the grain.

7.4.2.2. *Rate-controlling step: diffusion through the product layer*

This process is controlled by diffusion of the gaseous reactant in the external layer of the particle, see Figure 7.4.4b. The reaction occurs on a thin front separating the non-reacted core from the external layer of the product. The fractional conversion varies according to equation [7.4.5a] and the times of complete reaction vary with the square of the dimension of the particle (see equation [7.4.5b]).

		Film diffusion controls	"Ash" diffusion controls	Reaction controls
In situ transformation Constant size particles	Flat plate $X_B = 1 - \frac{l}{L}$	$\frac{t}{\tau} = X_B$ $\tau = \frac{\rho_B L}{b k_g C_{Ag}}$	$\frac{t}{\tau} = X_B^2$ $\tau = \frac{\rho_B L^2}{2b \mathcal{D}_e C_{Ag}}$	$\frac{t}{\tau} = X_B$ $\tau = \frac{\rho_B L}{b k_s C_{Ag}}$
	Cylinder $X_B = 1 - \left(\frac{r_c}{R}\right)^2$	$\frac{t}{\tau} = X_B$ $\tau = \frac{\rho_B R}{2b k_g C_{Ag}}$	$\frac{t}{\tau} = X_B + (1 - X_B)\ln(1 - X_B)$ $\tau = \frac{\rho_B R^2}{4b \mathcal{D}_e C_{Ag}}$	$\frac{t}{\tau} = 1 - (1 - X_B)^{1/2}$ $\tau = \frac{\rho_B R}{b k_s C_{Ag}}$
	Sphere $X_B = 1 - \left(\frac{r_c}{R}\right)^3$	$\frac{t}{\tau} = X_B$ $\tau = \frac{\rho_B R}{3b k_g C_{Ag}}$	$\frac{t}{\tau} = 1 - 3(1 - X_B)^{2/3} + 2(1 - X_B)$ $\tau = \frac{\rho_B R^2}{6b \mathcal{D}_e C_{Ag}}$	$\frac{t}{\tau} = 1 - (1 - X_B)^{1/3}$ $\tau = \frac{\rho_B R}{b k_s C_{Ag}}$
Gasification Srinking sphere	Small particle Stokes regime	$\frac{t}{\tau} = 1 - (1 - X_B)^{2/3}$ $\tau = \frac{\rho_B R_0^2}{3b \mathcal{D} C_{Ag}}$	Not applicable	$\frac{t}{\tau} = 1 - (1 - X_B)^{1/3}$ $\tau = \frac{\rho_B R_0}{b k_s C_{Ag}}$
	Large particle (u = constant)	$\frac{t}{\tau} = 1 - (1 - X_B)^{1/2}$ $\tau = (\text{const})\frac{R_0^{2/3}}{C_{Ag}}$	Not applicable	$\frac{t}{\tau} = 1 - (1 - X_B)^{1/3}$ $\tau = \frac{\rho_B R_0}{b k_s C_{Ag}}$

Table 7.2.2. *Conversion-time expressions for various non-porous shaped particles, shrinking core model [LEV 72]*

7.5. Conversion of a particle undergoing strong exo- or endothermic chemical reactions

7.5.1. *Exothermic chemical reactions*

The oxidation of sulfide particles is a strongly exothermic process, like the combustion of carbon.

The oxidation of particles is studied by blowing an oxidizing gas around a particle or through a particle bed. Determination of the oxidation rate of the particles, where a strong exothermic reaction occurs, poses a problem due to the increase in temperature of the reacting particles. Indeed, if the heat transfer between the particles and surrounding gas is low, each particle behaves as an adiabatic system and its temperature escalates rapidly (this is the case of the flash-smelting of sulfide particles).

The temperature increase depends on the size of the particles, their porosity and the operating conditions. The heating rate of particles is related to the initial temperature difference between the particle and gas phase and to the gas flow rate around the particles.

For instance, for the roasting of a dense and centimetric ZnS particle (see Chapter 5, reaction [5.5.2]), for a gas phase temperature ranging from 800–900°C, and a strong gas flow rate to remove the heat released, the temperature increase is small and ranges from 10–20°C [CAN 57]. The oxidation rate of a dense particle, with a large enough volume, can then be determined. Oxidation occurs topologically with the formation and growth of an external porous layer of ZnO. The oxidation proceeds at the sulfide-oxide interface, the penetration of oxygen through the external layer being possible as the layer is porous, see Chapter 6, section 6.3.1.1 and reaction [6.3.5a]. The limiting step is the diffusion of $O_2(g)$ in the pores and the variation of the fractional conversion is given by equation [7.4.5]

For a porous ZnS (from 30–40%) and centimetric particle with a gas phase temperature ranging from 643–843°C, and gas flowrate around the particle corresponding to a Reynolds number equal to 70, the increase in pellet temperature can reach 160°C, see Figure 7.5.1 and see [VIG 11b], Chapter 6, section 6.2.2 and Figure 6.2.4. For porous particles where the reaction occurs on the surface of the grains, the heat produced by the reaction inside the particle cannot be released and the pellet temperature increases rapidly when the reaction starts.

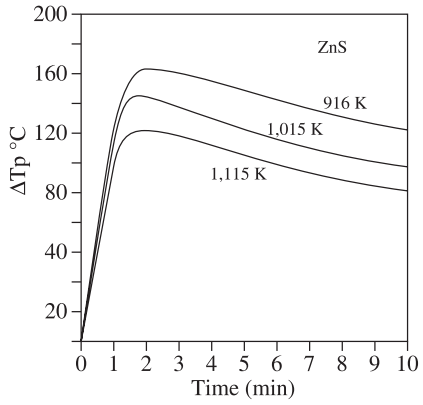

Figure 7.5.1. *Oxidation of porous zinc sulfide pellets (Φ = 1.29 cm, H = 0.73 cm, porosity = 0.34) in an air flow. Effect of the initial particle temperature on particle temperature history for a gas phase temperature of 1,073K (see [VIG 11b], Chapter 6, section 6.2.2 and Figure 6.2.4) [KIM 87]*

For micronic particles, the temperature increase is fast and quite high. The difference between the maximum temperature and temperature of the gas phase can reach 700°C, see Figure 7.5.4. The temperature variation of a particle injected into an oxidizing gas flow can be calculated by a heat balance, where the main terms are the enthalpy of the reaction, heat consumed by the vaporization of sulfur, and heat transferred to the atmosphere by conduction and radiation:

$$V_p \,.\, \rho C_p \,.\, dT_p / dt = S_p(-\Delta H_r) \,.\, r_S - (\Delta H_v) \,.\, dm / dt - h_T S_p(T_p - T_g) - \sigma \varepsilon S_p(T_p^{\,4} - T_g^{\,4}) \qquad [7.5.1]$$

the smaller the size of the particle, the higher dT_p / dt. As a result, the variation of the fractional conversion with time does not follow any of the kinetic law established in section 7.4.2. This is because the temperature of the particle varies during conversion.

The conversion of these micronic particles is studied in vertical drop tube furnaces also called laminar flow furnaces in which temperature, residence time and gas-phase composition are closely controlled. The particles carried by a primary gas flow are injected into a zone that is maintained at a high temperature by a heated element, where the combustion occurs. Some really sophisticated techniques allow the monitoring of particle temperature during heating and combustion. For a particle size, the variation in fractional conversion is determined as a function of time, and for different gas phase temperatures and oxygen contents (see Figure 7.5.2).

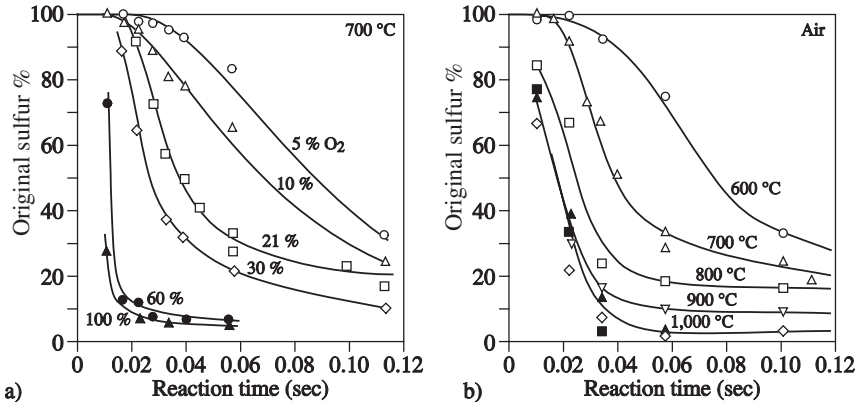

Figure 7.5.2. *Combustion of chalcopyrite ($CuFeS_2$) concentrates, in a laminar flow furnace in oxygen-nitrogen mixtures (37–53 μm screen size fraction). Fractional conversion (original sulfur content): a) for a gas phase temperature of 700°C and different oxygen contents (vol. %); and b) for different gas phase temperatures [JOR 01]*

Oxidation of the particles injected into a hot gas flow starts once the particles have reached a given temperature. The ignition temperature is the temperature above which the reaction starts and is self-sustained. As the heat produced by the exothermic reaction is higher than that released (by radiation and conduction phenomena), the particle temperature increases leading to an acceleration of the oxidation reaction. The ignition temperature depends on the particle features: size, porosity and on operating conditions: temperature of the gas flow, and initial temperature of the particle. Figure 7.5.3 presents the operating parameters Tg and p_{O2} in a laminar flow furnace leading to the ignition of chalcocite (Cu_2S) particles of different sizes.

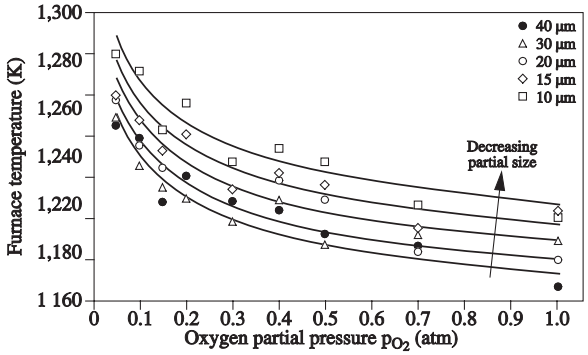

Figure 7.5.3. *Flash oxidation of chalcocite (Cu_2S) concentrates. Operating conditions (oxygen partial pressure and furnace temperature in a laminar flow furnace for particle ignition as a function of the particle size [MOR 96]*

The ignition temperatures of the unstable sulfides chalcopyrite $CuFeS_2$ and pyrite FeS_2 are significantly lower than the temperatures of more stable chalcocite Cu_2S sulfides. Ignition is triggered by decomposition of the sulfide, which liberates sulfur and produces a porous open structure, allowing the ingression of oxygen into the particle:

$$FeS_2 \rightarrow FeS_{(1+x)} + 0.5\ (1 - x)\ S_2(g)$$

$$1/2\ S_2(g) + O_2(g) \rightarrow SO_2(g)$$

For pyrite, the ignition temperature is about 530°C. Pyrrhotite (FeS) does not ignite until about 800°C.

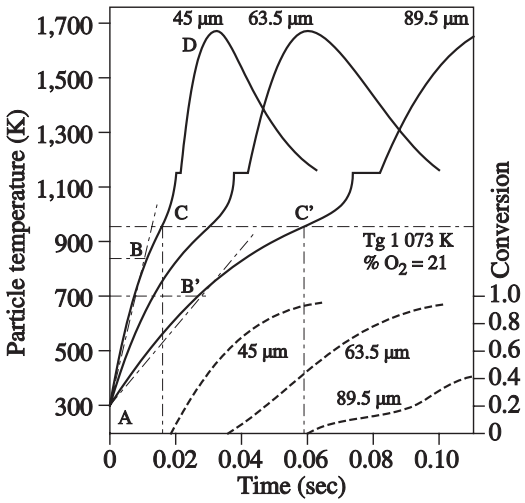

Figure 7.5.4. *Oxidation of chalcopyrite ($CuFeS_2$) particles of different sizes in a laminar flow furnace. Variations of the particle temperature and conversion as a function of time (Tg = 1,073K; $\%O_2$ = 21) [SOH 93]*

Figure 7.5.4 shows the temperature variation curves of chalcopyrite ($CuFeS_2$) of different sizes injected into an oxidizing gas flow (air) in a laminar flow furnace at 1,073°K. Each of these curves can be split into different segments:

– AB(AB') segment: heating of the particle. The heating rate depends on the size of the particle and on the gas flowrate around the particle;

– BC(B'C') segment: decomposition of the sulfide (endothermic process), releasing sulfur, at around 873°C: and simultaneously combustion of gaseous sulfur, (exothermic process), with slowing of the particle temperature increase.

$$4\ CuFeS_2 \rightarrow 2\ Cu_2S + 4\ FeS + S_2(g)$$

– CD segment: at point C, the oxidation of sulfide (an exothermic process) starts. This leads to a significant increase of the particle temperature: the smaller the particle, the higher the oxidation rate (higher surface/volume ratio). The temperature at point C corresponds to the ignition temperature (960K) for these particle sizes and operating conditions (see [VIG 11b], Chapter 6, reactions [6.2.11] and [6.2.12]):

$$3\ FeS\ (s, l) + 5\ O_2(g) \rightarrow Fe_3O_4(s, l) + 3\ SO_2(g)$$

$$Cu_2S + O_2(g) \rightarrow 2\ Cu(l) + SO_2(g)$$

At high oxygen pressures, Cu will be oxidized:

$$2\ Cu(l) + 5/2\ O_2(g) \rightarrow Cu_2O(s, l)$$

Fusion of the particles occurs at a temperature of 1,155K. The temperature continues to increase up to point D.

The curve reaches a maximum that is partly due to the vaporization of Cu.

The corresponding curves showing the variation in fractional conversion of the particles as a function of time are drawn in Figure 7.5.4. At high temperature, the conversion rate is controlled by the diffusion of the oxygen in the boundary layer surrounding the particle.

In the *flash-smelting* of chalcopyrite particles, particle size ranges from 20–200 μm and residence time in the gas stream is 0.5 s. For a gas stream temperature of 1,400°C for particles that are 20 μm, the time required to reach the ignition temperature is less than 6 ms, whereas for a particle of 100 μm, this ignition time is equal to 0.2 s. The smallest particles reach ignition point in very short times and their exothermic oxidation warms the surrounding gas and decreases the ignition time for the largest particles. The ignition of these particles produces a real flame and the kinetics of combustion of a relatively dense cloud of particles in this flame are quite complex.

Some pyrometry measurements of temperature evolution of chalcocite [MOR 96, SHO 95], galena and pyrite [TUF 95] particles during their flash roasting have been carried out. In the case of copper and lead sulfides, the phenomena involved are quite complex as the particles undergo decomposition and volatilization of metallic copper.

7.5.2. *Endothermic chemical reactions*

The thermal decomposition of a salt or hydroxide, or the calcination of calcium carbonate are examples of *in situ* endothermic conversion:

$$CaCO_3(s) \rightarrow CaO(s) + CO_2(g)$$

The reaction only occurs when:

$$A = (A° - RT \ln p_{CO2}) > 0 \text{ and when } p_{CO2} > P_{ext}\,(1 \text{ atm})$$

$$A° = -177{,}000 + 158\ T \text{ in J/mol}$$

or with T > 1,100 °C when $p_{CO2} = 1$ atm.

A porous CaO layer forms at the surface of the particles, which allows the release of CO_2 gas. The porosity of this layer comes from the difference between the molar volumes of the reactant and product. If the transport of gaseous CO_2 in the pores of the external layer is not the rate-limiting step due to the endothermicity of the reaction, the heat transfer between the surrounding and non-reacted core of the particle through the external porous layer is the rate-limiting step. The variation in fractional conversion is given by equation [7.4.5a]. The time for complete conversion is given by:

$$\tau = \rho_B \Delta H_r R_{po}^2 / 6\, h_T\, (T_{ext} - T_s) \qquad [7.5.2]$$

where h_T is the heat transfer coefficient within the external porous layer.

If transport of the gaseous product is the rate-limiting step, the progression of the conversion will correspond to a gasification , see section 7.2.

7.6. Transfer processes between two fluid phases, one phase being dispersed (as drops or bubbles) in the second phase

Transfer processes occur in many refining operations (see [VIG 11b], Chapter 7): steel desulphurization by dispersion of liquid steel in a slag; degassing of liquid metals (dehydrogenation, nitrogen removal) by injecting inert gas bubbles into a liquid metal; solvent extraction in hydrometallurgy; etc.

Simple kinetic laws can be only be established during the contact time between the globule (droplet or bubble) and the continuous phase when the amount of component A extracted is small, so the volume and surface of the globule do not vary, and if the globule is supposed to be perfectly mixed (i.e. full circulation within the globule), see Chapter 6, Figure 6.4.5b.

The number of moles of A in phase α extracted or absorbed by a globule β during time dt, see equation [7.2.3], can be written as:

$$dn_{A\beta} / dt = V_\beta\, dC_{A\beta} / dt = -\nu_A S_\beta (r_s \text{ or } \Phi_{A\alpha s}) \qquad [7.6.1]$$

7.6.1. *Heat transfer*

In the case of heat transfer between a perfectly mixed droplet β and a continuous phase α (droplet falling through a steady, continuous phase), the volume of the continuous phase being large compared to the droplet, during the contact time we can assume that the temperature of the continuous phase T_α does not vary. The

temperature of the droplet T_β, however, does vary. From the expression of the heat flux, see equation [6.3.1]:

$$\Phi_{T\alpha s} = h_{T\alpha} \,.\, (T_\beta - T_\alpha) \qquad [7.6.2]$$

The amount of heat extracted from the droplet with a volume V_β through its surface S during dt can be written as:

$$h_{T\alpha} \,.\, S_\beta (T_\beta - T_\alpha)\, dt = -V_\beta (\rho C)_\beta dT_\beta \qquad [7.6.3]$$

During the time $dt = dz / u_\beta$, the droplet travels dz, if we assume that the heat transfer coefficient $h_{T\alpha}$ in the continuous phase remains constant, see Chapter 6, equation [6.4.15], the integration of equation [7.6.3] leads to:

$$\ln \frac{\left(T_{\beta 2} - T\alpha\right)}{\left(T\beta 1 - T\alpha\right)} = \frac{h_{T\alpha}\left(z_2 - z_1\right)}{u_\beta . s_\beta \left(\rho C_p\right)_\beta} \qquad [7.6.4]$$

where u_β is the velocity of the droplet. It has been observed that $\ln (T_\beta - T_\alpha)$ varies linearly with the distance traveled by the droplet through the continuous phase.

7.6.2. *Mass transfer*

For the transfer (extraction) of a component (solute) from a continuous phase α to a dispersed phase β (see Chapter 6, section 6.3.2.2 and reaction [6.3.18]):

$$\nu_A A(\alpha) \rightarrow \nu_R R(\beta)$$

whose transfer flux is given by equation [6.3.21], the removal rate of solute A present in the continuous phase α by a drop β moving within the continuous phase can be obtained from equation [7.6.1]:

$$V_\beta dC_{R\beta} / dt = S_\beta h_{A\alpha} [C_{A\alpha} - C_{R\beta} / K_C] \qquad [7.6.5]$$

If we assume that the concentration of the solute in the continuous phase $C_{A\alpha}$ slightly varies during the contact time, $\tau = Z / u$, that the amount transferred remains small and the volume V_β and surface S_β of the drop do not vary, the variation of the solute A content within the drop as a function of time can be obtained by integration:

$$C_{A\beta}(t) = K_C C_{A\alpha} [1 - \exp(-\gamma t)] \text{ with } \gamma = S_\beta h_{A\alpha} / V_\beta \qquad [7.6.6]$$

and the fractional transfer of the solute defined as the ratio between the quantity extracted and maximum quantity that can be extracted, is:

$$C_{A\beta}(t) / C^*_{Ab} = C_{A\beta}(t) / K_C C_{A\alpha} \qquad [7.6.7]$$

The kinetics of steel desulphurization (transfer of the sulfur from the steel in a slag) is studied in [VIG 11b], Chapter 7, section 7.2.4.2. In this chapter we deal with the kinetics of steel dehydrogenation.

7.6.3. *Hydrogen removal from liquid steel bath by injection of inert gas bubbles*

$$2\ H_{(Fe)} \rightarrow H_2(g)$$

For this transfer (see Chapter 6, section 6.3.2.2), we can assume that there is an equilibrium at the interface (see Chapter 5, section 5.4.5.1.3 and equation [5.4.45]) and that the diffusion of hydrogen in the continuous metallic phase is the rate-limiting process. The transfer flux of hydrogen is given by equation [6.3.24b].

7.6.3.1. *Removal rate of by a single bubble under mass transfer control*

Consider extraction by an inert gas bubble of volume V_β and velocity u_β rising through a liquid height H. Over a height dH, the bubble remains in contact with the liquid phase during dt. During that time dt, the number of transferred hydrogen moles inside the bubble is:

$$dn_{H2} = V_\beta d\,(p_{H2} / p_{inert}) = h_{H(Fe)}\,(C_{H(Fe)} - K(p_{H2})^{1/2})\,S_\beta dt \qquad [7.6.8]$$

leading to:

$$\int \frac{dp_{H_2}}{P\left(C_{H(Fe)} - K\left(p_{H_2}\right)^{1/2}\right)} = \int h_{H(Fe)} \left(\frac{S_\beta}{V_\beta}\right) \frac{dH}{u_\beta} \qquad [7.6.9]$$

As we can assume that the hydrogen content in the metallic phase remains constant during extraction by a single bubble, the integration of this equation gives the pressure p_{H2} in the bubble and the amount of hydrogen moles extracted by the bubble after traveling the height H of the metallic phase.

7.6.3.2. *Stream degassing*

For a metallic bath with volume V_m, and an initial hydrogen content of $C°_{H(Fe)}$, we can calculate the hydrogen content reached after time t when an inert gas is injected at molar flow rate F_β. As this flow rate leads to the formation of $ñ_\beta$ bubbles

per second, with volume V_β and radius R_β, a bubble stays within the bath for a certain time τ, such as:

$$n_\beta = \frac{F_\beta}{\frac{4}{3}\pi R_\beta^3} \quad \text{and } \tau = H / u \qquad [7.6.10]$$

The number of bubbles present in the liquid phase at a given time is:

$$n_\beta = \tilde{n}_\beta \, . \, \tau \qquad [7.6.11]$$

and the contact surfaces between the bubbles and the liquid phase α is:

$$S = n_\beta \, . \, 4\pi \, R_\beta^2 = 3 \, F_\beta H / R_\beta u_\beta \qquad [7.6.12]$$

The overall degassing rate can be written as:

$$V_m C_{\underline{H}(Fe)} / dt = -h_{\underline{H}(Fe)} \, . \, S \, (C_{\underline{H}(Fe)} - K_H p_{H2}^{1/2}) = F_\beta \, (p_{H2} / p_{inert}) \qquad [7.6.13]$$

We can assume that the metallic bath is perfectly stirred by the injected gas bubbles so that the dissolved hydrogen concentration $C_{\underline{H}}$ in the metallic bath is uniform. In addition, we can suppose that the inert gas flowrate is quite high, and therefore that the partial hydrogen pressure in the gaseous bubbles, dispersed in the metallic phase, is quite low and can be neglected compared to the hydrogen concentration in the metallic phase. We can then write:

$$dC_{\underline{H}(Fe)} / C_{\underline{H}(Fe)} = -h_{\underline{H}(Fe)} \, . \, (S / V_m) \, dt \qquad [7.6.14]$$

During time t, an amount of inert gas F_β t has been injected, and, by integration:

$$C_{\underline{H}(Fe)} / C°_{\underline{H}(Fe)} = \exp(-\gamma' t) \qquad [7.6.15]$$

where:

$$\gamma' = h_{\underline{H}(Fe)} \, (S / V_m) = 3 \, h_{\underline{H}(Fe)} H F_\beta / (V_m R_\beta . u) \qquad [7.6.16]$$

Coefficient γ' therefore depends on the operating parameters: inert gas flow rate per unit volume of the liquid phase (F_β / V_m); H the height of the liquid phase; R_β the radius of the gas bubbles, which depends on the diameter of the submerged tuyere u_β; and u_β is velocity of the bubbles, which mainly depends on their radius R_β.

7.7. Bibliography

[CAN 57] K.J. CANNON, K.G. DENBIGH, *Chemical Engineering Science*, Vol.6, pp. 145-154, April-May 1987.

[DUT 06] J.E DUTRIZAC, *Metallurgical and Materials Transactions B*, Vol. 37B, pp. 161-170, April 2006.

[FIL 92] D. FILIPPOU, G.P. DEMOPOULOS, *Canadian Metallurgical Quarterly*, Vol. 31, No. 1, pp. 41-54, 1992.

[FRU 00] R.J. FRUEHAN *et al.*, *Metallurgical and Materials Transactions B*, Vol. 31B, p. 891, October 2000.

[FUE 86] M.C. FUERSTENAU *et al., Metallurgical Transactions B*, Vol. 17B, pp. 415-423, September 1986.

[JOR 01] F.R.A. JORGENSEN, P.T.L. KOH, *JOM*, pp. 16-20, May 2001.

[KIM 87] Y.H. KIM, N.J. THEMELIS, *Canadian Metallurgical Quarterly*, Vol. 26, No. 4, pp. 341-349, 1987.

[LEV 72] O. LEVENSPIEL, *Chemical Reaction Engineering*, Wiley International Edition, New York, 1972.

[LEV 89] O. LEVENSPIEL, *The Chemical Reactor Omnibook*, 2nd edition., OSU Book Stores, Ohio, 1989.

[LU 01] L. LU, V. SAHAJWALLA, D. HARRIS, *Metallurgical and Materials Transactions B*, Vol. 32B, pp. 811-820, October 2001.

[MCK 61] W.M. MC KEWAN, *Trans. AIME*, Vol. 221, pp. 140-145, February 1961.

[MOR 96] G.J. MORGAN, J.K. BRIMACOMBE, *Metallurgical and Materials Transactions B*, Vol. 27B, pp. 163-175, April 1996.

[NUN 84] C. NUNEZ, J. VINALS, *Metallurgical Transactions B*, Vol. 15B, pp. 221-228, June 1984.

[SHO 95] A.A. SHOOK, G.G. RICHARDS, J.K. BRIMACOMBE, *Metallurgical and Materials Transactions B*, Vol. 26B, pp. 719-729, August 1995.

[SOH 93] H.Y. SOHN, P.C. CHAUBAL, *Extractive Metallurgy of Cu*, *Ni and Co*, R.G. REDDY, R.N. WEIZENBACH (eds.), in TMS publication, Vol.1, pp. 537-565, 1993.

[STO 00] S.R. STORY, R.J. FRUEHAN, *Metallurgical and Materials Transactions B*, Vol. 31B, pp. 43-54, February 2000.

[SZE 76] J. SZEKELY, J.W. EVANS, H.Y. SOHN, *Gas-Solid Reactions*, Academic Press, New York, 1976.

[TSA 76] T. TSAY, W.H. RAY, J. SZEKELY, *AIchE Journal*, Vol. 22, 6, p. 1064, November 1976.

[TUF 95] N.E. TUFFREY, G.G. RICHARDS, J.K. BRIMACOMBE, *Metallurgical and Materials Transactions B*, Vol. 26B, pp. 929-941 and pp. 943-969, October 1995.

[VIG 11b] A. VIGNES, *Extractive Metallurgy 2:Metallurgical Reaction Processes*, ISTE Ltd, London and John Wiley and Sons, New York, 2011.

[VIG 11c] A. VIGNES, *Extractive Metallurgy 3: Processing Operations and Routes*, ISTE Ltd, London, John Wiley and Sons, Wiley, New York, 2011.

Chapter 8

Electrochemical Reactions

8.1. Overview of electrochemical processes

A chemical reaction is a reaction where only chemical species (neutral molecules and positively or negatively charged ions) are involved.

An electrochemical reaction is a reaction where chemical species and free electrons are involved. The two elementary electrochemical reactions are:

– *oxidation*: liberation of electrons. For a metal (in the solid state) immersed in an electrolytic solution, the reaction is a dissolution, which gives a metallic ion in solution (corrosion):

$$M(s) \rightarrow M^{z+} + ze \qquad [8.1.1]$$

– *reduction*: absorption of electrons. For a metallic ion in an aqueous solution (heterogeneous precipitation, see Chapter 5, section 5.6.1):

$$M^{z+} + ze \rightarrow M(s)\downarrow \qquad [8.1.2]$$

Various overall reactions are the result of elementary electrochemical reactions:

– *redox chemical reactions* resulting from two simultaneous elementary electrochemical reactions where the electrons are directly transferred between the reactants. They are homogeneous chemical reactions (see Chapter 5, section 5.2.1.1) (The charges of the ions involved in the purely chemical reactions are not active due to the electro-neutrality present at each point).

EXAMPLE.– The oxidation of ferrous salt by oxygen dissolved in water O_2 (aq) (see section 8.4.3):

Extractive Metallurgy 1: Basic Thermodynamics and Kinetics Alain Vignes
© 2011 ISTE Ltd. Published 2011 by ISTE Ltd.

$$2\ FeSO_4 + 1/2\ O_2(aq) + H_2SO_4 \rightarrow Fe_2(SO_4)_3 + H_2O \quad [8.1.3a]$$

$$2\ Fe^{2+} + 1/2\ O_2(aq) + 2\ H^+ \rightarrow 2\ Fe^{3+} + H_2O \quad [8.1.3b]$$

results from the completion of two simultaneous elementary electrochemical reactions:

$$\text{oxidation: } Fe^{2+} \rightarrow Fe^{3+} + e \quad [8.1.4a]$$

$$\text{reduction: } O_2(aq) + 4\ H^+ + 4\ e \rightarrow 2\ H_2O \quad [8.1.4b]$$

– Redox electrochemical reactions occur in heterogeneous systems, where the active charges are localized at the interfaces between the phases, consisting of separate (elementary electrochemical) reactions.

EXAMPLES.–

– *Water decomposition*:

$$2\ H_2O \rightarrow 2\ H_2(g) + O_2(g) \quad [8.1.5]$$

may be carried out by electrolysis of aqueous solutions by elementary reactions on electrodes (see [VIG 11b], Chapter 2 and Figure 2.2.1):

$$\text{negative electrode: } 4\ H^+ + 4\ e \rightarrow 2\ H_2(g) \quad [8.1.6]$$

$$\text{positive electrode: } 2\ H_2O \rightarrow O_2(g) + 4\ H^+ + 4\ e \quad [8.1.7]$$

– *Iron or zinc corrosion* by an aqueous medium with the release of hydrogen, which may be expressed by the overall reaction:

$$Fe(s) + 2\ H^+ \rightarrow Fe^{2+} + H_2(g) \quad [8.1.8]$$

This overall reaction is the result of two electrochemical reactions ([8.1.1] and [8.1.6]) occurring in different zones at the surface of the metal, which is an isolated electrode, with circulation of electrons from one zone to the other.

– The *cementation reaction* of copper by iron (see equation [8.5.1] and Figure 8.5.1) is also an electrochemical reaction:

$$Cu^{2+} + Fe(s) \rightarrow Cu(s)\downarrow + Fe^{2+} \quad [8.1.9]$$

In these electrochemical reactions, the electrons are transferred from one ion to the other by an electronic conductor over several atomic distances (see Figure 8.5.1).

This chapter deals with redox electrochemical reactions by elementary electrochemical reactions occurring on an isolated electrode that involve only thermal and chemical energies. The reactions involving electrical energy include electrolysis, where the electrochemical reactions occur on two electrodes connected by an electronic conductor. These are dealt with in [VIG 11b], Chapter 2. The electrochemical reactions of pyrometallurgy – reduction of an oxide by CO(g) or C(s) and the "metal-slag" reactions – are dealt with in [VIG 11b], Chapters 4 and 5, sections 4.1.3 and 5.4 respectively.

8.2. Equilibrium electric potential of an elementary electrochemical reaction

8.2.1. *Nernst equation*

The basic thermo-dynamic quantity of an elementary electrochemical reaction at equilibrium is the *equilibrium potential* of the reaction. This potential can be obtained from the electrochemical potential μ_{el} of an electrically charged species:

$$\mu_{el} = \mu_{chem} + q\Phi = \mu_{chem} + zF\Phi \qquad [8.2.1]$$

where μ_{chem} is the chemical potential, q is the charge of the species q = zF, and Φ is the electrical potential at the location of the charged species[1].

We consider the elementary electrochemical reduction [8.1.2]:

$$M^{z+} + ze \rightarrow M(s)\downarrow \qquad [8.2.2]$$

When an isolated metallic electrode is dipped into an aqueous solution of one of its salts, a "double layer" is formed at the metal-solution interface with a distribution of electric charges as in a condenser. The metal then reaches a potential Φ_M and the solution around the interface a potential $\Phi_{M^{z+}}$. The potential between the metal and the solution, which is called the *electrode potential* or *metal-solution potential*, is:

$$E_{M/M^{z+}} = \Phi_M - \Phi_{M^{z+}} \qquad [8.2.3]$$

Expression of the electrochemical potential of a metal ion M^{z+} in its metal, at the electric potential Φ_M is:

$$\mu_{M(el)} = \mu^\circ_M + zF\Phi_M \qquad [8.2.4]$$

where μ°_M is the standard chemical potential of the metal.

---

1 F = 96,485 coulomb/mole = 96,485 J/volt/eq.g. If μ is expressed in calories per mole, F = 23,060 cal/volt/eq.g.

Expression of the electrochemical potential of an ion in an electrolytic solution, see equations [1.3.46] and [4.2.6], is:

$$\mu_{M^{z+}(el)} = \mu_{M^{z+}} + zF\,\Phi_{M^{z+}} = \mu^{o}_{M^{z+}} + RT \ln \tilde{a}_{M^{z+}} + zF\,\Phi_{M^{z+}} \qquad [8.2.5]$$

where $\tilde{a}_{Mz+} = f_{Mz+} \,.\, [M^{z+}]$, where $[M^{z+}]$ is the molar concentration of the ion in the electrolytic solution and $\mu°_{Mz+}$ is the standard chemical potential of the ion (see the second note in Chapter 4).

When equilibrium is established between the isolated metallic electrode and the solution, the electrochemical potentials of the ions in their phases are identical and the equilibrium electrode potential is equal to[2]:

$$E^{*}_{M/M^{z+}} = (\mu_{M^{z+}} - \mu_{M}) / zF = A_{chem(reduction)} / zF \qquad [8.2.6]$$

The chemical affinity of the reduction reaction is defined by equation [1.3.14].

So, for the elementary reaction [8.2.2] for an electrode made of metal M, the equilibrium electrode potential is given by the Nernst equation:

$$E^{*}_{M/M^{z+}} = E^{o}_{M/M^{z+}} + (RT / zF) \,.\, \log\, \tilde{a}_{M^{z+}} \qquad [8.2.7]$$

where $E°_{M/Mz+}$ is the standard (normal) electrode potential:

$$E^{o}_{M/M^{z+}} = \{\mu^{o}_{M^{z+}} - \mu^{o}_{M}\} / zF = \mu^{o}_{M^{z+}} / zF \qquad [8.2.8a]$$

at 25°C:

$$E^{*}_{M/M^{z+}} = E^{o}_{M/M^{z+}} + (0.0591 / z) \,.\, \log\, \tilde{a}_{M^{z+}} \qquad [8.2.8b]$$

for the reaction:

$$Fe^{2+} + 2\,e \rightarrow Fe(s)$$

$$E^{*}_{Fe/Fe^{z+}} = -\,0.440 + 0.0295 \log[Fe^{2+}] \text{ in volts at 25°C}$$

---

2 If the reaction is written in the reverse order, $M(s) \rightarrow M_{z+} + ze$ (oxidation), the metal solution potential is equal to: $E^{*}_{M/Mz+} = (\mu_{M} - \mu_{M^{-z+}}) / -zF$.

If the potential of the electrode is changed to a more positive value than the equilibrium potential $E_{appl} > E^*_{M/Mz+}$, the reaction will proceed in the direction of oxidation (anodic dissolution), see reaction 8.1.1 and Figure 8.4.4:

$$\text{when } E_{appl} > E^*_{M/M^{z+}}, \text{ then } M(s) \rightarrow M^{z+}_{(dissolved)} + ze \qquad [8.2.9a]$$

If the potential of the electrode is changed to a more negative value than the equilibrium potential, the reaction will only proceed on this electrode in the direction of a reduction (see reaction [8.1.2]):

$$\text{when } E_{appl} < E^*_{M/M^{z+}}, \text{ then } M^{z+}_{(dissolved)} + ze \rightarrow M(s) \qquad [8.2.9b]$$

For an electrochemical reduction, such as:

$$\nu_A A_{(oxidized\ form)} + \nu_B B + ze \rightarrow \nu_R R_{(reduced\ form)} + \nu_S S \qquad [8.2.10a]$$

where species A, B, R or S can be ions or neutral species, the expression of equilibrium potential is:

$$E^* = A_{(chem)} / zF = -\Delta G_{(chem)} / zF \qquad [8.2.10b]$$

where:

$$E^\circ = A^\circ / zF = (\nu_A \mu^\circ_A + \nu_B \mu^\circ_B - \nu_R \mu^\circ_R - \nu_S \mu^\circ_S) / zF \qquad [8.2.10c]$$

For an electrochemical reduction in an aqueous medium:

$$\alpha A_{(oxidized\ form)} + cH_2O + ze \rightarrow \beta B_{(reduced\ form)} + mH^+ \qquad [8.2.11]$$

the expression of the equilibrium potential is:

$$E^* = E^\circ + (0.0591 / z) \,.\, \{m \,.\, pH + \log[A]^a / [B]^b\} \qquad [8.2.12]$$

with:

$$E^\circ = \{a\mu^\circ_A + c\mu^\circ_{H2O} - b\mu^\circ_B\} / 23{,}060\ z \qquad [8.2.13]$$

where $m > 0$ if a H^+ is in the second member of the reaction; $m < 0$ if H^+ is in the first member; $c > 0$ if H_2O is in the first member; and $c < 0$ if H_2O is in the second member of the reaction.

EXAMPLE 1.–

$$Cl_2(g) + 2\ e \rightarrow 2\ Cl^- \qquad [8.2.14]$$

$\mu°_{Cl^-} = -31{,}350$ cal

$E^* = 1.359 + 0.0295 \log\{p_{Cl2} / [Cl^-]^2\}$

EXAMPLE 2.–

$$CuO(s) + 2\ H^+ + 2\ e \rightarrow Cu(s) + H_2O \qquad [8.2.15]$$

$m = -2$; $\mu°_{CuO} = -30{,}400$ cal

$E^* = 0.570 - 0.0591\ pH$

EXAMPLE 3.–

$$Fe_3O_4(s) + 8\ H^+ + 2\ e \rightarrow 3\ Fe^{2+} + 4\ H_2O \qquad [8.2.16]$$

$m = -8$; $\mu°_{Fe3O4} = -242{,}400$ cal; $\mu°_{Fe2+} = -20{,}300$ cal

$E^* = 0.981 - 0.2364\ pH - 0.0885 \log [Fe^{2+}]$

EXAMPLE 4.–

$$CuO_2^- + 4\ H^+ + e \rightarrow Cu^{2+} + 2\ H_2O \qquad [8.2.17]$$

$m = -4$; $\mu°_{CuO_2^-} = -26{,}800$ cal; $\mu°_{Cu^{2+}} = 15{,}530$ cal

$E^* = 3.078 - 0.2364\ pH + 0.0591 \log [CuO_2^-] / [Cu^{2+}]$

8.2.2. *Electrode potentials in aqueous solutions*

The *metal/solution potential* that is also called the *electrode potential* can only be measured with respect to a reference electrode. To do so, we consider an electrolysis cell, see [VIG 11b], Chapter 2, Figure 2.1.1, with the metallic electrode

M, immersed in the considered solution on which the reaction [8.1.1] occurs, and a reference electrode. Let V stand for the voltage of the cell (without considering the Ohmic drop in the electrolyte):

$$V = E^{*}_{M/M^{z+}} - E_{ref} \qquad [8.2.18]$$

8.2.2.1. *Reference electrode*

In an aqueous solution, the reference electrode is the standard hydrogen electrode on which water is reduced with evolution of hydrogen, see reaction [8.1.6]:

$$2\ H^{+}_{(aq)} + 2\ e \rightarrow H_2(g) \qquad [8.2.19]$$

$$E^{*}_{(H2/H+)} = -0.0591\ pH - 0.0295\ p_{H_2} \qquad [8.2.20]$$

in standard conditions: under a hydrogen pressure of 1 atm and a value of pH = - log $[H^+]$ = 0 at a temperature of 298.1°K (see equation [4.2.15]):

$$E^{o}_{H_2/H^+} = (2\ \mu^{o}_{H^+} - \mu^{o}_{H_2}) / 2\ F = 0$$

By convention, the equilibrium potential of the standard hydrogen electrode is equal to zero. As $\mu^{o}_{H_2} = 0$, then $\mu^{o}_{H^+} = 0$ and:

$$E^{*}_{H_2/H^+} = E^{o}_{H_2/H^+} - 0.0591\ pH - 0.0295\ p_{H_2} \qquad [8.2.21]$$

8.2.2.2. *Standard electrode potentials* $E^{o}_{M/M^{z+}}$ *in aqueous solutions*

Table 8.2.1 presents the standard potentials in aqueous solutions for a given number of metals at 25°C. The standard electrode potentials of the noble metals (Au, Ag, Pt and Cu) are positive. The standard electrode potentials of the metals Pb, Sn, Ni, Fe, Zn and Al are negative. These standard potentials vary with the temperature. Some values of the electrode potentials of iron and nickel are available for temperatures of up to 300°C [CHE 83].

Metal	Ion	Potential (V)
Au	Au^{3+}	1.51
Pt	Pt^{2+}	1.2
Ag	Ag^{+}	0.799
Cu	Cu^{2+}	0.337
Pb	Pb^{2+}	-0.126
Sn	Sn^{2+}	-0.136
Ni	Ni^{2+}	-0.257
Cd	Cd^{2+}	-0.402
Fe	Fe^{2+}	-0.44
Cr	Cr^{3+}	-0.74
Zn	Zn^{2+}	-0.763
Al	Al^{3+}	-1.66
Ti	Ti^{4+}	-1.75
Mg	Mg^{2+}	-2.03
Na	Na^{+}	-2.71
K	K^{+}	-2.922
Li	Li^{+}	-3.02

Table 8.2.1. *Standard electrode potentials ($E^{O}_{M}/_{M^{2+}}$), also known as standard dissolution potentials or standard equilibrium potentials [POU 73, LAT 64]*

8.2.2.3. *Metal-complex electrode potential*

The oxidation potential of an redox electrochemical leaching reaction, and thus the leaching conditions, can be significantly lowered if the reaction occurs with the formation of a complex or if a complexing reaction occurs. The standard electrode potential of a electrochemical redox reaction with formation of a complex can be calculated from the standard potential M/M^{z+} and from the stability constant of the complex ion, see Chapter 4, section 4.2.3 and Table 4.2.5.

For the reaction leading to the formation of chloride complexes:

$$M(s) + nCl^- \rightarrow MCl^{(n-z)-}(aq) + ze \qquad [8.2.22]$$

The expression of the metal-complex equilibrium potential is:

$$E^*_{M/MCl^{(n-z)-}} = E^o_{M/M^{z+}} - (RT / zF)\ \ln \beta - (n\ RT / zF)\ \ln \tilde{a}_{Cl^-} + (RT / zF) \ln \tilde{a}_{MCl^{(n-z)-}} \qquad [8.2.23]$$

where β or $K_{(STxy)}$ is the stability coefficient of the complex, see equation [4.2.45a].

Table 8.2.2 presents some values of the standard electrode potentials of chloro-complexes for different Cl^- ion contents of the electrolyte.

$$E^O_{M/MCl^{(n-2)-}} - (0.059 / z) \ln \beta - (0.059 / z)\ \log\left[Cl^-\right]^n$$

Activity a_{Cl^-}			**0.1**	**1**	**5**	**50**
Cu	$CuCl_3^{2-}$	Cu^{2+} / Cu 0.340V	0.343	0.166	0.042	– 0.094
Ag	$AgCl_2^-$ / Ag	Ag^+ / Ag 0.799		0.480	0.397	0.279
Au	$AuCl_2^-$ / Au	Au^+/Au 1.71	1.27	1.15	1.07	0.95
	$AuCl_4^-$ / Au	$Au^{3+/}$Au 1.51	1.08	1.00	0.945	0.87
Pt	$PtCl_4^{2-}$ / Pt	Pt^{2+} / Pt 1.2	0.85	0.73	0.65	0.53
	$PtCl_6^{2-}$ / Pt		0.74	0.68	0.64	0.54
Pd	$PdCl_4^{2-}$ / Pd	Pd^{2+} / Pd 0.92	0.74	0.62	0.54	0.42
Rh	$RhCl_6^{3-}$ / Rh	Rh^{3+} / Rh 0.758	0.55	0.431	0.348	0.23

Table 8.2.2. *Electrode potentials of some metal-chloro-complexes at various chloride ion activities at 25°C (see equation [8.2.23]) [PUY 03]*

The electrolysis of a chloro-complex will require a higher consumption of electric energy than the electrolysis of a simple chloride, see [VIG 11b], Chapter 2, section 2.3.2. Conversely, the leaching of a metal forming complexes will be easier, see section 8.5.2.

The formation of a complex can change the redox properties of a redox couple. For instance, for the reaction:

$$Co^{3+} + e \rightarrow Co^{2+} \quad E°_1 = 1.82 \text{ V} \qquad [8.2.24]$$

The valence three of cobalt cannot exist in aqueous solutions. It is stabilized by cyanide ions (see Chapter 4, section 4.2.3.5, reactions [4.2.55] and [4.2.56]), and the equilibrium potential of the Co^{3+}/Co^{2+} couple in the presence of cyanide ions is:

$$E^*_2 = E°_1 + 0.06 \log \beta_2/\beta_1 + 0.06 \log[Co(CN)_6^{3-}] / [Co(CN)_6^{4-}] \qquad [8.2.25]$$

leading to a strong decrease of the standard equilibrium potential:

$$E°_2 = E°_1 + 0.06 \log \beta_2/\beta_1 = 1.82 - 2.64 = -0.78 \text{ V}$$

8.2.3. *Equilibrium potential metal/ion* $E_{M/M^{z+}}$ *in molten salts*

Lithium, sodium, calcium and magnesium are obtained by electrolysis in molten salts (see [VIG 11c], Chapter 9, sections 9.1 and 9.2).

8.3. Electrochemical equilibria of metals and metalloids (Pourbaix diagrams)

The Pourbaix diagrams [POU 73, POU 82] or potential-pH equilibrium diagrams have been designed and are used for the interpretation and prediction of corrosion phenomena. They are also quite useful for the prediction or rationalization of specific processes, such as:

– the leaching of metals, oxides and sulfides in hydrometallurgy;

– the precipitation of metals from aqueous phases (electrolytic deposition) that are reduction reactions;

– the precipitation of hydroxides from ions in solution (acid-base reactions).

These diagrams present the stability regions of the solid species and the predominance regions of the dissolved species: ions and complexes, as a function of two parameters: the pH of the solution and the potential where the electrochemical reaction occurs. This potential can be external in the case of electrolysis. In the case of an isolated electrode, or for an electrochemical reaction between two dissolved species (see reaction [8.1.4a]), the potential can be fixed by the partial pressure of oxygen above the solution, which sets the potential of the cathodic reduction of oxygen dissolved in water (see equation [8.1.4b]). The potential scale of a Pourbaix

diagram is an oxygen pressure scale. These diagrams indicate the operating conditions required for the desired reaction to occur.

8.3.1. *Diagram of electrochemical equilibria of water*

In Figure 8.3.1 there are two straight lines, a and b (line a corresponds to p_{H_2} = 1 atm, and line b corresponds to p_{O_2} = 1 atm), that *outline* the following regions:

– the thermodynamic stability of water between the two oblique lines a and b;

– reduction of hydrogen ions with the liberation of $H_2(g)$ below line a: water, under a pressure of hydrogen of 1 atm, will tend to decompose by reduction according to reaction [8.2.19];

– oxidation of water with the liberation of oxygen, above line b. Water under an oxygen pressure of 1 atm will tend to decompose according to the reaction:

$$2\ H_2O \rightarrow O_2(g) + 4\ H^+ + 4\ e \qquad [8.3.1a]$$

$$E^* = 1.28 - 0.59\ pH + 0.0148 \log\ p_{O_2} \qquad [8.3.1b]$$

(see reaction [8.1.7]).This expression is established in [VIG 11b], Chapter 2, section 2.3.1 and equation [2.3.4].

NOTE.– The oxidation of water can occur under potentials lower than those of line b in Figure 8.3.1, for oxygen partial pressures <1 atm.

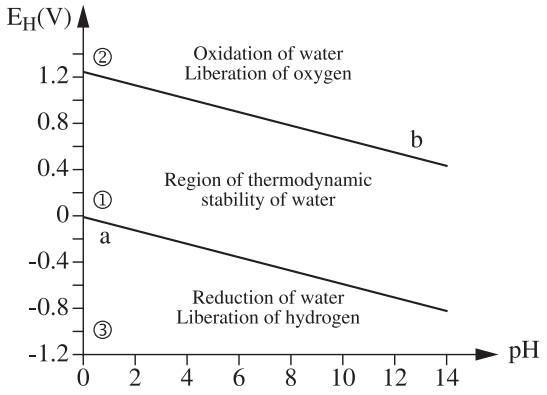

Figure 8.3.1. *Potential pH equilibrium diagram for water under a pressure of 1 atm at 25°C [POU 73]*

In regions 1 and 3, the reduction of oxygen dissolved in water (or reduction of hydrogen ions with the formation of water) occurs (see inverse reaction [8.3.1], and also Chapter 4, section 4.2.6):

$$O_2(aq) + 4\ H^+ + 4\ e \rightarrow 2\ H_2O \qquad [8.1.4b/8.3.2]$$

often written as (see reaction [8.2.11]):

$$O_2(aq) + 2\ H_2O + 4\ e \rightarrow 4\ OH^- \qquad [8.3.3]$$

The oxygen partial pressure above the bath sets the oxidizing power of the aqueous solution. This cathodic reaction is the driving force of the corrosion of a metal as it consumes the electrons released by reaction [8.1.1].

8.3.2. *Pourbaix diagram for metal-water systems*

NOTE.– The E-pH (E_H-pH)[3] Pourbaix diagrams of the M-H_2O systems are drawn by only considering the reactions that can occur between the solid species, metal, oxides, hydroxides, M^{x+} cations and MeO_2^{2-} anions, which can exist in a non-complexing acidic medium (the pH is obtained by adding ClO_4H). In alkaline media, only the predominance regions of the complexes formed with OH^- anions are shown on these diagrams. Some Pourbaix diagrams, taking into account the formation of complex ions in acidic medium (ClH, SO_4H_2) and basic medium (NH_3) are then presented.

8.3.2.1. *Pourbaix diagram for the copper-water system*

As an example, the basic diagram of the copper-water system at room temperature is presented[4] (see Figure 8.3.2a).

It is made up of:

– Parallel bold and continuous oblique straight lines separating the stability regions of two condensed (solid) phases (metal and oxide or hydroxide), such as line I, for instance, which corresponds to the equilibrium between copper and the copper oxide Cu_2O according to the reaction (see reaction [8.2.15]):

$$Cu_2O(s) + 2\ H^+ + 2\ e \rightarrow 2\ Cu(s) + H_2O \qquad [8.3.4a]$$

$$E° = 0.471 - 0.0591\ pH \qquad [8.3.4b]$$

3 E_H is used to indicate that the reference potential is the potential of the ESH (standard hydrogen) electrode.

4 For an exhaustive presentation of this diagram, see [POU 73].

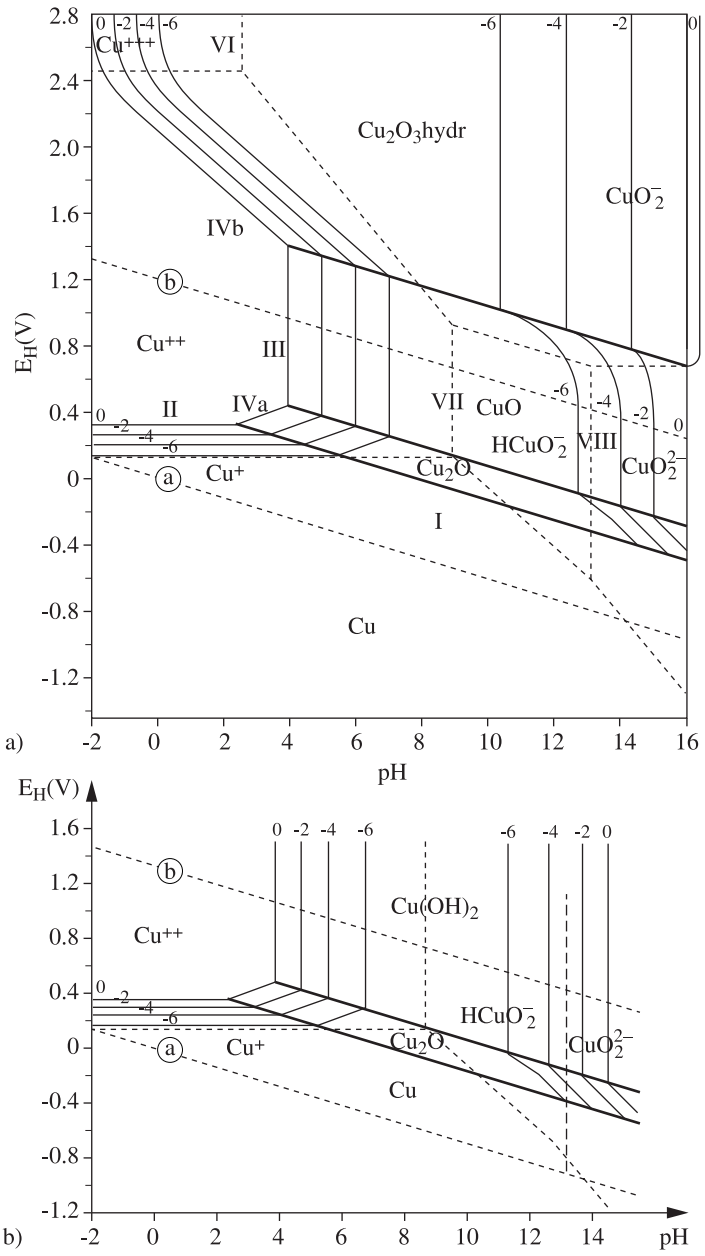

Figure 8.3.2. *Pourbaix diagrams for the copper-water system at 25°C (thick full lines – regions of relative stability of solid species; broken lines – regions of relative predominance of dissolved bodies; thin full lines – heterogeneous reactions in which one solid species participates (solubility of solid species) [POU 73]*

For pH and potential conditions below this line, reduction of the copper oxide occurs, and conversely, above this line oxidation of copper by H_2O. The oxidation potential of copper is above line a. Copper in contact with water is stable as long as there is no oxygen. Parallel oblique lines, which correspond to increasing oxygen potentials, separate the Cu_2O/CuO region from the CuO/Cu_2O_3 one. These lines are parallel to line a, the latter line corresponding to the cathodic reduction of water.

The lines for equilibria between solid phases are fixed and independent of the amounts of solids. The lines for equilibria between solid phases and dissolved species depend on their concentration.

– A family of thin parallel straight horizontal continuous lines II, marked $^{-}6$; $^{-}4$; $^{-}2$; 0 separating the copper stability region from the predominance region of ion Cu^{2+}. Each line corresponds to a given value of ion concentration ($\log[Cu^{2+}]$) in the solution in equilibrium with the metal, from 10^{-6} to 1 mol/kg (or 1 mol/L), in solution:

$$Cu \rightarrow Cu^{2+} + 2\ e \qquad [8.3.5a]$$

Each line gives the dissolution Cu/Cu^{2+} potential, corresponding to ions in the solution (see equation [8.2.8b]):

$$E^* = 0.337 + 0.0295 \log[Cu^{2+}] \qquad [8.3.5b]$$

The line marked as zero corresponds to a normal concentration of Cu^{2+} ions. In order to get an electrolytic copper deposit from an acidic solution of these ions, a potential has to be applied to the cathode, such as $E_{appl} < E$ of the electrode. Conversely, for a fixed applied potential dissolution of the metal continues as long as the concentration of Cu^{2+} ions in the solution remains lower than the concentration corresponding to the fixed potential.

For increasing p_{O2} pressures, the potential E of the solution increases. This makes the solution more oxidizing and the amount of Cu^{2+} ions that can be dissolved in water also increases. The concentration of ions, in equilibrium with copper, increases with p_{O2}. The potential scale is in fact an oxygen pressure scale p_{O2}.

– A family of vertical straight continuous lines separating the predominance region of the Cu^{2+} ion and stability region of the solid phase CuO or $Cu(OH)_2$. It gives the pH of the solution for ion concentration, beyond which the precipitation of $CuO(s)\downarrow$ (or of $Cu(OH)_2(s)$) occurs below which the oxide is dissolved to give ions (leaching). These lines correspond to acid-base reactions (see [VIG 11b], Chapter 1, reaction [1.2.1]). For instance:

$$CuO(s) + 2\ H^+ \rightarrow Cu^{2+} + H_2O \qquad [8.3.6a]$$

$$\log[Cu^{2+}] = 7.89 - 2\ pH \qquad [8.3.6b]$$

For a pH higher than the one corresponding to a vertical line, precipitation of the oxide occurs as long as the concentration of Cu^{2+} ions remains higher than the concentration corresponding to the considered line. For a lower pH, dissolution (leaching) of the oxide occurs as long as the ion concentration in solution is lower than the considered line's concentration.

For high pH, dissolution of the oxide in alkaline medium occurs:

$$CuO(s) + H_2O \rightarrow CuO_2^{2-} + H^+ \qquad [8.3.7a]$$

$$\log[CuO_2^{2-}] = -32 + 2\ pH \qquad [8.3.7b]$$

These dissolution reactions are written by considering that the ions present in the solution are $HCuO_2^-$ and CuO_2^{2-}:

$$CuO(s) + OH^- \rightarrow HCuO_2^- \qquad [8.3.8]$$

$$\log[HCuO_2^-] = -18.83 + pH \text{ at } 25°C$$

$$CuO(s) + 2\ OH^- \rightarrow CuO_2^{2-} + H_2O \qquad [8.3.9]$$

$$\log[CuO_2^{2-}] = -31.98 + pH \text{ at } 25°C$$

whereas the ions in solution are $Cu(OH)_4^{2-}$, see Chapter 4, Figure 4.2.14.

– A family of oblique continuous lines, IV a and b, corresponding to an electrochemical precipitation of Cu_2O and Cu_2O_3 oxides:

$$2\ Cu^{2+} + H_2O + 2\ e \rightarrow Cu_2O(s)\downarrow + 2\ H^+ \qquad [8.3.10a]$$

$$E^* = 0.203 + 0.0591\ pH + 0.0591 \log[Cu^{2+}] \qquad [8.3.10b]$$

and:

$$2\ Cu^{2+} + 3\ H_2O \rightarrow Cu_2O_3 \downarrow + 6\ H^+ + 2\ e \qquad [8.3.11a]$$

$$E = 2.114 - 0.18\ pH - 0.0591 \log[Cu^{2+}] \qquad [8.3.11b]$$

By increasing the pH, the oxide precipitates. By decreasing the pH, the oxide is dissolved.

– The dashed lines separate the predominance regions of two ions in solution. For the equilibrium between two species dissolved in solution, the line drawn

corresponds to equal ion concentrations in both phases. For instance, line VI (2.42 V) separates the predominance regions between the Cu^{2+} and Cu^{3+} ions. In the predominance region of the Cu^{2+} ion, the reaction $\{Cu^{3+} + e \rightarrow Cu^{2+}\}$ evolves in the indicated direction. In the predominance region of the Cu^{3+} ion, the above reaction evolves in the opposite direction.

– The vertical dashed line VII, at pH 8.9 separating the predominance regions of Cu^{2+} and $HCuO_2^-$ ions, corresponds to the equilibrium for which the activities of the ions are equal:

$$Cu^{2+} + 2\ H_2O \rightarrow HCuO_2^- + 3\ H^+ \qquad [8.3.12a]$$

with:

$$\log[HCuO_2^-] / [Cu^{2+}] = -26.72 + 3\ pH \qquad [8.3.12b]$$

It corresponds to a pH of 26.72 / 3 = 8.91.

– The vertical dashed line VIII corresponds to the equilibrium of $HCuO_2^-/CuO_2^{2-}$ ions. The concentrations of these complex ions are equal at pH 13. When pH <13, the $HCuO_2^-$ ion concentration is predominant and vice versa when pH >13. We can see that as the concentrations of these ions are quite low, the solubility of the CuO oxide is considered equal to zero, even for alkaline pHs.

– A horizontal dashed line separates the predominance regions of the Cu^+ and Cu^{2+} ions. We remember that the Cu^+ ion is not stable in aqueous solution, see Chapter 4, equation [4.2.51].

NOTE.– Different Pourbaix diagrams can be drawn for the same system, depending on the dissolved species (the ions) and the solid species taken into account, because different solid oxidized species − especially the hydroxide and oxide ones − can be thermodynamically stable at the same pH and potential. For instance, the CuO oxide, see reaction [8.3.6] and Figure 8.3.2a, or $Cu(OH)_2$ hydroxide, see Figure 8.3.2b:

$$Cu^{2+} + 2\ H_2O \rightarrow Cu(OH)_2(s) + 2\ H^+ \qquad [8.3.13a]$$

$$\log[Cu^{2+}] = 9.21 - 2\ pH \qquad [8.3.13b]$$

8.3.2.2. *Pourbaix diagram for the iron-water, aluminium-water, and nickel-water systems*

These systems are presented in Figures 8.3.3 to 8.3.5.

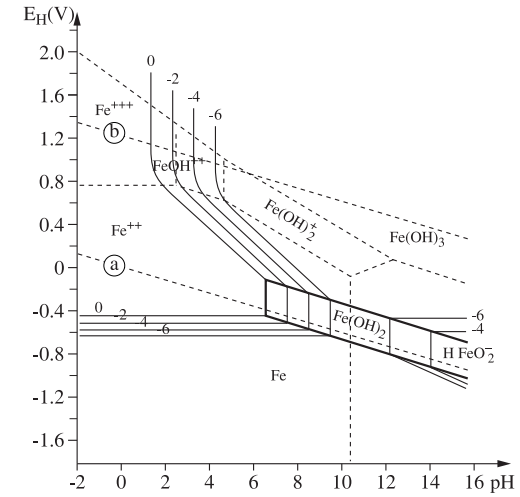

a)

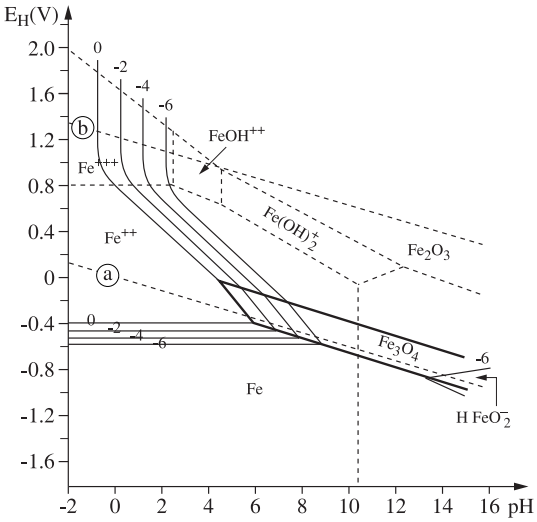

b)

Figures 8.3.3. *Pourbaix diagrams for the iron-water system at 25°C [POU 73]*

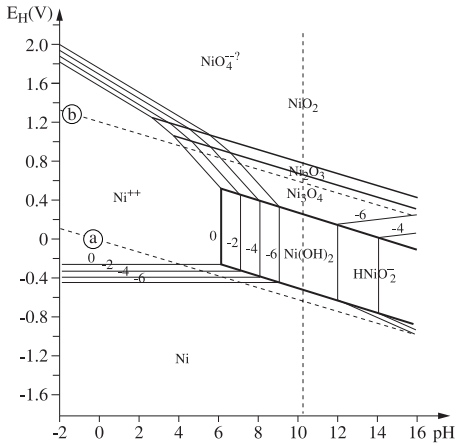

Figure 8.3.4. *Pourbaix diagram for the nickel-water system at 25°C [POU 73]*

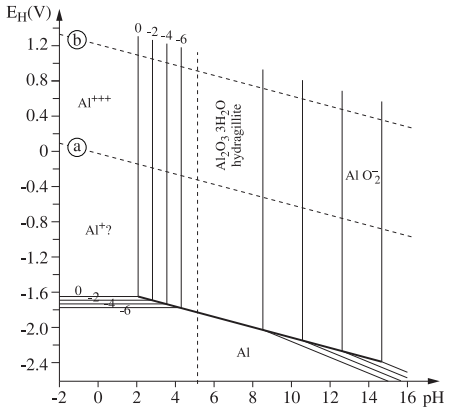

Figure 8.3.5. *Pourbaix diagram for the aluminum-water system at 25°C [POU 73]*

8.3.3. *Pourbaix diagram for the Fe, Cu and Zn-Cl-H_2O systems*

Fe^{2+}, Fe^{3+}, Ni^{2+}, Cu^{+}, Cu^{2+} and Zn^{2+} ions in aqueous chloride solutions form complexes that modify the stability and predominance regions of the redox couples, see Chapter 4, section 4.2.3.1. For the $FeCl_2(aq)$ and $FeCl_3(aq)$ species, the E-pH diagram (see Figure 8.3.6a) at a concentration of chloride ions $[Cl^-] = 1$, shows the existence regions of both compounds, for $[Fe^{2+}] = 1$ (continuous line) and 10^{-6} (dashed line):

$$Fe(s) + 2\ Cl^- \rightarrow FeCl_2(aq) + 2\ e \qquad [8.3.14]$$

$$E_2 = E_1 - 0.0591 \log[Cl^-]^2$$

and:

$$FeCl_2\,(aq) + Cl^- \rightarrow FeCl_3\,(aq) + e \qquad [8.3.15]$$

$$E_4 = E_3 - 0.0591 \log[Cl^-]$$

Pourbaix diagrams for different $[Cl^-]$ concentrations (see below and Figure 8.3.7) taking into account the complex $FeCl^+$ and $FeCl_2^+$ ions are presented in Figures 8.3.6b and c as a result of reactions:

$$Fe + Cl^- \rightarrow FeCl^+ + e$$

$$FeCl^+ + Cl^- \rightarrow FeCl_2^+ + e$$

$$FeCl^+ + 2\,H_2O \rightarrow \alpha\ FeOOH(s) + 3\,H^+ + Cl^- + 2e$$

$$FeCl_2^+ + 2H_2O \rightarrow \alpha\ FeOOH(s) + 3H^+ + 2\,Cl^-$$

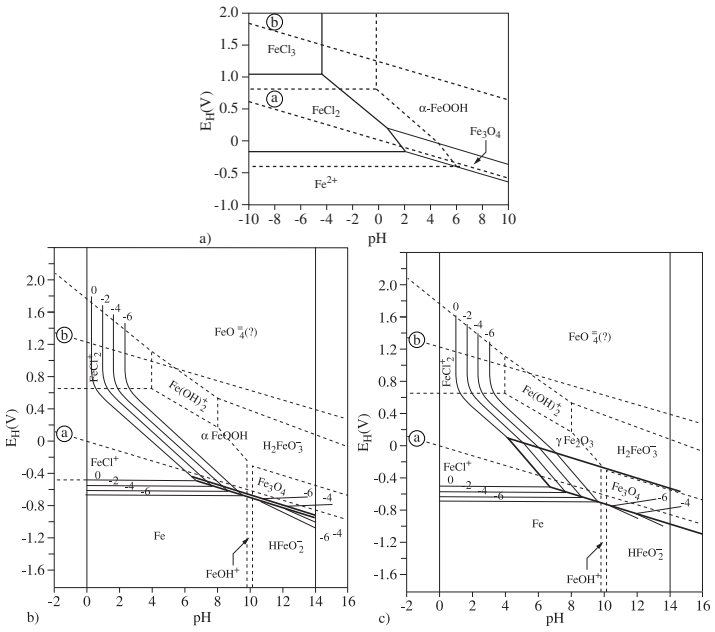

Figure 8.3.6. *Pourbaix diagrams for the Fe-Cl-H_2O system at 25°C: a) considering $FeCl_2$ and $FeCl_3$ ($a_{Cl^-} = 1$, $^-a_{Fe2+} = 1$, $a_{Fe2+} = 10^{-6}$); considering $FeCl^+$ and $FeCl_2^+$ complexes for b) the α ferric oxides and c) the γ ferric oxides [CHE 83]*

The oxidation potential of a metal with the formation of a complex ion depends on the complexing ion content in the solution, see equation [8.2.23]. The E-log a_{Cl^-} diagrams show the influence of Cl^- ion concentration on the predominance regions of the complex ions that can be formed, see Figure 8.3.7 and Chapter 4, Table 4.2.6. As in a Pourbaix diagram, we can observe two different types of separation lines: vertical lines corresponding to acid-base complexing reactions that are characterized by their stability coefficient (see Chapter 4, equation [4.2.45]); and oblique lines corresponding to elementary electrochemical reactions.

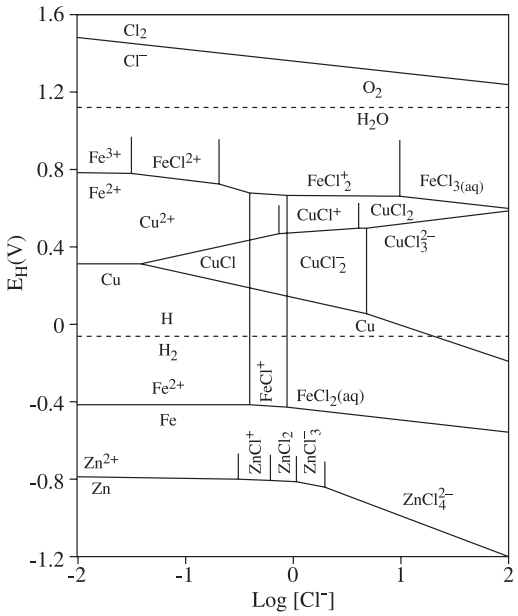

Figure 8.3.7. *Eh-log[Cl⁻] diagram at 25°C for the Fe-Cl-H_2O, Cu-Cl-H_2O and Zn-Cl-H_2O systems (pH = 1; $[M^{z+}] = 0.1$) [SEN 03]*

8.3.4. *Pourbaix diagrams for the M-NH_3-H_2O systems*

In an ammoniacal medium, metal ions such as copper, nickel, cobalt, silver, gold or platinum form complex ions that are soluble in water, see section 4.2.3.4:

$$Ni^{2+} + nNH_3(aq) \rightarrow Ni(NH_3)_n^{2+} \qquad [8.3.16]$$

where n can vary from 1 to 6, see section 4.2.3.5.

The formation of these complex ions increases Ni^{2+} or Co^{2+} ion solubility, which leads to a reduction in the stability region of the oxide or hydroxide. The predominance regions of these complex ions in a Pourbaix diagram take up part of the stability domain of the oxide or hydroxide, see Figures 8.3.8a and b. The vertical lines separating the two regions correspond to equal ion concentrations in their respective solutions. The complex ions' stability regions expand at the expense of NiO (or $Ni(OH)_2$ when the $[NH_3]$ / $[Ni^{2+}]$ ratio increases).

In the case of cobalt, the Pourbaix diagram shows the predominance region for the $Co(NH_3)_6^{3+}$ complex (see Figure 8.3.8b). The valence (III) of cobalt is stabilized in an aqueous ammoniacal medium, see Chapter 4, section 4.2.3.5.

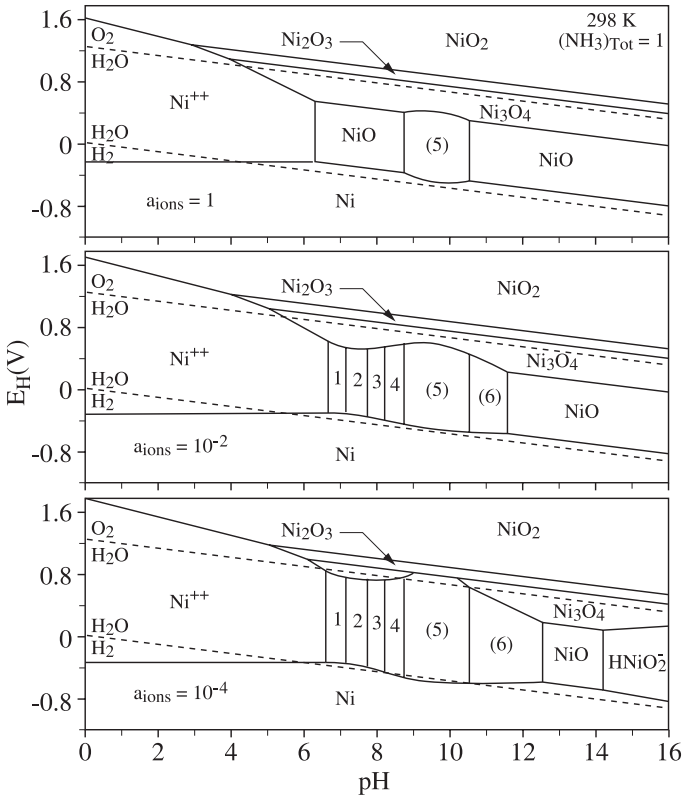

Figure 8.3.8a. *Pourbaix diagrams for the Ni-NH_3-H_2O system at 25°C at 1atm, a_{NH3} = 1 / 1-$Ni(NH_3)^{2+}$; 2-$Ni(NH_3)_2^{2+}$,... 6-$Ni(NH_3)_6^{2+}$ [HAN 93]*

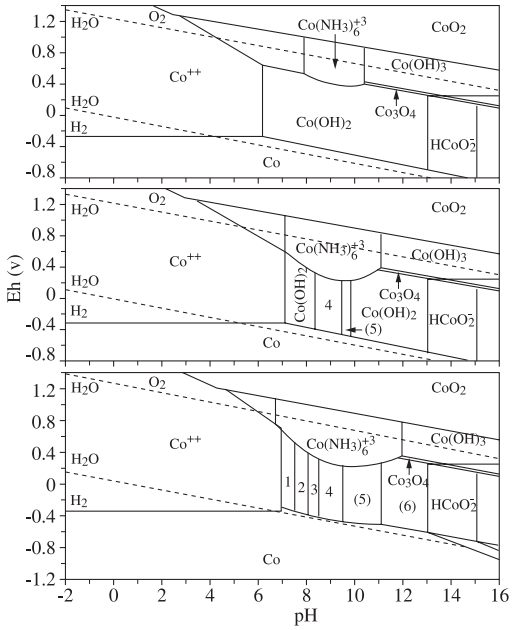

Figure 8.3.8b. *Diagrams for the Co-NH_3-H_2O system at 25°C at 1 atm, a_{NH3} =1 for $a_{CO}{}^{++}10^{-4}$, 10^{-2}, 1 (as in Figure 8.3.8a)/ 1-$Co(NH_3)^{2+;}$ 2-$Co(NH_3)_2{}^{2+}$,… and $Co(NH_3)_6{}^{3+}$ [HAN 93]*

8.3.5. *Pourbaix diagrams for the M-HCN-H_2O systems*

The diagram of the HCN-H_2O system is presented in Figure 8.3.9. Both the Au-H_2O and Au-HCN-H_2O diagrams (see Figures 8.3.10a and b) illustrate the increase of gold solubility due to the formation of the $Au(CN)_2^-$ complex, which stabilizes the Au^+ ion (see Chapter 4, reaction [4.2.54]).

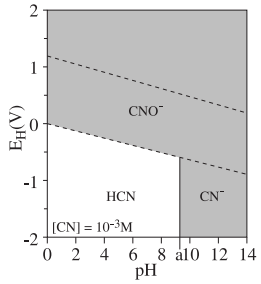

Figure 8.3.9. *Pourbaix diagram for the HCN-H_2O system at a -> $[CN^-]$ / [HCN] = 1*

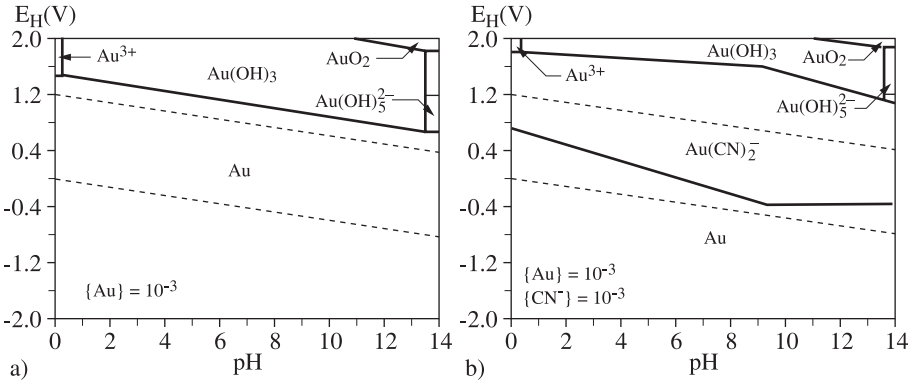

Figure 8.3.10. *Pourbaix diagrams: a) for the Au-H_2O system [Au] = 10^{-3}M; and b) Au-CN-H_2O system (gold in cyanide solution [Au] =[CN^-] = 10^{-3}M) [DAG 89]*

8.3.6. *Pourbaix diagrams for the M-S-H_2O systems*

A Pourbaix diagram of the S-H_2O system is presented in Figure 8.3.11. The stability region of S° is quite small although relatively large metastable existence region of S° exists, see [VIG 11b], Chapter 1, Figure 1.2.6. As the oxidizing leaching processes of sulfides are quite significant, M-S-H_2O diagrams have been established for many metals, see Figure 8.3.12 [PET 76].

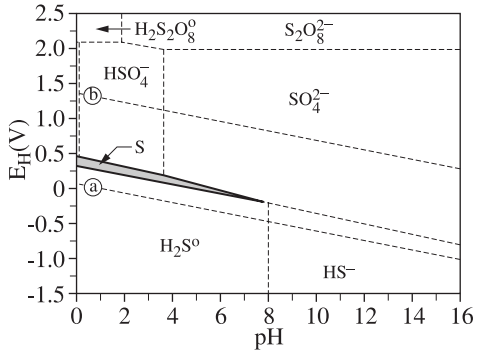

Figure 8.3.11. *Potential-pH diagram for the sulfur water system at 25°C [CHE 83]*

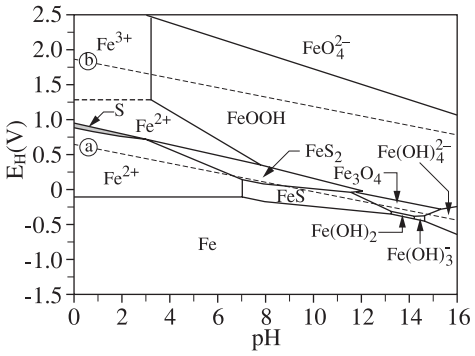

Figure 8.3.12. *Potential pH diagram for the iron-sulfur-water system at 25°C [CHE 83]*

8.4. Electrochemical kinetics

Figure 8.4.1 shows the different steps of the formation and growth of a metal deposit on an electrode, see reaction [8.1.2].

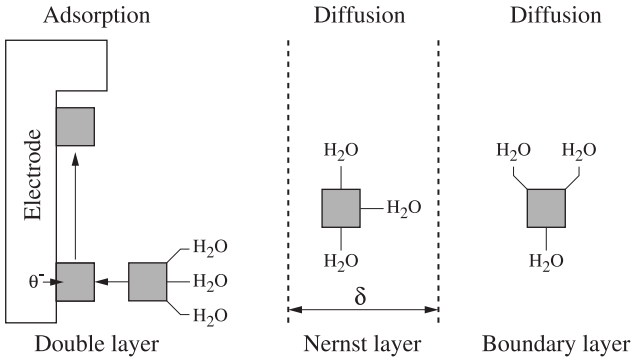

Figure 8.4.1. *Steps of the electrolytic deposition process: reaction M^{z+} + ze-> <M>(s) [OKE 92]*

The rate of an electrode process can be controlled by either the heterogeneous electrochemical reaction in the double layer or by a transport process in the Nernst diffusion layer or viscous boundary layer.

8.4.1. *Rate of an elementary electrochemical reaction: Tafel's Law*

The elementary electrochemical reaction is a heterogeneous reaction that occurs at the interface between a solution (electrolyte) and a metallic phase (electrode).

We consider an electrode made of metal M immersed in a solution of one of its salts. If there is no deposit (cathodic reduction) or dissolution of the metal (anodic oxidation), the system is in equilibrium and the potential of this electrode is given by equation [8.2.7].

An atom at the surface of the metal is an ion located in its own energy well. It is stabilized in this position by the gas of free electrons of the metal. In the same way, the M^{z+} ions are located in an energy well in the aqueous solution, see Figure 8.4.2.

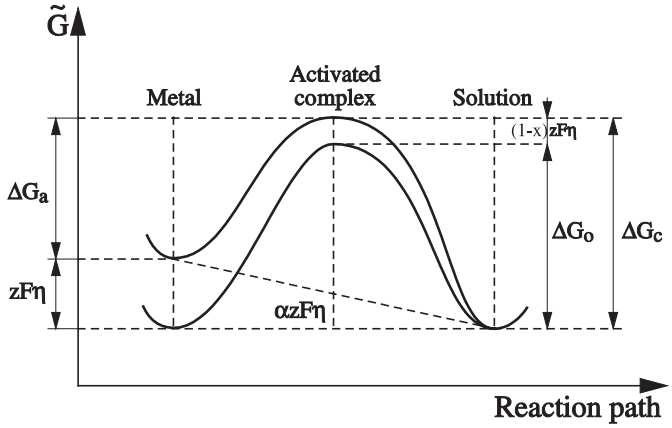

Figure 8.4.2. *Free energies diagram of a metal ion in its metal, in solution and as an activated complex*

Between two free energy minima, an energy extremum exists. For an atom to go into solution it has to jump over an energy barrier ΔG_a called the *activation energy*. Conversely, for the inverse reaction (deposition) the ion has to jump over an energy barrier ΔG_c. At equilibrium both activation energies are identical. If a potential is applied to the electrode that is higher or lower than its equilibrium potential E* (see Formula [8.2.9]), the activation energies become different. According to the theory of absolute reaction rates, the transfer rates towards one direction or the other can then be written, according to the Butler-Volmer's law, as:

$$i_a = zFk_a [M] \, . \, \exp(-\Delta G_a / RT) \qquad [8.4.1]$$

where:

$$\Delta G_a = \Delta G_0 - \alpha z F \eta \qquad [8.4.2]$$

and:

$$i_c = -zFk_c [M^{z+}] \,.\, \exp(-\Delta G_c / RT) \qquad [8.4.3]$$

where:

$$\Delta G_c = \Delta G_0 + (1 - \alpha)\, zF\eta \qquad [8.4.4]$$

where η is the over-potential:

$$\eta = E_{appl} - E^* \qquad [8.4.5]$$

The value of coefficient α, which is called the *transfer coefficient* is often close to 0.5. Much lower values have, however, been determined. For instance, for $Zn^{2+} \rightarrow Zn$ in a LiCl-KCl flux at 450 °C, $\alpha = 0.13$ (see Table 8.4.2).

Equations [8.4.1] and [8.4.3] can be rewritten[5]:

$$i_a = zFk_a [M] \,.\, \exp(-\Delta G_0 / RT) \,.\, \exp(\alpha\, z\, F\, \eta / PT) \qquad [8.4.6]$$

$$i_c = -zFk_c [M^{z+}] \,.\, \exp(-\Delta G_0 / RT) \,.\, \exp(-(1 - \alpha)\, z\, F\, \eta / PT) \qquad [8.4.7]$$

When the overpotential $\eta = 0$, we have:

$$i_a = i_c = i_0 \qquad [8.4.8]$$

where i_0 is called the *exchange current*:

$$i_0 = -zFk_c [M^{z+}] \,.\, \exp(-\Delta G_0 / RT) = zFk_a [M] \,.\, \exp(-\Delta G_0 / RT) \qquad [8.4.9]$$

which is usually written as:

$$i_0 = zFk'_c [M^{z+}] = zFk'_a [M] \qquad [8.4.10a]$$

5 In practice, for any reaction occurring on a pure metal (electrolytic deposit, cementation reactions): [M] = 1 ($a_M = 1$).

and that can also be written as:

$$i_0 = zF\ \{k'_a\,[M]\}^{(1-\alpha)}\ .\ \{k'_c\,[M^{z+}]\}^{\alpha} \qquad [8.4.10b]$$

when $\alpha = 1/2$:

$$i_0 = zF\ \{k'_a\,k'_c\}^{1/2}\,[M]^{1/2}\ .\ [M^{z+}]^{1/2} \qquad [8.4.10c]$$

By taking into account all these equations, we can re-write expressions [8.4.1] and [8.4.3] as:

$$i_a = i_O\ .\ \exp(\alpha zF\eta\ /\ RT) \qquad [8.4.11a]$$

and as:

$$i_c = -i_O\ .\ \exp(-(1-\alpha)\ zF\eta\ /\ RT) \qquad [8.4.11b]$$

which are known as *Tafel's law* or *equation* when written for the anodic branch, for instance, as:

$$\eta\ = a_a + b_a \log i_a \qquad [8.4.12]$$

The curves of the anodic and cathodic current variations as a function of over-potential η are drawn in Figure 8.4.3.

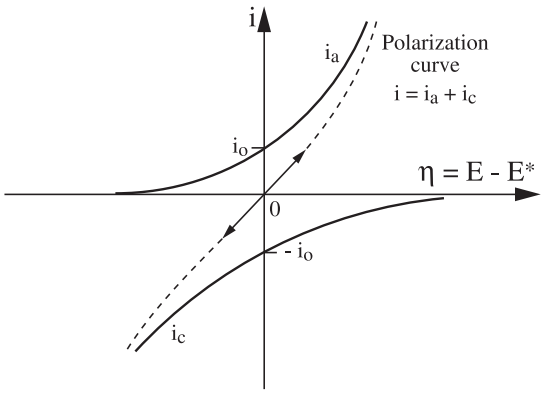

Figure 8.4.3. *Rate of an elementary electrochemical reaction (see formula [8.2.2]). Anodic and cathodic currents as a function of over-potential (polarization curve)*

The polarization curve is the sum of the anodic and cathodic currents:

$$i = i_a + i_c = f(\eta) \qquad [8.4.13]$$

is drawn as a function of the applied over-potential for a given concentration of the ion in solution.

If the potential applied to the electrode is lower than the Nernst reversible potential, $E_{app} < E^*$, the reaction will evolve towards a reduction (cathodic deposit). If a higher potential is applied, such as $E_{appl} > E^*$, the reaction will evolve towards a dissolution (anodic oxidation), see equations [8.2.9a] and [8.2.9b].

The polarization current i, proportional to i_O and the reversible potential E*, are a function of M^{z+} ion concentration in the double layer, see Figure 8.4.1. This concentration can be quite low due to the concentration gradient in the Nernst diffusion layer, see Figures 8.4.1 and 8.4.5a.

The exchange current i_O depends on the nature of the surface where the reaction occurs. Thus, for the reduction of water in a sulfuric solution, $H^+ + e \rightarrow 1/2\ H_2(g)$ (see equation [8.2.19]), the exchange current can vary be several orders of magnitude, see Table 8.4.1.

	i_O
Pt	$\times 10^{-2}$ to 10^{-3} A/cm^2
Pd, Rh	$\times 10^{-4}$ A/cm^2
Fe, Au	$\times 10^{-6}$ A/cm^2
Ni, Ag, Cu,	$\times 10^{-5}$ to 10^{-7} A/cm^2
Al, Sn	$\times 10^{-10}$ A/cm^2
Zn, Pb, Cd	$\times 10^{-11}$ A/cm^2

Table 8.4.1. *Exchange current densities for the reaction ($H^+ + e \rightarrow 1/2\ H_2(g)$) in sulfuric solution (1M H_2SO_4) [RIC 74, WES 65]*

In sulfuric aqueous solutions, the exchange currents for the cathodic reaction $Cu^{2+} + 2\ e \rightarrow Cu$ are of about 2×10^{-3} to 2×10^{-2} A/cm^2.

In molten salts (LiCl-KCL) at 450 °C, the exchange current densities are in the order of 1 to 2×10^2 A/cm^2 for ion concentration [1 mol/L], see Table 8.4.2.

Couple	*Electrode*	*i(A/cm²)*	*Coefficient of transfer α*
Cd^{2+}-Cd°	Cd	2.3×10^2	0.13
Zn^{2+}-Zn°	Zn	1.5×10^2	0.16
Pb^{2+}-Pb°	Pb	0.6×10^2	0.22
Ag^{2+}-Ag°	Ag	1.9×10^2	0.16
Ni^{2+}-Ni°	Ni	1.1×10^2	0.25
O^{2-}-O_2	Au	3×10^{-4}	

Table 8.4.2. *Exchange current densities and transfer coefficient α in molten salts (LiCl-KCl) at 450°C [RIC 74]*

In practice, a reaction is considered to be reversible when the value of its exchange current is equal to or greater than a value that has been relatively arbitrary chosen, such as 10^{-8} A/cm^2 for instance. It is considered to be irreversible for an exchange current lower than this value.

The polarization curves can present two different shapes, depending on the magnitude of the exchange current:

a) when the exchange current i_O is high (see Figure 8.4.4a), the reaction is reversible at low over-potentials. In this case, the diffusion limited current, imposed by the transport regime will be reached for low over-potentials η;

b) when the exchange current i_O is slow (see Figure 8.4.4b), the cathodic or anodic reaction rates become significant (appreciable) above an over-potential $\eta°_a$ or $\eta°_c$:

- an initial oxidation over-potential = $E^* + \eta°_a$, or
- an initial reduction over-potential = $E^* - \eta°_c$.

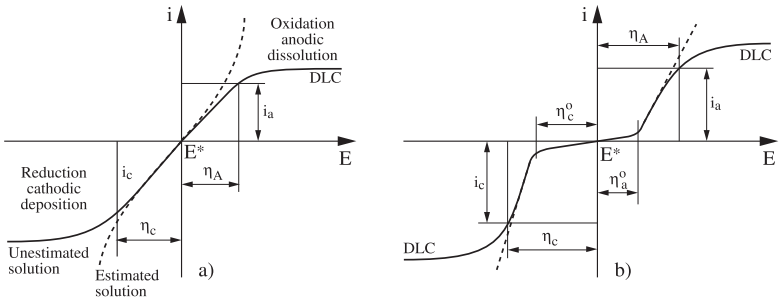

Figure 8.4.4. *Polarization curves of an elementary electrochemical reaction: a) exchange current i_0 high, $\eta°_a = \eta°_c \approx 0$, reversible reaction; and b) i_0 low, irreversible reaction (oxidation potential = $E^* + \eta°_a$ and reduction potential = $E^* - \eta°_c$)*

The more reversible the reaction is, the lower the over-voltage we need to apply, $\eta = E - E^*$, to achieve a current I, the lower the energy consumption is and vice versa. The cathodic reactions in chloride solutions are more reversible than in sulfate solutions, see [VIG 11b], Chapter 2, section 2.2.

NOTE.– These over-voltages lead us to construct Pourbaix diagrams, which not only represent the thermodynamic stability regions but also the metastability (or kinetic stability) regions of species, see [VIG 11b], Chapter 1, Figure 1.2.6.

8.4.2. *Diffusion-controlled rate of an elementary electrochemical reaction*

Above a certain over-potential, the rate of the electrochemical reaction becomes limited by the transport of the ion in the Nernst diffusion layer or in the viscous boundary layer, see Chapter 6, section 6.4.2. The diffusion limited current (DLC) is the current above which an increase in potential will not increase the rate of the electrochemical process, see Figures 8.4.4 and 8.4.5.

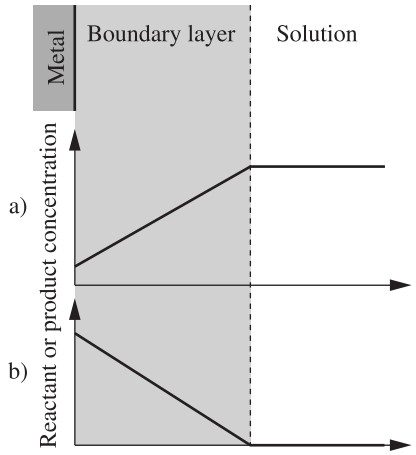

Figure 8.4.5. *Diffusion-controlled electrochemical process: concentration gradients of the reactant or product in the boundary layer, a) deposition, b) dissolution*

For the basic reactions, see equations [8.1.1] and [8.1.2], the diffusion flux of the M^{z+} ion can be written as:

$$\Phi_{Mz+} = -(D_{Mz+} / \delta) \, . \, \{[M^{z+}]_\infty - [M^{z+}]_i\} \qquad [8.4.14]$$

For a cathodic desposition (see reaction [8.1.2]), its concentration of the diffusing species at the interface is negligible as it is entirely consumed (see Figure 8.4.5a) and the diffusion current is:

$$i_{diff} = z\,F\,(D_{Mz^+} / \delta)\,.\,[M^{z+}]_\infty \qquad [8.4.15]$$

$$i(A/cm^2) = \{2 \times 96{,}485 / 10^4\}\,(D_{Mz^+} / \delta)\,.\,[M^{z+}]_\infty$$

where $D_{Fe2+} = 3.5 \times 10^{-10}$ m^2/s, $\delta \approx 0.0001$ m (thickness of the Nernst layer) and $[M^{z+}]_\infty$ is in mol/m^3.

For an anodic dissolution (see reaction [8.1.1]), the concentration of the diffusing species in the solution $[M^{z+}]_\infty$ is usually negligible compared to its concentration at the interface $[M^{z+}]_i$, at least at the start of the process (see Figure 8.4.5b):

$$i_{diff} = zF\,(D_{Mz^+} / \delta)\,.\,[M^{z+}]_i \qquad [8.4.16]$$

and by replacing the concentration at the interface $[M^{z+}]_i$ with its expression deduced from equation [8.2.7], we have:

$$i_{diff} = zF\,(D_{Mz^+} / \delta)\,.\,\exp\{zF\,(E_{app} - E^*) / RT\} \qquad [8.4.17]$$

If the deposition rate becomes limited by the diffusion process in the viscous limiting layer whose thickness is δ, we have:

$$J_{Fe^{2+}} = D_{Fe^{2+}}\,[M^{z+}] / \delta \qquad [8.4.18a]$$

$$J_{Fe^{2+}} = (2 \times 96\,485 / 10^4)\,D_{Fe^{2+}}\,[M^{z+}] / \delta \text{ in A/cm.}$$

8.4.3. *Rate of a redox chemical reaction*

In *chemical redox reactions* the electrons are directly transferred between the reactants.

In the oxidative leaching processes of sulfides (see [VIG 11b], Chapter 1, section 1.2.3), the oxidizing reactants are the ferric or cupric ions. The regeneration of the oxidizing reagent by oxygen occurs by the homogeneous redox chemical reaction:

$$2\,Fe^{2+}(aq) + 1/2\,O_2(aq) + 2\,H^+ \rightarrow 2\,Fe^{3+} + H_2O \qquad [8.4.18b]$$

which is the sum of two elementary electrochemical reactions, see equations [8.1.4a] and [8.1.4b]. At equilibrium and at 25°C:

$$\log[Fe^{3+}] / [Fe^{2+}] = 7.76 - pH + 1/4 \log p_{O2}$$

Under an oxygen pressure of 1 atm and pH < 2, the reaction can be considered as being complete. In a hydrochloric or sulfuric medium, the reaction rate is given by:

$$r = d [Fe^{2+}] / dt = k_r p_{O2} [Fe^{2+}]^2 \text{ (in mole/L.min)} \qquad [8.4.19]$$

of the first order with respect to oxygen pressure or to the concentration of dissolved oxygen and of second order with respect to Fe^{2+} ion concentration [CRU 97, PAP 90].

The rate constant k_r is a complex function of sulfuric acid content [SO_4H_2] and SO_4Zn, SO_4Na_2, $CuSO_4$ contents. We remember that depending on the temperature and pH, the predominant ions are different, see Chapter 4, Figures 4.2.11 and 4.2.12. Thus, for instance, for pH <2 at 100°C, the *prevailing* Fe(II) ion is $FeHSO_4^+$ and the predominant Fe(III) ion is $FeSO_4^+$. The reaction can then be written as:

$$2\ FeHSO_4^+ + 1/2\ O_2(aq) \rightarrow 2\ FeSO_4^+ + H_2O$$

The rate increases with the temperature up to 150°C and then significantly decreases, the solubility of iron sulfate becoming quite low beyond that point, see Figure 4.2.21.

We present only the expression established by Dreisinger and Peters [DRE 89] for 120°C < T < 150°C, which has been used by Baldwin for a 2.0 M $ZnSO_4$, 0.2 M $FeSO_4$, 0.5 M H_2SO_4 composition at 150°C. This can be written as [BAL 95]:

$$r = 4 \times 10^9 \exp(-80{,}300(J) / RT)\ (1 + 5[Cu^{2+}]^{1/2})\ [Fe^{2+}]^2\ p_{O2}\ [H_2SO_4]^{-1/2}\ .\ [SO_4^{2-}] \qquad [8.4.20]$$

where [$(SO_4^{2-})'$] is the concentration of sulfate ions.

8.5. Redox electrochemical reactions

In *redox electrochemical reactions*, both elementary electrochemical reactions occur on the same conducting but isolated surface without any current source. The electrons are transferred from one ion to the other by an electronic conductor over distances of more than several atoms. One of the reactions R_c (cathodic reaction) consumes the electrons released by the other reaction R_a (anodic reaction).

Three hydrometallurgical processes occur from a redox chemical reaction: *cementation*, *oxidative leaching* of metals and sulfides, and *precipitation* of a metal from one of its salts dissolved in an aqueous phase. Taking cementation as an example, we establish the expressions of the process rates under both chemical and diffusion regimes.

8.5.1. *Cementation or displacement reaction*

Cementation is an industrial process that is mainly performed to purify solutions before the electrolysis step or to recover metals, see [VIG 11b], Chapter 1, section 1.3.4.

8.5.1.1. *Thermodynamic analysis*

Cementation of copper by iron (recovering of copper from aqueous solutions) is represented by the reaction:

$$Cu^{2+} + Fe(s) \rightarrow Cu(s) \downarrow + Fe^{2+} \qquad [8.5.1]$$

$$A = A° \, (RT \ln K_C) + RT \ln([Cu^{2+}] / [Fe^{2+}]\} \qquad [8.5.2]$$

with deposition of copper on the iron substrate.

The reaction goes on as long as $A > 0$, so as long as:

$$\{[Cu^{2+}] / [Fe^{2+}]\} > 1 / K_C$$

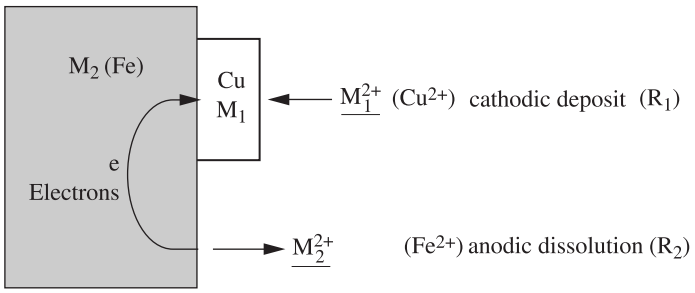

Figure 8.5.1. *Cementation mechanism, see reaction [8.5.1]*

The reaction is the sum of two elementary electrochemical reactions that occur simultaneously on nearby areas of the metallic surface. The reduction of the copper ions occurs on the iron cathodic areas (positive pole), see Figure 8.5.1; the electrons

travel in the iron from the anodic regions (negative pole) to the cathodic regions (positive pole):

$$R_1: Cu^{2+} + 2\,e \rightarrow Cu; \quad E^{o}_{Cu/Cu^{z+}} = +0.337 \text{ volt} \qquad [8.5.3a]$$

$$R_2: Fe \rightarrow Fe^{2+} + 2\,e; \quad E^{o}_{Fe/Fe^{z+}} = -0.44 \text{ volt} \qquad [8.5.3b]$$

The chemical affinity of the overall reaction [8.5.1] is given by:

$$A = (\mu_{Cu2+} - \mu°_{Cu}) + (\mu°_{Fe} - \mu_{Fe2+}) = \{E^*_{R1} - E^*_{R2}\} \qquad [8.5.4]$$

The overall reaction, like other redox electrochemical reactions, occurs in the direction indicated only if:

$$E^*_{R1} > E^*_{R2}$$

The standard affinity A° can be calculated from the reversible standard potentials of both elementary electrochemical reactions [8.2.6]:

$$A° = 2\,F\,.\,\{E°_{Cu} - E°_{Fe}\} = 2\,F \times 0.777 = RT \ln K_C \qquad [8.5.5]$$

thus: $K_C = 10^{26}$ at 25°C.

The reaction then continues until completion, i.e. until the concentration ratio of the ions in solution reaches 10^{-26}, which means it goes on until all the Cu^{2+} ions are removed from the solution.

The reaction rate can be controlled by either one of the elementary heterogeneous electrochemical reactions, or by the transport of anions in the solution towards the conducting surface or vice versa.

8.5.1.2. *Kinetics controlled by the elementary electrochemical reactions: mixed electrode*

When two electrochemical reactions R_1 and R_2 occur on the same surface at the contact of an electrolyte, the surface is called *mixed electrode*, see Figure 8.5.2.

One of the reactions R_1 (cathodic reduction) consumes the electrons released by the other reaction R_2 (anodic oxidation). On a mixed electrode, where the equilibrium potentials E^*_{R1} and E^*_{R2} of both reactions *a priori* are different, the law of conservation of electric neutrality can only be fulfilled if the sum of the reaction currents is equal to zero:

$$I = i_1 + i_2 = 0 \qquad [8.5.6]$$

The mixed potential E_m correspondings to the equality of the two currents ($i_1 = -i_2$). Its position with respect to the equilibrium potentials of both reactions is shown in Figure 8.5.2. The reaction rate per unit surface, *according to* Faraday's law, corresponds to the current thus determined (see VIG 11b, Chapter 2, section 2.2.2). Qualitatively, the greater $\{E^*_{R1} - E^*_{R2}\}$, the greater the reaction rate.

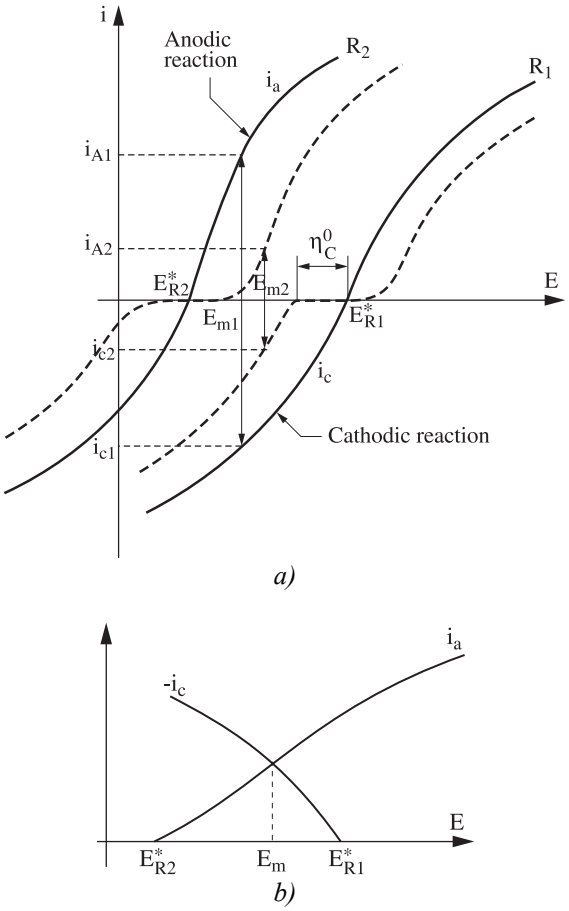

Figure 8.5.2. *a) Cementation or lixiviation kinetics for a mixed electrode. Polarization curves of the elementary reactions (full lines – reversible reaction; dashed lines – irreversible reactions). Graphical determination of the rate of overall reaction $i_a + i_c = 0$ and of the mixed potential E_m. b) Evans' diagram*

These two curves are usually drawn, as shown in Figure 8.5.2b, with only the anodic part of the curve representing reaction R_2 and with the cathodic part of the curve representing reaction R_1 drawn symmetrically. The resulting current corresponds to the kinetics of both simultaneous reactions. This diagram is the Evans' diagram, which is usually used in the analysis of the kinetics of leaching and cementation reactions.

The mixed potential E_m and resulting current can be determined thanks to equations [8.4.1] to [8.4.5]. Calculation, in the general case, leads to complex equations. In this section, we present the result obtained by considering that both polarization curves of the reduction R_1 and dissolution R_2 (see Figure 8.5.2) are far from each other, and that the exchange current of each reaction is quite high (see Figure 8.4.4a). In other words, we consider that the initial anodic and cathodic over-potentials $\eta°_a$ and $\eta°_c$ (see Figure 8.5.2) are low and we can mistake the oxidation polarization curve for its own anodic branch and the reduction polarization curve for its cathodic branch (see Figure 8.4.3). We thus obtain the expressions of the mixed potential and resulting current, and thus the expression of the overall reaction rate, from equations [8.4.10], [8.4.11] and [8.4.12]:

$$zFE_m / RT = \ln \{k''_{c(Cu)} / k''_{a(Fe)}\} \cdot [Cu^{2+}] \qquad [8.5.7]$$

and:

$$i = zF \{(k''_{c(Cu)})^{\alpha} \cdot (k''_{a(Fe)})^{(1-\alpha)}\} \cdot [Cu^{2+}]^{\alpha} \qquad [8.5.8]$$

In this example, $z = 2$ and when $\alpha = 1/2$ (value usually accepted), we have:

$$i = 2\,F \{(k''_{c(Cu)}) \cdot (k''_{a(Fe)})\}^{1/2} \cdot [Cu^{2+}]^{1/2} \qquad [8.5.9]$$

In this model, we assume that there were no complex ions formed.

When cathodic over-potentials $\eta°_c$ for the reduction (of oxygen on metals and sulfides, see Table 8.5.3) or/and anodic over-potentials $\eta°_a$ have to be taken into account (dashed curves in Figure 8.5.2), the mixed potential no longer fulfills equation [8.5.7]. The resulting currents (i_{A2}, i_{C2}) and therefore the overall reaction rate are therefore much lower than the one (i_{A1},i_{C1}) given by equation [8.5.9].

8.5.1.3. *Rate-controlled step: transport of an ion in the solution*

In most cases of cementation in dilute solution, the rate is of first-order kinetics with respect to ion concentration in the solution and the kinetics are controlled by the transport of the ion in the solution to the surface, with an activation energy of 8–14 kJ/mol.

When kinetics are controlled by:

– diffusion of the Cu^{2+} ion in the Nernst diffusion layer (see equation [8.4.15]):

$$i_{diff} = zF\,(D_{Mz+} / \delta)\,.\,[Cu^{z+}]_{\infty} \qquad [8.5.10]$$

– or by diffusion of the Fe^{2+} ion in the Nernst diffusion layer (see equation [8.4.17]):

$$i_{diff} = zF\,(D_{Mz+} / \delta)\,.\,\exp\{zF\,(E_m - E^*_{Fe}) / RT\} \qquad [8.5.11]$$

8.5.2. *Leaching (dissolution) of metals*

As another example of the kinetics of these redox electrochemical reactions, we consider the leaching of gold. The standard potential of the Au / Au^{3+} electrode in aqueous solution:

$$Au(s) \rightarrow Au^{3+} + 3\,e, \quad E°_{Au/Au3+} = 1.51\ V \qquad [8.5.12]$$

is higher than the standard reduction potential of oxygen (1.23 V), see reaction [8.3.2]. In addition, the initial *cathodic over-potential* $\eta°_c$ of the reduction of oxygen on gold being 0.8 V (see Figure 8.5.2), gold is extremely stable even in a strongly oxidizing medium.

Sodium cyanide solutions are used for gold and silver leaching. The reaction is carried out in an alkaline medium (pH > 10), see Figure 4.2.7, in the presence of oxygen:

$$2\,Au(s) + 1/2\,O_2(aq) + 4\,NaCN + H_2O \rightarrow 2\,NaAu(CN)_2 + 2\,NaOH \qquad [8.5.13]$$

with the formation of a complex ion $Au(CN)_2^-$ where the valence of gold is equal to 1 and whose stability constant $\beta(K_{STxy})$ is very high 2×10^{38}, see equation [4.2.45a] and Table 4.2.7. Complexation stabilizes the Au^+ ion, see section 4.2.3.5. The reaction occurs through the two following elementary reactions:

– reduction of the oxygen dissolved in water (see reaction [8.3.2]); and

– anodic reaction:

$$Au(s) + 2\,CN^- \rightarrow Au(CN)_2^- + e \qquad [8.5.14]$$

which can be considered as the sum of both successive reactions:

$$Au \rightarrow Au^+ + e \qquad (E^o_{Au/Au^+} = 1.715\ V \text{ at } 25°C) \qquad [8.5.15]$$

$$Au^{+} + 2\ CN^{-} \rightarrow Au(CN)_2^{-} \qquad [8.5.16]$$

The potential of the Au / Au^{+} electrode in presence of cyanide ions, see equation [8.2.23], is:

$$E^{*}_{Au/Au(CN)_2^-} - (RT / zF) \ln \beta - (nRT / zF) \ln \tilde{a}_{CN^-} + (RT / zF) \ln \tilde{a}_{Au(CN)_2^-} \qquad [8.5.17]$$

Complexation decreases the oxidation potential of gold and makes its dissolution possible (see Figure 8.5.2):

$$E^{o}_{Au/Au^{+}} - (RT / F) \ln \beta = 1.7 - 2.3 = -0.6\ V \qquad [8.5.18]$$

The higher the concentration in cyanide ions, the more significantly the potential is decreased. The Pourbaix diagrams $Au\text{-}H_2O$ and $Au\text{-}CN\text{-}H_2O$, see Figure 8.3.10, show the extension of the dissolution region of gold due to the formation of this complex. The pH of the solution has to be kept above pK = 9.38 (see Chapter 4, section 4.2.2, equation [4.2.32] and Figure 4.2.7) for the CN^- ion to be the predominant form in solution.

The mechanism of gold dissolution by cyanide solutions in alkaline media (pH >10) is represented in Figure 8.5.3.

Below a definite CN^- ion concentration, the kinetics are controlled by diffusion of the CN^- ion in the Nernst layer and is of the first order with respect to this concentration. Above this CN^- ion concentration, the kinetics are controlled by the diffusion of oxygen $O_2(aq)$ and are of the first order compared to this concentration.

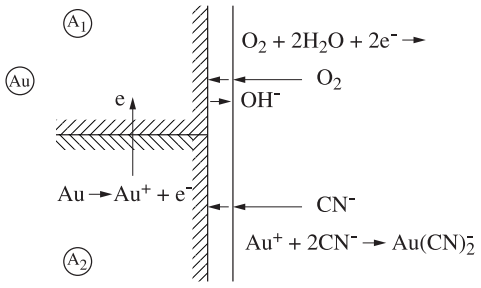

Figure 8.5.3. *Dissolution of gold in a cyanide solution where A_1 is the cathodic zone and A_2 the anodic zone*

The polarization curves of both reactions (see Figure 8.5.4) show that below a definite concentration in CN^- ions, the mixed potential is located on the plateau of the polarization curve of the anodic current. Above this concentration of CN^- ions, the mixed potential is located on the plateau of the polarization curve of the cathodic reaction for a solution saturated in air.

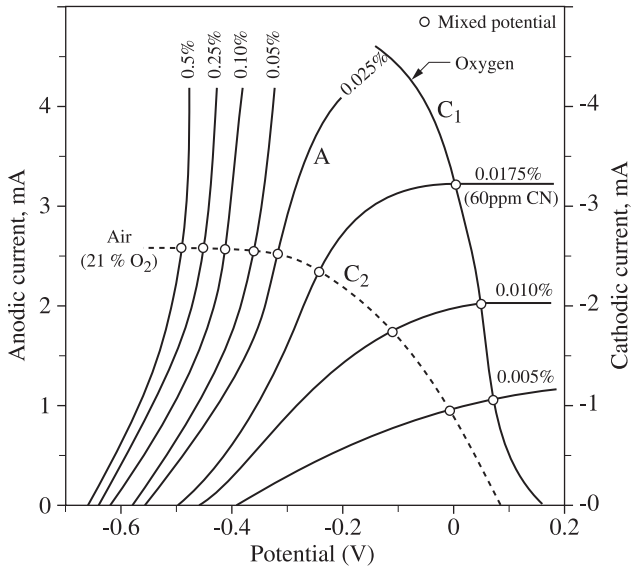

Figure 8.5.4. *Dissolution of gold in a cyanide solution. Effects of KCN concentration and oxygen partial pressure on the mixed potential and reaction rate. Evans' diagram. C – cathodic oxygen reduction curves (C_1 under oxygen and C_2 under air). A – gold anodic dissolution curves as a function of KCN concentration [FLE 99]*

In diffusion regime, we have [HAB 76]:

$$d(O_2(aq)) / dt = (D_O / \delta) \,.\, A_1 \,[O_2(aq)] \qquad [8.5.19]$$

$$d(CN^-) / dt = (D_{CN} / \delta) \,.\, A_2 \,[CN^-] \qquad [8.5.20]$$

in the steady state. As the dissolution of 1 M of gold corresponds to the consumption of 2 M of oxygen and 0.5 M of cyanide ion, we have:

$$2\,(D_{O2} / \delta) \,.\, A_1 .\, [O_2(aq)] = 1/2\,(D_{CN} / \delta) \,.\, A_2\,[CN^-] \qquad [8.5.21]$$

as $A = A_1 + A_2$, leading to:

$$\text{rate} = \frac{2AD_{CN}D_O\left[CN^-\right]\left[O_2\,(aq)\right]}{\delta\left\{D_{CN}\left[CN^-\right] + 4D_O\left[CN^-\right]\left[O_2\,(aq)\right]\right\}} \qquad [8.5.22]$$

At low cyanide concentrations, the rate of dissolution only depends on that concentration. At high cyanide concentrations, the rate of dissolution only depends on the oxygen concentration. These results are in agreement with experimental results.

The optimum cyanide concentration would be the concentration for which the diffusion fluxes of both reactants, according to the model of a diffusion layer of constant thickness:

$$[CN^-] = 4\ \{D_O / D_{CN^-}\}\ [O_2(aq)] \qquad [8.5.23]$$

and the dissolution rate reaches its limit value.

The D_O / D_{CN^-} ratio of the diffusion coefficient of both species being in the order of 1–1.5, the optimum ratio of the concentrations is then of the order 4–6.

For a solution saturated in air, the oxygen concentration is in the order of 8 ppm or 2.5×10^{-4} mol/L. The CN^- concentration is equal to 32–40 ppm, which corresponds to 75 ppm of NaCN.

In practice, the leaching of gold by this process is performed under pure oxygen and the kinetics are controlled by diffusion of the CN^- ions at low concentrations (<0.025% of KCN). At higher concentration, the kinetics are controlled by the diffusion of oxygen.

A model, considering the reaction as being controlled by electrochemical reactions, in agreement with its own experimental results has been established by Crundwell [CRU 97]. According to this model, the rate varies as the product of the concentrations in CN^- and $O_2(aq)$ raised to the power 1/2 (see equation [8.4.10c]):

$$r = i_a / F = 1 / F\ (k_a\ [CN^-])^{1/2}\ .\ (k_c\ [O_2(aq)])^{1/2} \qquad [8.5.24]$$

8.6. Bibliography

[AND 03] C.G. ANDERSON, *JOM*, pp. 32-36, April 2003.

[ANT 82] M.S. ANTELMAN, *The Encyclopedia of Chemical Electrode Potentials*, Plenum Press, New York, 1982.

[BAL 95] S.A. BALDWIN, G.P. DEMOPOULOS, V.G. PAPANGELAKIS, *Metallurgical and Materials Transactions B*, Vol. 62B, 1035-1047, October 1995.

[BER 99] R.M. BEREZOWSKY *et al*., *JOM*, pp. 36-40, December 1999.

[CHE 83] C. M. CHEN, K. ARAL, G. J. THEUS, "Computer-calculated potential-pH diagrams to 300°C", Vol 2, in: *Handbook of Diagrams*, EPRI, NP 3137 Report, Vol 2. project 1167, Final report, June 1983.

[CRU 97] F.K, CRUNDWELL, S.A. GODORR, *Hydrometallurgy*, 44, 47-162, 1997.

[CRU 05] F.K, CRUNDWELL, *Minerals Engineering*, Vol. 18, pp. 1315-1324, 2005.

[DAG 89] A. DAGDAR, *JOM*, 37, December 1989.

[DEM 99] G.P. DEMOPOULOS, *Leaching Fundamentals and Industrial Practice*, TMS Short Course, San Diego, 1999.

[DRE 89] D.B. DREISINGER, E. PETERS, *Hydrometallurgy*, Vol. 22, pp. 101-119, 1989.

[FLE 99] C.A. FLEMING, *Leaching of Gold Ores: Leaching Fundamentals and Industrial practice*, TMS short Course, San Diego, February 1999.

[HAB 67] F. HABASHI, *Montana Bur. Mines Geology*, Vol. 59, 1967.

[HAN 93] K.N. HAN, X. MENG, *Extractive Metallurgy of Copper, Nickel and Cobalt*, Vol. 1, TMS, pp. 709-733, 1993.

[LAT 64] W.M.M. LATIMER, *Oxidation Potentials*, Prentice Hall Inc., Englewood Cliff, 1964.

[LIN 87] H.K. LIN, H.Y. SOHN, *Metallurgical Transactions B*, Vol. 18, pp. 497-503, September 1987.

[OKE 92] T.J. O'KEEFE, *JOM*, 30-34, April 1992.

[PAP 90] V.P. PAPANGELAKIS, D. BERK, G.P. DEMOPOULOS, *Metallurgical Transactions B*, Vol. 21B, pp. 827-837, October 1990.

[POU 66] M. POURBAIX, *Atlas of Electrochemical Equilibria in Aqueous Solutions,* Pergamon, New York, 1966.

[POU 73] M. POURBAIX, *Lectures on Electrochemical Corrosion*, Plenum Press, New York, 1973.

[POU 82] M. POURBAIX and A. POURBAIX (eds.), *Diagrams of Chemical and Electrochemical Equilibria, Their Setting-up and Applications*, Cebelcor, 1982.

[PUY 03] G.V.K. PUYVADA, *JOM*, 39, August 2003.

[RIC 74] F.D. RICHARDSON, *Physical Chemistry of Melts in Metallurgy*, Vol. 2, Academic Press, London 1974.

[RUI 98] M.C. RUIZ, S. HONORES, R. PADILLA, *Metallurgical and Materials Transactions B*, Vol. 29B, pp. 961-969, October 1998.

[SEN 03] G. SENANAYAKE, D.M. MUIR, *Hydrometallurgy*, Vol. 1, pp. 518-531, 2003.

[VIG 11b] A. VIGNES, *Extractive Metallurgy 2: Metallurgical Reaction Processes*, ISTE Ltd, London and John Wiley and Sons, New York, 2011.

[VIG 11c] A. VIGNES, *Extractive Metallurgy 3: Processing Operations and Routes*, ISTE Ltd, London and John Wiley and Sons, New York, 2011.

[WES 65] J.M. WEST, *Electrodeposition and Corrosion Processes*, D. Van Nostrand, New York, 1965.

[WIN 91] R. WINAND, *Hydrometallurgy*, Vol. 23, pp. 285-316, 1991.

List of Symbols

Superscripts:

° indicates standard state

* indicates quantity at equilibrium

$\bar{}$ indicates mean value

Subscripts for a component X or for a quantity such as a flowrate F or a flux:

X(s,l,g) indicates the physical state of the component

$\underline{X}_{(metal)}$ indicates a component X dissolved in a metallic phase

$(X)_{(slag)}$ indicates a component (element or compound) dissolved in a slag

$\{X\}_{(matte)}$ indicates a component (element or compound) dissolved in a matte

X(aq) indicates a component X dissolved in an aqueous solution

[X] $= C_X$ is the molar concentration of component X in a solution

For the content (mole fraction, concentration, mass fraction) or for the flux (flow rate) of a component X in a phase α at a specific location, for example at the (in the vicinity of the) interface between two phases, this is indicated by subscript s:

$x_{X(\alpha)s}$; $C_{X(\alpha)s}$; $\%X_{(\alpha)s}$ ($\%\underline{X}_{(M)s}$, $\%X_{(slag)s}$, $\%X_{\{matte\}}$), $F_{X(\alpha)s}$

Extractive Metallurgy 1: Basic Thermodynamics and Kinetics Alain Vignes
© 2011 ISTE Ltd. Published 2011 by ISTE Ltd.

a, b: partial order of the rate of a chemical reaction (see [VIG 11a], formula [5.2.12])

a_j, $a_{j(\alpha)}$: activity of component j, $a_{j(\alpha)}$ activity of component j (dissolved) in phase α:

Raoultian activity of component j: $a_j = \gamma_j \cdot x_j$ (see [VIG 11a], formula [1.3.21] and [1.3.31])

a°_j: standard activity of component j relative to its standard potential μ°_j (reference state: standard state of the pure component, i.e.: its physical state at the temperature T and p = 1 atm) (see [VIG 11a], formula [1.3.22])

$\tilde{a}_j = f_j x_j$: Henrian activity of component j = $f_j x_j$ (see [VIG 11a], formula [1.3.37])

$\tilde{a}_{j(1\%)} = f_j \cdot \%j$; $\tilde{a}_{j©} = f_j.C_j$; $\tilde{a}_{j(<m>)} = f_j.\langle m_j \rangle$ (see [VIG 11a], formula [1.3.41], [1.3.46-47])

$\tilde{a}_{(MaAb)}$: activity (of an electrolyte (salt)) of the fraction of the content of a compound in an aqueous solution in an undissociated state (see [VIG 11a], formula [4.2.27])

$a_{\pm}$: mean (ionic) activity of the fraction of the content of a compound (electrolyte (salt), in an aqueous solution in a dissociated state (function of the activities of the two ions) (see [VIG 11a], formula [4.2.8])

$\hat{a}_{MaXb}$: pseudo-activity of an electrolyte in an aqueous solution (see [VIG 11a], formula [4.2.10])

$\hat{a}_{MaXb}$: pseudoactivity of an unstoichiometric compound in an intermediate phase (see [VIG 11a], formula [2.3.11])

a_w: activity of water in aqueous solutions (see [VIG 11a], formula [4.2.13])

A_r: affinity of a chemical reaction r ($A_r = -\Delta G_r$) (see [VIG 11a], formula [1.3.14] and [1.3.53])

A°_r: standard affinity of a reaction r : $A^\circ (T, P = 1atm) = -\Delta G^\circ_r$ (see [VIG 11a], formula [1.3.16])

b: ratio of stoichiometric coefficients of reactants A and B : ν_B/ν_A (see [VIG 11a], formula [7.2.1])

B: slag basicity (see [VIG 11a], formula [3.4.1])

C: total molar density of a solution

$C_{j(\alpha)}$: molar concentration (molarity) of component (species) j in α phase, $C_A = [A]$ (moles/L^3) (see [VIG 11a], formula [1.2.34])

C_{pj}: molar heat capacity at constant pressure of species j (J/°K.mole) (see [VIG 11a], formula [1.3.5])

C_p: steel dephosphorization (phosphate) capacity of a slag (see [VIG 11b], formula [5.4.18])

d_p: diameter of a particle (= 2 R_p)

$D_{j(\alpha)}$: diffusion coefficient of a component j in a phase α (L^2/t) (see [VIG 11a], formula [6.2.18])

D_{AR}: interdiffusion coefficient (binary diffusivity) for mixture of A+R (see [VIG 11a], formula [6.2.12])

D_{eff}: effective diffusion coefficient of a gas in a porous particle

e^k_j: interaction coefficients (see [VIG 11a], formula [1.3.44])

E_a: activation energy for an elementary reaction (cal/mole or J/*mole) (see [VIG 11a], formula [5.2.27])

E: EMF: electromotive force (see [VIG 11b], formula [2.2.6])

$E^*_{(decomposition)}$: decomposition voltage of a salt (see [VIG 11b], formula [2.2.12])

$E_{M/M^{z+}}$: electrode potential (see [VIG 11a], formula [8.2.3])

$E^*_{M/M^{z+}}$: electrode potential at equilibrium between the electrode and its solution (Nernst equation) (see [VIG 11a], formula [8.2.6-7])

$E^\circ_{M/M^{z+}}$: standard electrode potential (see [VIG 11a], formula [8.2.8])

$E_{ESH} = E_H$: electrode potential relative to standard hydrogen reference electrode (see [VIG 11a], Table 8.2.1)

E_m: mixed (electrical) potential (potential at which the rates of the two reactions are balanced) (see [VIG 11a], Figure 8.5.2)

f_j: Henrian activity coefficient of component j, relative to a standard which makes f equal to unity at infinite dilution (see [VIG 11a], formula [1.3.37])

f_j^i: Henrian activity coefficient of component j function of the content of component i in a multicomponent solution (see [VIG 11a], formula [1.3.43])

$f_{\pm}$: mean activity coefficient of a dissociated compound in an aqueous solution (see [VIG 11a], formula [4.2.9])

F: Faraday number = 96,485 coulombs/mole = 96,485 J/volt/eqg = 23,060 cal/volt/eqg

F_j: molar flow rate of component j (see [VIG 11a], formula [1.2.42])

F_jM_j: mass flow rate of component j (see [VIG 11a], formula [1.2.42])

$G = Q\,\rho$: mass flow rate of a stream (see [VIG 11a], formula [1.2.42])

$G^{(sys)}$: "Gibbs free energy" or "free enthalpy" of a system (see [VIG 11a], formula [1.3.6]) (see ΔG)

g_p: linear growth or shrinkage rate of a particle = dR_p/dt (see [VIG 11a], formula [7.2.4] and [VIG 11c], formula [2.2.6])

h: hydratation number (see [VIG 11a], formula [4.2.22])

h_T: heat transfer coefficient (see [VIG 11a], formula [6.3.1])

$h_{T(\alpha)s}$: heat transfer coefficient in phase α (see [VIG 11a], formula [6.3.1b])

$h_{A(\alpha)}$: mass transport conductance (mass transfer coefficient) of component A in a phase α (see [VIG 11a], formula [6.3.2])

H: enthalpy of a phase per unit mass (see [VIG 11a], formula [6.2.9])

H: distribution (partition) coefficient in solvent extraction (see [VIG 11b], formula [1.4.6])

i: basicity of a slag (see [VIG 11a], formula [3.4.1b])

i_0: exchange current (see [VIG 11a], formula [8.4.9])

i_a: anodic current (see [VIG 11a], formula [8.4.6] and [8.4.11])

i_c: cathodic current (see [VIG 11a], formula [8.4.7] and [8.4.12])

i_{diff}: diffusion controlled current (DLC) (see [VIG 11a], formula [8.4.15])

I: (electrolysis) cell (line) current (see [VIG 11b], formula [2.2.3])

$i = i_a + i_c$: polarization current (see [VIG 11a], formula [8.4.13])

I: ionic strength of an aqueous solution relative to component concentrations (see [VIG 11a], formula [4.2.16])

I_m: ionic strength of an aqueous solution relative to component molalities (see [VIG 11a], formula [4.2.17])

j_j: molar flux of component j relative to the molar average velocity (see [VIG 11a], formula [6.2.7] and [6.2.13])

J_j: molar (barycentric) diffusion flux molar flux of component j relative to the mass average velocity (see [VIG 11a], formula [6.2.4] and [6.2.12])

J_T: heat flux by conduction: law of heat conduction (see [VIG 11a], formula [6.2.9] and [6.2.10])

k_r: rate constant of a chemical reaction (see [VIG 11a], formula [5.2.11])

k_{rp}; k_{rc}: rate constants (rate expressed as a function of component concentration or pressure) (see [VIG 11a], formula [5.2.12] and [5.2.13] and [5.2.26])

k_B: rate constant of the fractional conversion of a particle B kinetic law ([VIG 11a], formula [7.2.7])

K°(T): equilibrium constant of a reaction expressed in terms of the standard activities of components (see [VIG 11a], formula [1.3.54])

K_p: equilibrium constant of a reaction expressed in terms of the partial pressures of components (see [VIG 11a], formula [1.3.59])

K_C: equilibrium coefficient of a reaction expressed in terms of the concentrations of components (see [VIG 11a], formula [5.2.19])

$K_{\%}$: equilibrium coefficient of a reaction expressed in terms of the mass fraction of components

K_{ads}: equilibrium constant of an adsorption reaction (see [VIG 11a], formula [5.4.3])

K_D: dissociation (acidity) constant of a weak electrolyte in an aqueous solution (see [VIG 11a], formula [4.2.27])

K_{STxy}: stability constant (stability product) i.e. equilibrium constant of a formation reaction of a complex ion defined as a product of activities) (see [VIG 11a], formula [4.2.45a])

K_{sxy}: solubility constant of an hydroxo-complex (see [VIG 11a], formula [4.2.60])

K_{ps}: solubility product of an oxide or a sulphide in a metallic phase (see formula [3.2.16]), of an hydroxide (see formula [4.2.74]) and a salt (see formula [4.2.81] in an aqueous solution [VIG 11a].

K_{Xn}: equilibrium constant for the formation reaction of a complex ion (see [VIG 11a], formula [4.2.71])

K_w: dissociation constant of water (see [VIG 11a], formula [4.2.13])

L_S: sulfur partition ratio between a slag and a metallic (Fe) phase (see [VIG 11b], formula [7.2.5])

L_P: phosphorus partition ratio between a slag and a metallic (Fe) phase (see [VIG 11b], formula [5.4.10])

m_j: mass of component j in a phase α (see [VIG 11a], formula [1.2.27])

m: mass of metal deposited at an electrode (Faraday law) (see [VIG 11b], formula [2.2.3])

m_B: mass of a particle B (see [VIG 11a], formula [7.2.17])

M_j: molar (atomic) weight of component j (see [VIG 11a], formula [1.2.27])

$<m_j>$: molality of component (see [VIG 11a], formula [1.2.37])

mol%j: mole percentage of component j in a solution = x_j (see [VIG 11a], formula [1.2.29])

n: number of reactants and products in a chemical system (see [VIG 11a], formula [1.2.3])

$\mathbf{n_{j(\alpha)}}$: number of moles of component j in a phase α (see [VIG 11a], formula [1.2.5])

$\mathbf{n_B}$: number of moles of component B in a particle (see [VIG 11a], formula [7.2.2])

$\mathbf{p_j}$: partial pressure of component j (see [VIG 11a], formula [1.2.38])

$\mathbf{p^*_j}$: equilibrium partial pressure of component j

pH: (see [VIG 11a], formula [4.2.15])

pK_w: ionic product of water (see formula [4.2.13b])

$pK_D = -\log K_D$ (dissociation constant) (see formula [4.2.28])

P: pressure (see [VIG 11a], formula [1.3.27])

q: electric charge of an ion = zF (see [VIG 11a], formula [8.2.1])

Q: volumetric flow rate (L^3 /t) (see [VIG 11a], formula [1.2.41])

Q_{STxy}: stability coefficient (called also quotient) of a complex ion (equilibrium coefficient of the formation reaction of a complex expressed as a product of molar concentrations) (see [VIG 11a], formula [4.2.45b])

Q_{Sxy}: solubility coefficient of an hydroxide (equilibrium constant) (see [VIG 11a], formula [4.2.60])

Q_{Hxy}: hydrolysis coefficient of a cation M^{z+} (equilibrium coefficient) (see [VIG 11a], formula [4.2.47])

r: current efficiency (see [VIG 11b], formula [2.2.3])

r: number of independent reactions of a reaction system (see [VIG 11a], formula [1.2.3])

r_S: reaction rate of an heterogeneous reaction (per unit surface) (mole/cm^2.sec) (see [VIG 11a], formula [5.2.10])

$\mathbf{r_V}$: reaction rate of an homogeneous reaction (per unit volume) (mole/cm^3.sec) (see [VIG 11a], formula [5.2.5])

R: Boltzman constant = 1.986 cal/mole.K ; 8.314×107 ergs/mole.K ; 9.325 J/mole.K; 82.1 cm^3.atm/mole.K

R_g: nucleus radius (see [VIG 11a], formula [5.3.4])

R_p: particle radius (see [VIG 11a], formula [7.2.2])

s: solubility of an oxide or a salt in an aqueous solution (see [VIG 11a], formula [4.2.57] and [4.2.86])

$s_{\mathbf{m}}$: area of a particle per unit mass (see [VIG 11a], formula [7.2.17])

s_v: area of a particle per unit volume $\rho\, s_m$

S: area of interface for bulk phase

S_p: area of a particle, drop or bubble

t_S: residence time of a unit volume of fluid in a flow reactor (see [VIG 11c], formula [2.1.1] and [3.2.13])

$\bar{t}_S$: reactor holding time; mean residence time of a unit volume of fluid in a CSTR reactor (see [VIG 11c], formula [2.1.2] and [3.2.14])

T: temperature

u: mass average velocity of a fluid flow (see [VIG 11a], formula [1.2.41] and [6.2.1])

v_{MB}: molar volume of component B (see [VIG 11a], formula [7.2.2])

V: volume of a phase

V; V_{cell}: electrolytic cell voltage (see [VIG 11b], formula [2.2.6])

v_{MS}: molar volume of the solvent (see [VIG 11a], formula [1.2.35])

v_{MB}: molar volume of component B (see [VIG 11a], formula [7.2.2])

w: number of intensive variables (see the phase rule) (see [VIG 11a], formula [1.2.4])

w_j = wt%j: mass fraction of component j (see [VIG 11a], formula [1.2.30])

W: energy consumption to produce by electrolysis to one ton of metal (see [VIG 11b], formula [2.2.10])

%j: mass percentage of component j (see [VIG 11a], formula [1.2.31])

x_j: mole fraction of component j in a phase (see [VIG 11a], formula [1.2.29])

X_j: fractional extraction (removal) or absorption of a component j by or from a drop or a bubble (see [VIG 11a], formula [6.4.19] and [7.6.7])

X_B: fractional volumetric conversion of a particle B (see [VIG 11a], formula [7.2.5])

z_j: electric charge (valency) of an ion, z^+ charge of a cation z^- charge of an anion j (see [VIG 11a], formula [4.2.2])

Greek letters

α: transfer coefficient of an electrochemical reaction (see [VIG 11a], formula [8.4.2] and [8.4.4])

α: dissociation degree of a weak electrolyte in an aqueous solution (see [VIG 11a], formula [4.2.29])

α: stoichiometric excess of reactant A with respect to reactant B (see [VIG 11a], formula [1.3.58a] and Figure [1.3.4])

α_T: thermal diffusivity (cm^2/sec)(see [VIG 11a], formula [6.2.10b])

$\beta_{(STxy)} = K_{STxy}$: stability constant (see [VIG 11a], formula [4.2.45])

δ: thickness of the Nernst layer (see [VIG 11a], formula [8.4.14])

δ_v, δ_M, δ_T: boundary layer thicknesses (see [VIG 11a], formula [6.4.9], [6.4.10] and [6.4.11])

ε_A: $(\nu_R - \nu_A) / \nu_A$ (see [VIG 11a], formula [6.2.28])

ε_A: (see [VIG 11a], formula [1.2.55])

ε: mixing power: rate of energy dissipation (see [VIG 11b], formula [7.2.15])

χ_A: fractional conversion of a reactant A (fraction of reactant A converted into product) (see [VIG 11a], formula [1.2.7])

Φ: number of phases of a system (see [VIG 11a], formula [1.2.4])

Φ: osmotic coefficient (see [VIG 11a], formula [4.2.22])

Φ: electrical potential (voltage) (see [VIG 11a], formula [8.2.1])

$\Phi_{j(\alpha)}$: molar flux of component j in a phase α relative to stationary coordinates (with respect to fixed axes) (see [VIG 11a], formula [6.2.2])

$\Phi_{A(\alpha)s}$: molar flux of component A in a phase α at the interface between two phases relative to stationary coordinates (see [VIG 11a], formula [6.2.27])

$\Delta G_r(\xi)$: variation of the Gibbs free energy (free enthalpy) of a reaction for a "degree of advancement" ξ (see [VIG 11a], formula [1.3.9])

$\Delta G°_r$: standard Gibbs free energy of a reaction (see [VIG 11a], formula [1.3.13b])

$\Delta G°_{f(A)}$: standard Gibbs free energy (free enthalpy) of formation of a compound A (see [VIG 11a], formula [1.3.11])

ΔG_a: energy barrier (see [VIG 11a], formula [8.4.2])

ΔG_a: free energy of formation of a stable nucleus (see [VIG 11a], formula [5.3.5])

Δg_j^{sc}: molar free energy of a physical state change of a component j (see [VIG 11a], formula [1.3.25])

Δg_j^{fusion}: molar free energy of fusion of a component (see [VIG 11a], formula [1.3.26])

$\Delta g°_{j(0)}^{(diss)}$: molar free energy of dissolution of a component j in its standard state, in a dilute solution at infinite dilution (see [VIG 11a], formula [1.3.39])

$\Delta g°_{j(1\%)}^{(diss)}$: molar free energy of fusion of a component j in its standard state in a solution with 1% of component j (see [VIG 11a], formula [1.3.42])

γ_j: Raoultian activity coefficient $\gamma_j \,.\, a_j = \gamma_j \,.\, x_j$ (see [VIG 11a], formula [1.3.31] and [1.3.36] and Figure [1.3.2])

$\gamma_{j(0)}$: Raoultian activity coefficient at infinite dilution (see formula [1.3.35])

ΔH_r: enthalpy (heat) of reaction r (see [VIG 11a], formula [1.3.3])

$\Delta H°_r$: standard enthalpy (heat) of reaction r (see [VIG 11a], formula [1.3.2])

$\Delta H°_{f(A)}$: standard enthalpy (heat) of formation of a pure species (compound) A (see [VIG 11a], formula [1.3.5])

λ_T: thermal conductivity (cal(joule)/cm K) (see [VIG 11a], formula [6.2.10a])

$\lambda(g)$: $\Delta v / \{\sum n_{ji}(g) + n_{inertes}(g)\}$ (see [VIG 11a], formula [1.2.50])

$\mu_j \,.\, \mu_{j\,chem}$: chemical potential of component j (see [VIG 11a], formula [1.3.7], [1.3.21] and [8.2.1])

μ°_j: chemical potential of component j in standard state (potential of the pure species in its physical state at temperature T and pressure p = 1 atm) (see [VIG 11a], formula [1.3.22])

$\mu_\pm$: mean chemical potential of both ions of a compound dissociated in an aqueous solution (see [VIG 11a], formula [4.2.7])

$\mu_{j(el)}$: electrochemical potential of component (ion) j (see [VIG 11a], formula [8.2.1])

μ: viscosity (poise = g/cm/s dyn.s/cm2)

η°_j: Henrian chemical potential of a pure component j (see [VIG 11a], formula [1.3.38], [1.3.46] and [4.2.5])

η: overvoltage (see [VIG 11a], formula [8.4.5])

η_c , η_a: cathode and anode polarization (see [VIG 11b], formula [2.2.8] and [VIG 11a], Figure 8.4.4)

ν_A: stoichiometric coefficient of reactant A in a chemical reaction (see [VIG 11a], formula [1.2.1])

$\Delta\nu$: $(\nu_R + \nu_S - \nu_A - \nu_B)$ (see [VIG 11a], formula [1.2.47])

ν: kinematic viscosity (cm^2/s)

$\theta_{A(ads)}$, θ_T: number of sites per unit surface covered by adsorbed species (see [VIG 11a], formula [5.4.3] and [5.4.12])

θ_v: number of empty sites per unit surface (see [VIG 11a], formula [5.4.2])

ρ: (mass) density of a solution (see [VIG 11a], formula [1.2.28])

ρ_j: mass concentration of component j

ρ_B: (mass) density of a particle B (see [VIG 11a], formula [7.2.20])

ρ_{mC}: carbon reactivity (combustion rate per unit mass of the particle) (see [VIG 11a], formula [7.2.24])

$\sigma_{\alpha/\beta}$: surface tension α/β

τ: time for complete conversion of a single solid particle (see [VIG 11a], formula [7.2.8], [7.2.13], [7.4.3] and [7.4.7])

Ω: cross-sectional area

$\xi(t)$: "extent" or "degree of completion" or "degree of advancement" of a reaction (moles) (see [VIG 11a], formula [1.2.5] and [1.2.6])

ψ_T: heat flux across the interface (phase boundary) between two phases (see [VIG 11a] formula [6.3.1])

ψ_A: flux of a component A across the interface between two phases) (see [VIG 11a], [6.3.21])

$\psi(Rp)$: size distribution function of particles (volumetric density function) (see [VIG 11c], formula [2.1.11])

ζ_j: chemical potential of a pure component j in the same physical state than the phase in which it is dissolved (see Formula [1.3.21])

Dimensionless numbers (see Table 6.1)

Nu: Nusselt number = $2\, h_{T\alpha}\, R_p / \alpha_{T\alpha}$ (see [VIG 11a], formula [6.4.15b])

Pr: Prandtl number = $\nu_\alpha / \alpha_{T\alpha}$ (see [VIG 11a], formula [6.4.12b])

Re: Reynolds number = $2R_p u_\infty \rho_f / \mu_f$ ( ) (see [VIG 11a], formula [6.4.15a])

Sc: Schmidt number = $\nu_\alpha / D_{A\alpha}$ (see [VIG 11a], formula [6.4.12a])

Sh: Sherwood number = $2\, h_{A\alpha}\, R_p / D_{A\alpha}$ (see [VIG 11a], formula [6.4.15c])

Index

A

activities
  of metals in liquid copper, 77
  of metals in liquid iron, 78
  Ag-Cu system, 75
  $CaO\text{-}FeO\text{-}Fe_2O_3$ slags, 119
  $CaO\text{-}SiO_2\text{-}Al_2O_3$ slag, 112
  $CaO\text{-}SiO_2\text{-}Al_2O_3\text{-}MgO$ slag, 114
  $CaO\text{-}SiO_2$-CrO slag, 125
  $CaO\text{-}SiO_2$-FeO slags, 123
  Cu-S matte, 95
  Cu-Zn system, 75
  Fe-Cu system, 79
  Fe-Cu-S matte, 98
  Fe-Cu-S-O, 104
  Fe-Mn system, 79
  Fe-Ni-S matte, 98
  Fe-S matte, 95
  Fe-Si system, 79
  Pb-S matte, 95
  $SiO_2\text{-}FeO\text{-}Fe_2O_3$ slags, 117
activity
  in dilute metal solutions, 26
  of a metalloid in metal solutions, 27, 48
  of an ion in aqueous solutions, 136
affinity of a reaction, 19, 28
alumina (Al_2O_3) solubility in cryolite (Na_3AlF_6), 177
aluminum sulfate ($Al_2(SO_4)_3$)
  solubility in aqueous solutions, 167
Arrhenius' law activation energy, 189

B

blast furnaces slags, 114
Boehmite (γ-AlOOH) solubility in aqueous solutions, 162
Boudouard reaction, 68
  mechanism and rate (chemical reaction control), 200
  rate (mixed regime), 262
boundary layer
  flow past flat plate, 240
  heat transfer coefficient, 241
  mass transport conductance, 242
  thicknesses ratios, 242
  viscous boundary layer thickness, 241
Butler-Volmer law, 307

C

calcium carbonate (CO_3Ca)
  calcination, 276

Extractive Metallurgy 1: Basic Thermodynamics and Kinetics Alain Vignes
© 2011 ISTE Ltd. Published 2011 by ISTE Ltd.

carbon
activity in liquid iron, 81
Boudouard reaction rate (mixed regime), 262
combustion rate (chemical reaction control), 199
combustion reactions, 67
combustion reactivity, 262
solubility in Fe-Si alloy, 83
solubility in liquid iron, 82
solubility in liquid manganese, 83
cation hydrolysis hydroxocomplexes, 154
cementation
redox electrochemical reaction, 315
chalcocite (Cu_2S): flashroasting, 273
chalcoptyrite ($CuFeS_2$): flash roasting, 273
chemical potential, 21
chemical potential in aqueous solutions, 26, 132
of a metalloid in metal solutions, 27
of component j, 18
chemical vapor deposition (CVD)
silicon, 215
chlorides solubility in aqueous solutions, 168
chlorination rate (chemical reaction control), 198
chlorocomplexes stability constant, 149
coals features, 70
cobalt
(II): chlorocomplexes, 152
(III): cyanide complex stability constant, 156
coke compositions, 70
complexes: stability constant in aqueous solution, 149
conservation equations of elements in a closed system, 8
convection flux of component j, 224
conversion *in situ*
of a porous particle: grain pellet model, 269
of a porous particle: heat balance, 272
of a porous particle: rate (chemical reaction control), 269
of a porous particle: rate (product layer diffusion control), 269
of a dense particle: rate (chemical reaction control), 267
of a dense particle: rate (fluid diffusion control), 266
of a dense particle: rate (product layer diffusion control), 266
of a dense particle: shrinking unreacted core model, 265
copper oxide (CuO)
acid leaching (chemical reaction control), 205
solubility in aqueous solutions, 159
copper (I): chlorocomplexes, 156
copper (II): chlorocomplexes
speciation diagram, 151
stability contants, 151
cryolite
(AlF_6Na_3): standard free energy of formation, 176
(Na_3AlF_6): dissociated ions, 176
cyanhydric acid (HCN)
dissociation in aqueous solutions, 144
De Donder equation, 20, 187
Debye-Hückel law, 135
decarburization of liquid iron
chemical reaction control, 210
mass transport control, 232
degree of advancement of a reaction
closed system, 6
open system, 9
degree of dissociation of a weak electrolyte in aqueous solutions, 143

diffusion
coefficient in multicomponent systems, 227
flux of component j, 224
dissociation constant of a weak electrolyte in aqueous solutions, 143
Duhem theorem, 5

E

electrochemical irreversible reaction
oxidation potential, 311
reduction potential, 311
electrochemical potential of
charged species, 285
an ion in its metal, 285
an ion in its solution, 286
electrochemical reaction, 308
equilibrium potential, 286
exchange current, 308
polarization curve, 309
transfer coefficient, 308
electrode potential, 285
at equilibrium, 286
metal-complex, 290
standard dissolution potentials of metals, 289
standard electrode potential, 286
Ellingham-Richardson diagrams
carbides, 66
chlorides, 62
Fe-O system, 55
oxides, 51
sulfides, 58
enthalpy
balance (for a reacting system), 225
of a reaction, 17
of formation of a component, 17
equilibrium constant of a reaction, 29
Evans diagram
redox electrochemical reaction, 318
evaporation rate of a component: mass transport control, 239
exchange current: electrochemical reaction, 308

F

ferric sulfate ($Fe_2(SO_4)_3$)
solubility in aqueous solutions, 167
ferrous
salts in aqueous solutions: oxidation by O_2 (rate), 314
sulfate ($FeSO_4$): solubility in aqueous solutions, 167
Fick's
first law, 226
second law, 227
flash roasting, 271
ignition temperature, 273
laminar flow furnace, 272
Fourier's law, 225
fractional conversion of a
particle, 255
reactant in a closed system, 7
reactant in a semi-batch system, 10
reactant in an open system, 9

G

gasification of a dense particle
fractional conversion rate (chemical reaction control), 255
fractional conversion rate (fluid film diffusion control), 256
gasification of a porous particle
fractional conversion rate (chemical reaction and pore diffusion control), 260
fractional conversion rate (chemical reaction control), 259
Gibbs free energy
of a system, 18
of formation: Al2O, 54

of formation: CO, 67
of formation: Cr3C2, 66
of formation: FeO, 56
of formation: FeS, 58
of formation: SiO, 54
of formation: ZnO, 53
Gibbs Phase rule, 5
Gibbs-Duhem equation, 28
Gibbsite (a-$Al(OH)_3$)
solubility in aqueous solutions, 159
gold
complexes: stability constants, 153
(I) cyanide complex: stability constant, 156
leaching in cyanide (CNNa) solution, 319
grain model of a porous particle
gasification rate (chemical reaction control), 259

H

heat
balance, 226
conduction flux, 225
transfer coefficient, 228, 238
transport conductance, 228
Henrian activity, 24, 25
coefficient f_j, 24
Henry's law, 24
heterogeneous precipitation
growth rate of a particle (chemical reaction control), 264
growth rate of a particle (mass transport control), 264
mechanism, 216
heterogeneous reaction
adsorption rate, 195
mechanism, 194, 196
reaction rate, 197
Higbie's model: mass transport
conductance in a continuous phase around a fluid particle, 246
homogeneous precipitation
critical supersaturation, 191
incubation time, 193
kinetics, 192
mechanism, 190
primary nucleation, 191
secondary nucleation, 193
hydratation number of a cation, 138
hydrochloric acid (HCl)
dissociation constant in aqueous solutions, 138
mean activity coefficient in aqueous solutions, 139
hydrogen activity
in liquid copper, 86
in liquid iron, 90
in liquid nickel, 87
hydrogen
solubility in liquid iron, 90
sulfide (H_2S): dissociation in aqueous solutions, 145
removal of steel (mass transfer control), 236
removal of steel, 278
stream degassing, 279
hydrolysis constant of a cation, 154
hydroxides: solubility products in aqueous solutions, 162

I, K

ignition temperature, 273
ilmenite ($FeTiO_3$): leaching by H_2SO_4(chemical reaction control), 257
interaction coefficients in dilute metal solutions, 26
ionic
product, 134
product: water, 134

strength of an aqueous solution I, 135
iron oxide
(Fe_2O_3): acid leaching(chemical reaction control), 203
(Fe_2O_3): reduction by H_2 (chemical reaction control), 212
(Fe_3O_4): reduction by H_2 (chemical reaction control), 213
(Fe_3O_4): reduction of a pellet by H_2, 267
(FeO(l)): reduction by CO (chemical reaction control), 209
(FeO(s)): reduction by CO (chemical reaction control), 188
(FeOOH) (goethite): solubility in aqueous solutions, 159
Iron
(II) sulfate complexes: speciation diagram, 152
(III) chlorocomplexes: speciation diagram, 151
(III) chlorocomplexes: stability contants, 150
(III) sulfate complexes: speciation diagram, 152
kinetics: additivities of resistances, 251

L

law of definite proportions
closed system, 6
open system, 8
law of mass action, 29
leaching
by H_2SO_4(chemical reaction control), 257
of a dense particle: fractional conversion rate (chemical reaction control), 255
of a dense particle: fractional conversion rate (fluid film diffusion control), 256
lead sulfide(PbS):
acid leaching (chemical reaction control), 205
leaching by $FeCl_3$, 266
lead(II) chlorocomplexes: stability constants, 150
Lewis and Whitman theory, 251
ligands, 132, 148

M

magnetherm process: slags, 115
mass
transfer coefficient, 235
transport conductance : rigid sphere, 246
transport conductance, 228
mattes
conductivities, 94
viscosities, 94
mean activity of
a strong electrolyte $a_{\pm}$ in aqueous solutions, 135
an electrolyte $a_{\pm}$ in aqueous solutions, 133
mean chemical potential of an electrolyte in aqueous solutions, 133

N

Nernst equation, 286
Newton’s law (heat transfer), 228
nickel
oxide (NiO): reduction by H_2, 212
(II) ammoniacal complexes: stability constant, 155
nitrogen
activity in liquid iron, 90
solubility in liquid iron, 90

absorption by liquid iron (chemical reaction control), 207
absorption by liquid iron (effect of sulfur and oxygen), 208
removal of steel (chemical reaction control), 208
Nusselt number
heat transfer between a particle and a fluid phase, 244
Nusselt number: Higbie model, 246

O

Onsager relations, 225
osmotic coefficient, 138
Ostwald law, 144
oxygen
adsorption by liquid iron, 208
solubility phase diagrams: Ag-Cu system, 75
oxygen activity
in liquid copper, 85
in liquid iron, 88
in liquid nickel, 87
in slags, 116
oxygen solubility
Cu-O-S matte, 102
in aqueous solutions, 171
in Fe-Cu-S-O mattes, 103
in liquid iron, 88
phase diagrams, 36

P

phase diagrams
CaO-FeO-Fe_2O_3 system, 117
CaO-SiO_2-Al_2O_3 system, 111
CaO-SiO_2-Cr_2O_3, 125
CaO-SiO_2-CrO, 125
CaO-SiO_2-Fe_2O_3, 121
CaO-SiO_2-FeO, 121
CaO-SiO_2-MgO-Al_2O_3 system, 113
Cu-O system, 44
Cu-O-S system, 102
Cu-Zn system, 75
Fe-Cu system, 79
Fe-Cu-O-S system, 103
Fe-Cu-S system, 97
Fe-Ni-S system, 98
Fe-O-S system, 101
Fe-S system, 47
MgO-SiO_2-Al_2O_3 system, 113
Na_3AlF_6-Al_2O_3 system, 177
NaF-AlF_3 system, 175
Ni-O-S system, 100
Pb-Zn system, 74
SiO_2-FeO-Fe_2O_3 system, 117
Zr-O system, 45
potential-pH diagrams, 36
Pourbaix diagrams
cobalt-NH_3-H_2O, 303
iron-H_2O system, 298
nickel-NH_3-H_2O, 303
sulfur-H_2O system, 305
water, 293
Prandtl number (Pr), 242
predominance diagrams, 36
pseudo-activity
âCu2S, 56
$â_{FeO}$, 117
âFeO, 57
âMaAb, 56
of an electrolyte $â_{(MaAb)}$ in aqueous solutions, 133
of unstoechiometric compound âMaAb, 56
pyrite (FeS_2)

R

Raoultian activity, 21, 24
coefficient γ_j, 24
Raoult's law, 21
reaction rate
activation energy, 189
elementary reversible reaction, 187
heterogeneous reaction, 186

homogeneous reaction, 185
near equilibrium, 187
redox chemical reaction rate, 313
redox electrochemical reaction, 314
Evans diagram, 318
mixed electrode, 316
mixed potential, 317
reference electrode: hydrogen electrode, 289

S

salt melts
melting temperatures, 174
viscosities, 174
Schmidt number (Sc), 242
Sherwood number: mass transfer between a particle and a fluid phase, 244
silica carbothermic reduction, 34
silicon: chemical vapor deposition (CVD), 217
silver chloride (AgCl): solubility in aqueous solutions, 169
silver cyanide (AgCN): solubility in aqueous solutions, 171
slags
basicity, 108
conductivities, 107
iron ore smelting reduction, 124
magnetherm process, 115
steel converting, 124
steel desulfurization, 114
viscosities, 107, 109
sodium
chloride (NaCl): mean activity in aqueous solutions, 136
hydroxide (NaOH): dissociation constant in aqueous solutions, 138
hydroxide (NaOH): mean activity in aqueous solutions, 142
sulfate (SO_4Na_2): mean activity in aqueous solutions:, 136
solubilities
hydroxides in aqueous solutions, 157
salts in aqueous solutions, 165
solubility
diagrams: gibbsite (α-$Al(OH)_3$), 158
products: hydroxides in aqueous solutions, 162
products: sulfides in aqueous solutions, 169
speciation diagrams:
chlorocomplexes, 151
sphalerite (ZnFe)S)
stability diagrams, 36
Cr-O2-Cl2 system, 62
Cu-O-S system, 83, 102
Fe-O2-Cl2 system, 62
Fe-O-S system, 102
M-O-S, 60
Ni-O-S system, 100
Pb-O_2-S_2 system, 102
Zn-O2-Cl2 system, 62
standard
activity, 22
affinity, 20
chemical potential, 18
Gibbs free energy of a reaction, 19
Gibbs free energy of formation: oxide, 51
sulfates: solubility in aqueous solutions, 166
sulfides
acid leaching, 205
solubilities in aqueous solutions, 169
solubility products in aqueous solutions, 169
sulfur activity
in liquid copper, 85
in liquid iron, 89

in liquid nickel, 87
sulfuric acid (SO_4H_2):
dissociation in aqueous solutions, 145
ion H^+ activity in aqueous solutions, 145
sulfuric monoprotonic acid (HSO_4^-):
dissociation constant in aqueous solutions, 146

T, U, W

Tafel law, 309
Temkin law, 94
Ternary phase diagrams, 36
thermal
conductivity, 225
diffusivity, 225
transfer
coefficient
processes: mechanism, 207
unstoichiometric compound
vapor pressures of metals in liquid copper, 77
water (H_2O): activity, 134

Z

zinc ferrite ($ZnFe_2O_4$):
(dense particles) leaching by HCl (chemical reaction control), 257
(porous particles) leaching by SO_4H_2 (chemical reaction control), 260
zinc oxide (ZnO)
reduction by CO (mass transport control), 232
reduction by CO (chemical reaction control), 198
zinc sulfide (ZnS)
acid activities of metalloids in liquid iron, 78
dense particle: roasting(porous layer diffusion control), 271
porous particle
leaching (chemical reaction control), 205
roasting (chemical reaction control), 214
zinc sulfide (ZnS): roasting (mass transport control), 231
zirconium oxide (ZrO_2)

Summary of Volume 2

Metallurgical Reaction Processes

Preface

Chapter 1. Hydrometallurgical Extraction Processes

1.1. Overview of hydrometallurgical processes
1.2. Leaching processes
1.3. Precipitation processes
1.4. Solvent extraction
1.5. Hydrometallurgical processing routes of ores, concentrates and residue (flowsheets)
1.6. Bibliography

Chapter 2. Electrometallurgical Extraction Processes

2.1. Overview of electrometallurgical processes
2.2. Electrolysis – bases
2.3. Aqueous electrolysis: bases
2.4. Electrowinning of copper
2.5. Electrowinning of nickel
2.6. Electrowinning of zinc
2.7. Electrorefining of lead
2.8. Electrorefining of tin
2.9. Cobalt electrowinning
2.10. Bibliography

Extractive Metallurgy 1: Basic Thermodynamics and Kinetics Alain Vignes
© 2011 ISTE Ltd. Published 2011 by ISTE Ltd.

Chapter 3. Halide Extraction Processes

3.1. Overview of the halide extraction processes
3.2. Chlorination processes
3.3. Reduction of halides
3.4. Bibliography

Chapter 4. Reduction of Metal Oxides

4.1. Introduction
4.2. Solid state oxide reduction by a gaseous reducing agent
4.3. Solid-state carbothermic reduction
4.4. Carbothermic smelting reduction
4.5. Smelting reduction by slag-metal reactions
4.6. Carbothermic reduction of silica and alumina
4.7. Metallothermic reductions
4.8. Bibliography

Chapter 5. Oxygen Steelmaking

5.1. Overview of steel converting and refining operations
5.2. Converting and refining reactions
5.3. Oxidation of hot metal elements by gaseous oxygen
5.4. “Slag-metal” reactions
5.5. Stainless steel making
5.6. Ultra-low carbon steel making
5.7. Bibliography

Chapter 6. Sulfide Extraction Processes

6.1. Introduction
6.2. Oxidation of sulfides (in the solid state)
6.3. Matte oxidation by gaseous oxygen
6.4. Reactions occurring in smelting and converting operations
6.5. Smelting reduction of a roasted concentrate and primary converting
6.6. Secondary converting of Cu_2S, Ni_3S_2 and PbS mattes
6.7. Bibliography

Chapter 7. Metal Refining Processes

7.1. Introduction
7.2. Steel refining/secondary steelmaking
7.3. Aluminium refining
7.4. Copper refining
7.5. Lead refining

7.6. Tin refining
7.7. Zinc refining
7.8. Titanium and zirconium refining
7.9. Nickel refining
7.10. Bibliography

List of Symbols

Index

Summary of Volume 3

Processing Operations and Routes

Preface

Chapter 1. Physical Extraction Operations

1.1. Solid-solid and solid-fluid separation operations
1.2. Separation operations of the components of a fluid phase
1.3. Bibliography

Chapter 2. Hydrometallurgical Operations

2.1. Leaching and precipitation operations
2.2. Reactor models based on particle residence time distribution functions
2.3. Reactor models based on the population balance equation model
2.4. Solvent extraction operations
2.5. Bibliography

Chapter 3. Gas-solid and Solid-solid Reactors and Particle Conversion Operations

3.1. Overall presentation of gas-solid and solid-solid reactors
3.2. Gas-solid reactor hydrodynamic behavior and heat transfer between phases
3.3. The performance equations of gas-solid packed-bed reactors
3.4. The performance equations of fluidized-bed reactors
3.5. Solid-solid reactors
3.6. Bibliography

Chapter 4. Blast Furnaces

4.1. Overview of blast furnaces
4.2. Iron blast furnace
4.3. Ferromanganese blast furnace
4.4. Zinc blast furnace: the Imperial smelting furnace
4.5. Lead blast furnace
4.6. Bibliography

Chapter 5. Smelting Reduction Operations

5.1. Overview of smelting reduction operations
5.2. Production of (iron) “hot metal” by carbothermic smelting reduction
5.3. Tin and zinc smelting reduction operations
5.4. Magnetherm process
5.5. Bibliography

Chapter 6. Steelmaking Operations

6.1. Overview of steelmaking operations
6.2. Hot metal pretreatment operations
6.3. The hot metal converting operation
6.4. Stainless steelmaking operations
6.5. Ultra-low carbon steel-making operation
6.6. Bibliography

Chapter 7. Sulfide and Matte Smelting and Converting Operations

7.1. Overview of the operations and processes
7.2. Flash-smelting operations and processes
7.3. In-bath smelting and converting operations in bottom-blown converters
7.4. In-bath smelting and converting operations in top-blown converters
7.5. Top-submerged lance (TSL) blown converters: Ausmelt/Isasmelt process
7.6. Bibliography

Chapter 8. Electric Melting and Smelting Furnaces

8.1. Introduction
8.2. Performance of electric furnaces
8.3. Electric arc melting furnaces
8.4. Electric smelting reduction furnaces
8.5. Consumable-electrode remelting furnaces
8.6. Bibliography

Chapter 9. Molten Salt Electrolysis Operations

9.1. Overview of molten salt electrolysis operations
9.2. Chloride electrolysis
9.3. Reduction of alumina by electrolysis
9.4. Electro-reduction of metal oxides and deoxidation of metals by molten salt electrolysis
9.5. Bibliography

Chapter 10. Extractive Processing Routes

10.1. Features of extractive processing routes
10.2. Hot metal, steel and ferroalloys
10.3. Aluminum (gallium)
10.4. Copper and other valuable metals
10.5. Nickel (cobalt)
10.6. Zinc (cadmium, indium, germanium, gallium)
10.7. Lead (silver, gold, bismuth)
10.8. Tin
10.9. Magnesium
10.10. Titanium, zirconium and hafnium
10.11. Chromium
10.12. Molybdenum and tungsten
10.13. Niobium and tantalum
10.14. Gold
10.15. Metals belonging to the PGM
10.16. Silicon
10.17. Bibliography

List of Symbols

Index